

PACIFIC EARTHQUAKE ENGINEERING RESEARCH CENTER

Response Modification of Structures with Supplemental Rotational Inertia

Gholamreza Moghimi

Nicos Makris

**Department of Civil and Environmental Engineering
Southern Methodist University, Dallas, Texas**

PEER Report No. 2024/01

Pacific Earthquake Engineering Research Center
Headquarters at the University of California, Berkeley
January 2024

Response Modification of Structures with Supplemental Rotational Inertia

Gholamreza Moghimi

Nicos Makris

Department of Civil and Environmental Engineering
Southern Methodist University, Dallas, Texas

PEER Report No. 2024/01
Pacific Earthquake Engineering Research
Center Headquarters,
University of California, Berkeley
January 2024

ABSTRACT

Tall, multistory, buildings are becoming increasingly popular in large cities as a result of growing urbanization trends (United Nations Department of Economic and Social Affairs 2018). As cities continue to grow, many of them along the coasts of continents which are prone to natural hazards, the performance of tall, flexible buildings when subjected to natural hazards is a pressing issue with engineering relevance. The performance of structures when subjected to dynamic loads can be enhanced with various response modification strategies which have been traditionally achieved with added stiffness, flexibility, damping and strength (Kelly et al. 1972; Skinner et al. 1973, 1974; Clough and Penzien 1975; Zhang et al. 1989; Aiken 1990; Whittaker et al. 1991; Makris et al. 1993a,b; Skinner et al. 1993; Inaudi and Makris 1996; Kelly 1997; Soong and Dargush 1997; Constantinou et al. 1998; Makris and Chang 2000a; Chang and Makris 2000; Black et al. 2002, 2003; Symans et al. 2008; Sarlis et al. 2013; Tena-Colunga 1997).

Together with the elastic spring that produces a force proportional to the relative displacement of its end-nodes and the viscous dashpot that produces a force proportional to the relative velocity of its end-nodes; the inerter produces a force proportional to the relative acceleration of its end-nodes and emerges as the third elementary mechanical element (in addition to the spring and dashpot) capable for modifying structural response. Accordingly, in this report we examine the seismic performance of multistory and seismically isolated structures when equipped with inerters.

In view that the inerter emerges as the third elementary mechanical element for the synthesis of mechanical networks, in Chapter 2 we derive the basic frequency- and time-response functions of the inerter together with these of the two-parameter inertoelastic and inertoviscous mechanical networks.

Chapter 3 examines the response of a two-degree-of-freedom (2DOF) structure where the first story is equipped with inerters. Both cases of a stiff and a compliant support of the inerters are examined. The case of two parallel clutching inerters is investigated and the study concludes that as the compliance of the frame that supports the inerters increases, the use of a single inerter offers more favorable response other than increasing the force transferred to the support frame.

Chapter 4 examines the seismic response analysis of the classical two-degree-of-freedom isolated structure with supplemental rotational inertia (inerter) in its isolation system. The analysis shows that for the “critical” amount of rotational inertia which eliminates the participation of the second mode, the effect of this elimination is marginal on the structural response since the participation of the second mode is invariably small even when isolation systems without inerters are used. Our study, upon showing that the reaction force at the support of the inerter is appreciable, proceeds with a non-linear response analysis that implements a state-space formulation which accounts for the bilinear behavior of practical isolation system (single concave sliding bearings or lead-rubber bearings) in association with the compliance of the support of the inerter. Our study concludes that supplemental rotational inertia aggravates the displacement and acceleration response of the elastic superstructure and as a result, for larger isolation periods ($T_b > 2.5s$) the use of inerters in isolation systems is not recommended.

Chapter 5 first examines the response analysis of a SDOF elastoplastic and bilinear structure and

reveals that when the yielding structure is equipped with supplemental rotational inertia, the equal-displacement rule is valid starting from lower values of the pre-yielding period given that the presence of inerters lengthens the apparent pre-yielding period. The analysis concludes that supplemental rotational inertia emerges as an attractive response modification strategy for elastoplastic and bilinear SDOF structures with pre-yielding periods up to $T_1 = 1.5sec$. For larger pre-yielding periods (say $T_1 > 2.0sec$), the effectiveness of inerters to suppress the inelastic response of 2DOF yielding structures reduces; and for very flexible first stories; as in the case of isolated structures examined in chapter 4, the use of inerter at the first level (isolation system) is not recommended.

Finally, chapter 6 shows that, in spite of the reduced role of inerters when placed at floor levels other than the first level (they no-longer suppress the induced ground acceleration nor they can eliminate the participation of higher modes), they still manifest a unique role since it is not possible to replace a structure with solitary inerters at higher levels with an equivalent traditional structure without inerters.

Keywords: Supplemental rotational inertia, Response modification, Inerter, Nonlinear analysis, Seismic protection, Earthquake Engineering.

ACKNOWLEDGMENTS AND DISCLAIMER

The current post-doctoral fellowship of Dr. Gholamreza Moghimi (first author) is supported by the SMU/Bush Institute post-doctoral program. The opinions, findings, conclusions, and recommendations expressed in this publication are those of the author(s) and do not necessarily reflect the view of Pacific Earthquake Engineering Research (PEER) Center, or the Regents of the University of California.

CONTENTS

ABSTRACT	iii
ACKNOWLEDGMENTS	vi
TABLE OF CONTENTS	ix
LIST OF TABLES	xi
LIST OF FIGURES	xiii
1 INTRODUCTION	1
1.1 Suppression of the induced ground acceleration	3
2 BASIC RESPONSE FUNCTIONS OF SIMPLE INERTOELASTIC AND INERTO-VISCOUS MODELS	5
2.1 Basic Response Functions of the Linear Spring	8
2.2 Basic Response Functions of the Inerter	10
2.3 Basic Response Functions of the Two-Parameter Inertoelastic “Solid”	13
2.4 Basic Response Functions of the Two-Parameter Inertoelastic “Fluid”	17
2.5 Basic Response Functions of the “rotational inertia damper” (dashpot and inerter in parallel)	20
2.6 Basic Response Functions of a Dashpot and Inerter Connected in Series	22
2.7 Conclusions	24
3 DISPLACEMENTS AND FORCES IN STRUCTURES WITH INERTERS WHEN SUBJECTED TO EARTHQUAKES	27
3.1 Open Soft First Story: From Aesthetics, Functionality and Seismic Isolation to a Lateral Failure Mechanism	27
3.2 Inertia Forces from the Flywheel Supported on a Stiff Chevron Frame	30
3.3 Equations of Motion of a 2DOF Structure Supported on a Stiff Chevron Frame	30
3.4 Two Parallel Rotational Inertia Systems	32
3.5 Response Spectra of the 2DOF Structure with a Stiff Chevron Frame	34
3.6 Equations of Motion of a 2DOF Structure with a Compliant Chevron Frame with Finite Stiffness and Damping	38
3.7 Response Spectra of the 2DOF structure with a Compliant Chevron Frame with Finite Stiffness and Damping	42
3.8 Conclusions	44

4	RESPONSE OF SEISMICALLY ISOLATED STRUCTURES WITH SUPPLEMENTAL ROTATIONAL INERTIA	45
4.1	Linear Theory of Seismic Isolation with Supplemental Rotational Inertia	45
4.1.1	Eigenvalue Analysis	47
4.2	Modal Response Contributions and Seismic Response Analysis	51
4.3	Seismic Response of a 2DOF Structure Supported on a Bilinear Isolation System with Supplemental Rotational Inertia	58
4.3.1	Response of Isolated Structure with Inerters Supported on a Non-Compliant Support	59
4.3.2	Response of Isolated Structure with Inerter Supported on a Compliant Support	60
4.4	Conclusions	65
5	SEISMIC RESPONSE OF YIELDING STRUCTURES EQUIPPED WITH INERTERS	67
5.1	Inertia Forces From an Inerter Supported on a Stiff Chevron Frame	67
5.2	Equation of Motion of a Yielding SDOF Structure with Inerters Supported on a Stiff Chevron Frame	68
5.2.1	The use of a pair of clutching inerters	70
5.3	Response Spectra of a Yielding SDOF Structure with Inerters Supported on a Stiff Chevron Frame	71
5.4	Equation of Motion of a Yielding 2DOF Structure with Inerters Supported on a Compliant Chevron Frame	76
5.5	Response Spectra of a Yielding 2DOF Structure with Inerters Supported on a Compliant Chevron Frame	81
5.6	Conclusions	86
6	THE ROLE OF INERTERS WHEN PLACED AT FLOOR-LEVELS OTHER THAN THE FIRST LEVEL	87
6.1	Multi-Story Structures	87
6.2	Inerters manifests a unique role even when placed at floor-levels other than the first level	93
6.3	Conclusions	97
7	CONCLUSIONS	99
	REFERENCES	101

LIST OF TABLES

2.1	Basic frequency-response functions and their corresponding causal time-response functions of elementary inertoelastic and inertoviscous models.	9
-----	---	---

LIST OF FIGURES

1.1	A physical realization of the inerter in which the force output is proportional only to the relative acceleration between nodes 1 and 2.	1
1.2	A rack-and-pinion-flywheel realization of the inerter, which is the mechanical analogue of the capacitor in a force–current/velocity–voltage analogy.	2
1.3	Single-degree-of-freedom structure with mass m and stiffness k with supplemental rotational inertia from a flywheel with radius R supported on a chevron frame with stiffness k_f that is much larger than k	4
2.1	Left: The two-parameter inertoelastic “solid”. Right: The two-parameter inertoelastic “fluid”.	14
2.2	Left: The rotational inertia damper which is an inertoviscous model in parallel. Right: The inertoviscous model in series.	20
3.1	(a) 2DOF structure engaged with a rotational flywheel system;(b) 2DOF structure retrofitted with supplemental damper at firstsoft story; and (c) classical two-degree-of-freedom seismic isolationsystem.	28
3.2	Iconic soft-story failure of Olive View Hospital during 1971 San Fernando, California earthquake. (Image courtesy of the USGS).	29
3.3	Response of a 2DOF structure that is engaged to an inerter at the first story supported on an infinite stiff chevron frame: (a) single inerter which may induce deformation; (b) pair of inerters that can only resist the motion as described by equations (3.14) and (3.16a); force from the inerter only opposes the motion.	33
3.4	Acceleration time histories recorded during (a) 1979 Coyote Lake, California earthquake; and (b) 1995 Kobe, Japan earthquake.	35
3.5	Response spectra of a two-degree-of-freedom (2DOF) structure equipped with supplemental rotational inertia (heavy solid lines) or supplemental damping (dashed lines) supported on a stiff frame when excited by the Gilroy Array 6/230 ground motion recorded during the 1979 Coyote Lake, USA earthquake.	36
3.6	Response spectra of a two-degree-of-freedom (2DOF) structure equipped with supplemental rotational inertia (heavy solid lines) or supplemental damping (dashed lines) supported on a stiff frame when excited by Takarazuka /000 ground motion recorded during the 1995 Kobe, Japan earthquake.	37

3.7	Response spectra of a two-degree-of-freedom (2DOF) structure equipped with supplemental rotational inertia (heavy solid lines) or supplemental damping (dashed lines) supported on a compliant frame ($\lambda = 0.05s$, $\lambda_d = 0.5s$, $\lambda\omega_R = 0.5$) when excited by the Gilroy Array 6/230 ground motion recorded during the 1979 Coyote Lake, USA earthquake.	43
4.1	Classical two-degree-of-freedom seismic isolation structure (Kelly 1990, 1997) with supplemental rotational inertia at the isolation system.	46
4.2	Reduction of the first and second modal damping ratios ξ_1 and ξ_2 due to supplemental rotational inertia with inertance $M_R = \sigma M = \sigma(m_b + m_s)$. The graphs also compare the modal damping ratio values offered by equation (4.24) (where only terms up to order ϵ have been retained) against the corresponding values before taking the Taylor expansions offered by equation (4.23).	51
4.3	Participation factors, L_1 and L_2 of the first and second modes respectively as a function of supplemental rotational inertia $\sigma = M_R/M$. For values of $\sigma = \epsilon(1 - \gamma)$, the participation factor $L_2 = 0$ and the contribution of the second vibration mode in the seismic response of the 2DOF structure vanishes. The graphs also compare the approximate values of L_1 and L_2 as offered by equation (4.28) with the exact expressions appearing in the right-hand-side of equations (4.26) and (4.27).	53
4.4	Response of the 2DOF isolated structure shown in Figure 4.1 with isolation period $T_b = 2\pi/\omega_b = 2 \text{ sec}$, superstructure period $T_s = 2\pi/\omega_s = 0.4 \text{ sec}$ ($\epsilon = 0.04$), $\gamma = m_s/M = 0.75$, $\xi_b = 15\%$ and $\xi_s = 3\%$ when subjected to the C02, N65E ground motion recorded during the 1966 Parkfield, California earthquake. Plots (a) and (b) are without supplemental rotational inertia ($\sigma = 0$); whereas plots (c) and (d) are for the critical value $\sigma = \epsilon(1 - \gamma) = 0.01$ that vanishes the participation of the second mode.	55
4.5	Left: Peak base u_b^{max} , and superstructure, u_s^{max} displacements of the 2DOF isolated structure shown in Figure 4.1 for a wide range of isolation periods ($1.5 \text{ sec} \leq T_b = 2\pi/\omega_b \leq 3.5 \text{ sec}$) and a constant value $\epsilon = \omega_b^2/\omega_s^2 = 0.04$, $\gamma = m_s/M = 0.75$, $\xi_b = 15\%$, $\xi_s = 3\%$ for various values of supplemental rotational inertia, $\sigma = 0, \epsilon(1 - \gamma) = 0.01, 0.2$ and 0.4 when subjected to the C02, N65E ground motion recorded during the 1966 Parkfield, California earthquake shown in Figure 4.4. The differences between the superstructure response when $\sigma = 0$ and when $\sigma = \epsilon(1 - \gamma)$ are marginal and within the error due to the approximations inherent to the approximate modal analysis procedure. Top-Right: Total superstructure accelerations. Bottom-Right: Force transferred to a non-compliant inerter-support.	56

- 4.6 Left: Peak base u_b^{max} , and superstructure, u_s^{max} displacements of the 2DOF isolated structure shown in Figure 4.1 for a wide range of isolation periods ($1.5 \text{ sec} \leq T_b = 2\pi/\omega_b \leq 3.5 \text{ sec}$) and a constant value $\epsilon = \omega_b^2/\omega_s^2 = 0.04$, $\gamma = m_s/M = 0.75$, $\xi_b = 15\%$, $\xi_s = 3\%$ for various values of supplemental rotational inertia, $\sigma = 0$, $\epsilon(1 - \gamma) = 0.01$, 0.2 and 0.4 when subjected to the Pacoima Dam/164 ground motion recorded during the 1971 San Fernando, California earthquake shown at the bottom. The differences between the superstructure response when $\sigma = 0$ and when $\sigma = \epsilon(1 - \gamma)$ are marginal and within the error due to the approximations inherent to the approximate modal analysis procedure. Top-Right: Total superstructure accelerations. Bottom-Right: Force transferred to a non-compliant inerter-support. 57
- 4.7 Bilinear idealization. From the five control parameters, k_1 , $k_b = \alpha k_1$, u_y , $F = k_1 u_y$ and $Q = (\frac{1}{\alpha} - 1) k_b u_y$ only three parameters are needed to define the bilinear behavior. 58
- 4.8 Left: Peak base u_b^{max} , and superstructure, u_s^{max} displacements of the 2DOF isolated structure shown in Figure 4.1 for a wide range of isolation periods ($1.5 \text{ sec} \leq T_b = 2\pi/\omega_b \leq 3.5 \text{ sec}$) for a constant value $\epsilon = \omega_b^2/\omega_s^2 = 0.04$, $\gamma = m_s/M = 0.75$, $\xi_b = 0$, $\xi_s = 3\%$, coefficient of friction μ as shown in bottom-right subplot, $u_y = 0.25 \text{ mm}$ and various values of supplemental rotational inertia, $\sigma = 0$, $\epsilon(1 - \gamma) = 0.01$, 0.2 and 0.4 when subjected to the C02, N65E ground motion recorded during the 1966 Parkfield, California earthquake. The bottom-right plot offers the equivalent value of the friction coefficient μ as results from equation (4.44) for $\xi_b = 15\%$ (which is the isolation damping used in the approximate model analysis) for every isolation period value; whereas the top-right plot offers the total superstructure accelerations. 61
- 4.9 Left: Peak base u_b^{max} , and superstructure, u_s^{max} displacements of the 2DOF isolated structure shown in Figure 4.1 for a wide range of isolation periods ($1.5 \text{ sec} \leq T_b = 2\pi/\omega_b \leq 3.5 \text{ sec}$) for a constant value $\epsilon = \omega_b^2/\omega_s^2 = 0.04$, $\gamma = m_s/M = 0.75$, $\xi_b = 0$, $\xi_s = 3\%$, coefficient of friction μ as shown in bottom-right subplot, $u_y = 0.25 \text{ mm}$ and various values of supplemental rotational inertia, $\sigma = 0$, $\epsilon(1 - \gamma) = 0.01$, 0.2 and 0.4 when subjected to the Pacoima Dam/164 ground motion recorded during the 1971 San Fernando, California earthquake. The bottom-right plot offers the equivalent value of the friction coefficient μ as results from equation (4.44) for $\xi_b = 15\%$ (which is the isolation damping used in the approximate model analysis) for every isolation period value; whereas the top-right plot offers the total superstructure accelerations at a non-compliant support of the inerter. . . . 62

4.10	Left: Peak base u_b^{max} , and superstructure, u_s^{max} displacements of the 2DOF isolated structure shown in Figure 4.1 for a wide range of isolation periods ($1.5 \text{ sec} \leq T_b = 2\pi/\omega_b \leq 3.5 \text{ sec}$) for a constant value $\epsilon = \omega_b^2/\omega_s^2 = 0.04$, $\gamma = m_s/M = 0.75$, $\xi_b = 0$, $\xi_s = 3\%$, coefficient of friction μ as shown in bottom-right sub-plot, $u_y = 0.25 \text{ mm}$ and various values of supplemental rotational inertia, $\sigma = 0$, $\epsilon(1-\gamma) = 0.01, 0.2$ and 0.4 on a compliant support ($\omega_b/\omega_R = \epsilon/4$) when subjected to the C02, N65E ground motion recorded during the 1966 Parkfield, California earthquake. The bottom-left plot offers the equivalent value of the friction coefficient μ as results from equation (4.44) for $\xi_b = 15\%$ for every isolation period value; whereas the top-right plot offers the total superstructure accelerations.	63
4.11	Left: Peak base u_b^{max} , and superstructure, u_s^{max} displacements of the 2DOF isolated structure shown in Figure 4.1 for a wide range of isolation periods ($1.5 \text{ sec} \leq T_b = 2\pi/\omega_b \leq 3.5 \text{ sec}$) for a constant value $\epsilon = \omega_b^2/\omega_s^2 = 0.04$, $\gamma = m_s/M = 0.75$, $\xi_b = 0$, $\xi_s = 3\%$, coefficient of friction μ as shown in bottom-right sub-plot, $u_y = 0.25 \text{ mm}$ and various values of supplemental rotational inertia, $\sigma = 0$, $\epsilon(1-\gamma) = 0.01, 0.2$ and 0.4 on a compliant support ($\omega_b/\omega_R = \epsilon/4$) when subjected to the Pacoima Dam/164 ground motion recorded during the 1971 San Fernando, California earthquake. The bottom-left plot offers the equivalent value of the friction coefficient μ as results from equation (4.44) for $\xi_b = 15\%$ for every isolation period value; whereas the top-right plot offers the total superstructure accelerations.	64
5.1	(a) SDOF yielding structure engaged with a rotational flywheel system; (b) Bilinear idealization of the inelastic behavior of the yielding SDOF structure; (c) SDOF yielding structure with supplemental damping; (d) 2DOF yielding structure engaged with a flywheel system; (e) Bilinear idealization of the inelastic behavior of each story of the 2DOF yielding structure;(f) 2DOF yielding structure with supplemental damping at its first story.	68
5.2	The Cholame, Array 2/360 acceleration time history recorded during the 2004 Parkfield, California earthquake.	71
5.3	Response spectra of an elastoplastic ($\alpha = 0$) SDOF structure equipped with inerters (heavy solid black lines) or supplemental viscous damping (dashed lines) supported on a stiff frame when excited by the Gilroy Array 6/230 ground motion recorded during the 1979 Coyote Lake earthquake: (a) Single inerter; (b) Pair of clutching inerters. Red lines are for the corresponding elastic structures without (thin red lines) or with (heavier red lines) inerters.	72
5.4	Response spectra of a bilinear ($\alpha = 0.05$) SDOF structure equipped with inerters (heavy solid black lines) or supplemental viscous damping (dashed lines) supported on a stiff frame when excited by the Gilroy Array 6/230 ground motion recorded during the 1979 Coyote Lake earthquake: (a) Single inerter; (b) Pair of clutching inerters. Red lines are for the corresponding elastic structures without (thin red lines) or with (heavier red lines) inerters.	73

5.5	Response spectra of an elastoplastic ($\alpha = 0$) SDOF structure equipped with inerters (heavy solid black lines) or supplemental viscous damping (dashed lines) supported on a stiff frame when excited by the Cholame Number 2/360 ground motion recorded during the 2004 Parkfield California earthquake: (a) Single inerter; (b) Pair of clutching inerters. Red lines are for the corresponding elastic structures without (thin red lines) or with (heavier red lines) inerters.	74
5.6	Response spectra of a bilinear ($\alpha = 0.05$) SDOF structure equipped with inerters (heavy solid black lines) or supplemental viscous damping (dashed lines) supported on a stiff frame when excited by the Cholame Number 2/360 ground motion recorded during the 2004 Parkfield California earthquake: (a) Single inerter; (b) Pair of clutching inerters. Red lines are for the corresponding elastic structures without (thin red lines) or with (heavier red lines) inerters.	75
5.7	Response spectra of a yielding 2DOF structure equipped with inerters (heavy solid lines) or supplemental viscous damping (dashed lines) supported on a stiff frame when excited by the Gilroy Array 6/230 ground motion recorded during the 1979 Coyote Lake earthquake: (a) Single inerter; (b) Pair of clutching inerters.	82
5.8	Response spectra of a yielding 2DOF structure equipped with inerters (heavy solid lines) or supplemental viscous damping (dashed lines) supported on a stiff frame when excited by the Cholame Number 2/360 ground motion recorded during the 2004 Parkfield California earthquake: (a) Single inerter; (b) Pair of clutching inerters.	83
5.9	Response spectra of a yielding 2DOF structure equipped with inerters (heavy solid lines) or supplemental viscous damping (dashed lines) supported on a compliant chevron frame when excited by the Gilroy Array 6/230 ground motion recorded during the 1979 Coyote Lake earthquake: (a) Single inerter; (b) Pair of clutching inerters.	84
5.10	Response spectra of a yielding 2DOF structure equipped with inerters (heavy solid lines) or supplemental viscous damping (dashed lines) supported on a compliant chevron frame when excited by the Cholame Number 2/360 ground motion recorded during the 2004 Parkfield California earthquake: (a) Single inerter; (b) Pair of clutching inerters.	85
6.1	Multi-story structure with supplemental rotational inertia at its first level (left); or at some higher level j without any inerters at the levels below (right).	88
6.2	Three degree-of-freedom (3DOF) structure with supplemental rotational inertia at its 2^{nd} and 3^{rd} floors.	92
6.3	Two-degree-of-freedom (2DOF) structure with inerter installed only at its 2nd level	95

6.4 Comparison of modal frequencies ω_1 and ω_2 of the 2DOF structure as the rotational inertia at the second level increases (additional inertia forces are proportional to the relative acceleration of the second floor) with the modal frequencies of the traditional 2DOF structure (no inerters) by increasing the mass m_2 of the second level (additional inertia D'Alembert forces are proportional to the total acceleration of the second level). 96

1 Introduction

Response modification of civil structures has been traditionally achieved with added stiffness, flexibility damping and strength (Kelly et al. 1972; Skinner et al. 1974; Clough and Penzien 1975; Skinner et al. 1993; Kelly 1997; Soong and Dargush 1997; Constantinou et al. 1998; Makris and Chang 2000a; Whittaker et al. 1991; Black et al. 2003; Symans et al. 2008; Sarlis et al. 2013 and references reported therein). Nevertheless, together with the elastic spring that produces a force proportional to the relative displacement of its end-nodes and the viscous dashpot that produces a force proportional to the relative velocity of its end nodes, the inerter produces a force proportional to the relative acceleration of its end-nodes and emerges as the third elementary mechanical element (in addition to the spring and dashpot) for the synthesis of mechanical networks (Smith 2002; Makris 2017, 2018; Makris and Efthymiou 2020). While a driving spinning top, as the one shown in Figure 1.1 which is a physical realization of the inerter, has been familiar to several generations; inerters were apparently first proposed for the response modification of buildings in the mid-1980s by Kawamata (1986) and subsequently by Ishimaru (1994) and Arakaki et al. (1999a,b) in the mid to late 1990s in Japan.

Following the pioneering work in Japan and the subsequent theoretical and experimental studies by Smith and coworkers (Smith 2002; Papageorgiou and Smith 2005; Papageorgiou et al. 2009;



Figure 1.1: A physical realization of the inerter in which the force output is proportional only to the relative acceleration between nodes 1 and 2.

Chen et al. 2009; Kuznetsov et al. 2011) who established, within the context of linear networks, the analogy of the inerter to the electric capacitor; a growing number of publications have proposed the use of inerters for the response modification of buildings by installing them at all floor levels (Furuhashi and Ishimaru 2008; Ikago et al. 2012a,b; Takewaki et al. 2012); at selected levels (Sugimura et al. 2012; Ogino and Sumiyama 2014; Lazar et al. 2014; Marian and Giaralis 2014; Taflanidis et al. 2019) or at the ground level, either within the context of protecting a first soft-story (Makris and Kampas 2016; Makris and Moghimi 2019; Moghimi and Makris 2021), or within the context of enhancing a seismic isolation system (Saitoh 2007, 2012; De Domenico and Ricciardi 2018b; Ye et al. 2019; Makris and Moghimi 2022).

Supplemental rotational inertia can be achieved either with a rack-and-pinion- flywheel arrangement schematically shown in Figure 1.2, a ball-screw assembly as shown in Figure 1.1 (Arakaki et al. 1999a,b; Papageorgiou and Smith 2005; Hwang et al. 2007; Ikago et al. 2012a; Takewaki et al. 2012; Watanabe et al. 2012; Ishii et al. 2014) or fluid inerters (Swift et al. 2013; Wang et al. 2011; Liu et al. 2018; De Domenico et al. 2019). The mechanical system shown in Figure 1.2 is a mechanical analogue of the electrical capacitor in a force-current/velocity-voltage analogy between mechanical and electrical networks. This missing analogy was first recognized by Smith (2002) who coined the term inerter for any mechanical arrangement where the output force is proportional only to the relative acceleration between its end-nodes. The constant of proportionality of the inerter is coined the inertance = M_R (Smith 2002) and has units of mass [M]. Accordingly, if F_1 , u_1 and F_2 , u_2 are the forces and displacements at the end-nodes of the inerter with inertance, M_R , its constitutive relation is (Saitoh 2007; Makris 2018; Makris and Moghimi 2019)

$$\begin{Bmatrix} F_1(t) \\ F_2(t) \end{Bmatrix} = \begin{bmatrix} M_R & -M_R \\ -M_R & M_R \end{bmatrix} \begin{Bmatrix} \ddot{u}_1(t) \\ \ddot{u}_2(t) \end{Bmatrix} \quad (1.1)$$

The basic frequency and time-response functions of the mechanical element defined by equation (1.1) have been derived by Makris (2017, 2018) and are summarized in Chapter 2 together with

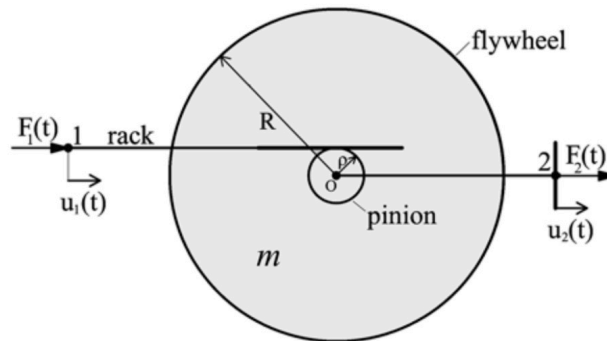


Figure 1.2: A rack-and-pinion-flywheel realization of the inerter, which is the mechanical analogue of the capacitor in a force–current/velocity–voltage analogy.

those of simple inertoelastic and inertoviscous elements. The unique characteristic of the inerter is that it has an appreciable inertia mass as opposed to a small gravitational mass.

The potential unfavorable situation when the rotational inertia stored in the inerter may drive the structure was first recognized by Makris and Kampas (2016) who introduced the implementation of two parallel inerters together with the use of a clutch (pair of clutching inerters), so that the rotating flywheels only resist the motion of the structure without inducing any deformations. The benefits of using a pair of counter-rotating clutching inerters were subsequently examined on a 2DOF elastic structure (Makris and Moghimi 2019). About the same time, De Domenico and Ricciardi (2018b) examined the response of a multi-degree-of-freedom seismic isolated elastic structure where the isolation system was enhanced with a tuned mass damper inerter. In that study the nonlinear behavior of the isolator is accounted for, and subsequently, the study proceeds with a stochastic linearization technique.

A seminal contribution among the aforementioned studies is the work of Furuhashi and Ishimaru (2008) who showed that when inerters are installed without being interrupted, starting from the first level, then the inertance of the inerters can be adjusted to eliminate the participation of higher modes. At the same time, the unique ability of the inerters to eliminate the contribution of higher modes vanishes when they are placed at a higher level without having inerters at all the floors down below to the first level. Following Furuhashi and Ishimaru's (2008) seminal contribution, Takewaki et al. (2012) explained that for inerters to suppress the induced ground acceleration they need to be installed without being interrupted, starting from the ground level; otherwise, the inerters which are installed above the "interrupted" level can no-longer suppress the ground induced acceleration. In spite of Takewaki et al. (2012) important finding—that solitary inerters when placed at higher levels do not suppress the ground induced acceleration, several subsequent publications investigated the response of structures equipped with a solitary inerter at a floor level other than the first level (Sugimura et al. 2012; Ogino and Sumiyama 2014; Lazar et al. 2014; Marian and Giaralis 2014; Taflanidis et al. 2019) within the context of proposing an enhanced tuned mass damper. Soon after Takewaki et al. (2012) publication, Lazar et al. (2014) examined in detail the role of a tuned inerter damper (TID)—which is essentially an inerter supported on a compliant support (a spring-dashpot parallel connection), as an alternative tuned mass damper (TMD) and they correctly concluded that the TID is more effective when placed at the ground level, reaffirming the findings of Takewaki et al. (2012).

In view of the appreciable number of publications that examine the response of tall buildings when equipped at a higher level with a solitary mechanical network that involves inerters (Marian and Giaralis 2014; Giaralis and Taflanidis 2018; Taflanidis et al. 2019), in association that this concept has enjoyed full-scale implementations (Sugimura et al. 2012; Ogino and Sumiyama 2014), this report reviews, the dynamics of structures equipped with inerters and how inerters modify elastic and inelastic structural response.

1.1 SUPPRESSION OF THE INDUCED GROUND ACCELERATION

Figure 1.3 depicts a single-degree-of-freedom undamped structure with stiffness k and mass m . A stiff chevron frame supports a flywheel with radius R and mass m_W that can rotate about an

axis O. In the interest of simplicity, we consider the case of a non-compliant chevron frame whose deformation is negligible to the translational displacement, $u(t)$, of the SDOF structure. The case of a compliant chevron frame has been examined in depth in past publications (Makris and Kampas 2016; Makris and Moghimi 2019; Moghimi and Makris 2021). Concentric to the flywheel, there is an attached pinion with radius ρ engaged to a linear rack connected to the bottom of the vibrating mass m of the SDOF. With this arrangement when the mass m undergoes a positive displacement, $u(t)$, the flywheel is subjected to a clockwise rotation, $\theta(t)$. Given that there is no slipping between the rack and the pinion, $u(t) = \rho\theta(t)$, the internal force $F_I(t)$ that develops along the rack-pinion interface satisfies dynamic moment equilibrium

$$F_I(t)\rho = I_W\ddot{\theta}(t) \quad (1.2)$$

where $I_W(t) = (1/2)m_W R^2 =$ moment of inertia of the flywheel about point O. With reference to Figure 1.3, for a positive displacement, $u(t)$, to the right, the internal force, $F_I(t)$ given by equation (1.2) opposes the motion of the mass, m (to the left). Accordingly, dynamic equilibrium of the vibrating mass when subjected to a ground acceleration, \ddot{u}_g , gives (Makris and Kampas 2016)

$$\ddot{u}(t) + \frac{\omega_0}{1 + \frac{1}{2}\frac{m_W R^2}{m \rho^2}} u(t) = -\frac{1}{1 + \frac{1}{2}\frac{m_W R^2}{m \rho^2}} \ddot{u}_g(t) \quad (1.3)$$

where $\omega_0 = \sqrt{k/m}$ = natural frequency of the structure when the pinion-flywheel is disengaged and m_W is the mass of the flywheel.

Equation (1.3) indicates that the engagement of the flywheel lengthens the vibration period of the structure (Chen et al. 2014); yet, most importantly, it suppresses the level of ground shaking given that the denominator in the right-hand side is always larger than unity (Makris and Kampas 2016). The quantity $M_R = (1/2)M_W(R^2/\rho^2)$ is defined as the inertance of the inerter with units of mass $[M]$, whereas the ratio $\sigma = M_R/m$ appearing in the denominators of equation (1.3) is the inertance ratio.

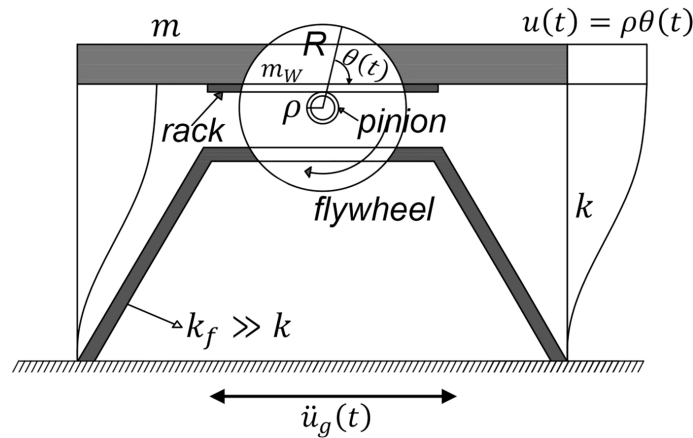


Figure 1.3: Single-degree-of-freedom structure with mass m and stiffness k with supplemental rotational inertia from a flywheel with radius R supported on a chevron frame with stiffness k_f that is much larger than k .

2 Basic Response Functions of Simple Inertoelastic and Inertoviscous Models

Given that the inerter emerges as the third elementary mechanical element for the synthesis of mechanical networks (Smith 2002; Makris 2017, 2018; Makris and Efthymiou 2020), in this chapter we derive the basic frequency- and time-response functions of the inerter and these of the two-parameter inertoelastic and inertoviscous mechanical networks.

When a mechanical network with a fixed end-node (one terminal fixed), consists of springs, dashpots and inerters, the constitutive equation of the mechanical network is of the form

$$\left[\sum_{m=0}^M a_m \frac{d^m}{dt^m} \right] F(t) = \left[\sum_{n=0}^N b_n \frac{d^n}{dt^n} \right] u(t) \quad (2.1)$$

where $F(t)$ and $u(t)$ are the force and displacement acting on the end-node that is free to move. In equation (2.1) the coefficients a_m and b_n are restricted to real numbers and the order of differentiation m and n is restricted to integers. The linearity of equation (2.1) permits its transformation in the frequency domain by applying the Fourier transform

$$F(\omega) = [K_1(\omega) + iK_2(\omega)] u(\omega) \quad (2.2)$$

where $F(\omega) = \int_{-\infty}^{\infty} F(t) e^{-i\omega t} dt$ and $u(\omega) = \int_{-\infty}^{\infty} u(t) e^{-i\omega t} dt$ are the Fourier transforms of the force and displacement histories respectively; and $K(\omega) = K_1(\omega) + iK_2(\omega)$ is the dynamic stiffness of the model

$$K(\omega) = \frac{F(\omega)}{u(\omega)} = K_1(\omega) + iK_2(\omega) = \frac{\left[\sum_{n=0}^N b_n (i\omega)^n \right]}{\left[\sum_{m=0}^M a_m (i\omega)^m \right]} \quad (2.3)$$

The dynamic stiffness, $K(\omega)$, expressed by equation (2.3), is a transfer function that relates a displacement input to a force output and is the ratio of two polynomials where the numerator is of degree n and the denominator of degree m . Accordingly, $K(\omega)$ has m poles and n zeros. A transfer function that has more poles than zeros ($m > n$) is called “strictly proper” and results in a “strictly causal” time-response function. A strictly proper transfer function means that the output of the model is finite and follows the input modulations.

The force output $F(t)$ in equation (2.1) can be computed in the time domain with the convolution integral

$$F(t) = \int_{-\infty}^t q(t - \tau) u(\tau) d\tau \quad (2.4)$$

where $q(t)$ is the “memory function” of the model defined as the resulting force at present time t due to an impulsive displacement input at time τ ($\tau < t$); and is the inverse Fourier transform of the dynamic stiffness

$$q(t) = \frac{1}{2\pi} \int_{-\infty}^{\infty} K(\omega) e^{i\omega t} d\omega \quad (2.5)$$

The notation $q(t)$ used for the memory function is the same as the notation used by Veletsos and Verbic (1974). The inverse Fourier transform given by equation (2.5) converges only when $\int_{-\infty}^{\infty} |K(\omega)| d\omega < \infty$; therefore, $q(t)$ exists in the classical sense only when $K(\omega)$ is a strictly proper transfer function ($m > n$). When the number of poles is equal to the number of zeros ($m = n$), the transfer function of the model is “simply proper” and results to a time-response function, $q(t)$, that has a singularity at the time origin because of the finite limiting value of the associated transfer function at high frequencies. This means that the model instantaneously produces an output at a given input.

The inverse of the dynamic stiffness is the dynamic flexibility

$$H(\omega) = H_1(\omega) + iH_2(\omega) = \frac{1}{K_1(\omega) + iK_2(\omega)} \quad (2.6)$$

which is the transfer function that relates a force input to a displacement output. From equations (2.3) and (2.6) it is clear that when a mechanical network has a strictly proper dynamic flexibility it has an improper dynamic stiffness and vice versa. Consequently, when the causality of a proposed mechanical model (network) is a concern, it is most important to specify what is the input and what is the output. When the dynamic flexibility $H(\omega)$ is a proper transfer function, the displacement, $u(t)$, in equation (2.1) can be computed in the time domain via the convolution integral

$$u(t) = \int_{-\infty}^t h(t - \tau) F(\tau) d\tau \quad (2.7)$$

where $h(t)$ is the “impulse response function” defined as the resulting displacement at time t for an impulsive force input at time τ ($\tau < t$) and is the inverse Fourier transform of the dynamic flexibility

$$h(t) = \frac{1}{2\pi} \int_{-\infty}^{\infty} H(\omega) e^{i\omega t} d\omega \quad (2.8)$$

The notation $h(t)$ for the impulse response function used by Veletsos and Verbic (1974) and Clough and Penzien (1975) is adopted in this study.

An equally useful transfer function of a phenomenological model is the impedance, $Z(\omega) = Z_1(\omega) + iZ_2(\omega)$; which relates a velocity input to a force output

$$F(\omega) = [Z_1(\omega) + iZ_2(\omega)] v(\omega) \quad (2.9)$$

where $v(\omega) = i\omega u(\omega)$ is the Fourier transform of the velocity time history. For the linear inerto-viscoelastic model given by equation (2.1), the impedance of the model is

$$Z(\omega) = Z_1(\omega) + iZ_2(\omega) = \frac{\left[\sum_{n=0}^N b_n (i\omega)^n \right]}{\left[\sum_{m=0}^M a_m (i\omega)^{m+1} \right]} \quad (2.10)$$

The force output $F(t)$ appearing in equation (2.1) can be computed in the time domain with an alternative convolution integral

$$F(t) = \int_{-\infty}^t k(t-\tau) \dot{u}(\tau) d\tau \quad (2.11)$$

where k is the relaxation stiffness of the model (Ferry 1980; Giesekus 1995; Tschoegl 2012) defined as the resulting force at the present time, t , due to a unit step displacement input at time τ ($\tau < t$) and is the inverse Fourier transform of the impedance

$$k(t) = \frac{1}{2\pi} \int_{-\infty}^{\infty} Z(\omega) e^{i\omega t} d\omega \quad (2.12)$$

Equation (2.12) indicates that if the dynamic stiffness of a phenomenological model is a simple proper transfer function, then the impedance is a strictly proper transfer function; therefore, the relaxation stiffness, $k(t)$, of the model is finite; whereas, the memory function, $q(t)$, has a singularity at the time origin. The inverse of the impedance is called in structural mechanics ‘‘mobility’’; while, in the electrical engineering literature the term ‘‘admittance’’ is used (Bode et al. 1945; Smith 2002).

$$Y(\omega) = Y_1(\omega) + iY_2(\omega) = \frac{1}{Z_1(\omega) + iZ_2(\omega)} \quad (2.13)$$

The mobility (admittance) is a transfer function that relates a force input to a velocity output. When the mobility is a proper transfer function, the velocity history of the node that is free to move can be computed in the time domain via the convolution

$$v(t) = \int_{-\infty}^t y(t-\tau) F(\tau) d\tau \quad (2.14)$$

where $y(t)$ is the ‘‘impulse velocity response function’’ defined as the resulting velocity at time t for an impulsive force input at time τ ($\tau < t$) and is the inverse Fourier transform of the mobility (admittance).

$$y(t) = \frac{1}{2\pi} \int_{-\infty}^{\infty} Y(\omega) e^{i\omega t} d\omega \quad (2.15)$$

At negative times ($t < 0$), all four time-response functions given by equations (2.5), (2.8), (2.12) and (2.15) need to be zero in order for the phenomenological model (mechanical network) to be causal. The requirement for a time-response function to be causal in the time domain implies that its corresponding frequency response function, $Z(\omega) = Z_1(\omega) + iZ_2(\omega)$, is analytic on the bottom-half complex plane (Bendat and Piersol 1986; Papoulis 1987; Makris 1997a,b, 2020a). The analyticity condition on a complex function, $Z(\omega) = Z_1(\omega) + iZ_2(\omega)$, relates the real part $Z_1(\omega)$ and the imaginary part $Z_2(\omega)$ with the Hilbert transform (Morse and Feshbach 1953; Papoulis 1987).

$$Z_1(\omega) = -\frac{1}{\pi} \int_{-\infty}^{\infty} \frac{Z_2(x)}{x-\omega} dx, \quad Z_2(\omega) = \frac{1}{\pi} \int_{-\infty}^{\infty} \frac{Z_1(x)}{x-\omega} dx \quad (2.16)$$

2.1 BASIC RESPONSE FUNCTIONS OF THE LINEAR SPRING

For the linear elastic spring with spring-constant k , equation (2.1) reduces to

$$F(t) = ku(t) \quad (2.17)$$

therefore, its dynamic stiffness $k(\omega) = k$ and its dynamic flexibility $H(\omega) = 1/k$ are real-valued constants. Accordingly, both these transfer functions are simply proper ($m = n = 0$); and their corresponding time response functions exhibit a singularity at the time origin:

$$q(t) = k\delta(t - 0) \quad (2.18)$$

and

$$h(t) = \frac{1}{k}\delta(t - 0) \quad (2.19)$$

where $\delta(t - 0)$ is the Dirac delta function at the time origin (Lighthill 1958; Papoulis 1987).

The Fourier transform of equation (2.17) is merely $F(\omega) = ku(\omega)$ and by using that $v(\omega) = i\omega u(\omega)$, the impedance of the linear spring as defined by equation (2.9) assumes the form

$$Z(\omega) = \frac{k}{i\omega} = -ki\frac{1}{\omega} \quad (2.20)$$

The inverse Fourier transform of $-i/\omega$ is $(1/2)sgn(t)$ (Morse and Feshbach 1953); where, $sgn(t)$, is the signum function. Accordingly, by using the expression of the impedance of the linear spring as given by equation (2.20), the resulting relaxation stiffness as defined by equation (2.12) is $k(t) = (k/2)sgn(t)$; which is clearly a non-causal function. In fact the signum function, $sgn(t)$, indicates that there is as much response before the induced step displacement as the response upon the excitation is induced. 1/4 century ago, Makris (1997a) resolved this impasse by extending the relation between the analyticity of a transfer function and the causality of the corresponding time-response function to the case where generalized functions are involved. Given that the Hilbert pair of the reciprocal function $1/\omega$ is $-\pi\delta(\omega - 0)$, Makris (1997a) explained that a Dirac delta function needs to be appended as a real part in equation (2.21) and the correct expression of the impedance of the linear spring is

$$Z(\omega) = k \left[\pi\delta(\omega - 0) - i\frac{1}{\omega} \right] \quad (2.21)$$

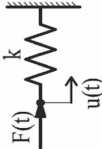
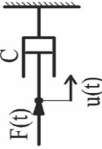
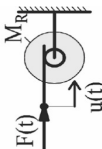
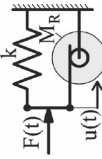
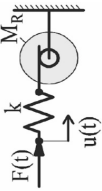
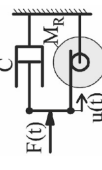
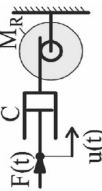
By “manually” appending the real part, $\pi\delta(\omega - 0)$, in equation (2.20), the Fourier transform of the correct impedance of the linear spring given by equation (2.21) gives

$$k(t) = \frac{1}{2\pi} \int_{-\infty}^{\infty} Z(\omega) e^{i\omega t} d\omega = \frac{k}{2\pi} \int_{-\infty}^{\infty} \left[\pi\delta(\omega - 0) - i\frac{1}{\omega} \right] e^{i\omega t} d\omega \quad (2.22)$$

By recalling that the Fourier transform of $-i/\omega$ is $(1/2)sgn(t)$, equation (2.21), gives

$$k(t) = k \left[\frac{1}{2} \int_{-\infty}^{\infty} \delta(\omega - 0) e^{i\omega t} d\omega + \frac{1}{2}sgn(t) \right] = k \left[\frac{1}{2} + \frac{1}{2}sgn(t) \right] = kU(t - 0) \quad (2.23)$$

Table 2.1: Basic frequency-response functions and their corresponding causal time-response functions of elementary inertioelastic and inertioviscous models.

	Elastic Spring	Viscous Dashpot	Inertner	Inertioelastic Solid	Inertioelastic Fluid	Inertioviscous in Parallel the Rotational Inertia Damper	Inertioviscous in Series
Constitutive Equation	 $F(t) = ku(t)$	 $F(t) = C \frac{du(t)}{dt}$	 $F(t) = M_R \frac{d^2u(t)}{dt^2}$	 $F(t) = ku(t) + M_R \frac{d^2u(t)}{dt^2}$	 $F(t) + \frac{1}{\omega^2} \frac{d^2F(t)}{dt^2} = M_R \frac{d^2u(t)}{dt^2}$	 $F(t) = C \frac{du(t)}{dt} + M_R \frac{d^2u(t)}{dt^2}$	 $F(t) + \frac{M_R}{C} \frac{dF(t)}{dt} = M_R \frac{d^2u(t)}{dt^2}$
Dynamic Stiffness	$k + i0$	$0 + i\omega C$	$-\omega^2 M_R + i0$	$K - M_R \omega^2 = -M_R(\omega^2 - \omega_R^2)$	$k + \frac{k\omega_R}{2} [\frac{2\omega_R}{\omega^2 - \omega_R^2} + i\pi(\delta(\omega - \omega_R) - \delta(\omega + \omega_R))]$	$-\omega^2 M_R + i\omega C$	$-M_R \frac{\omega^2}{1 + i\omega \frac{M_R}{C}}$
Dynamic Flexibility	$\frac{1}{k} + i0$	$\frac{1}{C} [\pi\delta(\omega - 0) - i\frac{1}{\omega}]$	$\frac{1}{M_R} [\frac{1}{\omega^2} + i\pi \frac{d\delta(\omega - 0)}{d\omega}]$	$\frac{1}{2M_R\omega_R} [\frac{2\omega_R}{\omega^2 - \omega_R^2} + i\pi(\delta(\omega + \omega_R) - \delta(\omega - \omega_R))]$	$\frac{1}{k} + \frac{1}{M_R} [\frac{1}{\omega^2} + i\pi \frac{d\delta(\omega - 0)}{d\omega}]$	$\frac{1}{C} [\pi\delta(\omega - 0) - i\frac{1}{\omega}] - \frac{M_R}{C} \frac{1}{1 + i\omega \frac{M_R}{C}}$	$\frac{1}{C} [\pi\delta(\omega - 0) - i\frac{1}{\omega}]$
Impedance	$k[\pi\delta(\omega - 0) - i\frac{1}{\omega}]$	$C + i0$	$0 + i\omega M_R$	$k[\pi\delta(\omega - 0) - i\frac{1}{\omega}] + i\omega M_R$	$\frac{k}{2} [\pi\delta(\omega - \omega_R) + \pi\delta(\omega + \omega_R) - 2i\frac{\omega_R}{\omega^2 - \omega_R^2}]$	$C + i\omega M_R$	$M_R \frac{i\omega}{1 + i\omega \frac{M_R}{C}}$
Mobility or Admittance	$i\omega \frac{1}{k}$	$\frac{1}{C} + i0$	$\frac{1}{M_R} [\pi\delta(\omega - 0) - i\frac{1}{\omega}]$	$\frac{1}{2M_R} [\pi\delta(\omega - \omega_R) + \pi\delta(\omega + \omega_R) - 2i\frac{\omega_R}{\omega^2 - \omega_R^2}]$	$\frac{1}{k} i\omega + \frac{1}{M_R} [\pi\delta(\omega - 0) - i\frac{1}{\omega}]$	$\frac{1}{C} + \frac{1}{M_R} \frac{1}{1 + i\omega \frac{M_R}{C}}$	$\frac{1}{C} + \frac{1}{M_R} [\pi\delta(\omega - 0) - i\frac{1}{\omega}]$
Memory Function	$k\delta(t - 0)$	$C \frac{d\delta(t - 0)}{dt}$	$M_R \frac{d^2\delta(t - 0)}{dt^2}$	$k\delta(t - 0) + M_R \frac{d^2\delta(t - 0)}{dt^2}$	$k[\delta(t - 0) - \omega_R U(t - 0) \sin(\omega_R t)]$	$C \frac{d\delta(t - 0)}{dt} + M_R \frac{d^2\delta(t - 0)}{dt^2}$	$C [\frac{d\delta(t - 0)}{dt} - \frac{C}{M_R} \delta(t - 0) + (\frac{C}{M_R})^2 e^{-\frac{C}{M_R} t}]$
Impulse Response Function	$\frac{1}{k} \delta(t - 0)$	$\frac{1}{C} U(t - 0)$	$\frac{1}{M_R} U(t - 0) t$	$\frac{1}{M_R \omega_R} \frac{U(t - 0) \sin(\omega_R t)}{0}$	$\frac{1}{k} \delta(t - 0) + \frac{1}{M_R} U(t - 0) t$	$\frac{1}{C} [U(t - 0) - e^{-\frac{C}{M_R} t}]$	$C [1 + \frac{C}{M_R} t] U(t - 0)$
Relaxation Stiffness	$kU(t - 0)$	$C\delta(t - 0)$	$M_R \frac{d\delta(t - 0)}{dt}$	$kU(t - 0) + M_R \frac{d\delta(t - 0)}{dt}$	$kU(t - 0) \cos(\omega_R t)$	$C\delta(t - 0) + M_R \frac{d\delta(t - 0)}{dt}$	$C [\frac{\delta(t - 0)}{C} - \frac{M_R}{C} e^{-\frac{C}{M_R} t}]$
Impulse Velocity Response Function	$\frac{1}{k} \frac{d\delta(t - 0)}{dt}$	$\frac{1}{C} \delta(t - 0)$	$\frac{1}{M_R} U(t - 0)$	$\frac{1}{M_R} U(t - 0) \cos(\omega_R t) t$	$\frac{1}{k} \frac{d\delta(t - 0)}{dt} + \frac{1}{M_R} U(t - 0)$	$\frac{1}{M_R} e^{-\frac{C}{M_R} t}$	$\frac{1}{C} \delta(t - 0) + \frac{1}{M_R} U(t - 0)$

where $U(t - 0)$ is the Heaviside unit-step function at the time origin; and therefore, the relaxation stiffness, $k(t) = kU(t - 0)$, is causal. The notation $U(t - 0)$ for the Heaviside unit-step function used by Papoulis (1987) is adopted in this study.

The mobility (admittance) of the linear spring is the inverse of its impedance,

$$Y(\omega) = i\frac{\omega}{k} \quad (2.24)$$

and is an improper transfer function. Accordingly, its inverse Fourier transform, that is the impulse velocity response function $y(t)$, as defined by equation (2.15) does not exist in the classical sense. Nevertheless, it can be constructed mathematically with the calculus of generalized functions and more specifically with the property of the derivative of the Dirac delta function (Lighthill 1958)

$$\int_{-\infty}^{\infty} \frac{d\delta(t-0)}{dt} f(t) dt = - \int_{-\infty}^{\infty} \delta(t-0) \frac{df(t)}{dt} dt = -\frac{df(0)}{dt} \quad (2.25)$$

By employing equation (2.25), the Fourier transform of $d\delta(t-0)/dt$ is

$$\int_{-\infty}^{\infty} \frac{d\delta(t-0)}{dt} e^{-i\omega t} dt = - \int_{-\infty}^{\infty} \delta(t-0) (-i\omega) e^{-i\omega t} dt = i\omega \quad (2.26)$$

Consequently, based on equation (2.26), the inverse Fourier transform of the mobility given by equation (2.24) is

$$y(t) = \frac{1}{k} \frac{d\delta(t-0)}{dt} \quad (2.27)$$

Equation (2.27) shows that the impulse velocity response function of the linear spring exhibits a strong singularity at the time origin given that its mobility increases linearly with frequency. Table 2.1 summarizes the basic frequency and time-response functions of the linear spring computed in this section. In the interest of completeness, next to these functions, Table 2.1 summarizes the corresponding functions of the linear dashpot which have been computed by following the same reasoning (Makris 1997a; Makris and Kampas 2009).

2.2 BASIC RESPONSE FUNCTIONS OF THE INERTER

With reference to Figure 1.1, when node 2 is fixed ($u_2 = 0$), equation (2.1) reduces to

$$F(t) = M_R \frac{d^2 u(t)}{dt^2} \quad (2.28)$$

The Fourier transform of equation (2.29) is

$$F(\omega) = -M_R \omega^2 u(\omega) \quad (2.29)$$

therefore, the dynamic stiffness of the inerter, $k(\omega) = -M_R \omega^2$, is improper to the second degree. Accordingly, the memory function $q(t)$, as defined by equation (2.9) does not exist in the classical sense. The reader needs to recall that $q(t)$ is the resulting force due to an induced impulsive

displacement. Clearly an impulsive displacement is not physically realizable on the inerter given that it is not possible to rotate instantaneously a flywheel with finite rotational inertia—the only thing that may be achieved is to buckle the supports of the flywheel or to fail the gears along the rack-pinion interface. Nevertheless, a mathematical expression for $q(t)$ can be reached by using the properties of the higher-order derivatives of the Dirac delta function (Lighthill 1958),

$$\int_{-\infty}^{\infty} \frac{d^n \delta(t-0)}{dt^n} f(t) dt = (-1)^n \frac{d^n f(0)}{dt^n} \quad (2.30)$$

By employing equation (2.30), the Fourier transform of $d^2\delta(t-0)/dt^2$ is

$$\int_{-\infty}^{\infty} \frac{d^2 \delta(t-0)}{dt^2} e^{-i\omega t} dt = (-1)^2 (-i\omega)^2 = -\omega^2 \quad (2.31)$$

Consequently, based on equation (2.31), the inverse Fourier transform of the dynamic stiffness of the inerter, $k(\omega) = -M_R\omega^2$, is

$$q(t) = M_R \frac{d^2 \delta(t-0)}{dt^2} \quad (2.32)$$

Equation (2.32) shows that the memory function of the inerter exhibits a strong singularity at the time origin given that its dynamic stiffness increases quadratically with frequency.

While the dynamic stiffness of the inerter, $k(\omega) = -M_R\omega^2$, is an improper transfer function, its inverse, that is the dynamic flexibility as defined by equation (2.6) is a proper transfer function

$$H(\omega) = -\frac{1}{M_R\omega^2} \quad (2.33)$$

Nevertheless, while the dynamic flexibility of the inerter as expressed by equation (2.33) is a proper transfer function, the inverse Fourier transform of $-1/\omega^2$ is $(t/2)\text{sgn}(t)$, where $\text{sgn}(t)$ is the signum function. Accordingly, the expression given by equation (2.33) faces similar challenges as those faced by the expression of the impedance of the linear spring given by equation (2.20), since the appearance of the signum function alone renders the corresponding time-response function, $h(t)$, non-causal. Given that the dynamic flexibility of the inerter, as expressed by equation (2.33), is a purely real quantity, we are in search of the imaginary Hilbert pair of $-1/\omega^2$.

The Hilbert pair of $-1/\omega^2$ is constructed by employing the first of equations (2.16), together with the help of (2.25) By letting $H_2(\omega) = \pi \frac{d\delta(\omega-0)}{d\omega}$, its Hilbert transform gives:

$$H_1(\omega) = -\frac{1}{\pi} \int_{-\infty}^{\infty} \pi \frac{d\delta(x-0)}{dx} \frac{1}{x-\omega} dx \quad (2.34)$$

and with the change of variables $\xi = x - \omega$, $d\xi = dx$, equation (2.34) becomes

$$H_1(\omega) = \int_{-\infty}^{\infty} \frac{d\delta(\xi - (-\omega))}{d\xi} \frac{1}{\xi} d\xi = \int_{-\infty}^{\infty} \delta(\xi - (-\omega)) \left(-\frac{1}{\xi^2}\right) d\xi = -\frac{1}{\omega^2} \quad (2.35)$$

The result of equation (2.35) indicates that the right-hand side of (2.33) cannot stand alone and has to be accompanied by its imaginary Hilbert pair, $\pi d\delta(\omega-0)/d\omega$. Consequently, the correct expression of the dynamic flexibility of the inerter is

$$H(\omega) = \frac{1}{M_R} \left[-\frac{1}{\omega^2} + i\pi \frac{d\delta(\omega-0)}{d\omega} \right] \quad (2.36)$$

By comparing Equations (2.21) and (2.36), the reader recognizes that the stronger is the singularity of the frequency term ($1/\omega$ or $1/\omega^2$), the stronger is the singularity of its Hilbert companion ($\pi\delta(\omega - 0)$ or $\pi d\delta(\omega - 0)/d\omega$). By “manually” appending the imaginary part, $\pi d\delta(\omega - 0)/d\omega$, in equation (2.33), the inverse Fourier transform of the correct dynamic flexibility of the inerter given by Equation (2.36) gives

$$h(t) = \frac{1}{2\pi} \int_{-\infty}^{\infty} H(\omega) e^{i\omega t} d\omega = \frac{1}{M_R} \frac{1}{2\pi} \int_{-\infty}^{\infty} \left[-\frac{1}{\omega^2} + i\pi \frac{d\delta(\omega - 0)}{d\omega} \right] e^{i\omega t} d\omega \quad (2.37)$$

By recalling that the Fourier transform of $-1/\omega^2$ is $(t/2)sgn(t)$, equation (2.37) gives

$$h(t) = \frac{1}{M_R} \left[\frac{t}{2} sgn(t) + \frac{i}{2} \int_{-\infty}^{\infty} \frac{d\delta(\omega - 0)}{d\omega} e^{i\omega t} d\omega \right] \quad (2.38)$$

and after employing equation (2.25), the second term in the right-hand-side of equation (2.38) gives

$$\frac{i}{2} \int_{-\infty}^{\infty} \frac{d\delta(\omega - 0)}{d\omega} e^{i\omega t} d\omega = -\frac{i}{2} \int_{-\infty}^{\infty} \delta(\omega - 0) ite^{i\omega t} d\omega = \frac{t}{2} \quad (2.39)$$

Substitution of the result of equation (2.39) into equation (2.38)), gives the causal expression for the impulse response function of the inerter

$$h(t) = \frac{1}{M_R} \left[\frac{t}{2} sgn(t) + \frac{t}{2} \right] = \frac{1}{M_R} U(t - 0) t \quad (2.40)$$

where $U(t - 0)$ is again the Heaviside unit-step function at the time origin. Equation (2.40)) indicates that an impulse force on the inerter creates a causal response that grows linearly with time and is inverse proportional to the inertance, M_R .

The impedance of the inerter derives directly from equation (2.28)) by using that $v(\omega) = i\omega u(\omega)$; therefore, it is given by

$$Z(\omega) = i\omega M_R \quad (2.41)$$

which is an improper transfer function and is of the same form as the mobility (admittance) of the linear spring given by equation (2.24)). By following the same operations described by equation (2.26)), the inverse Fourier transform of the impedance of the inerter is

$$k(t) = M_R \frac{d\delta(t - 0)}{dt} \quad (2.42)$$

Equation (2.42)) indicates that the relaxation stiffness of the inerter exhibits a strong singularity (not as strong as the memory function, $q(t)$) at the time origin given that it is not physically realizable to impose a step displacement to the inerter.

The mobility (admittance) of the inerter is the inverse of its impedance given by equation (2.41))

$$Y(\omega) = \frac{1}{M_R i\omega} = -\frac{1}{M_R} i \frac{1}{\omega} \quad (2.43)$$

The mobility of the inerter given by equation (2.43)), while a strictly proper transfer function, faces the same challenges as the impedance of the linear spring given by equation (2.20)); since

the inverse Fourier transform of $-i/\omega$ is $(1/2)sgn(t)$ —a non-causal function. By following the same reasoning described to construct the correct impedance of the linear spring given by equation (2.21)), a Dirac delta function is appended as a real part in equation (2.43)), and the correct expression of mobility of the inerter is

$$Y(\omega) = \frac{1}{M_R} \left[\pi\delta(\omega - 0) - i\frac{1}{\omega} \right] \quad (2.44)$$

By “manually” appending the real part, $\pi\delta(\omega - 0)$, in equation (2.43)), the inverse Fourier transform of the correct mobility of the inerter given by equation (2.44)) is

$$y(t) = \frac{1}{M_R} \left[\frac{1}{2} + \frac{1}{2} sgn(t) \right] = \frac{1}{M_R} U(t - 0) \quad (2.45)$$

which is a causal function since $U(t - 0)$ is the Heaviside unit-step function at the time origin.

The eight basic response functions of the inerter computed in this section are summarized in Table 2.1 next to the basic response functions of the linear spring and the viscous dashpot.

2.3 BASIC RESPONSE FUNCTIONS OF THE TWO-PARAMETER INERTOELASTIC “SOLID”

Upon we have derived and established the correct basic frequency-response functions of the linear spring and the inerter that result to the corresponding causal time-response functions, we now proceed with the derivation of the basic time-response functions of the two-parameter inertoelastic “solid” element—that is a spring and an inerter connected in parallel as shown in Figure 2.1(left). The term “solid” is used to express that this network sustains a finite displacement under a static load. The constitutive equation of the mechanical network shown in Figure 2.1(left) is

$$F(t) = ku(t) + M_R \frac{d^2u(t)}{dt^2} \quad (2.46)$$

and its Fourier transform gives

$$F(\omega) = [k - M_R\omega^2] u(\omega) \quad (2.47)$$

Equation (2.47)) indicates that the dynamic stiffness, $K(\omega) = k - M_R\omega^2$ of the inertoelastic solid element is improper to the second degree because of the inerter that is connected in parallel with the elastic spring. Clearly, given this parallel arrangement, the memory function, $q(t)$, of the inertoelastic solid element is the summation of the memory functions of the elastic spring given by equation (2.18)) and that of the inerter given by equation (2.32))

$$q(t) = k\delta(t - 0) + M_R \frac{d^2\delta(t - 0)}{dt^2} \quad (2.48)$$

Equation (2.48)) shows that the memory function (inverse Fourier transform of the dynamic stiffness) of the inertoelastic solid element exhibits a strong singularity (second order) at the time origin because of the inerter ($d^2\delta(t - 0)/dt^2$) and a weak singularity ($\delta(t - 0)$) because of the linear

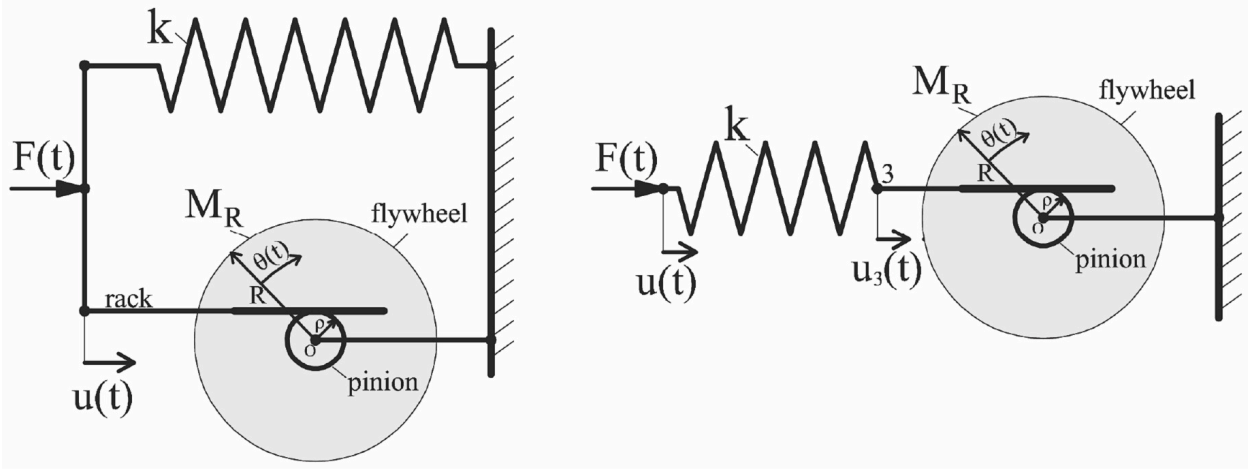


Figure 2.1: Left: The two-parameter inertoelastic “solid”. Right: The two-parameter inertoelastic “fluid”.

spring. While the dynamic stiffness of the two-parameter inertoelastic solid, $k(\omega) = k - M_R\omega^2 = M_R[\omega_R^2 - \omega^2]$ is an improper transfer function, its inverse, that is the dynamic flexibility is a proper transfer function,

$$H(\omega) = -\frac{1}{M_R(\omega^2 - \omega_R^2)} \quad (2.49)$$

in which $\omega_R^2 = k/M_R$, is the natural frequency of the systems shown in Figure 2.1. The poles of the dynamic flexibility given by equation (2.49) are $\omega = \pm\omega_R$; and partial fraction expansion gives

$$H(\omega) = -\frac{1}{2M_R\omega_R} \left[\frac{1}{\omega - \omega_R} - \frac{1}{\omega + \omega_R} \right] \quad (2.50)$$

The transfer function given by equation (2.50) is a purely real quantity with singularities at $\omega = \omega_R$ and $\omega = -\omega_R$; therefore, it faces similar challenges as those faced by the expression of the impedance of the linear spring given by equation (2.20) which has a singularity at $\omega = 0$. Given that the dynamic flexibility of the two-parameter inertoelastic solid as expressed by equation (2.50) is a purely real quantity, we are in search of the imaginary Hilbert pairs of $1/(\omega - \omega_R)$ and $1/(\omega + \omega_R)$.

We first set $\Omega = \omega - \omega_R$ and we let $H_2(\Omega) = \pi\delta(\Omega - 0)$. Its Hilbert transform as expressed by the first of equation (2.16) gives

$$H_1(\omega) = -\frac{1}{\pi} \int_{-\infty}^{\infty} \frac{\pi\delta(x - 0)}{x - \Omega} dx \quad (2.51)$$

and with the change of variables $\xi = x - \Omega$, $d\xi = dx$, equation (2.51) becomes

$$H_1(\omega) = -\int_{-\infty}^{\infty} \frac{\delta(\xi - (-\Omega))}{\xi} d\xi = -\frac{1}{-\Omega} = \frac{1}{\omega - \omega_R} \quad (2.52)$$

Equation (2.52) indicates that the imaginary Hilbert pair of $1/(\omega - \omega_R)$ is $\pi\delta(\omega - \omega_R)$. Following the same reasoning one can show that the imaginary Hilbert pair of $1/(\omega + \omega_R)$ is $\pi\delta(\omega + \omega_R)$;

and the correct expression of the dynamic flexibility of the two-parameter inertoelastic solid is

$$H(\omega) = \frac{1}{2M_R} \frac{1}{\omega_R} \left[\frac{1}{\omega + \omega_R} - \frac{1}{\omega - \omega_R} + i\pi (\delta(\omega + \omega_R) - \delta(\omega - \omega_R)) \right] \quad (2.53)$$

By “manually” appending the imaginary part $\pi(\delta(\omega - \omega_R) - \delta(\omega + \omega_R))$ within the brackets of equation (2.50), the inverse Fourier transform of the dynamic flexibility of the network shown in Figure 2.1(left) is evaluated by rearranging equation (2.54) as

$$H(\omega) = \frac{1}{2M_R} \frac{i}{\omega_R} \left[\pi\delta(\omega + \omega_R) - \frac{i}{\omega + \omega_R} - \left(\pi\delta(\omega - \omega_R) - \frac{i}{\omega - \omega_R} \right) \right] \quad (2.54)$$

The inverse Fourier transform of the first two terms in the bracket of equation (2.54) is

$$F_1(t) = \frac{1}{2\pi} \int_{-\infty}^{\infty} \left[\pi\delta(\omega + \omega_R) - \frac{i}{\omega + \omega_R} \right] e^{i\omega t} d\omega \quad (2.55)$$

and with the change of variables, $\Omega = \omega + \omega_R$, $d\Omega = d\omega$, equation (2.55) gives

$$F_1(t) = e^{-i\omega_R t} \frac{1}{2\pi} \int_{-\infty}^{\infty} \left[\pi\delta(\Omega - 0) - \frac{i}{\Omega} \right] e^{i\Omega t} d\Omega = U(t - 0) e^{-i\omega_R t} \quad (2.56)$$

where again $U(t - 0)$ is the Heaviside unit-step function at the time origin.

The Fourier integral in equation (2.56) is computed by following the steps outlined in equations (2.22) and (2.23). Similarly, the inverse Fourier transform of the last two terms in the brackets of equation (2.54) is

$$F_2(t) = \frac{1}{2\pi} \int_{-\infty}^{\infty} \left[\pi\delta(\omega - \omega_R) - \frac{i}{\omega - \omega_R} \right] e^{i\omega t} d\omega = U(t - 0) e^{i\omega_R t} \quad (2.57)$$

Substitution of the results of equations (2.56) and (2.57) into equation (2.54) gives

$$h(t) = \frac{1}{2M_R} \frac{i}{\omega_R} U(t - 0) (e^{-i\omega_R t} - e^{i\omega_R t}) = \frac{1}{M_R \omega_R} U(t - 0) \sin(\omega_R t) \quad (2.58)$$

Equation (2.58) indicates that the impulse response function, $h(t)$, of the two-parameter inertoelastic solid shown in Figure 2.1(left), is a causal sinusoidal function (oscillatory response that initiates upon the application of the input impulse force) with frequency, $\omega_R = \sqrt{k/M_R}$; where the elastic spring and the inerter exchange continuously their strain and kinetic energies. Most importantly, equation (2.58) indicates that when an impulsive force is exerted on a spring that is connected in parallel with an inerter, the impulse response function is a finite oscillatory response; therefore, the presence of the inerter “absorbs” the weak singularity, $\delta(t - 0)$, that exists in the impulse response function of the solitary spring given by equation (2.19). This observation indicates the potential benefits of the inerter as a response modification device.

In the limiting case of a very soft spring ($\omega_R \rightarrow 0$), the limiting expression for the impulse response function given by equation (2.58) is

$$\lim_{\omega_R \rightarrow 0} h(t) = \frac{1}{M_R \omega_R} U(t - 0) \omega_R t = \frac{1}{M_R} U(t - 0) t \quad (2.59)$$

and the impulse response function of the solitary inerter given by equation (2.40) is recovered.

The impedance of the two-parameter inertoelastic solid derives directly from equation (2.46) by using that $v(\omega) = i\omega u(\omega)$; and it is given by

$$Z(\omega) = -k\frac{i}{\omega} + i\omega M_R \quad (2.60)$$

The first term in equation (2.60) is merely the impedance of the linear spring given by equation (2.20), while its second improper term is the impedance of the inerter given by equation (2.41). The imaginary reciprocal function, i/ω , is enhanced with its Hilbert pair according to equation (2.21) and the correct expression for the impedance of the two-parameter inertoelastic solid is

$$Z(\omega) = k \left[\pi\delta(\omega - 0) - i\frac{1}{\omega} \right] + i\omega M_R \quad (2.61)$$

By following the same mathematical operations described by equation (2.22), (2.23) and (2.26), the inverse Fourier transform of the impedance of the two-parameter inertoelastic solid is

$$k(t) = kU(t - 0) + M_R \frac{d\delta(t - 0)}{dt} \quad (2.62)$$

The mobility (admittance) of the two-parameter inertoelastic solid shown in Figure 2.1(left) is the inverse of its impedance expressed by equation (2.60),

$$Y(\omega) = -\frac{1}{M_R} \frac{i\omega}{\omega^2 - \omega_R^2} \quad (2.63)$$

in which $\omega_R^2 = k/M_R$, is the natural frequency of the system. The poles of the mobility given by equation (2.63) are $\omega = \pm\omega_R$ and partial fraction expansion gives

$$Y(\omega) = -\frac{i}{2M_R} \left(\frac{1}{\omega - \omega_R} + \frac{1}{\omega + \omega_R} \right) \quad (2.64)$$

The transfer function given by equation (2.64) is a purely imaginary quantity with singularities at $\omega = \omega_R$ and $\omega = -\omega_R$; therefore, it faces similar challenges as those faced by the expression of the impedance of the linear spring given by equation (2.20), which has a singularity at $\omega = 0$. Given that the mobility (admittance) of the two parameter inertoelastic solid, as expressed by equation (2.64), is a purely imaginary quantity, we are in search of the real Hilbert pairs of $1/(\omega - \omega_R)$ and $1/(\omega + \omega_R)$. We first set $\Omega = \omega - \omega_R$ and we let $Y_1(\Omega) = \pi\delta(\Omega - 0)$. Its Hilbert transform as expressed by the second of equations (2.16) gives (see also equations (2.51) and (2.52)):

$$Y_2(\omega) = \frac{1}{\pi} \int_{-\infty}^{\infty} \pi \frac{\delta(x - 0)}{x - \Omega} dx = -\frac{1}{\omega - \omega_R} \quad (2.65)$$

Equation (2.65) indicates that the real Hilbert pair of $-1/(\omega - \omega_R)$ is $\pi\delta(\Omega - \omega_R)$. Following the same reasoning one can show that the real Hilbert pair of $-1/(\omega + \omega_R)$ is $\pi\delta(\Omega + \omega_R)$ and the correct expression for the mobility of the two-parameter inertoelastic solid given by equation (2.64) is

$$Y(\omega) = \frac{1}{2M_R} \left[\pi\delta(\omega - \omega_R) - i\frac{1}{\omega - \omega_R} + \pi\delta(\omega + \omega_R) - i\frac{1}{\omega + \omega_R} \right] \quad (2.66)$$

The inverse Fourier transform of equation (2.66) is computed in a similar way as we computed the inverse Fourier transform of equation (2.54) and it gives:

$$y(t) = \frac{1}{M_R} U(t-0) \cos(\omega_R t) \quad (2.67)$$

where $U(t-0)$ is again the Heaviside unit-step function at the time origin. Equation (2.67) indicates that the impulse velocity response function, $y(t)$, of the two-parameter inertoelastic solid shown in Figure 2.1(left) is acausal cosine function with frequency $\omega_R = \sqrt{k/M_R}$. Similar to equation (2.58), equation (2.67) indicates that when an impulsive force is exerted on a spring that is connected in parallel with an inerter, the impulse velocity response function is a finite oscillatory response; therefore, the presence of the inerter “absorbs” the singularity, $d\delta(t-0)/dt$, that exists in the impulse velocity response function of the solitary spring given by equation (2.27).

In the limiting case of a very soft spring ($\omega_R \rightarrow 0$), the limiting expression for the impulse velocity response function given by equation (2.67) is

$$\lim_{\omega_R \rightarrow \infty} y(t) = \frac{1}{M_R} U(t-0) \quad (2.68)$$

and the impulse velocity response function of the solitary inerter given by equation (2.45) is recovered. The eight basic response functions of the two-parameter viscoelastic solid computed in this section are also summarized in Table 2.1 next to the basic response functions of the linear spring, the viscous dashpot and the inerter.

2.4 BASIC RESPONSE FUNCTIONS OF THE TWO-PARAMETER INERTOELASTIC “FLUID”

We are now interested in deriving the basic time-response functions of the two-parameter inertoelastic “fluid” element—that is a spring and an inerter connected in series as shown in Figure 2.1(right). The term “fluid” is used to express that this network undergoes an infinite displacement under a static loading. Given that the force, $F(t)$, is common at the spring and the inerter

$$F(t) = k(u(t) - u_3(t)) \quad (2.69)$$

while at the same time,

$$F(t) = M_R \frac{d^2 u_3(t)}{dt^2} \quad (2.70)$$

where $u_3(t)$ is the nodal displacement of the internal node, 3, where the spring and the inerter connect. Upon differentiating equation (2.69) two times and substituting $d^2 u_3(t)/dt^2$ from equation (2.70), the constitutive equation of the mechanical network shown in Figure 2.1(right) is expressed by

$$F(t) + \frac{1}{\omega_R^2} \frac{d^2 F(t)}{dt^2} = M_R \frac{d^2 u(t)}{dt^2} \quad (2.71)$$

The Fourier transform of (2.71) gives

$$F(\omega) = \omega_R^2 M_R \frac{\omega^2}{\omega^2 - \omega_R^2} u(\omega) \quad (2.72)$$

and by recalling that $k = \omega_R^2 M_R$, the dynamic stiffness of the mechanical network as results from equation (2.72) is $K(\omega) = k\omega^2/(\omega^2 - \omega_R^2)$, which is a simple proper transfer function, reaching the constant value, k , at the high-frequency limit. By separating the high-frequency limiting value, k , the dynamic stiffness of the two parameter inertoelastic “fluid” as results from equation (2.72) is expressed as

$$K(\omega) = k \left[1 + \frac{\omega_R^2}{\omega^2 - \omega_R^2} \right] \quad (2.73)$$

The second term within the bracket in equation (2.73), $\omega_R^2/(\omega^2 - \omega_R^2)$, is of the same form as the dynamic flexibility of the two-parameter inertoelastic “solid” given by equation (2.49). Accordingly, the purely real term, $\omega_R^2/(\omega^2 - \omega_R^2)$, is equation (2.73) which has poles at $\omega \pm \omega_R$ needs to be enhanced with its corresponding imaginary delta functions. By following a procedure similar to the one outlined by equations (2.51) to equation (2.54), the correct expression of the dynamic stiffness of the two-parameter viscoelastic fluid described by equation (2.71) is

$$K(\omega) = k + \frac{k\omega_R}{2} \left[\frac{1}{\omega - \omega_R} - \frac{1}{\omega + \omega_R} + i\pi (\delta(\omega - \omega_R) - \delta(\omega + \omega_R)) \right] \quad (2.74)$$

By “manually” appending the imaginary part $\pi(\delta(\omega - \omega_R) - \delta(\omega + \omega_R))$ in equation (2.73), the inverse Fourier transform of the dynamic stiffness of the two-parameter viscoelastic fluid shown in Figure 2.1(right) is evaluated by following a procedure similar to the one outlined in equations (2.54) to (2.57); and the resulting memory function is

$$q(t) = k [\delta(t - 0) - \omega_R U(t - 0) \sin \omega_R t] \quad (2.75)$$

Under an impulsive displacement input the two-parameter viscoelastic fluid shown in Figure 2.1 (right), initially behaves like the linear spring; given that the inerter provides “infinite” resistance at the initiation of motion. Accordingly, at the time origin, the memory function given by equation (2.75) is singular, exactly as is the memory function of the solitary elastic spring given by equation (2.18); and subsequently the inerterengages in motion and follows a causal sinusoidal response with frequency $\omega_R = \sqrt{k/M_R}$.

Equation (2.72) also indicates that the dynamic flexibility $H(\omega) = u(\omega)/F(\omega)$ of the two-parameter inertoelastic fluid is a simply proper transfer function

$$H(\omega) = \frac{1}{k} - \frac{\omega_R^2}{k} \frac{1}{\omega^2} = \frac{1}{k} - \frac{1}{M_R} \frac{1}{\omega^2} \quad (2.76)$$

The constant term $1/k$ in equation (2.76) results to a weak singularity in the time domain; while, the second term is precisely the dynamic flexibility of the solitary inerter given by equation (2.33). By following the same procedure as the one presented by equations (2.34) to (2.36), the correct expression for the dynamic flexibility of the two-parameter inertoelastic fluid is

$$H(\omega) = \frac{1}{k} + \frac{1}{M_R} \left[-\frac{1}{\omega^2} + i\pi \frac{d\delta(\omega - 0)}{d\omega} \right] \quad (2.77)$$

By “manually” appending the imaginary part $\pi d\delta(\omega - 0)/d\omega$ in equation (2.76), the inverse Fourier transform of the correct dynamic flexibility of the two-parameter inertoelastic fluid given by equation (2.77) is computed by following the steps outlined in equations (2.37) to (2.40) and gives

$$h(t) = \frac{1}{k} \delta(t - 0) + \frac{1}{M_R} U(t - 0) t \quad (2.78)$$

where $U(t - 0)$ is again the Heaviside unit-step function at the time origin. Equation (2.78) indicates that when an impulsive force is exerted on the two-parameter inertoelastic fluid, the impulse is initially taken entirely by the elastic spring, $\delta(t - 0)/k$, and subsequently the inerter enters a causal response that grows linearly with time during which the “idle” spring is carried along.

The impedance of the two-parameter viscoelastic fluid shown in Figure 2.1(right) derives directly from equation (2.72) by using that $v(\omega) = i\omega u(\omega)$; therefore, is given by

$$Z(\omega) = -k \frac{i\omega}{\omega^2 - \omega_R^2} \quad (2.79)$$

Equation (2.79) is of the same form as the mobility (admittance) of the two-parameter inertoelastic solid given by equation (2.63); so by following the steps outlined by equations (2.64) to equation (2.66), the correct expression of the impedance of the two-parameter inertoelastic fluid is

$$Z(\omega) = \frac{k}{2} \left[\pi\delta(\omega - \omega_R) - \frac{i}{\omega - \omega_R} + \pi\delta(\omega + \omega_R) - \frac{i}{\omega + \omega_R} \right] \quad (2.80)$$

The inverse Fourier transform of equation (2.80) is computed in a similar way as we computed the inverse Fourier transform of equation (2.54) and it gives

$$K(t) = kU(t - 0) \cos(\omega_R t) \quad (2.81)$$

where $U(t - 0)$ is again the Heaviside unit-step function at the time origin. Equation (2.81) indicates that the imposed unit-step displacement is initially accommodated entirely by the elastic spring which subsequently sets the inerter in motion with the elastic and kinetic energies being continuously interchanged between the elastic spring and the inerter.

The mobility (admittance) of the two-parameter inertoelastic fluid shown in Figure 2.1(right) is the inverse of 389 its impedance expressed by equation (2.79)

$$Y(\omega) = \frac{1}{k}i\omega - \frac{\omega_R^2}{k} \frac{i}{\omega} = \frac{1}{k}i\omega - \frac{1}{M_R} \frac{i}{\omega} \quad (2.82)$$

Equation (2.82) is of the same form as the impedance of the two-parameter inertoelastic solid given by equation (2.60). It includes an improper term, $i\omega/k$, which results from the mobility of the solitary linear spring given by equation (2.24) together with the reciprocal function, $1/\omega$, which results from the mobility of the solitary inerter given by equation (2.43). Accordingly, the imaginary reciprocal function, i/ω , is enhanced with its Hilbert pair according to equation (2.21) and the correct expression for the mobility of the two-parameter inertoelastic fluid is

$$Y(\omega) = \frac{1}{k}i\omega + \frac{1}{M_R} \left[\pi\delta(\omega - 0) - i\frac{1}{\omega} \right] \quad (2.83)$$

By following the same mathematical operations described by Equations (2.22), (2.23) and (2.26), the inverse Fourier transform of the mobility of the two-parameter inertoelastic fluid given by equation (2.83) is

$$y(t) = \frac{1}{k} \frac{d\delta(t - 0)}{dt} + \frac{1}{M_R} U(t - 0) \quad (2.84)$$

The eight basic response functions of the two-parameter viscoelastic fluid computed in this section are also summarized in Table 2.1 next to the basic response functions of the two-parameter viscoelastic solid.

2.5 BASIC RESPONSE FUNCTIONS OF THE “ROTATIONAL INERTIA DAMPER” (DASHPOT AND INERTER IN PARALLEL)

About a decade ago, Hwang et al. (2007) proposed a rotational inertia damper which consists of a cylindrical mass that is driven by a ball screw and rotates within a chamber that contains some viscous fluid. In this way the resistance to the driving force originates partly from the difficulty to mobilize the rotational inertia of the rotating mass and partly from the viscous stresses that develop on the circumference of the rotating mass as it shears the viscous fluid. Consequently, the mechanical analogue of the rotational inertia damper proposed by Hwang et al. (2007) and later by Ikago et al. (2012a) is essentially a dashpot and an inerter connected in parallel as shown in Figure 2.2(left). The constitutive equation of the mechanical network shown in Figure 2.2(left) is

$$F(t) = C \frac{du(t)}{dt} + M_R \frac{d^2u(t)}{dt^2} \quad (2.85)$$

and its Fourier transform gives

$$F(\omega) = [Ci\omega - M_R\omega^2] u(\omega) \quad (2.86)$$

Equation (2.86) indicates that the dynamic stiffness $k(\omega) = Ci\omega - M_R\omega^2$ of the rotational inertia damper is an improper transfer function of the first degree because of the dashpot and of the second degree because of the inerter. Clearly, given this parallel arrangement, the memory function, $q(t)$, of the rotational inertia damper shown in Figure 2.2(left) is the summation of the memory function of the dashpot (see Makris 1997a, Table 2.1 and the Fourier transform of equation (2.24) given by equation (2.27)) and that of the inerter given by equation (2.32).

$$q(t) = C \frac{d\delta(t-0)}{dt} + M_R \frac{d^2\delta(t-0)}{dt^2} \quad (2.87)$$

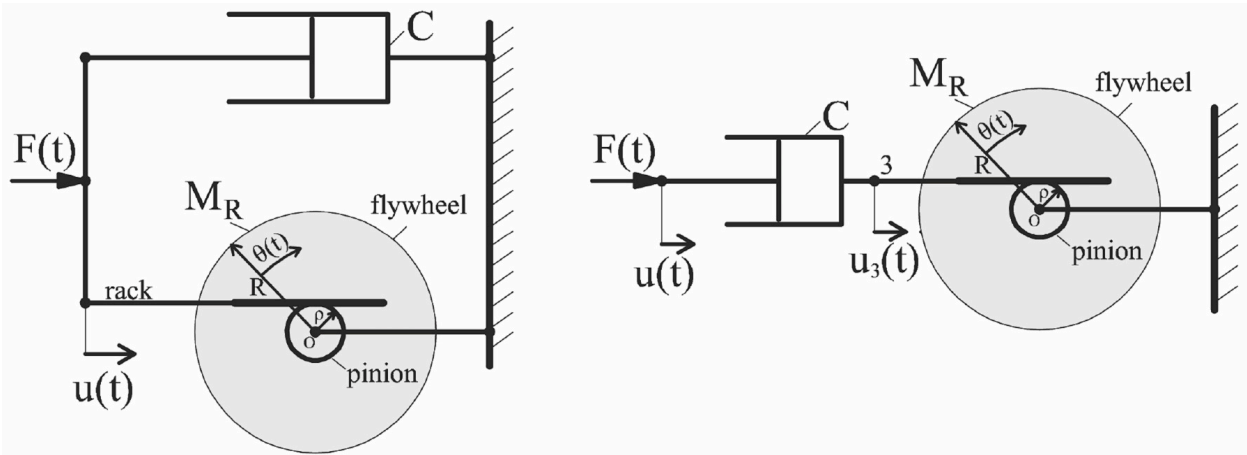


Figure 2.2: Left: The rotational inertia damper which is an inertoviscous model in parallel. Right: The inertoviscous model in series.

The improper dynamic stiffness appearing in equation (2.86) indicates that it is not physically realizable to impose an impulse displacement on a rotational inertia damper. Nevertheless, a mathematical expression of its memory functions can be reached via the use of the derivatives of the Dirac delta function as shown by equation (2.87).

While the dynamic stiffness of the rotational inertia damper, $k(\omega) = Ci\omega - M_R\omega^2$, is an improper transfer function, its inverse, that is the dynamic flexibility is a proper function,

$$H(\omega) = \frac{1}{i\omega C - \omega^2 M_R} = \frac{1}{C} \frac{1}{\omega(-\omega \frac{M_R}{C} + i)} \quad (2.88)$$

where the ratio M_R/C is the retardation time of the network and has units of time [T].

The poles of the dynamic flexibility given by equation (2.88) are $\omega = 0$ and $\omega = iC/M_R$; therefore, partial fraction expansion of the right-hand side of equation (2.88) gives

$$H(\omega) = \frac{1}{C} \left[-i \frac{1}{\omega} - \frac{M_R}{C} \frac{1}{1 + i\omega \frac{M_R}{C}} \right] \quad (2.89)$$

The first term within the brackets in equation (2.89) is the imaginary reciprocal function, i/ω , which faces the same challenges as the impedance of the linear spring given by equation (2.20); therefore, it is enhanced with its Hilbert pair according to equation (2.21). The second term with the brackets in equation (2.89) is a strictly proper transfer function; therefore, its inverse Fourier transform converges in the classical sense. Consequently, the correct expression for the dynamic flexibility of the rotational inertia damper is

$$H(\omega) = \frac{1}{C} \left[\left[\pi\delta(\omega - 0) - i \frac{1}{\omega} \right] - \frac{M_R}{C} \frac{1}{1 + i\omega \frac{M_R}{C}} \right] \quad (2.90)$$

The inverse Fourier transform of equation (2.90) is evaluated by following the same mathematical operations described by equations (2.22) and (2.23) for the term $\pi\delta(\omega - 0) - i/\omega$; while, the last term is integrated by employing the method of residues (Morse and Feshbach 1953). Accordingly,

$$h(t) = \frac{1}{C} \left[U(t - 0) - e^{-\frac{C}{M_R}t} \right] \quad (2.91)$$

where again, $U(t - 0)$ is the Heaviside unit-step function at the time origin. Equation (2.91) indicates that the impulse response function of the rotational inertia damper assumes the value of $1/C$ at the time origin and subsequently decays exponentially to zero.

The impedance of the rotational inertia damper shown in Figure 2.2(left) derives directly from equation (2.86), by using that $v(\omega) = i\omega u(\omega)$ and is given by

$$Z(\omega) = \frac{Ci\omega - M_R\omega^2}{i\omega} = C + i\omega M_R \quad (2.92)$$

where to constant C is the impedance of the viscous dashpot and $i\omega M_R$ is the impedance of the inerter given by equation (2.41). With this parallel arrangement, the inverse Fourier transform of the impedance of the rotational inertia damper is

$$k(t) = C\delta(t - 0) + M_R \frac{d\delta(t - 0)}{dt} \quad (2.93)$$

The mobility of the rotational inertia damper is the inverse of its impedance given by equation (2.92)

$$Y(\omega) = \frac{1}{C + i\omega M_R} = \frac{1}{C} \frac{1}{1 + i\omega \frac{M_R}{C}} \quad (2.94)$$

The transfer function given by equation (2.94) is a strictly proper transfer function and its inverse Fourier transform is evaluated with the method of residues.

$$y(t) = \frac{1}{M_R} e^{-\frac{C}{M_R}t} \quad (2.95)$$

The eight basic response functions of the rotational inertia damper (dashpot and inerter connected in parallel) are summarized in Table 2.1 next to the inertoelastic elements examined in this study.

2.6 BASIC RESPONSE FUNCTIONS OF A DASHPOT AND INERTER CONNECTED IN SERIES

We are now interested in deriving the basic time-response function of a dashpot and an inerter in series as shown in Figure 2.2(right). Given that the force, $F(t)$, is common at the dashpot and the inerter

$$F(t) = C \left(\frac{du(t)}{dt} - \frac{du_3(t)}{dt} \right) \quad (2.96)$$

while at the same time, $F(t)$ satisfies equation (2.70). In equation (2.96), $u_3(t)$ is the nodal displacement of the internal node, 3, where the dashpot and the inerter connect. Upon differentiating equation (2.96) and substituting $d^2u_3(t)/dt^2$ from equation (2.70), the constitutive equation of the mechanical network shown in Figure 2.2(right) is expressed by

$$F(t) + \frac{M_R}{C} \frac{dF(t)}{dt} = M_R \frac{d^2u(t)}{dt^2} \quad (2.97)$$

The Fourier transform of equation (2.97) gives

$$F(\omega) = -M_R \frac{\omega^2}{1 + i\omega \frac{M_R}{C}} u(\omega) \quad (2.98)$$

Equation (2.98) indicates that the dynamic stiffness of a dashpot and an inerter connected in series is $-M_R\omega^2/(1 + i\omega M_R/C)$; therefore, it is an improper transfer function. By first separating the improper high-frequency limit, $i\omega C$, and subsequently separating the simple-proper high-frequency limit $-C_2/M_R$, the dynamic stiffness of the mechanical network shown in Figure 2.2(right) as results from equation (2.98) is expressed as

$$K(\omega) = i\omega C - \frac{C^2}{M_R} + \frac{C^2}{M_R} \frac{1}{1 + i\omega \frac{M_R}{C}} \quad (2.99)$$

The inverse Fourier transform of the first term which is the dynamic stiffness of the linear dashpot (Makris 1997a) is evaluated by employing equation (2.26); while, the inverse Fourier transform of the constant C_2/M_R results to a weak singularity $(C_2/M_R)\delta(t - 0)$. The last term in equation

(2.99) is a strictly proper transfer function; therefore, its inverse Fourier transform converges in the classical sense and is evaluated with the method of residues. Accordingly, the memory function of a dashpot and an inerter connected in series is given by

$$q(t) = C \left[\frac{d\delta(t-0)}{dt} - \frac{C}{M_R} \delta(t-0) + \frac{C^2}{M_R^2} e^{-\frac{C}{M_R}t} \right] \quad (2.100)$$

The dynamic flexibility of a dashpot and an inerter connected in series is the inverse of the dynamic stiffness given by equation (2.98)

$$H(\omega) = -\frac{1}{M_R} \frac{1 + i\omega \frac{M_R}{C}}{\omega^2} = -\frac{1}{M_R} \frac{1}{\omega^2} - \frac{1}{C} i \frac{1}{\omega} \quad (2.101)$$

The first term in the right-hand side of equation (2.101) is the dynamic flexibility of the inerter as expressed by equation (2.33); while, the second term is the dynamic flexibility of the linear dashpot (Makris 1997a). Consequently both terms are enhanced with their Hilbert pairs as shown by equations (2.21) and (2.36), and the correct expression of the dynamic flexibility given by equation (2.101) is

$$H(\omega) = \frac{1}{M_R} \left[-\frac{1}{\omega^2} + i\pi \frac{d\delta(\omega-0)}{d\omega} \right] + \frac{1}{C} \left[\pi\delta(\omega-0) - i \frac{1}{\omega} \right] \quad (2.102)$$

By “manually” appending the Hilbert pair singularities $\pi d\delta(\omega-0)/d\omega$ for the inerter and $\pi\delta(\omega-0)$ for the dashpot, the inverse Fourier transform of the dynamic flexibility given by equation (2.102) is

$$h(t) = \frac{1}{C} \left[1 + \frac{C}{M_R} t \right] U(t-0) \quad (2.103)$$

where $U(t-0)$ is the Heaviside unit-step function at the time origin. Equation (2.103) indicates that the causal impulse response function of a dashpot and an inerter in series assumes a constant value, $1/C$, at the time origin and subsequently grows linearly with time.

The impedance of a dashpot and an inerter connected in series derives directly from equation (2.98) by using that $v(\omega) = i\omega u(\omega)$ and is given by

$$Z(\omega) = M_R \frac{i\omega}{1 + i\omega \frac{M_R}{C}} \quad (2.104)$$

The transfer function given by equation (2.104) is a simple proper transfer function, reaching the constant value, C , at the high-frequency limit. By separating the high-frequency limit, C , the impedance of the mechanical network shown in Figure 2.2(right) as results from Equation (2.104) is expressed as

$$Z(\omega) = C \left[1 - \frac{1}{1 + i\omega \frac{M_R}{C}} \right] \quad (2.105)$$

The inverse Fourier transform of a constant is the Dirac delta function; while the inverse Fourier transform of the strictly proper second term within the brackets of equation (2.105) is evaluated

with the method of residues. Accordingly, the relaxation stiffness of a dashpot and an inerter connected in series is given by

$$k(t) = C \left[\delta(t - 0) - \frac{C}{M_R} e^{-\frac{C}{M_R}t} \right] \quad (2.106)$$

The mobility (admittance) of a dashpot and an inerter connected in series is the inverse of the impedances as expressed by equation (2.104)

$$Y(\omega) = \frac{1}{M_R} \frac{1 + i\omega \frac{M_R}{C}}{i\omega} = \frac{1}{C} - \frac{1}{M_R} i \frac{1}{\omega} \quad (2.107)$$

The first constant term, $1/C$, in the right hand side of equation (2.107) is the mobility of the linear dashpot (Makris 1997a); and yields in the time domain a weak singularity; while the second term is the mobility of the inerter given by equation (2.43). Consequently, the imaginary reciprocal function, i/ω , is enhanced with its Hilbert pair according to equation (2.44), and the correct expression for the mobility of the mechanical network shown in Figure 2.2(right) is

$$Y(\omega) = \frac{1}{C} + \frac{1}{M_R} \left[\pi \delta(\omega - 0) - i \frac{1}{\omega} \right] \quad (2.108)$$

By following the same mathematical operations described by equations (2.22) and (2.23), the inverse Fourier transform of the mobility given by equation (2.108) is

$$Y(t) = \frac{1}{C} \delta(t - 0) - \frac{1}{M_R} U(t - 0) \quad (2.109)$$

To this end, the eight basic response functions of a dashpot and an inerter connected in series are summarized in Table 2.1 next to the basic response functions of the rotational inertia damper.

Recently, the concept of the inerter and its associated time response functions have been used to model the fluctuation component of the perpetual fluctuation-dissipation process that characterizes Brownian motion and has been essential in deriving a fundamental viscous-viscoelastic correspondence principle for Brownian motion (Makris 2020b). This correspondence principle led to the definition of the *impulsive response function for Brownian motion* (Makris 2021a) and allowed for the construction of a rheological analogue for Brownian motion when hydrodynamic memory effects need to be accounted for (Makris 2021b).

2.7 CONCLUSIONS

This chapter examines and constructs the basic frequency-response functions and subsequently derives the corresponding causal time-response functions of elementary mechanical networks which involve the inerter—a two-node element in which the force-output is proportional to the relative acceleration of its end-nodes. This is achieved by extending the relation between the causality of a time-response function with the analyticity of its corresponding frequency response function to the case of generalized functions.

The chapter shows that when the frequency-response function has as singularity the reciprocal function, $1/(\omega - \omega_R)$ (with $\omega_R = \text{constant or zero}$), the complex frequency-response function needs to be enhanced with the addition of a Dirac delta function, $\delta(\omega - \omega_R)$, so that the real and imaginary parts of the correct frequency-response function are Hilbert pairs; therefore, yielding a causal time-response function in the time domain. Similarly, when the singularity of the frequency-response function is $1/\omega^2$, the complex frequency-response function needs to be enhanced with the addition of $d\delta(\omega - 0)/d\omega$, so that the real and imaginary parts of the correct frequency-response function are Hilbert pairs.

Because of the participation of the inerter, some basic time-response functions of the examined mechanical networks exhibit a causal oscillatory response and this behavior complements the decaying-exponential response due to the participation of the dashpot. Most importantly, the chapter shows that the inerter emerges as an attractive response-modification element given that in some cases it “absorbs” the impulsive response of the solitary spring or dashpot.

Finally, the basic response-functions derived in this chapter and summarized in Table 2.1 in association with the mathematical operations outlined in this work extends the well-established theory of linear viscoelasticity to the inertoelastic and inertoviscoelastic behavior (combination of inerters, dashpots and springs) and introduce the subject of inertoviscoelasticity.

3 Displacements and Forces in Structures with Inerters when Subjected to Earthquakes

In view of the effectiveness of supplemental rotational inertia to suppress the seismic displacements of a SDOF system as shown by equation (1.3) (see also Makris and Kampas 2016), this chapter investigates the seismic response of the two-degree-of-freedom (2DOF) structure shown in Figure 3.1(a). This 2DOF system can be viewed as the idealization of a structure supported on solitary columns, known in modern architecture as a structure *on pilotis*. In this configuration, only the first story (pilotis) is engaged to a rotational flywheel system in an effort to investigate to what extent the use of supplemental rotational inertia (use of inerters as a retrofit strategy) can limit large displacements versus the use of large values of supplemental damping. The chapter compares the computed response quantities of the 2DOF system shown in Figure 3.1(a) with those when the pilotis is retrofitted with large values of supplemental damping [Figure 3.1(b)] and with those from the “classical” two-degree-of-freedom system shown in Figure 3.1(c) that has been used to introduce the linear theory of seismic isolation (Kelly 1997; Kelly and Konstantinidis 2011).

3.1 OPEN SOFT FIRST STORY: FROM AESTHETICS, FUNCTIONALITY AND SEISMIC ISOLATION TO A LATERAL FAILURE MECHANISM

The concept of lifting the bulk of the structure above the ground level and supporting it merely on solitary columns was introduced by Le Corbusier (1925; 1986) who developed a set of architectural principles that marked the architecture of the 20th century. Le Corbusier’s five points of New Architecture (in French: cinq points de l’architecture moderne) are: (1) pilotis—a grid of solitary columns either from reinforced concrete or steel that support the gravity loads of the structure above without any bearing or shear walls at the ground floor on the basis of the new aesthetics; (2) the open floor plan which is free of supporting walls, therefore the internal use of the floor plan is unrestricted; (3) the free facade where the exterior of the building is separated from its structural function, allowing for more natural light to enter the building; (4) the strip windows which in addition of allowing for more natural light give the impression of a floating structure—an impression that is also accentuated from point (1) = the pilotis; and (5) roof gardens—which make buildings cooler in the summer and warmer in the winter—a pioneering vision for sustainable cities that is receiving growing acceptance only a century later.

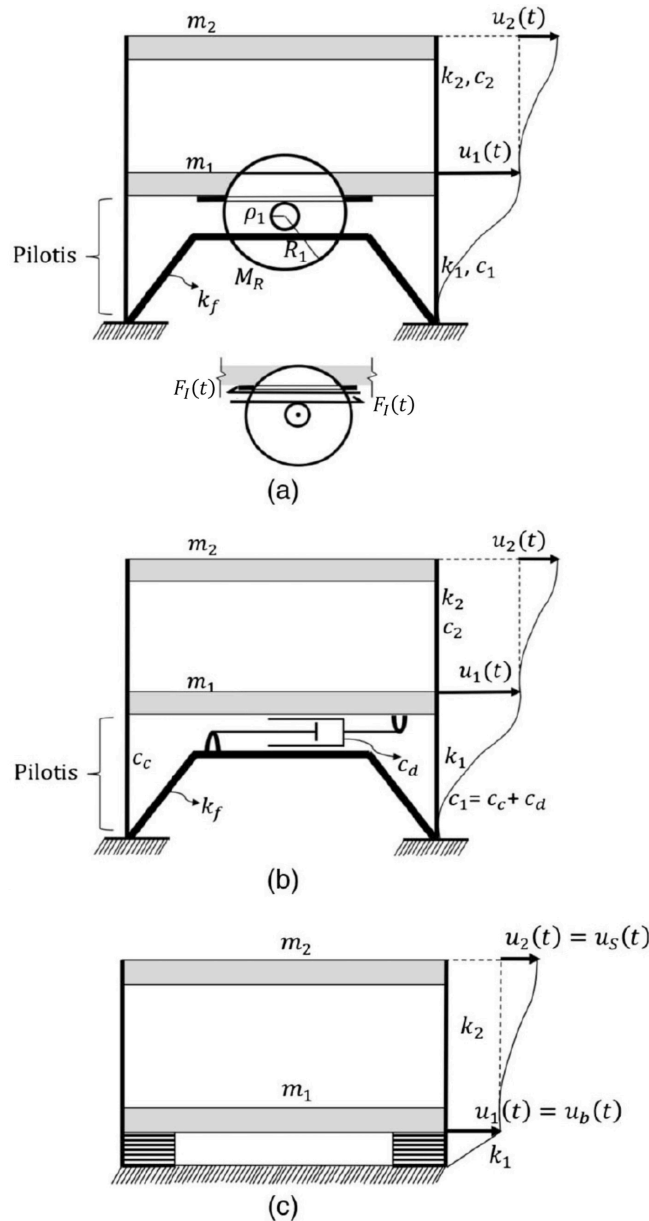


Figure 3.1: (a) 2DOF structure engaged with a rotational flywheel system;(b) 2DOF structure retrofitted with supplemental damper at first soft story; and (c) classical two-degree-of-freedom seismic isolation system.

The unique aesthetics of the "floating" structure atop the pilotis in association with the functionality advantages of an open ground floor in urban design which creates continuity between the ground floor and the surrounding open space, had such a major impact in modern architecture that the open ground floor has been enthusiastically adopted in the design of major buildings world-wide. As an example, the emblematic Ministry of Education and Health Building (Palácio Gustavo Capanema) in Rio de Janeiro Brazil completed in 1943 is supported by a pilotis. Its mid 1930s design was drastically influenced by Le Corbusier (1925) concepts of modern architecture.

About the same time that Le Corbusier (1925; 1986) was developing his new architecture in France, structural engineers at the California Institute of Technology (Martel 1929) and at Stanford University (Jacobsen 1938) viewed the flexible first story—that is Le Corbusier’s pilotis—as a way to lengthen the period of the structure and reduce the shear forces at the base of the structure. Because of the low lateral stiffness of the solitary columns of the “soft” first story, the deformation demands would be concentrated in these first-story columns which essentially isolate the superstructure from the ground shaking. This early concept of seismic isolation (Martel 1929; Green 1935; Jacobsen 1938) assumed that the solitary columns would remain elastic during the earthquake shaking. In the late 1960s, Fintel and Khan (1969) after examining first-story failures from several earthquakes, further advanced the concept of the soft first-story seismic isolation by indicating that the solitary columns will deform inelastically; therefore, offering some energy dissipation. In their remarkable paper, Fintel and Khan (1969) recognized that the yielding columns of the soft, first-story will convert the first-story into a mechanism; therefore, they suggested the construction of core stabilizing walls that will support the weight of the structure via elastomeric (polychloroprene= neoprene) bearings with low lateral stiffness. Accordingly, the Fintel and Khan (1969) paper suggested an early concept of seismic isolation with bilinear behavior where recentering is offered by the neoprene bearings and dissipation is offered by the yielding first-story columns. Soon after the Fintel and Khan paper and immediately after the devastating 1971 San Fernando California earthquake, extensive numerical studies at the University of California, Berkley (Chopra et al. 1972) showed that the displacement demands due to a “soft” first story may be exceedingly large, to the extent that the effect of the gravity loads from the upper levels during this sideways deformation lead to collapse of the entire structure. This lateral failure mechanism was responsible for the spectacular failure of the Olive View Hospital during the 1971 San Fernando, California earthquake shown in Figure 3.2 (Bertero et al. 1978). By the end of the 1970, it became clear to the civil engineering profession that the pilotis, while an architectural concept with several aesthetic and functionality advantages, has poor seismic performance (Bertero et al. 1978; Arnold 1984; Bertero et al. 1991; Repapis et al. 2006; Antonopoulos and Anagnostopoulos 2017). Despite its poor seismic performance, the pilotis is widely used by architects around the world (Arnold 1984); therefore, the chapter examines to what extent supplemental rotational inertia can control the displacements of the two-story structure shown in Figure 3.2(a). In other words, the chapter explores the effectiveness of supplemental rotational inertia on enhancing the response of a structure with a soft first story.



Figure 3.2: Iconic soft-story failure of Olive View Hospital during 1971 San Fernando, California earthquake. (Image courtesy of the USGS).

3.2 INERTIA FORCES FROM THE FLYWHEEL SUPPORTED ON A STIFF CHEVRON FRAME

Figure 3.1(a) depicts a 2DOF structure where the mass, m_1 , of the first story is engaged to a flywheel with radius R_1 and mass M_{w1} that can rotate about an axis O. We first consider the case of a very stiff chevron frame whose deformation is negligible to the translational displacements, $u_1(t)$ and $u_2(t)$, of the 2DOF structure. Concentric to the flywheel, there is an attached pinion with radius ρ_1 engaged to a linear rack connected to the bottom of the vibrating mass m_1 of the 2DOF. With this arrangement when the mass m_1 undergoes a positive displacement, $u_1(t)$, the flywheel is subjected to a clockwise rotation, $\theta_1(t)$. Given that, there is no slipping between the rack and the pinion

$$\theta_1(t) = \frac{u_1(t)}{\rho_1} \quad (3.1)$$

With reference to Figure 3.1(a) for a positive displacement, $u_1(t)$, to the right, the internal force, $F_I(t)$ at the rack-pinion interface opposes the motion (to the left). Moment equilibrium of the flywheel about point O, gives

$$I_{W1}\ddot{\theta}_1(t) = F_I(t)\rho_1 \quad (3.2)$$

In equation (3.2), $I_{W1} = (1/2)m_{w1}R_1^2 =$ moment of inertia of the flywheel about point O. Substituting of equation (3.1) into equation (3.2) gives:

$$F_I(t) = \frac{1}{2}m_{w1}\frac{R_1^2}{\rho_1^2}\ddot{u}_1(t) = M_R\ddot{u}_1(t) \quad (3.3)$$

Equation (3.3) offers the inertial force, $F_I(t)$, at the rack-pinion inerter face—that is the force transferred to the stiff chevron frame. The constant of proportionality, $M_R = (1/2)m_{w1}(R_1^2/\rho_1^2)$ is the inertance of the supplemental rotational inertia system and it has units of mass [M]. The inertance, M_R , can be amplified by adding two (or more) flywheels in series, where the first flywheel is a gearwheel (Smith 2002; Makris and Kampas 2016).

3.3 EQUATIONS OF MOTION OF A 2DOF STRUCTURE SUPPORTED ON A STIFF CHEVRON FRAME

With reference to Figure 3.1(a), dynamic equilibrium of the entire structure above the chevron frame gives

$$m_2[\ddot{u}_1(t) + \ddot{u}_2(t) + \ddot{u}_g(t)] + m_1[\ddot{u}_1(t) + \ddot{u}_g(t)] = -k_1u_1(t) - c_1\dot{u}_1(t) - F_I(t) \quad (3.4)$$

where $F_I(t)$ is the internal force from the flywheel given by equation (3.3). Dynamic equilibrium of the second story gives

$$m_2[\ddot{u}_1(t) + \ddot{u}_2(t) + \ddot{u}_g(t)] = -k_2u_2(t) - c_2\dot{u}_2(t) \quad (3.5)$$

Following the notation introduced by Kelly (1997), the nominal frequencies and nominal damping ratios are

$$\omega_1^2 = \frac{k_1}{m_1 + m_2}, \quad \omega_2^2 = \frac{k_2}{m_2} \quad (3.6)$$

$$2\xi_1\omega_1 = \frac{c_1}{m_1 + m_2}, \quad 2\xi_2\omega_2 = \frac{c_2}{m_2} \quad (3.7)$$

Furthermore, the mass ratio, γ , and the inertance ratio, σ , are defined as:

$$\gamma = \frac{m_2}{m_1 + m_2}, \quad \sigma = \frac{M_R}{m_1 + m_2} \quad (3.8)$$

Equations (3.4) and (3.7) can be expressed in matrix form in terms of the parameters defined in equations (3.6), (3.7) and (3.8).

$$\begin{bmatrix} 1 + \sigma & \gamma \\ 1 & 1 \end{bmatrix} \begin{Bmatrix} \ddot{u}_1(t) \\ \ddot{u}_2(t) \end{Bmatrix} + \begin{bmatrix} 2\xi_1\omega_1 & 0 \\ 0 & 2\xi_2\omega_2 \end{bmatrix} \begin{Bmatrix} \dot{u}_1(t) \\ \dot{u}_2(t) \end{Bmatrix} + \begin{bmatrix} \omega_1^2 & 0 \\ 0 & \omega_2^2 \end{bmatrix} \begin{Bmatrix} u_1(t) \\ u_2(t) \end{Bmatrix} = - \begin{Bmatrix} 1 \\ 1 \end{Bmatrix} \ddot{u}_g(t) \quad (3.9)$$

When $\sigma = 0$, equation (3.9) is identical to the matrix equation of a two-degree-of-freedom seismic isolated structure (Kelly 1997; Kelly and Konstantinidis 2011).

By multiplying equation (3.9) from the left with the inverse of the normalized mass matrix:

$$\begin{bmatrix} 1 + \sigma & \gamma \\ 1 & 1 \end{bmatrix}^{-1} = \begin{bmatrix} \frac{1}{1 + \sigma - \gamma} & -\frac{\gamma}{1 + \sigma - \gamma} \\ -\frac{1}{1 + \sigma - \gamma} & \frac{1 + \sigma}{1 + \sigma - \gamma} \end{bmatrix} \quad (3.10)$$

the relative accelerations, $\ddot{u}_1(t)$ and $\ddot{u}_2(t)$, of each story become explicit expressions of the relative displacements, and velocities of the two stories

$$\ddot{u}_1(t) = -\frac{1 - \gamma}{\mu} \ddot{u}_g(t) - \frac{2\xi_1\omega_1}{\mu} \dot{u}_1(t) + \frac{2\gamma\xi_2\omega_2}{\mu} \dot{u}_2(t) - \frac{\omega_1^2}{\mu} u_1(t) + \frac{\gamma\omega_2^2}{\mu} u_2(t) \quad (3.11)$$

and

$$\ddot{u}_2(t) = -\frac{\sigma}{\mu} \ddot{u}_g(t) + \frac{2\xi_1\omega_1}{\mu} \dot{u}_1(t) - \frac{2(1 + \sigma)\xi_2\omega_2}{\mu} \dot{u}_2(t) + \frac{\omega_1^2}{\mu} u_1(t) - \frac{(1 + \sigma)\omega_2^2}{\mu} u_2(t) \quad (3.12)$$

The solution of the system of equations given by equations (3.11) and (3.12) is computed numerically via a state-space formulation (Konstantinidis and Makris 2005; Pitilakis and Makris 2010; Vassiliou and Makris 2012; Aghagholizadeh and Makris 2018 among the others). The state vector of the system is

$$\{y(t)\} = \begin{Bmatrix} y_1(t) \\ y_2(t) \\ y_3(t) \\ y_4(t) \end{Bmatrix} = \begin{Bmatrix} u_1(t) \\ \dot{u}_1(t) \\ u_2(t) \\ \dot{u}_2(t) \end{Bmatrix} \quad (3.13)$$

and the time-derivative state-vector, $\{\dot{y}(t)\}$ is expressed solely in terms of the state variables appearing in the state vector given by equation (3.13).

$$\{\dot{y}(t)\} = \begin{Bmatrix} \dot{u}_1(t) \\ \ddot{u}_1(t) \\ \dot{u}_2(t) \\ \ddot{u}_2(t) \end{Bmatrix} = \begin{Bmatrix} y_2(t) \\ \frac{1}{\mu} [-(1 - \gamma)\ddot{u}_g(t) - 2\xi_1\omega_1 y_2(t) + 2\gamma\xi_2\omega_2 y_4(t) - \omega_1^2 y_1(t) + \gamma\omega_2^2 y_3(t)] \\ y_4(t) \\ \frac{1}{\mu} [-\sigma\ddot{u}_g(t) + 2\xi_1\omega_1 y_2(t) - 2(1 + \sigma)\xi_2\omega_2 y_4(t) + \omega_1^2 y_1(t) - (1 + \sigma)\omega_2^2 y_3(t)] \end{Bmatrix} \quad (3.14)$$

where $\mu = 1 + \sigma - \gamma = 1 + (M_R - m_2) / (m_1 + m_2) > 0$.

With reference to Figure 3.1, the entire base-shear of the structure is

$$V_1(t) = k_1 u_1(t) + c_1 \dot{u}_1(t) + M_R \ddot{u}_1(t) = m_2 \ddot{u}_2(t) + (m_1 + m_2) (\ddot{u}_1(t) + \ddot{u}_g(t)) \quad (3.15)$$

Equation (3.15) brings forward the role of the inerter in association with the framing action of the first story since the base shear of the structure is proportional to the relative displacement, velocity and acceleration of the first story multiplied with the corresponding lateral stiffness, k_1 , damping constant, c_1 , and inertance, M_R .

3.4 TWO PARALLEL ROTATIONAL INERTIA SYSTEMS

The previous sections introduced the concept of supplemental rotational inertia for the seismic protection or retrofit of a 2DOF framing systems and it was shown that the proposed concept is physically realizable with the arrangement of one or more flywheels in series.

Equation (3.3) describes an undamped force-acceleration relation according to which part of the ground-induced energy is transferred in to the flywheels. Figure 3.3(a) plots the relative displacement, $u_1(t)$, velocity, $\dot{u}_1(t)$, force transferred to the first floor by the pinion (opposite of force transferred to the chevron frame given by equation (3.3),) and absolute acceleration of the first story show in Figure 3.1(a) with $T_1 = 1.0s$, $T_2 = 0.3s$, when subjected to a one-sine acceleration pulse with acceleration amplitude $a_p = 0.5g$ and pulse duration $T_p = 0.5s$. In the interest of simplicity in this analysis, zero damping is assumed ($\xi_1 = \xi_2 = 0$). The shaded stripes in Figure 3.3 correspond to the time-segments where the magnitude of the relative velocity of the first story, $\dot{u}_1(t)$, reduces on its way to reach a peak displacement. During this interval, the flywheels have built angular momentum and now, as the translating mass tends to move slower, the flywheels may drive the mass, therefore inducing deformations—a situation that is not desirable. One challenge with the proposed concept is that the rotating flywheels should only resist the motion of the structure without inducing any deformations. This is feasible with the use of a clutch so that the pinion of the first gearwheel that is engaged to the rack is unable to drive the rack and only the motion of the translating rack can drive the pinion-gearwheel (Makris and Kampas (2016)). This is similar to the motion of a bicycle, where the cyclist can drive the wheel through the pedals; yet, when the bicycle is rolling, the pedals may remain idle. Without loss of generality, assume that upon initiation of motion, the structure moves to the left; therefore, the front gearwheel rotates counterclockwise and the force on m_1 from the gearwheel is to the right (positive). As the mass, m_1 , keeps moving to the left, it will slow down and at the instant where the gearwheel will tend to drive m_1 due to its angular momentum, the force transmission needs to become idle. With the proposed arrangement, upon m_1 reaching its first maximum displacement, to the left $[\dot{u}_1(t)] < 0$; the front gearwheel keeps rotating freely counterclockwise without inducing any force to the structure. When the motion reverses and the structure starts moving to the right $[\dot{u}_1(t)] > 0$, a second, parallel rotational inertia system (back flywheels) is needed to oppose the motion, and during the course of this motion, the first gearwheel of the back system engaged to the rack and rotates clockwise. The sequential engagement of the two parallel rotational inertial systems that can only resist the motion is expressed mathematically as

$$\frac{F_I(t)}{m_1 + m_2} = \sigma \ddot{u}_1(t) \quad \text{when} \quad \text{sgn} \left[\frac{\ddot{u}_1(t)}{\dot{u}_1(t)} \right] > 0 \quad (3.16a)$$

$$T_1 = 2T_p = 1s, T_2 = 0.3s, \sigma = 0.5, \xi_1 = \xi_2 = 0, \gamma = 0.5$$

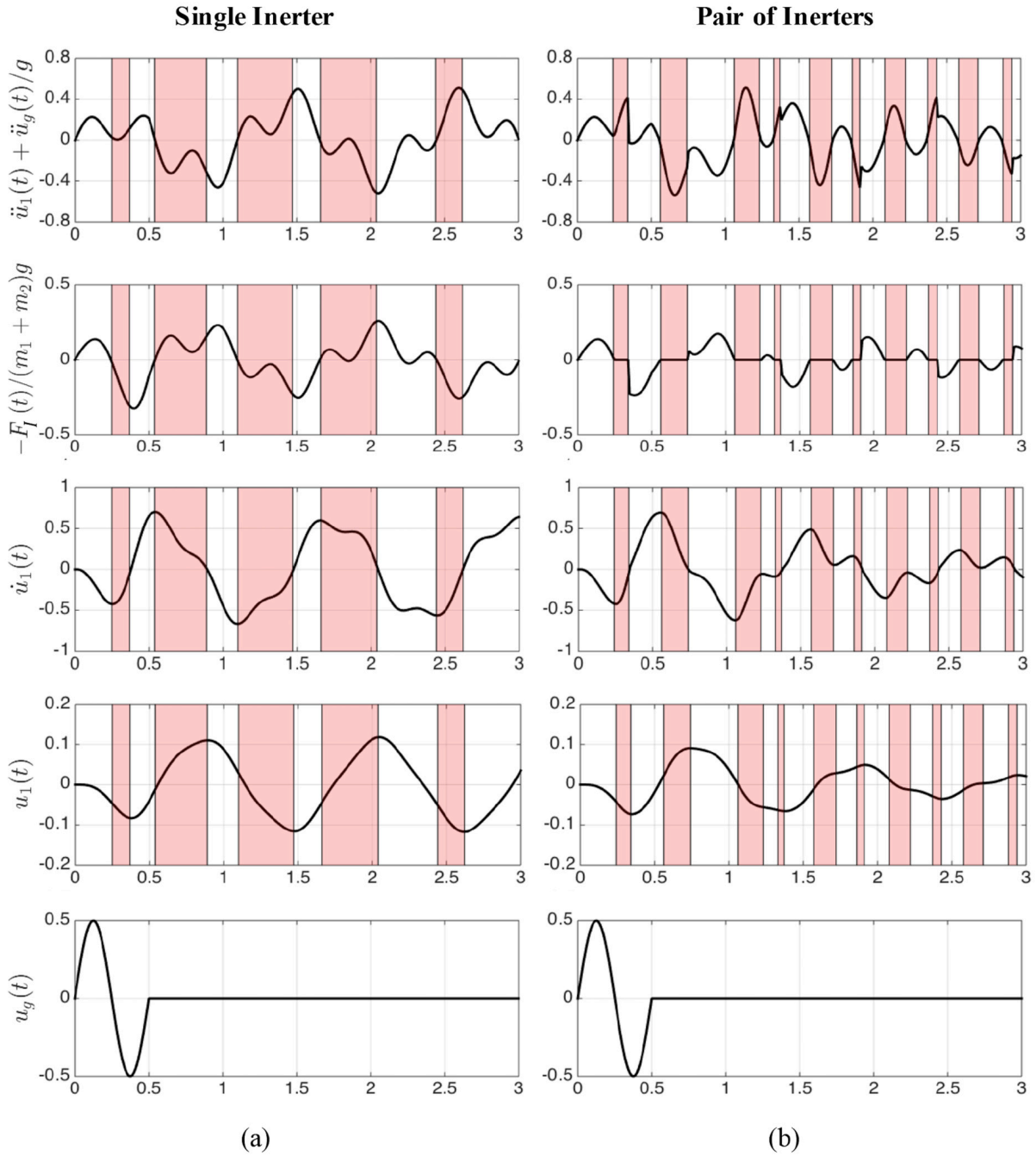


Figure 3.3: Response of a 2DOF structure that is engaged to an inerter at the first story supported on an infinite stiff chevron frame: (a) single inerter which may induce deformation; (b) pair of inerters that can only resist the motion as described by equations (3.14) and (3.16a); force from the inerter only opposes the motion.

and

$$\frac{F_I(t)}{m_1 + m_2} = 0 \quad \text{when } \text{sgn} \left[\frac{\ddot{u}_1(t)}{\dot{u}_1(t)} \right] < 0 \quad (3.16b)$$

Accordingly, for the two parallel rotational inertia systems that only resist the motion of the structure, the equation of motion given in equation (3.9) is modified to

$$\begin{bmatrix} 1 + \delta\sigma & \gamma \\ 1 & 1 \end{bmatrix} \begin{Bmatrix} \ddot{u}_1(t) \\ \ddot{u}_2(t) \end{Bmatrix} + \begin{bmatrix} 2\xi_1\omega_1 & 0 \\ 0 & 2\xi_2\omega_2 \end{bmatrix} \begin{Bmatrix} \dot{u}_1(t) \\ \dot{u}_2(t) \end{Bmatrix} + \begin{bmatrix} \omega_1^2 & 0 \\ 0 & \omega_2^2 \end{bmatrix} \begin{Bmatrix} u_1(t) \\ u_2(t) \end{Bmatrix} = - \begin{Bmatrix} 1 \\ 1 \end{Bmatrix} \ddot{u}_g(t) \quad (3.17)$$

in which

$$\delta = \begin{cases} 1, & \text{when } \text{sgn} \left[\frac{\ddot{u}_1(t)}{\dot{u}_1(t)} \right] > 0 \\ 0, & \text{when } \text{sgn} \left[\frac{\ddot{u}_1(t)}{\dot{u}_1(t)} \right] < 0 \end{cases} \quad (3.18)$$

Clearly, with the two parallel front and back rotational inertia systems, the flywheels only resist the motion of the structure and do not give back any energy to the structure. During the time-period when one of the flywheel systems is rotating idle, its rotation needs to decelerate appreciably so that when it is again engaged into motion, it will be capable of resisting the motion through its rotational inertia. This can be achieved by appending an induction generator to the axis of the flywheel, therefore the opportunity for energy harvesting. With this arrangement, part of the earthquake-induced energy is converted into electricity.

3.5 RESPONSE SPECTRA OF THE 2DOF STRUCTURE WITH A STIFF CHEVRON FRAME

The seismic response of the 2DOF structure equipped with an inerter at the first story as described by equation (3.9) or equations (3.17) and (3.18) is compared with the seismic response of the same 2DOF structure where the inerter is replaced with a supplemental viscous damper. In this case the value of the damping coefficient $C_1 = C_c + C_d$, where C_c is the damping originating from the first-story columns and C_d is the damping originating from the supplemental viscous damper. Together with the drift responses u_1 and u_2 (relative displacements), of interest are the total acceleration of the first story, $\ddot{u}_1 + \ddot{u}_g$, the total acceleration of second story, $\ddot{u}_1 + \ddot{u}_2 + \ddot{u}_g = V_2/m_2$, which is the normalized shear force just above the first story, the total base shear of the structure given by equation (3.15) and the normalized force transferred to the mounting of the flywheel, $F_I(t) / (m_1 + m_2) g$, or to the mounting of the supplemental damper, $c_d \dot{u}_1 / (m_1 + m_2) g = 2\xi_d \omega_1 \dot{u}_1 / g$.

Figure 3.4 shows the recorded acceleration time-histories used for the response spectrum analysis presented in this study: (a) The Gilroy Array 6/230 ground motion recorded during the 1979 Coyote Lake, USA earthquake and (b) The Takarazuka/000 ground motion recorded during the 1995 Kobe, Japan earthquake.

The response spectra shown in Figures 3.5, and 3.6 are the results of the solution of equation (3.9) for a single inerter (left plots) or equations (3.17) and (3.18) when a pair of inerters is used (right plots). When $\sigma = 0$ (thin line), the solution offers the response of the structural systems

shown in Figures 3.1(b) and 3.1(c). For the structural system shown in Figures 3.1(a) values of the normalized inertance $\sigma = 0.5$ and $\sigma = 1.0$ are used. For the structural system shown in Figure 3.1(b) values of $\xi_c = 2\%$ and $\xi_d = 23\%$ are used so that $\xi_1 = \xi_c + \xi_d = 0.02 + 0.23 = 0.25$. In all spectra, the period of the superstructure is $T_2 = 0.2 \text{ sec}$, with viscous damping ratio $\xi_2 = 0.02$, and mass ratio, $\gamma = 0.5$. Figure 3.5 presents response spectra for the three configurations of the 2DOF structure shown in Figure 3.1(a), (b) and (c) when subjected to the GilroyArray 6/230 ground motion recorded during the 1979 Coyote Lake, USA earthquake. Across the spectra we indicate two shaded strips. The first strip is for $0.5s \leq T_1 \leq 1.0s$ and it represents the period range of T_1 for a 2DOF structure with the first story being a pilotis. The second shaded strip in the long period range, $T_1 \geq 2.0s$, corresponds to seismic isolated structures.

The first observation in Figure 3.5 is that supplemental rotational inertia is most effective in suppressing the displacement of the first story, u_1 , in particular for long period structures. When two parallel rotational inertia systems (pair of inerters, right plots) are used, the effectiveness of supplemental rotational inertia (Figure 3.1(a)) in suppressing u_1 outperforms the effectiveness of large values of supplemental damping ($\xi_1 = 25\%$) along the entire frequency range. At the same time, in the period range $0.5s \leq T_1 \leq 1.0s$ the base shear of the entire structure, V_1 , is lower when supplemental rotational inertia is used. This situation reverses in the neighborhood of $T_1 = 1.5s$ upon which supplemental damping results in lower base shears. At the same time the forces transferred at the support of the flywheels (chevron frame) are appreciable; however, when a pair of inerters is used these forces are comparable to the case where large values of supplemental damping is used (see bottom plots of Figure 3.5).

In view of the results presented in Figure 3.5, supplemental rotational inertia ($0.5 \leq \sigma \leq 1.0$), emerges as an attractive alternative to suppress both displacements and base shears of structures supported on pilotis—that is $0.5s \leq T_1 \leq 1.0s$. Among the three configurations examined, seis-

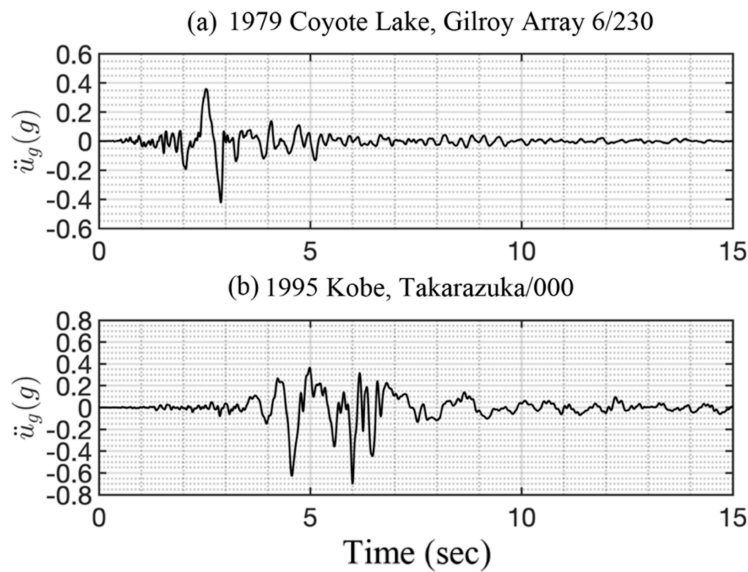


Figure 3.4: Acceleration time histories recorded during (a) 1979 Coyote Lake, California earthquake; and (b) 1995 Kobe, Japan earthquake.

1979 Coyote Lake, Gilroy Array 6/230

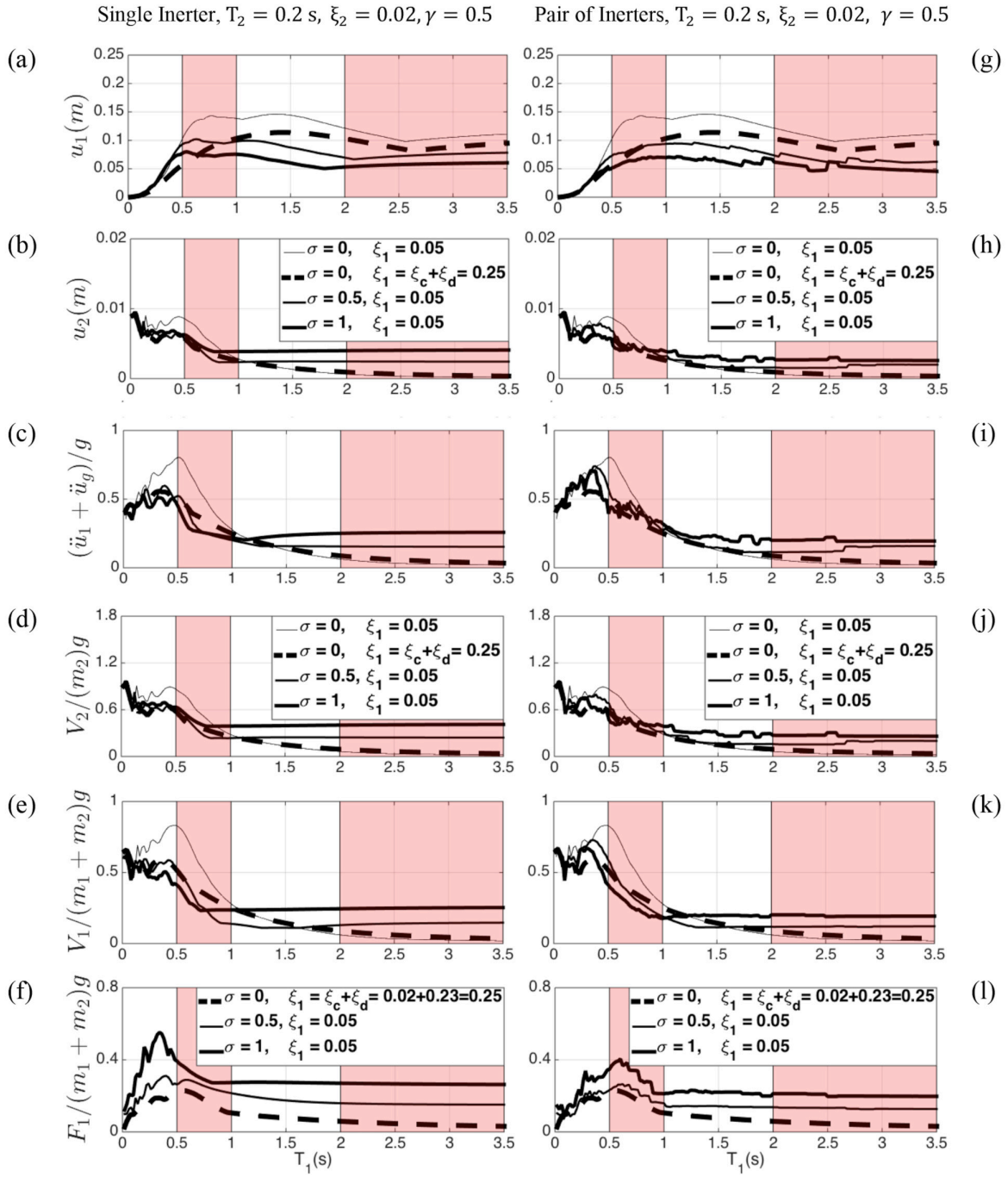


Figure 3.5: Response spectra of a two-degree-of-freedom (2DOF) structure equipped with supplemental rotational inertia (heavy solid lines) or supplemental damping (dashed lines) supported on a stiff frame when excited by the Gilroy Array 6/230 ground motion recorded during the 1979 Coyote Lake, USA earthquake.

1995 Kobe Takarazuka/000

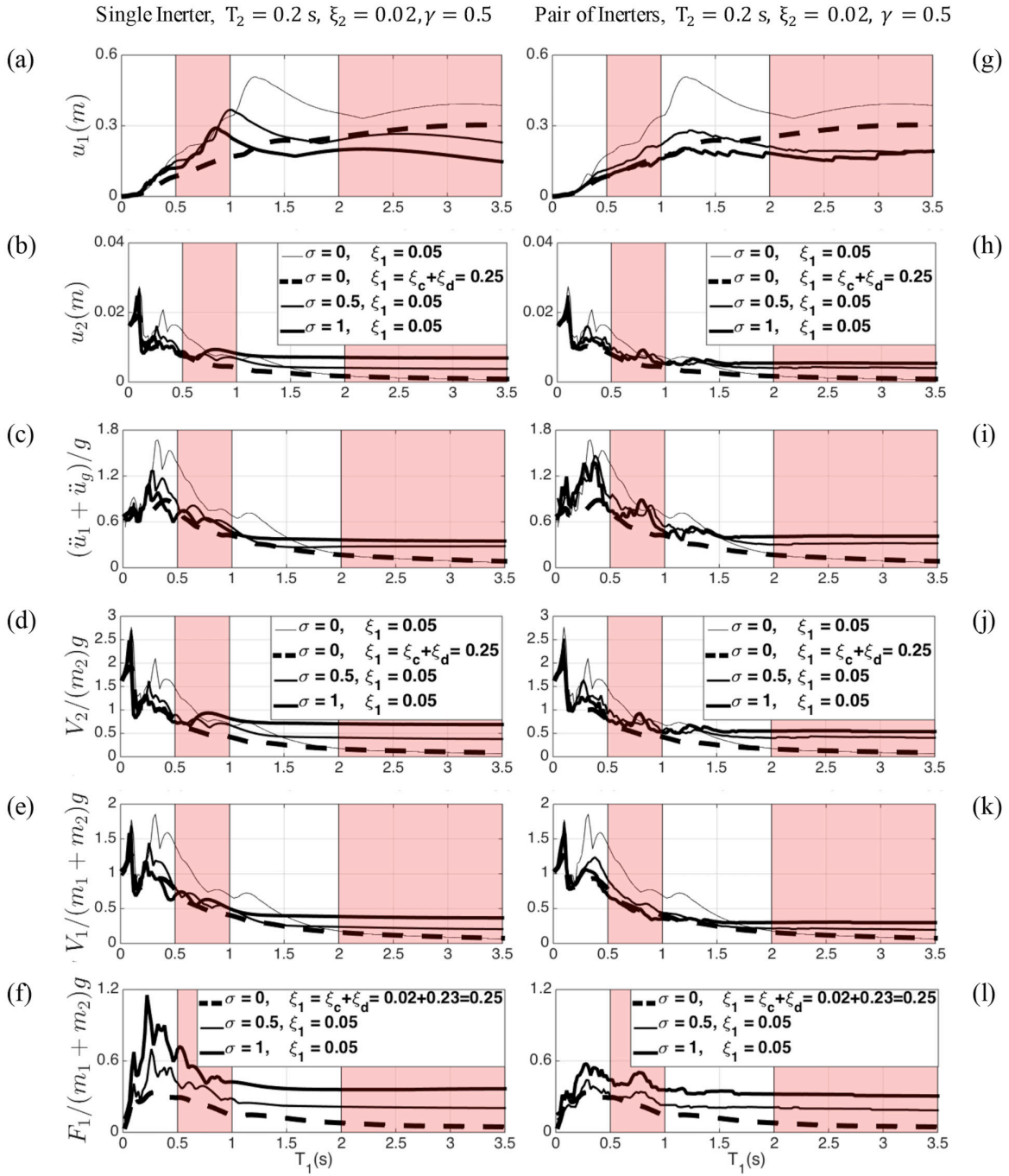


Figure 3.6: Response spectra of a two-degree-of-freedom (2DOF) structure equipped with supplemental rotational inertia (heavy solid lines) or supplemental damping (dashed lines) supported on a stiff frame when excited by Takarazuka /000 ground motion recorded during the 1995 Kobe, Japan earthquake.

mic isolation ($T_1 \geq 2.0s$) is most effective in reducing floors accelerations and base shears at the expense of producing the largest displacements, u_1 . However, isolation systems are designed to accommodate these high displacements above isolators. Figure 3.6 presents response spectra for the three configurations of the 2DOF structure shown in Figure 3.1(a), (b) and (c) when subjected to the Takarazuka/000 ground motion recorded during the 1995, Kobe Japan earthquake and reveals similar trends as those observed from the response spectra shown in Figure 3.5.

3.6 EQUATIONS OF MOTION OF A 2DOF STRUCTURE WITH A COMPLIANT CHEVRON FRAME WITH FINITE STIFFNESS AND DAMPING

Now the case where the chevron frame that supports the rotational inertia system shown in Figure 3.1(a) has a finite stiffness, k_f , and damping constant, c_f , is considered. Because of its compliance, under the force transferred by the mounting of the flywheel, the chevron frame deforms and this deformation, influences the resisting force, $F_I(t)$, from the flywheel. Accordingly, $F_I(t)$, is no longer expressed with equation (3.3)—that is for a rigid chevron frame, but from (Makris and Kampas 2016; Makris 2018).

$$F_I(t) + \frac{c_f}{k_f} \frac{dF_I(t)}{dt} + \frac{M_R}{k_f} \frac{d^2F_I(t)}{dt^2} = M_R \left(\frac{d^2u_1(t)}{dt^2} + \frac{c_f}{k_f} \frac{d^3u_1(t)}{dt^3} \right) \quad (3.19)$$

Equation (3.19) is the constitutive law of a spring-dashpot parallel connection (k_f , c_f) that is connected in series with an inerter (M_R). This mechanical network is also known as the tuned inerter damper (TID) (Lazar et al. 2014), and was coined recently as the inertoviscoelastic fluid A (Makris and Kampas 2016). The term fluid expresses that the network undergoes infinite displacement under a static loading. By defining the relaxation time, $\lambda = c_f/k_f$ and the rotational frequency $\omega_R = \sqrt{k_f/M_R}$ (Makris 2017, 2018), equation (3.19) assumes the form.

$$F_I(t) + \lambda \frac{dF_I(t)}{dt} + \frac{1}{\omega_R^2} \frac{d^2F_I(t)}{dt^2} = M_R \left(\frac{d^2u_1(t)}{dt^2} + \lambda \frac{d^3u_1(t)}{dt^3} \right) \quad (3.20)$$

Clearly the product $\lambda\omega_R$ is dimensionless. The mechanical system described by equation (3.20) becomes critically damped when $\lambda\omega_R = 2$ (Makris 2018). In the special case where the damping within the chevron frame is neglected, $c_f = 0$, equation (3.20) reduces to

$$F_I(t) + \frac{1}{\omega_R^2} \frac{d^2F_I(t)}{dt^2} = M_R \frac{d^2u_1(t)}{dt^2} \quad (3.21)$$

which is the constitutive equation of the inertoelastic fluid (Makris 2017).

The equations of motion of the 2DOF structure shown in Figure 3.1 are given by equations (3.4) and (3.5); however, now for the case of a chevron frame with finite stiffness, k_f , and damping, c_f , the force from the flywheel, $F_I(t)$ appearing in equation (3.3) is described by equation (3.20).

By using the frequencies, damping, mass and inertance ratios defined by equations (3.6) to (3.8), the equations of motion of the 2DOF structure shown in Figure 3.1(a) with a compliant chevron frame with finite stiffness, k_f , and damping, $c_f = \lambda k_f$ can be expressed in matrix form.

$$\begin{bmatrix} 1 & \gamma \\ 1 & 1 \end{bmatrix} \begin{Bmatrix} \ddot{u}_1(t) \\ \ddot{u}_2(t) \end{Bmatrix} + \begin{bmatrix} 2\xi_1\omega_1 & 0 \\ 0 & 2\xi_2\omega_2 \end{bmatrix} \begin{Bmatrix} \dot{u}_1(t) \\ \dot{u}_2(t) \end{Bmatrix} + \begin{bmatrix} \omega_1^2 & 0 \\ 0 & \omega_2^2 \end{bmatrix} \begin{Bmatrix} u_1(t) \\ u_2(t) \end{Bmatrix} = - \begin{bmatrix} 1 & 1 \\ 0 & 1 \end{bmatrix} \begin{Bmatrix} \frac{F_I(t)}{m_1+m_2} \\ \ddot{u}_g(t) \end{Bmatrix} \quad (3.22)$$

in which $F_I(t)$ is solution of equation (3.20).

By multiplying equation (23) from the left with the inverse of the normalized mass matrix

$$\begin{bmatrix} 1 & \gamma \\ 1 & 1 \end{bmatrix}^{-1} = \begin{bmatrix} \frac{1}{1-\gamma} & -\frac{\gamma}{1-\gamma} \\ -\frac{1}{1-\gamma} & \frac{1}{1-\gamma} \end{bmatrix} \quad (3.23)$$

the relative accelerations, $\ddot{u}_1(t)$ and $\ddot{u}_2(t)$ are expressed as

$$\ddot{u}_1(t) = -\frac{1}{1-\gamma} f_I(t) - \ddot{u}_g(t) - \frac{2\xi_1\omega_1}{1-\gamma} \dot{u}_1(t) + \frac{2\gamma\xi_2\omega_2}{1-\gamma} \dot{u}_2(t) - \frac{\omega_1^2}{1-\gamma} u_1(t) + \frac{\gamma\omega_2^2}{1-\gamma} u_2(t) \quad (3.24)$$

and

$$\ddot{u}_2(t) = \frac{1}{1-\gamma} f_I(t) + \frac{2\xi_1\omega_1}{1-\gamma} \dot{u}_1(t) - \frac{2\xi_2\omega_2}{1-\gamma} \dot{u}_2(t) + \frac{\omega_1^2}{1-\gamma} u_1(t) - \frac{\omega_2^2}{1-\gamma} u_2(t) \quad (3.25)$$

where $f_I(t) = F_I(t) / (m_1 + m_2)$ has units of acceleration.

In this case, the state vector of the system is

$$\{y(t)\} = \begin{Bmatrix} y_1(t) \\ y_2(t) \\ y_3(t) \\ y_4(t) \\ y_5(t) \\ y_6(t) \end{Bmatrix} = \begin{Bmatrix} u_1(t) \\ \dot{u}_1(t) \\ u_2(t) \\ \dot{u}_2(t) \\ f_I(t) \\ \dot{f}_I(t) \end{Bmatrix} \quad (3.26)$$

From equation (3.20) it is evident that the time-derivative of $y_6(t)$, that is $\dot{y}_6(t) = \ddot{f}_I(t)$, involves the third derivative of $u_1(t)$ which is given by

$$\ddot{u}_1(t) = -\frac{1}{1-\gamma} \dot{f}_I(t) - \ddot{u}_g(t) - \frac{2\xi_1\omega_1}{1-\gamma} \dot{u}_1(t) + \frac{2\gamma\xi_2\omega_2}{1-\gamma} \dot{u}_2(t) - \frac{\omega_1^2}{1-\gamma} u_1(t) + \frac{\gamma\omega_2^2}{1-\gamma} u_2(t) \quad (3.27)$$

In terms of the state variables given by equation (27), equation (28) assumes the form

$$\begin{aligned} \ddot{u}_1(t) = & -\left(\frac{1}{1-\gamma} y_6(t) + \ddot{u}_g(t)\right) \\ & - \frac{2\xi_1\omega_1}{1-\gamma} \left(-\frac{1}{1-\gamma} y_5(t) - \ddot{u}_g(t) - \frac{2\xi_1\omega_1}{1-\gamma} y_2(t) + \frac{2\gamma\xi_2\omega_2}{1-\gamma} y_4(t) - \frac{\omega_1^2}{1-\gamma} y_1(t) + \frac{\gamma\omega_2^2}{1-\gamma} y_3(t)\right) \\ & + \frac{2\gamma\xi_2\omega_2}{1-\gamma} \left(\frac{1}{1-\gamma} y_5(t) + \frac{2\xi_1\omega_1}{1-\gamma} y_2(t) - \frac{2\xi_2\omega_2}{1-\gamma} y_4(t) + \frac{\omega_1^2}{1-\gamma} y_1(t) - \frac{\omega_2^2}{1-\gamma} y_3(t)\right) \\ & - \frac{\omega_1^2}{1-\gamma} y_2(t) + \frac{\gamma\omega_2^2}{1-\gamma} y_4(t) \end{aligned} \quad (3.28)$$

The solution of the system of differential equations given by equations (3.20), (3.24) and (3.25) is computed by integrating the time-derivative of the state vector given by equation (3.26)

$$\{\dot{y}(t)\} = \begin{Bmatrix} \dot{u}_1(t) \\ \ddot{u}_1(t) \\ \dot{u}_2(t) \\ \ddot{u}_2(t) \\ \dot{f}_I(t) \\ \ddot{f}_I(t) \end{Bmatrix} = \begin{Bmatrix} y_2(t) \\ -\frac{1}{1-\gamma} y_5(t) - \ddot{u}_g(t) - \frac{2\xi_1\omega_1}{1-\gamma} y_2(t) + \frac{2\gamma\xi_2\omega_2}{1-\gamma} y_4(t) - \frac{\omega_1^2}{1-\gamma} y_1(t) + \frac{\gamma\omega_2^2}{1-\gamma} y_3(t) \\ y_4(t) \\ \frac{1}{1-\gamma} y_5(t) + \frac{2\xi_1\omega_1}{1-\gamma} y_2(t) - \frac{2\xi_2\omega_2}{1-\gamma} y_4(t) + \frac{\omega_1^2}{1-\gamma} y_1(t) - \frac{\omega_2^2}{1-\gamma} y_3(t) \\ y_6(t) \\ \omega_R^2 \sigma (\dot{u}_1(t) + \lambda \ddot{u}_1(t)) - \omega_R^2 y_5(t) - \omega_R^2 \lambda y_6(t) \end{Bmatrix} \quad (3.29)$$

In the last row of equation (3.29), the acceleration of the first story, $\ddot{u}_1(t)$, is given by the second row of equation (3.29) and the derivative of the acceleration, $\dot{\ddot{u}}_1(t)$, is given by equation (3.28). The numerical integration of equation (3.29) is performed with standard ordinary differential equation (ODE) solvers available in MATLAB¹.

Alternatively, given that equations (3.24), (3.25) and (3.20) are linear differential equations, the response history of the 2DOF structure shown in Figure 3.1 can be computed with frequency domain analysis. The Fourier transform of equation (3.20) gives

$$f_I(\omega) = \frac{F_I(\omega)}{m_1 + m_2} = \frac{-\sigma\omega^2(1+i\omega\lambda)}{1+i\omega\lambda - \frac{\omega^2}{\omega_R^2}} u_1(\omega) \quad (3.30)$$

whereas the Fourier transform of equations (3.24) and (3.25) give

$$\left[\omega^2 - \frac{2\xi_1 i \omega_1 \omega}{1-\gamma} - \frac{\omega_1^2}{1-\gamma} - \frac{-\sigma\omega^2(1+i\omega\lambda)}{1-\gamma\left(1+i\omega\lambda - \frac{\omega^2}{\omega_R^2}\right)} \right] u_1(\omega) + \left[\frac{2\gamma\xi_2 i \omega_2 \omega}{1-\gamma} + \frac{\gamma\omega_2^2}{1-\gamma} \right] u_2(\omega) - \left[\frac{1}{1-\gamma} \right] f_I(\omega) = \ddot{u}_g(\omega) \quad (3.31)$$

and

$$\left[\frac{2\xi_1 i \omega_1 \omega}{1-\gamma} + \frac{\omega_1^2}{1-\gamma} + \frac{-\sigma\omega^2(1+i\omega\lambda)}{1+i\omega\lambda - \frac{\omega^2}{\omega_R^2}} \right] u_1(\omega) + \left[\omega^2 - \frac{2\xi_2 i \omega_2 \omega}{1-\gamma} - \frac{\omega_2^2}{1-\gamma} \right] u_2(\omega) + \left[\frac{1}{1-\gamma} \right] f_I(\omega) = 0 \quad (3.32)$$

Substitution of the expression for $f_I(\omega)$ given by equation (3.30) into equations (3.31) and (3.32) the solution of the system of equations (3.31) and (3.32) gives

$$u_1(\omega) = \frac{B_2(\omega)}{A_1(\omega) B_2(\omega) - A_2(\omega) B_1(\omega)} \ddot{u}_g(\omega) \quad (3.33)$$

$$u_2(\omega) = \frac{B_1(\omega)}{A_2(\omega) B_1(\omega) - A_1(\omega) B_2(\omega)} \ddot{u}_g(\omega) \quad (3.34)$$

where

$$A_1(\omega) = \omega^2 - \frac{2\xi_1 i \omega_1 \omega}{1-\gamma} - \frac{\omega_1^2}{1-\gamma} - \frac{-\sigma\omega^2(1+i\omega\lambda)}{1-\gamma\left(1+i\omega\lambda - \frac{\omega^2}{\omega_R^2}\right)} \quad (3.35a)$$

$$A_2(\omega) = \frac{2\gamma\xi_2 i \omega_2 \omega}{1-\gamma} + \frac{\gamma\omega_2^2}{1-\gamma} \quad (3.35b)$$

$$B_1(\omega) = \frac{2\xi_1 i \omega_1 \omega}{1-\gamma} + \frac{\omega_1^2}{1-\gamma} + \frac{-\sigma\omega^2(1+i\omega\lambda)}{1+i\omega\lambda - \frac{\omega^2}{\omega_R^2}} \quad (3.36a)$$

¹ MATLAB. (2021). High performance numerical computation and visualization software. The Math works, Natick, Mass.

$$B_2(\omega) = \omega^2 - \frac{2\xi_2 i \omega_2 \omega}{1 - \gamma} - \frac{\omega_2^2}{1 - \gamma} \quad (3.36b)$$

and the time-domain solution for the responses of stories 1 and 2 is given by the inverse Fourier transform

$$u_j(t) = \frac{1}{2\pi} \int_{-\infty}^{\infty} u_j(\omega) e^{i\omega t} d\omega, \quad j \in \{1, 2\} \quad (3.37)$$

When a single rotational inertia system is used, the frequency domain solution given by equation (3.37) is attractive since it does not involve the numerical differentiation of the ground acceleration which in most cases is only available in digital form (i.e. acceleration recordings). The agreement between the time-domain solution by integrating the derivative of the state-vector given by equation (3.29) and the frequency domain solution given by equation (3.37) has been confirmed during the course of this study.

When the two parallel rotational inertia system (pair of inerters) is employed that can only resist the motion of the structure without inducing any deformation (the pinion of the gearwheel that is engaged in the rack of the first story is unable to drive the rack and only the motion of the translating rack can drive the pinion), the normalized force, $f_1(t) = F_I(t) / (m_1 + m_2)$ appearing in equations (3.24) and (3.25) is given by equation (3.20) when $\text{sgn} [\ddot{u}_1(t) / \dot{u}_1(t)] \geq 0$ and by

$$f_1(t) = \frac{F_I(t)}{m_1 + m_2} = 0 \quad \text{when} \quad \text{sgn} \left[\frac{\ddot{u}_1(t)}{\dot{u}_1(t)} \right] < 0 \quad (3.38)$$

In the case when $f_I(t) = 0$, the equations of motion of our 2DOF structure become piecewise linear and only a time-domain solution is feasible. The state vector of the system is given by equation (3.29) when $\text{sgn} [\ddot{u}_1(t) / \dot{u}_1(t)] > 0$ and by

$$\{\dot{y}(t)\} = \begin{Bmatrix} \dot{u}_1(t) \\ \dot{u}_1(t) \\ \dot{u}_2(t) \\ \dot{u}_2(t) \end{Bmatrix} = \begin{Bmatrix} y_2(t) \\ -\ddot{u}_g(t) - \frac{2\xi_1\omega_1}{1-\gamma} y_2(t) + \frac{2\gamma\xi_2\omega_2}{1-\gamma} y_4(t) - \frac{\omega_1^2}{1-\gamma} y_1(t) + \frac{\gamma\omega_2^2}{1-\gamma} y_3(t) \\ y_4(t) \\ -\ddot{u}_g(t) - \frac{2\xi_1\omega_1}{1-\gamma} y_2(t) + \frac{2\gamma\xi_2\omega_2}{1-\gamma} y_4(t) - \frac{\omega_1^2}{1-\gamma} y_1(t) + \frac{\gamma\omega_2^2}{1-\gamma} y_3(t) \end{Bmatrix} \quad (3.39)$$

when $\text{sgn} [\ddot{u}_1(t) / \dot{u}_1(t)] < 0$.

The response of the 2DOF structure with supplemental rotational inertia shown in Figure 3.1(a) with a compliant chevron frame with finite stiffness, k_f and damping c_f is compared with the response of a heavily damped 2DOF structure with supplemental viscous damping at the first story with damping constant $c_d = 2\xi_d\omega_1(m_1 + m_2)$. The mechanical network of a spring-dashpot parallel connection (k_f, c_f) that is connected in series with a dashpot (c_d) is known as the Jeffreys fluid (Jeffreys 1929; Bird et al. 1987; Makris and Kampas 2016) and its constitutive law is

$$F_I(t) + \frac{c_d + c_f}{k_f} \frac{dF_I(t)}{dt} = c_d \left[\frac{du_1(t)}{dt} + \frac{c_f}{k_f} \frac{d^2u_1(t)}{dt^2} \right] \quad (3.40)$$

By defining the relaxation time $\lambda_d = (c_d + c_f)/k_f$ and recognizing that $c_f/k_f = \lambda$, (3.40) assumes the form

$$f_I(t) + \lambda_d \frac{df_I(t)}{dt} = 2\xi_d \omega_1 \left[\frac{du_1(t)}{dt} + \lambda \frac{d^2 u_1(t)}{dt^2} \right] \quad (3.41)$$

where again $f_I(t) = F_I(t)/(m_1 + m_2)$.

For the case of a 2DOF structure with supplemental damping supported by a compliant chevron frame with finite stiffness shown in Figure 3.1(b), the state-vector of the system is

$$\{y(t)\} = \begin{Bmatrix} y_1(t) \\ y_2(t) \\ y_3(t) \\ y_4(t) \\ y_5(t) \end{Bmatrix} = \begin{Bmatrix} u_1(t) \\ \dot{u}_1(t) \\ u_2(t) \\ \dot{u}_2(t) \\ f_I(t) \end{Bmatrix} \quad (3.42)$$

The solution of the system of differential equations given by equations (3.24), (3.25) and (3.41) is computed by integrating the time-derivative of the state-vector given by equation (3.42)

$$\{\dot{y}(t)\} = \begin{Bmatrix} \dot{u}_1(t) \\ \ddot{u}_1(t) \\ \dot{u}_2(t) \\ \ddot{u}_2(t) \\ \dot{f}_I(t) \end{Bmatrix} = \begin{Bmatrix} y_2(t) \\ -\frac{1}{1-\gamma} y_5(t) - \ddot{u}_g(t) - \frac{2\xi_1 \omega_1}{1-\gamma} y_2(t) + \frac{2\gamma \xi_2 \omega_2}{1-\gamma} y_4(t) - \frac{\omega_1^2}{1-\gamma} y_1(t) + \frac{\gamma \omega_2^2}{1-\gamma} y_3(t) \\ y_4(t) \\ \frac{1}{1-\gamma} y_5(t) + \frac{2\xi_1 \omega_1}{1-\gamma} y_2(t) - \frac{2\xi_2 \omega_2}{1-\gamma} y_4(t) + \frac{\omega_1^2}{1-\gamma} y_1(t) - \frac{\omega_2^2}{1-\gamma} y_3(t) \\ \frac{1}{\lambda_d} [-y_5(t) + 2\xi_d \omega_1 (y_2(t) + \lambda (\ddot{u}_1(t)))] \end{Bmatrix} \quad (3.43)$$

3.7 RESPONSE SPECTRA OF THE 2DOF STRUCTURE WITH A COMPLIANT CHEVRON FRAME WITH FINITE STIFFNESS AND DAMPING

The response spectrum shown in Figure 3.7 are the results of the solution of equation (3.29) (single inerter with a time-domain formulation) or equation (3.37) (single inerter with a frequency domain formulation) and equations (3.29) and (3.39) when a pair of inerters is used. Again, when $\sigma = 0$ (thin line), the solution offers the response of the structural systems shown in Figures 3.1(b) and (c). For the structural system shown in Figure 3.1(a), values of the normalized inertance, $\sigma = 0.5$ and $\sigma = 1.0$ are used. The compliance of the chevron frame is expressed with the relaxation time, $\lambda = c_f/k_f = 0.05$, while the stiffness of the chevron frame compared to the supplemental inertance M_R , is expressed with the dimensionless product $\lambda \omega_R = 0.5$. For the structural system shown in Figure 3.1(b), values of $\xi_c = 2\%$ and $\xi_d = 23\%$ are used so that $\xi_1 = \xi_c + \xi_d = 0.02 + 0.23 = 0.25$. When supplemental damping c_d , is used, the compliance of the chevron frame is $\lambda_d = (c_d + c_f)/k_f = 0.5$. In all spectra, the period of the superstructure is $T_2 = 0.2s$ with viscous damping ratio $\xi_2 = 0.02$ and mass ratio $\gamma = 0.5$. Figure 3.7 presents response spectra for the three configuration of the 2DOF structure shown in Figure 3.1 when the chevron frame has finite stiffness k_f and damping c_f and is subjected to the Gilroy Array 6/230 ground motion recorded during the 1979 Coyote Lake, USA earthquake. Across the spectra we indicate the same two shaded strips as explained when discussing the spectra shown in Figure 3.5. The first observation in Figure 3.7 is that even when a compliant chevron frame is used, supplemental rotational inertia remains on effective strategy in suppressing displacements of the first story, $u_1(t)$, along the entire frequency

1979 Coyote Lake, Gilroy Array 6/230

$$T_2 = 0.2 \text{ s}, \xi_2 = 0.02, \gamma = 0.5, \lambda = 0.05 \text{ s}, \lambda_d = 0.5 \text{ s}, \lambda\omega_R = 0.5$$

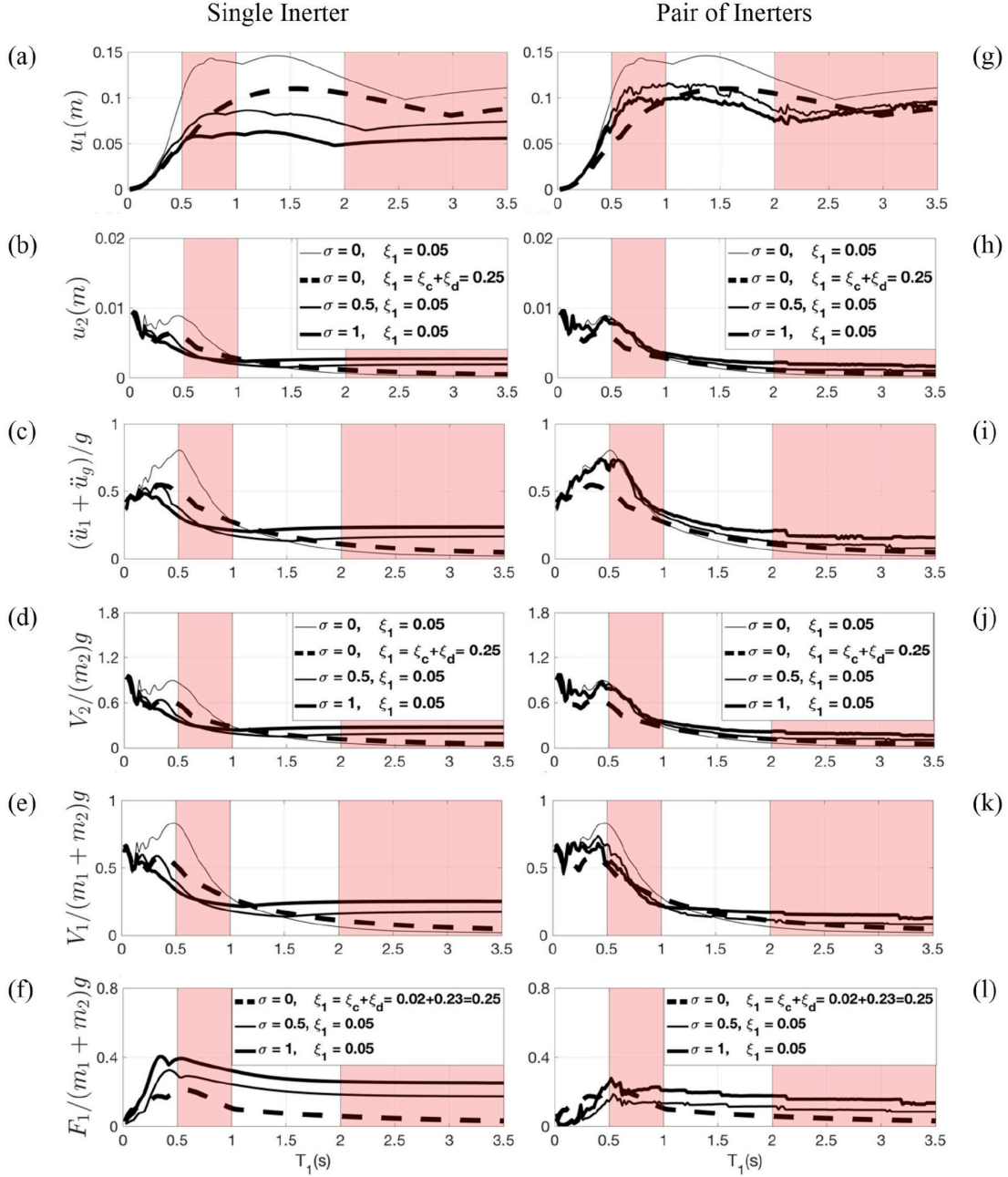


Figure 3.7: Response spectra of a two-degree-of-freedom (2DOF) structure equipped with supplemental rotational inertia (heavy solid lines) or supplemental damping (dashed lines) supported on a compliant frame ($\lambda = 0.05\text{s}$, $\lambda_d = 0.5\text{s}$, $\lambda\omega_R = 0.5$) when excited by the Gilroy Array 6/230 ground motion recorded during the 1979 Coyote Lake, USA earthquake.

range. Interestingly, Figure 3.7 reveals, that the compliance of the chevron frame reduces the effectiveness of the pair of inerters (right plots) when compared to the case of a single inverter (left plots) which produces the most favorable response other than increasing the forces transferred to the chevron frame (bottom plots). In summary, the results presented in Figure 3.7 in association with the results presented in Figures 3.5 and 3.6 (for a stiff chevron frame) reveal that supplemental rotational inertia is an effective response modification strategy for controlling the response of a structure with a soft first-story at the expense of transferring appreciable forces at the support of the inverter. Accordingly, assuming that the chevron frame is properly designed, supplemental rotational inertia is a competitive alternative to the use of supplemental damping, in particular for cases with large relative displacement demands.

3.8 CONCLUSIONS

This chapter investigates the potential advantages of using supplemental rotational inertia for the seismic protection of moment-resisting frames. The chapter examines the response of a 2DOF structure where the first story employs a rack-pinion-flywheel system whose resisting force is proportional to the relative acceleration between the vibrating mass and the support of the flywheels. Both cases of a stiff and a compliant support of the inverter are examined and the corresponding equations of motion have been derived. The chapter shows that the supplemental rotational inertia controls effectively the displacements of the first story along a wide range of the response spectrum. Furthermore, the proposed seismic protection strategy can accommodate large relative displacements without suffering from the issue of viscous heating (Makris 1998; Makris et al. 1998; Black and Makris 2007) and potential leaking that challenges the implementation of fluid dampers under prolonged cyclic loading.

The chapter also examines the dynamic response of the 2DOF structure when two parallel rotational inertia systems are installed so that they can only resist the motion of the structure without inducing any deformation. This can be achieved with a pair of inerters and the use of a simple clutch (Makris and Kampas 2016). When the chevron frame that supports the rotational inertia system is stiff, the use of two parallel rotational inertia systems offers improved results for the response of the 2DOF structure. However, as the compliance of the chevron frame that supports the inerters increases, the use of a single rotational inertia system offers more favorable response other than increasing the forces transferred to the chevron frame.

4 Response of Seismically Isolated Structures with Supplemental Rotational Inertia

This chapter was partly motivated from the ability of inerters to control the response of flexible and yielding structures as shown in chapter 3 and chapter 5 of this report (see also Makris and Moghimi 2019; Makris and Kampas 2016; Moghimi and Makris 2021) and partly from their known property to eliminate the participation of higher modes (Furuhashi and Ishimaru 2008; Ye et al. 2019). Our study shows that while a small amount of supplemental rotational inertia is needed to eliminate the participation of the second mode of the two-degree-of-freedom isolated structure shown in Figure 4.1, the effect of this elimination is marginal on the structural response, since the participation of the second mode is invariably small even when isolation systems without inerters are used (Kelly 1990, 1997). Our study also brings forward and corrects issues regarding the orthogonality of eigenmodes in a recent study (Ye et al. 2019); and revisits how supplemental rotational inertia at the isolation level influences the modal frequencies, mode shapes and participation factors of the classical two-degree-of-freedom (2DOF) linear seismic isolated, structure shown in Figure 4.1 (Kelly 1990, 1997). Our study upon showing that the reaction force at the support of the inerter is appreciable; proceeds with the nonlinear response analysis of the same 2DOF isolated structure by adopting a bilinear behavior for the isolation system (either lead rubber bearings (LRB) or single concave sliding bearings (SCSB)) in association with a formulation that accounts for the compliance of the support of the inerters and discusses advantages and challenges that emerge when supplemental rotational inertia is used in the isolation system. Our study concludes that the presence of inerters aggravates both the displacement and acceleration response of the superstructure and as a result for larger isolation periods ($T_b > 2.5 \text{ sec}$) the use of inerters is not recommended.

4.1 LINEAR THEORY OF SEISMIC ISOLATION WITH SUPPLEMENTAL ROTATIONAL INERTIA

Our analysis starts with the eigenvalue analysis of the 2DOF isolated structure shown in Figure 4.1 where the isolation system has elastic stiffness k_b and damping constant c_b , whereas the superstructure has elastic stiffness k_s and damping constant c_s . In this section we adopt the notation and the degrees of freedom used by Kelly (1990, 1997) where u_b is the relative to the ground displacement of m_b and u_s is the relative displacement of m_s to m_b as shown in Figure 4.1. At the base level a non-compliant (rigid) pedestal supports a flywheel with radius R and mass m_w that can rotate about point O. Concentric to the flywheel, there is an attached pinion with radius ρ engaged

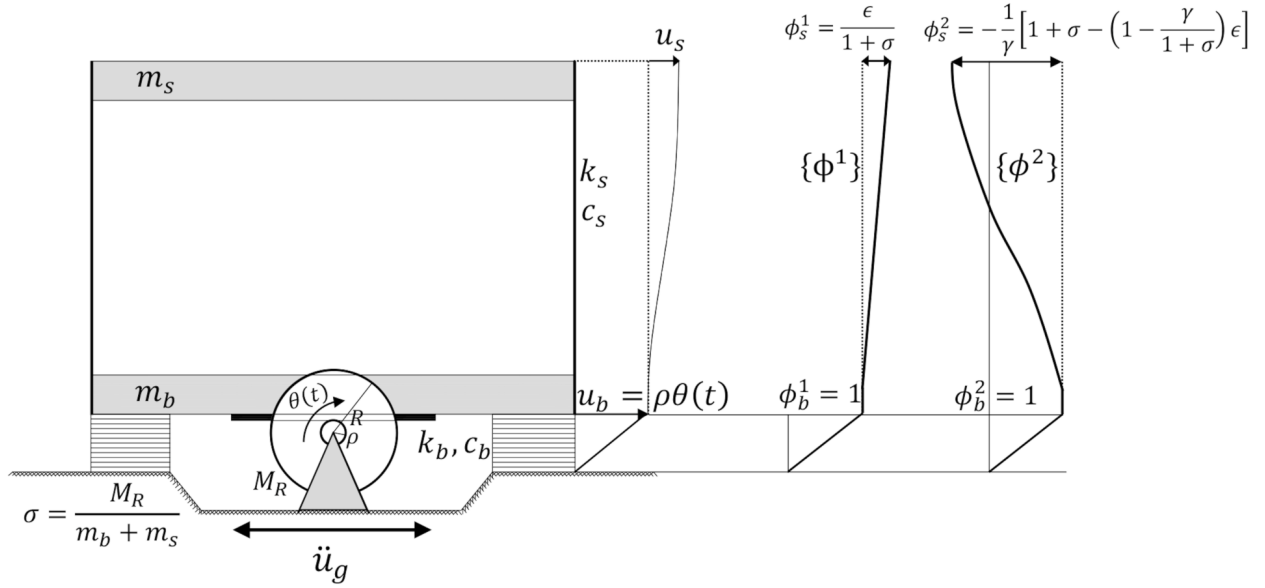


Figure 4.1: Classical two-degree-of-freedom seismic isolation structure (Kelly 1990, 1997) with supplemental rotational inertia at the isolation system.

to a linear rack connecting to the bottom of mass m_b . With this arrangement, when the mass m_b undergoes a displacement, $u_b(t)$ to the left, the flywheel is subjected to a clockwise rotation $\theta(t)$. Given that there is no slipping between the rack and the pinion, $u_b(t) = \rho\theta(t)$; whereas, the internal force $F_I(t)$, that develops along the rack-pinion interface needs to satisfy dynamic moment equilibrium given by equation (1.2).

With reference to Figure 4.1, for a displacement $u_b(t)$ to the right, the internal force

$$F_I(t) = \frac{I_w \ddot{\theta}(t)}{\rho} = \frac{1}{2} m_w \frac{R^2}{\rho^2} \ddot{u}_b(t) = M_R \ddot{u}_b(t) \quad (4.1)$$

oppose the motion of the mass m_b (to the left). In equation (4.1), $M_R = (1/2) m_w (R^2/\rho^2)$ is the inertance of the inerter with units of mass Smith (2002). Accordingly, dynamic equilibrium of the entire structure above isolators gives

$$(m_b + m_s + M_R) \ddot{u}_b + m_s \ddot{u}_s + c_b \dot{u}_b + k_b u_b = -(m_b + m_s) \ddot{u}_g \quad (4.2)$$

and dynamic equilibrium of mass m_s gives

$$m_s \ddot{u}_b + m_s \ddot{u}_s + c_s \dot{u}_s + k_s u_s = -m_s \ddot{u}_g \quad (4.3)$$

Following the notation introduced by Kelly (1990, 1997), the nominal frequencies and nominal damping ratios are

$$\omega_b^2 = \frac{k_b}{m_b + m_s}, \quad \omega_s^2 = \frac{k_s}{m_s}, \quad 2\xi_b \omega_b = \frac{c_b}{m_b + m_s}, \quad 2\xi_s \omega_s = \frac{c_s}{m_s} \quad (4.4)$$

whereas, the mass ratio, γ , and inertance ratio, σ , are defined as

$$\gamma = \frac{m_s}{m_b + m_s} = \frac{m_s}{M} \quad \sigma = \frac{M_R}{m_b + m_s} = \frac{M_R}{M} \quad (4.5)$$

where $M = m_b + m_s$ (Kelly 1990, 1997). Equations (4.2) and (4.3) can be expressed in a matrix form in terms of the parameters defined in equations (4.4) and (4.5).

$$\begin{bmatrix} M + M_R & m_s \\ m_s & m_s \end{bmatrix} \begin{Bmatrix} \ddot{u}_b(t) \\ \ddot{u}_s(t) \end{Bmatrix} \begin{bmatrix} 2\xi_b M \omega_b & 0 \\ 0 & 2\xi_s m_s \omega_s \end{bmatrix} \begin{Bmatrix} \dot{u}_b(t) \\ \dot{u}_s(t) \end{Bmatrix} \begin{bmatrix} M \omega_b^2 & 0 \\ 0 & m_s \omega_s^2 \end{bmatrix} \begin{Bmatrix} u_b(t) \\ u_s(t) \end{Bmatrix} = - \begin{Bmatrix} M \\ m_s \end{Bmatrix} \ddot{u}_g(t) \quad (4.6)$$

When $M_R = 0$, equation (4.6) is identical to the matrix equation of the two-degree-of-freedom seismically isolated, elastic structure (Kelly 1990, 1997). The earthquake response of the two-degree-of-freedom isolated structure shown in Figure 4.1 can be evaluated directly with modal analysis (Kelly 1997; Clough and Penzien 1975; Chopra 2000). In addition to the response time-histories, a modal analysis provides insight into the dynamics of the isolated structure and the conceptual results may be applicable to more elaborate structures.

4.1.1 Eigenvalue Analysis

Upon dropping the damping matrix in equation (4.6) its homogeneous version (free vibrations) yields

$$\begin{bmatrix} \omega_b^2 - \omega^2(1 + \sigma) & -\omega^2\gamma \\ -\omega^2 & \omega_s^2 - \omega^2 \end{bmatrix} \begin{Bmatrix} \Phi_b \\ \Phi_s \end{Bmatrix} = \begin{Bmatrix} 0 \\ 0 \end{Bmatrix} \quad (4.7)$$

where ω are the eigenvalues and $\langle \phi_b \ \phi_s \rangle^T$ are the eigenvectors. The characteristic equation of the homogeneous equation (4.7) gives

$$(1 + \sigma - \gamma)\omega^4 - (\omega_b^2 + (1 + \sigma)\omega_s^2)\omega^2 + \omega_b^2\omega_s^2 = 0 \quad (4.8)$$

which has also been presented by (Ye et al. 2019). The lower of the two roots, ω_1 , of equation (4.8) represents the shifted isolation frequency due to the flexibility of the isolation bearings and the presence of the inerter; whereas, the higher root, ω_2 , represents the modified superstructure frequency due to the presence of the isolation bearings and the inerter

$$\omega_{1,2}^2 = \frac{1}{2(1 + \sigma - \gamma)} \left\{ \omega_b^2 + (1 + \sigma)\omega_s^2 \mp \left[(\omega_b^2 + (1 + \sigma)\omega_s^2)^2 - 4(1 + \sigma - \gamma)\omega_b^2\omega_s^2 \right]^{\frac{1}{2}} \right\} \quad (4.9)$$

The radical in the right-hand side of equation (4.9) can be expressed as

$$\left[(\omega_b^2 + (1 + \sigma)\omega_s^2)^2 - 4(1 + \sigma - \gamma)\omega_b^2\omega_s^2 \right]^{\frac{1}{2}} = ((1 + \sigma)\omega_s^2 - \omega_b^2) \left[1 + 4\gamma \frac{\omega_b^2\omega_s^2}{((1 + \sigma)\omega_s^2 - \omega_b^2)^2} \right]^{\frac{1}{2}} \quad (4.10)$$

We now follow the same approach presented by Kelly (1990, 1997) by expanding the radical appearing in the right-hand side of equation (4.10) in Taylor series after recognizing that for isolated structures with well-separated frequencies, $\omega_b^2 \ll \omega_s^2$. By defining $\epsilon = \omega_b^2/\omega_s^2 \ll 1$ and after using

that $\omega_b^2 = \epsilon\omega_s^2$, the Taylor series expansion of the radical in the right-hand side of Equation (4.10) gives

$$\left[1 + 4\gamma \frac{\epsilon}{(1 + \sigma - \epsilon)^2}\right]^{\frac{1}{2}} = 1 + 2\gamma \frac{\epsilon}{(1 + \sigma - \epsilon)^2} - 2\gamma^2 \frac{\epsilon^2}{(1 + \sigma - \epsilon)^4} + \dots \quad (4.11)$$

Substitution of the right-hand side of equation (4.11) into the first equation (4.9) gives

$$\omega_1^2 = \frac{\omega_b^2}{1 + \sigma - \gamma} \left[1 - \frac{\gamma}{(1 + \sigma) \left(1 - \frac{\epsilon}{1 + \sigma}\right)} \left(1 - \gamma \frac{\epsilon}{(1 + \sigma)^2 \left(1 - \frac{\epsilon}{1 + \sigma}\right)^2}\right)\right] \quad (4.12)$$

Upon expanding $1/(1 - \epsilon/(1 + \sigma)) = 1 + \epsilon/(1 + \sigma) + \dots$ and $1/(1 - \epsilon/(1 + \sigma))^2 = 1 + 2\epsilon/(1 + \sigma) + \dots$ and after retaining terms of order ϵ , equation (4.12) yields the following result

$$\omega_1^2 = \frac{\omega_b^2}{1 + \sigma} \left(1 - \frac{\gamma\epsilon}{(1 + \sigma)^2}\right) \quad (4.13)$$

For the classical case where there is no inerter in the isolation system ($\sigma = M_R/(m_b + m_s) = 0$), equation (4.13) offers the known result, $\omega_1^2 = \omega_b^2 (1 - \gamma\epsilon)$ (Kelly 1990, 1997). The first modal frequency ω_1^2 of the isolated structure shown in Figure 4.1 has also been derived by Ye et al. 2019, however the term $(1 + \sigma)^2$ in the denominator of $\gamma\epsilon$ appearing in Equation (4.13) is missing. This is a minor omission since the $\gamma\epsilon$ term has a negligible influence on ω_1 when the frequencies ω_s and $\omega_b = \sqrt{\epsilon}\omega_s$ are well separated.

Equation (4.13) indicates that the presence of the inerter with inertance ratio $\sigma = M_R/(m_b + m_s)$ reduces the isolation frequency, ω_b ; therefore, the first modal period is lengthened by $\sqrt{1 + \sigma}$ showing that the presence the inerter in the isolation system of the 2DOF structure depicted in Figure 4.1 produces the same period lengthening that happens in the single-degree-of-freedom structure equipped with an inerter as shown in (Furuhashi and Ishimaru 2008; Makris and Kampas 2016; Moghimi and Makris 2021). Substitution of the right-hand side of equation (4.11) into the second equation (4.9) gives

$$\omega_2^2 = \frac{\omega_s^2}{1 + \sigma - \gamma} \left[1 + \sigma + \gamma \frac{\epsilon}{1 + \sigma - \epsilon} \left(1 - \gamma \frac{\epsilon}{(1 + \sigma - \epsilon)^2}\right)\right] \quad (4.14)$$

By performing the same Taylor expansions as in equation (4.12) and after retaining terms of order ϵ , equation (4.14) yields the following result

$$\omega_2^2 = \frac{\omega_s^2}{1 + \sigma - \gamma} \left[1 + \sigma + \frac{\gamma\epsilon}{1 + \sigma}\right] \quad (4.15)$$

The second modal frequency ω_2 given by equation (4.15) has also been derived correctly in (Ye et al. 2019).

For the classical case where there is no inerter in the isolation system ($\sigma = M_R/(m_b + m_s) = 0$), equation (4.15) offers the known result $\omega_2^2 = \omega_s^2 (1 + \gamma\epsilon) / (1 - \gamma)$ (Kelly 1990, 1997). The first mode shape $\{\phi^1\}$ is extracted from equation (4.7) by setting $\omega^2 = \omega_1^2$ which is given by equation (4.13). Upon setting $\phi_b^1 = 1$ and after retaining terms of order ϵ , the first eigenmode is

$$\{\phi^1\} = \left\{ \begin{matrix} \phi_b^1 \\ \phi_s^1 \end{matrix} \right\} = \left\{ \begin{matrix} 1 \\ \frac{\epsilon}{1 + \sigma} \end{matrix} \right\} \quad (4.16)$$

Equation (4.16) indicates that the presence of an inerter with inertance ratio $\sigma = M_R / (m_b + m_s) = M_R / M$ in the isolation system further suppresses the superstructure drift $= \epsilon / (1 + \sigma)$ when compared to the drift $= \epsilon$ that results from the classical linear isolation system without inerter. The first mode shape $\{\phi^1\}$ has also been presented in (Ye et al. 2019), however the term $(1 + \sigma)$ appears incorrectly in the numerator of ϕ_s^1 rather than in the denominator as shown by equation (4.16) and leads to flawed, unfavorable conclusion. This inadvertent error is also brought forward because it violates the orthogonality conditions of normal modes.

By setting $\omega^2 = \omega_2^2$, which is given by equation (4.15) and after retaining terms of order ϵ in equation (4.9), the second eigenmode is

$$\{\phi^2\} = \begin{Bmatrix} \phi_b^2 \\ \phi_s^2 \end{Bmatrix} = \begin{Bmatrix} 1 \\ -\frac{1}{\gamma} \left[1 + \sigma - \left(1 - \frac{\gamma}{1+\sigma} \right) \epsilon \right] \end{Bmatrix} \quad (4.17)$$

which has been also presented in (Ye et al. 2019) correctly. Figure 4.1 plots the eigenmode ϕ^1 and ϕ^2 next to schematic of the 2DOF isolated linear structure that is equipped with supplemental rotational inertia at the isolation level. Because of the linearity of the structure shown in Figure 4.1, the eigenmodes $\{\phi^1\}$ and $\{\phi^2\}$ given by equations (4.16) and (4.17) shall be orthogonal to the mass and stiffness matrices appearing in Equation (4.6). Accordingly,

$$\begin{aligned} [\Phi]^T [m] [\Phi] &= M \begin{bmatrix} 1 & \frac{\epsilon}{1+\sigma} \\ 1 & \phi_s^2 \end{bmatrix} \begin{bmatrix} 1 + \sigma & \gamma \\ \gamma & \gamma \end{bmatrix} \begin{bmatrix} 1 & 1 \\ \frac{\epsilon}{1+\sigma} & \phi_s^2 \end{bmatrix} \\ &= M \begin{bmatrix} 1 + \sigma + 2\gamma\epsilon \frac{1+\sigma+\frac{\epsilon}{2}}{(1+\sigma)^2} & \epsilon^2 \frac{1+\sigma-\gamma}{(1+\sigma)^2} \\ \epsilon^2 \frac{1+\sigma-\gamma}{(1+\sigma)^2} & \frac{1+\sigma-\gamma}{\gamma(1+\sigma)^2} \left[(1+\sigma)(1+\sigma-\epsilon)^2 + 2\gamma\epsilon \left(1 + \sigma - \frac{\epsilon}{2} \right) \right] \end{bmatrix} \end{aligned} \quad (4.18)$$

where $\phi_s^2 = -\frac{1}{\gamma} \left[1 + \sigma - \left(1 - \frac{\gamma}{1+\sigma} \right) \epsilon \right]$ appears in equation (4.17). The off-diagonal terms are identical and of order ϵ^2 ; therefore zero, given that in our entire analysis we retain terms up to order ϵ . The diagonal terms are the modal masses, which upon retaining terms up to order ϵ simplify to

$$M_1 = M \left(1 + \sigma + 2 \frac{\gamma\epsilon}{1+\sigma} \right) \quad \text{and} \quad M_2 = M \frac{(1+\sigma-\gamma)(1+\sigma)}{\gamma} \left(1 - 2\epsilon \frac{1+\sigma-\gamma}{(1+\sigma)^2} \right) \quad (4.19)$$

In the absence of rotational inertia ($\sigma = 0$) the expressions of M_1 and M_2 given by equation (4.19) reduce to the modal masses reported by Kelly (1990, 1997). The modal stiffnesses are given by

$$[\Phi]^T [k] [\Phi] = M\omega_s^2 [\Phi]^T \begin{bmatrix} \epsilon & 0 \\ 0 & \gamma \end{bmatrix} [\Phi] = M\omega_s^2 \begin{bmatrix} \epsilon + \frac{\gamma\epsilon^2}{(1+\sigma)^2} & \epsilon^2 \frac{1+\sigma-\gamma}{(1+\sigma)^2} \\ \epsilon^2 \frac{1+\sigma-\gamma}{(1+\sigma)^2} & \epsilon + \frac{[(1+\sigma)^2 - \epsilon(1+\sigma-\gamma)]^2}{\gamma(1+\sigma)^2} \end{bmatrix} \quad (4.20)$$

where again the off-diagonal terms are of order ϵ^2 , confirming the orthogonality of the eigenmodes on the stiffness matrix. The ratios $K_j/M_j = \omega_j^2$, $j = 1, 2$ return the modal frequencies ω_1^2 and ω_2^2 given by equations (4.13) and (4.15). For instance, with reference to equations (4.20) and (4.19)

when $j = 1$

$$\frac{K_1}{M_1} = \frac{\omega_b^2 \left(1 + \frac{\gamma\epsilon}{(1+\sigma)^2}\right)}{1 + \sigma + 2\frac{\gamma\epsilon}{1+\sigma}} = \frac{\omega_b^2}{1 + \sigma} \frac{1 + \frac{\gamma\epsilon}{(1+\sigma)^2}}{1 + 2\frac{\gamma\epsilon}{(1+\sigma)^2}} \approx \frac{\omega_b^2}{1 + \sigma} \left(1 - \frac{\gamma\epsilon}{(1 + \sigma)^2}\right) = \omega_1^2 \quad (4.21)$$

and equation (4.13) is recovered. While the eigenmodes $\{\Phi^1\}$ and $\{\Phi^2\}$ given by equations (4.16) and (4.17) are orthogonal to the mass and stiffness matrices as shown by equations (4.18) and (4.20), the product

$$\begin{aligned} [\Phi]^T [c] [\Phi] &= 2M\omega_s \begin{bmatrix} 1 & \frac{\epsilon}{1+\sigma} \\ 1 & \phi_s^2 \end{bmatrix} \begin{bmatrix} \sqrt{\epsilon}\xi_b & 0 \\ 0 & \gamma\xi_s \end{bmatrix} \begin{bmatrix} 1 & 1 \\ \frac{\epsilon}{1+\sigma} & \phi_s^2 \end{bmatrix} \\ &= 2M\omega_s \begin{bmatrix} \sqrt{\epsilon}\xi_b + \epsilon^2 \frac{\gamma}{(1+\sigma)^2} \xi_s & \sqrt{\epsilon}\xi_b - \epsilon\xi_s + \epsilon^2 \frac{1+\sigma-\gamma}{(1+\sigma)^2} \\ \sqrt{\epsilon}\xi_b - \epsilon\xi_s + \epsilon^2 \frac{1+\sigma-\gamma}{(1+\sigma)^2} & \sqrt{\epsilon}\xi_b + \frac{[1+\sigma+\epsilon(\frac{\gamma}{1+\sigma}-1)]^2}{\gamma} \xi_s \end{bmatrix} \end{aligned} \quad (4.22)$$

yields off-diagonal terms that couple the equations of motion when expressed in terms of the modal coordinates q_j . However, it is worth noting that the presence of the inerter does not contribute to this coupling which is entirely due to the damping of the isolation system ξ_b and of the superstructure, ξ_s . This result was anticipated since the inertance of the inerter, σ , appears only in the mass matrix (see equation (4.6)) on which the eigenmodes are orthogonal as shown by equation (4.18).

In view of the simplicity of modal analysis, this mild coupling due to the term $\sqrt{\epsilon}\xi_b - \epsilon\xi_s$, is neglected as is adopted in the works by Kelly Kelly (1990, 1997), and one can merely proceed with the modal damping offered by the diagonal terms of equation (4.22)

$$2\xi_1\omega_1 = \frac{2M\omega_s\sqrt{\epsilon}\xi_b}{M_1}, \quad 2\xi_2\omega_2 = \frac{2M\omega_s \left[\sqrt{\epsilon}\xi_b + \frac{[1+\sigma+\epsilon(\frac{\gamma}{1+\sigma}-1)]^2}{\gamma} \xi_s \right]}{M_2} \quad (4.23)$$

where ξ_1 and ξ_2 are the modal damping ratios, ω_1 and ω_2 are the modal frequencies given by equations (4.13) and (4.15) and M_1 and M_2 are the modal masses given by equation (4.19). Upon substitution of these expression into equation (4.23), and after retaining terms up to order ϵ , (we have also neglected terms of the order of $\epsilon^{3/2}$) one obtains

$$\xi_1 = \frac{\xi_b}{\sqrt{1+\sigma}} \left(1 - \frac{3}{2} \frac{\gamma\epsilon}{(1+\sigma)^2}\right), \quad \text{and} \quad \xi_2 = \frac{\xi_b\gamma\sqrt{\epsilon} + \xi_s [(1+\sigma)^2 - \frac{1}{2}\gamma\epsilon]}{(1+\sigma)^{3/2} \sqrt{1+\sigma-\gamma}} \quad (4.24)$$

The modal damping ratios presented by equation (4.24) have also been presented in (Ye et al. 2019) where the result for ξ_2 is correct and also contains term of the order of $\epsilon^{3/2}$; whereas, the result for ξ_1 has a minor error since the term $(1+\sigma)^2$ in the denominator of the $\gamma\epsilon$ term in ξ_1 is missing. Equation (4.24) reveals that supplemental rotational inertia ($\sigma > 0$) suppress both modal damping ratios ξ_1 and ξ_2 which become nearly independent of $\epsilon = \omega_b^2/\omega_s^2$ as σ increases (see Figure 4.2).

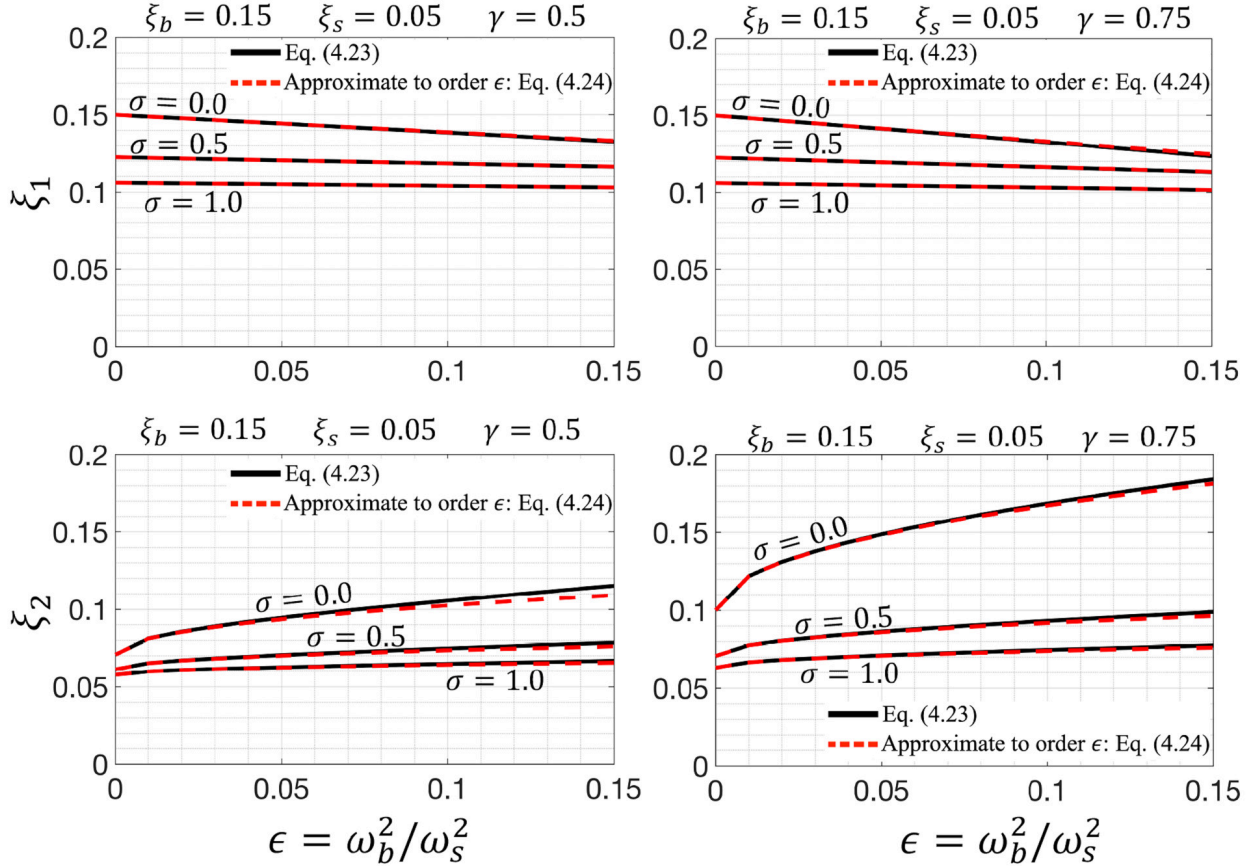


Figure 4.2: Reduction of the first and second modal damping ratios ξ_1 and ξ_2 due to supplemental rotational inertia with inertance $M_R = \sigma M = \sigma (m_b + m_s)$. The graphs also compare the modal damping ratio values offered by equation (4.24) (where only terms up to order ϵ have been retained) against the corresponding values before taking the Taylor expansions offered by equation (4.23).

4.2 MODAL RESPONSE CONTRIBUTIONS AND SEISMIC RESPONSE ANALYSIS

With the two eigenmodes of the 2DOF structure shown in Figure 4.1 being offered by equations (4.16) and (4.17), its linear response history can be expressed with modal superposition

$$\begin{Bmatrix} u_b(t) \\ u_s(t) \end{Bmatrix} = \{\phi\} \begin{Bmatrix} q_1(t) \\ q_2(t) \end{Bmatrix} = \begin{bmatrix} 1 & 1 \\ \frac{\epsilon}{1+\sigma} & -\frac{1}{\gamma} \left[1 + \sigma - \left(1 - \frac{\gamma}{1+\sigma} \right) \epsilon \right] \end{bmatrix} \begin{Bmatrix} q_1(t) \\ q_2(t) \end{Bmatrix} \quad (4.25)$$

where $[\phi]$ is the modal matrix and $q_1(t)$, $q_2(t)$ are the modal coordinates (Clough and Penzien 1975; Chopra 2000) which are scalar, time dependent participation functions.

Substitution of the displacement vector given by equation (4.25) into the matrix equation of motion given by equation (4.6) and upon multiplying from the left with the transpose of the modal matrix $[\phi]^T$, the coupled equations of motion decouple due to the orthogonality of modes on the mass and stiffness matrices (see equations (4.18) and (4.20)); after neglecting the small coupling due to the

off-diagonal damping terms (see equation (4.22)).

$$\ddot{q}_1(t) + 2\xi_1\omega_1\dot{q}_1(t) + \omega_1^2q_1(t) = -\frac{M}{M_1} \left(1 + \frac{\gamma\epsilon}{1+\sigma}\right) \ddot{u}_g(t) = -L_1\ddot{u}_g(t) \quad (4.26)$$

$$\ddot{q}_2(t) + 2\xi_2\omega_2\dot{q}_2(t) + \omega_2^2q_2(t) = -\frac{M}{M_2} \left[-\sigma + \left(1 - \frac{\gamma}{1+\sigma}\right)\epsilon\right] \ddot{u}_g(t) = -L_2\ddot{u}_g(t) \quad (4.27)$$

In the decoupled equations (4.26) and (4.27) ω_1 and ω_2 are the eigenvalues of the 2DOF structure given by equations (4.13) and (4.15), ξ_1 and ξ_2 are its modal damping ratios given by equation (4.24) and M_1 and M_2 are the modal masses given by equation (4.19).

By virtue of the results presented by equation (4.19), the modal response contributions (participation factors) L_1 and L_2 appearing on the right of equations (4.26) and (4.26) after retaining terms up to order ϵ are given by

$$L_1 = \frac{1}{1+\sigma} - \frac{\gamma\epsilon}{(1+\sigma)^2} \left(\frac{2}{1+\sigma} - 1\right) \quad \text{and} \quad L_2 = \frac{\gamma}{1+\sigma} \left[-\frac{\sigma}{1+\sigma-\gamma} + \epsilon\frac{1-\sigma}{(1+\sigma)^2}\right] \quad (4.28)$$

In the absence of supplemental rotational inertia in the isolation system ($\sigma = 0$), the participation factors reduce to $L_1 = 1 - \gamma\epsilon$ and $L_2 = \gamma\epsilon$ reported by Kelly Kelly (1990, 1997).

In his insightful publications, Kelly (1990, 1997) explains that the classical result for the participation factor of the second mode (the mode that involves structural deformations $L_2 = \gamma\epsilon$)-that is of order ϵ further contributes to the effectiveness of seismic isolation since the frequency separation ($\omega_b^2 = \epsilon\omega_s^2$, with $\epsilon \ll 1$) suppresses the participation of the second mode $\{\phi^2\}$. In the case where the isolation system is enhanced with supplemental rotational inertia, the participation factor L_2 is no-longer a function of ϵ alone since it involves the negative quantity, $-\sigma/(1+\sigma-\gamma)$, which appears due to the presence of the inertance $\sigma = M_R/M$. Nevertheless, because of the negative sign there is a critical value of the inertance, σ , for which the participation of the second mode, vanishes ($L_2 = 0$) as was initially uncovered by Furuhashi and Ishimaru (2008) and recently reiterated by Ye et al. (2019).

By setting the bracket in the right-hand side of L_2 given by the second equation (4.28) equal to zero, one obtains a cubic equation for σ as was suggested in (Ye et al. 2019). However, we recall that the expressions appearing in equation (4.28) are approximate expressions that involve additional fictitious roots for σ that result from the Taylor expansions of the modal masses M_1 and M_2 appearing in the denominators of the right-hand sides of equations (4.26) and (4.27). Accordingly, the correct critical value of σ for which the participation factor L_2 vanishes is obtained by setting the quantity in the brackets in the right-hand side of equation (4.27) equal to zero; and the following quadratic (not cubic) equation is obtained

$$\sigma^2 + (1 - \epsilon)\sigma - \epsilon(1 - \gamma) = 0 \quad (4.29)$$

Upon performing Taylor series expansions similar to the one offered by equation (4.11) and after retaining terms of order ϵ , the roots of equation (4.29) are

$$\sigma_1 = \epsilon(1 - \gamma) \quad \text{and} \quad \sigma_2 = -1 + \gamma\epsilon \quad (4.30)$$

The only physically admissible root for $\sigma > 0$ is the first of equation (4.30) which offers the intriguing result, that a small amount of inertance $\sigma = \epsilon(1 - \gamma)$ is sufficient to vanish the participation of the second mode $\{\Phi^2\}$ which is responsible for most of the deformation of the superstructure (see Figure 4.1-left).

Figure 4.3 plots the dependance of the participation factors L_1 and L_2 on the values of the inertance σ for various values of the frequency ratio $\epsilon = \omega_b^2/\omega_s^2$. The graphs also compare the approximate values of L_1 and L_2 offered by equation (4.28) (where only terms up to order ϵ have been retained) against the corresponding exact values offered by the right-hand sides of equations (4.26) and (4.27). The graphs of L_2 cross the zero axis at values of $\sigma = \epsilon(1 - \gamma)$. For the modal seismic response analysis we follow the formulation presented by Chopra (2000) where the modal coordinate functions $q_1(t)$ and $q_2(t)$ appearing in equation (4.26) and (4.27) are expressed in terms of the response of solitary single-degree-of-freedom (SDOF) structures.

$$\ddot{D}_j(t) + 2\xi_j\omega_j\dot{D}_j(t) + \omega_j^2D_j(t) = -\ddot{u}_g(t) \quad j \in \{1, 2\} \quad (4.31)$$

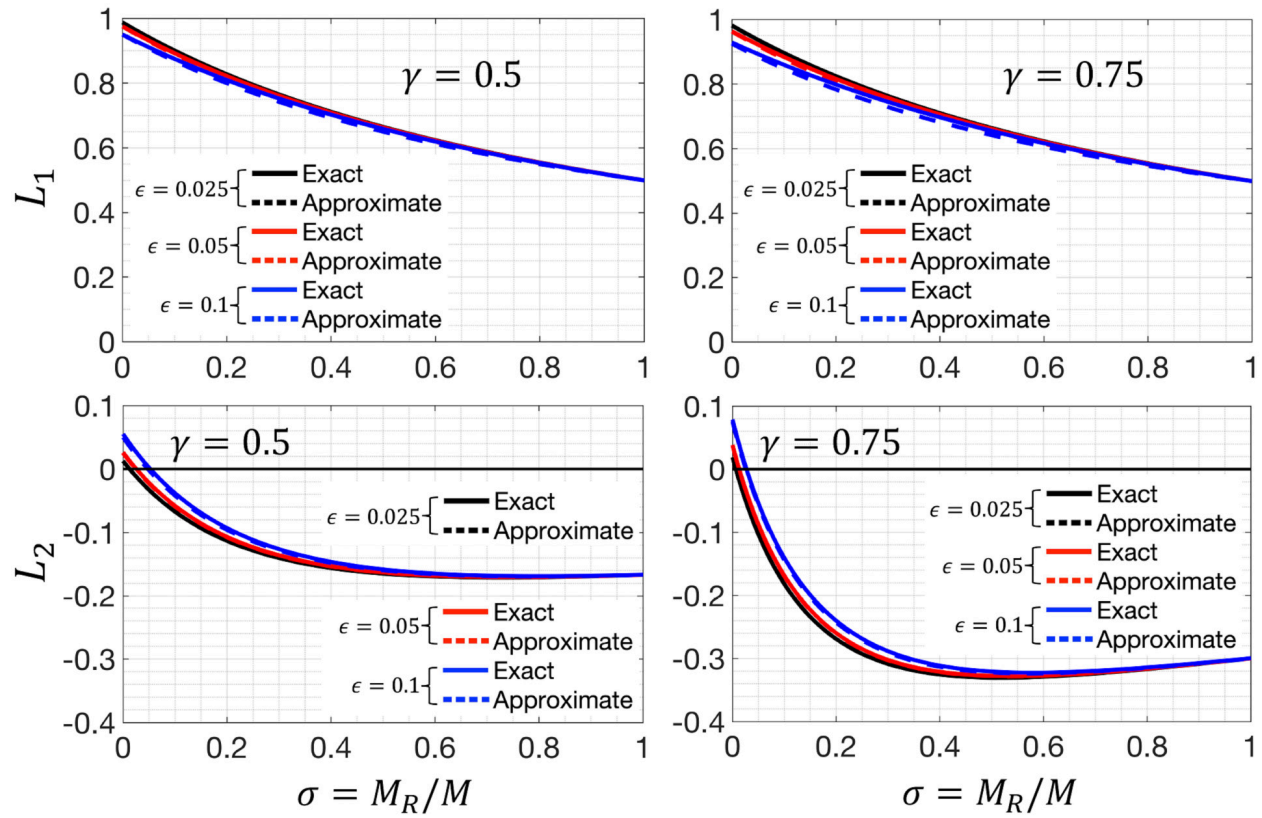


Figure 4.3: Participation factors, L_1 and L_2 of the first and second modes respectively as a function of supplemental rotational inertia $\sigma = M_R/M$. For values of $\sigma = \epsilon(1 - \gamma)$, the participation factor $L_2 = 0$ and the contribution of the second vibration mode in the seismic response of the 2DOF structure vanishes. The graphs also compare the approximate values of L_1 and L_2 as offered by equation (4.28) with the exact expressions appearing in the right-hand-side of equations (4.26) and (4.27).

By comparing equation (4.31) with equations (4.26) and (4.27) with $j \in \{1, 2\}$, then $q_j(t) = L_j D_j(t)$, and equation (4.25) assumes the form

$$\begin{Bmatrix} u_b(t) \\ u_s(t) \end{Bmatrix} = \sum_{j=1}^2 L_j D_j(t) \begin{Bmatrix} \phi_b^j \\ \phi_s^j \end{Bmatrix} \quad (4.32)$$

Figure 4.4 plots the base, $u_b(t)$ and the superstructure, $u_s(t)$ displacement histories of the 2DOF isolated structure shown in Figure 4.1 with $\omega_b = \pi$ rad/sec ($T_b = 2$ sec), $\omega_s = 1/\sqrt{\epsilon}\omega_b = 5\pi$ rad/sec ($T_s = 0.4$ sec), $\epsilon = \omega_b^2/\omega_s^2 = 0.04$, $\gamma = m_s/M = 0.75$, $\xi_b = 15\%$ and $\xi_s = 3\%$ when subjected to the C02, N65E ground motion recorded during the 1966 Parkfield, California earthquake. Plots (a) and (b) are for the case where there is no supplemental rotational inertia ($\sigma = 0$) in the isolation system; whereas plots (c) and (d) are for the critical value of $\sigma = \epsilon(1 - \gamma)$. While for the case where $\sigma = \epsilon(1 - \gamma) = 0.01$, the participation of the second mode vanishes, this mathematical intriguing property of supplemental rotational inertia is of marginal engineering interest since the participation of the second mode in the classical isolated structure (no inerters) is anyhow marginal—that is of order ϵ ($L_2 = \gamma\epsilon$, Kelly 1990, 1997).

The displacement histories $u_b(t)$ and $u_s(t)$ computed in Figure 4.4 with the approximate modal analysis procedure presented in this study (we have only retained terms of order ϵ and we have neglected the mild coupling of the equations of motion due to damping) are compared with the rigorous numerical results after integrating the coupled equations of motion of the matrix equation (4.6) by employing a state-space formulation (Makris and Chang 2000b; Makris and Kampas 2016; Makris and Moghimi 2019; Moghimi and Makris 2021; Moghimi 2022) that is outlined in the next section which presents the nonlinear response analysis. The excellent comparison of the response histories shown in in Figure 4.4 confirms the practical value of the approximate modal analysis procedure given its simplicity. Figure 4.5(left) plots the base, u_b^{max} , and the superstructure, u_s^{max} peak displacements of the 2DOF isolated structure shown in Figure 4.1 for a wide range of isolation periods ($1.5 \text{ sec} \leq T_b = 2\pi/\omega_b \leq 3.5 \text{ sec}$) for a constant value $\epsilon = \omega_b^2/\omega_s^2 = 0.04$, $\gamma = 0.75$, $\xi_b = 15\%$, $\xi_s = 3\%$ and various values of supplemental rotational inertia, $\sigma = 0, \epsilon(1 - \gamma) = 0.01, 0.2$ and 0.4 when subjected to the C02, N65E ground motion recorded during the 1966 Parkfield, California earthquake. Figure 4.5(left) reveals that the approximate modal analysis summarized in the first part of this chapter (solid lines) predicts very well the peak base displacement, u_b^{max} for the entire range of isolation periods; whereas, for the peak structural displacement, u_s^{max} minor differences are observed between the approximate modal analysis (solid lines) and the rigorous state-space formulation (dashed lines) at larger isolation periods. More specifically, the differences between the superstructure response without supplemental rotational inertia ($\sigma = 0$) and with the critical value of $\sigma = \epsilon(1 - \gamma)$ is marginal and within the error due to the approximations inherent to the approximate modal analysis (we have only retained terms of order ϵ and neglected the coupling due to the off-diagonal damping terms). Figure 4.5(left) reveals that larger values of supplemental rotational inertia ($\sigma = 0.2$ or 0.4) are effective in suppressing the large peak base displacements due to the flexibility of the isolation system. However, for larger isolation periods ($T_b > 2.5 \text{ sec}$) this happens at the expense of increasing the superstructure displacements, u_s^{max} to drift levels that the superstructure may enter the nonlinear range (drifts $> 1\%$). Figure 4.5(right) shows that supplemental rotational inertia also aggravates the superstructure accelerations at larger isolation periods ($T_b > 2.5 \text{ sec}$).

Figure 4.6 plots the base, u_b^{max} , and the superstructure, u_s^{max} peak displacements of the 2DOF isolated structure shown in Figure 4.1 for a wide range of isolation periods ($1.5 \text{ sec} \leq T_b = 2\pi/\omega_b \leq 3.5 \text{ sec}$) for a constant value $\epsilon = \omega_b^2/\omega_s^2 = 0.04$, $\gamma = m_s/M = 0.75$, $\xi_b = 15\%$, $\xi_s = 3\%$ and various values of supplemental rotational inertia, $\sigma = 0, \epsilon(1 - \gamma) = 0.01, 0.2$ and 0.4 when subjected to the Pacoima Dam/164 ground motion recorded during the 1971 San Fernando, California earthquake. Trends similar to those discussed in Figure 4.5 are observed where at larger isolation

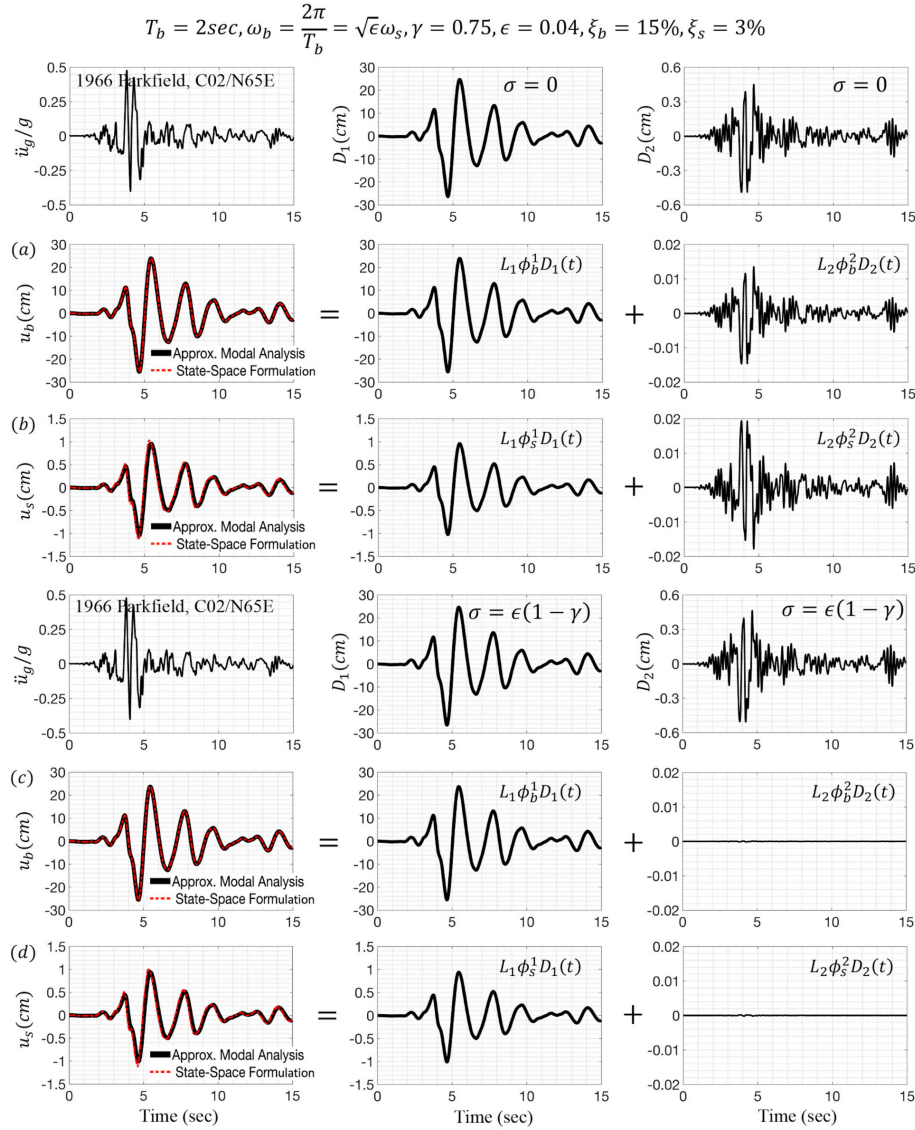


Figure 4.4: Response of the 2DOF isolated structure shown in Figure 4.1 with isolation period $T_b = 2\pi/\omega_b = 2 \text{ sec}$, superstructure period $T_s = 2\pi/\omega_s = 0.4 \text{ sec}$ ($\epsilon = 0.04$), $\gamma = m_s/M = 0.75$, $\xi_b = 15\%$ and $\xi_s = 3\%$ when subjected to the C02, N65E ground motion recorded during the 1966 Parkfield, California earthquake. Plots (a) and (b) are without supplemental rotational inertia ($\sigma = 0$); whereas plots (c) and (d) are for the critical value $\sigma = \epsilon(1 - \gamma) = 0.01$ that vanishes the participation of the second mode.

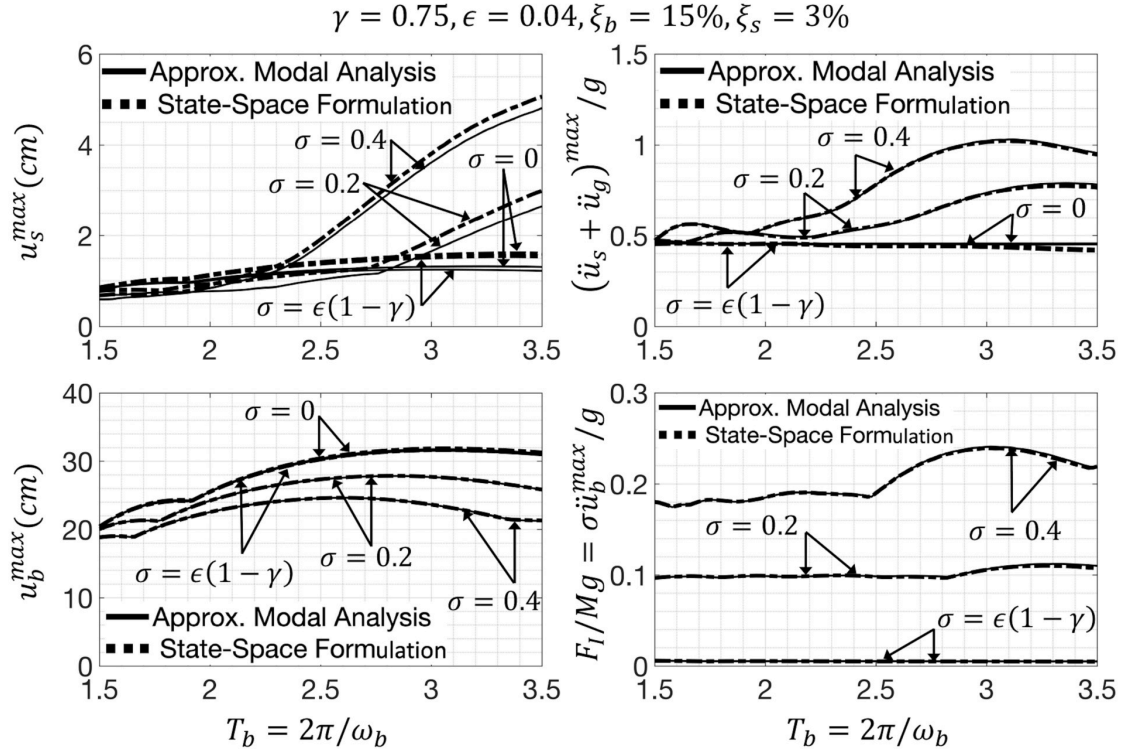


Figure 4.5: Left: Peak base u_b^{max} , and superstructure, u_s^{max} displacements of the 2DOF isolated structure shown in Figure 4.1 for a wide range of isolation periods ($1.5 \text{ sec} \leq T_b = 2\pi/\omega_b \leq 3.5 \text{ sec}$) and a constant value $\epsilon = \omega_b^2/\omega_s^2 = 0.04, \gamma = m_s/M = 0.75, \xi_b = 15\%, \xi_s = 3\%$ for various values of supplemental rotational inertia, $\sigma = 0, \epsilon(1 - \gamma) = 0.01, 0.2$ and 0.4 when subjected to the C02, N65E ground motion recorded during the 1966 Parkfield, California earthquake shown in Figure 4.4. The differences between the superstructure response when $\sigma = 0$ and when $\sigma = \epsilon(1 - \gamma)$ are marginal and within the error due to the approximations inherent to the approximate modal analysis procedure. Top-Right: Total superstructure accelerations. Bottom-Right: Force transferred to a non-compliant inverter-support.

periods ($T_b > 2.5 \text{ sec}$) both superstructure displacements and accelerations are increased.

The bottom-right subplots in Figures 4.5 and 4.6 show the reaction force at the non-compliant support of the inerter, F_I , given by equation(4.1). Clearly, the reaction force at the support of the inerter is an appreciable fraction of the weight of the entire structure, therefore a formulation that accounts for the deformation of the support of the inerter will offer superior results. This formulation is presented in the following section of the chapter which presents the response analysis of the 2DOF structure when the behavior of the isolation system is bilinear.

Our response analysis employs the C02, N65E ground motions from the 1966 Parkfield, California earthquake and the Pacoima Dam/164 ground motion from the 1971 San Fernando, California earthquake. Both these ground motions are characterized as pulse-like ground motions (Vassiliou

and Makris 2011; Efthymiou and Makris 2022); which are known to be responsible for appreciable displacement demands on flexible seismic isolated structures. In addition to their distinguishable long-duration pulse ($T_p = 0.6 \text{ sec}$ for the 1966 Parkfield motion and $T_p = 1.35 \text{ sec}$ for the San Fernando motion), both motions have a rich frequency content that is pertinent to the potential engagement of higher vibration modes.

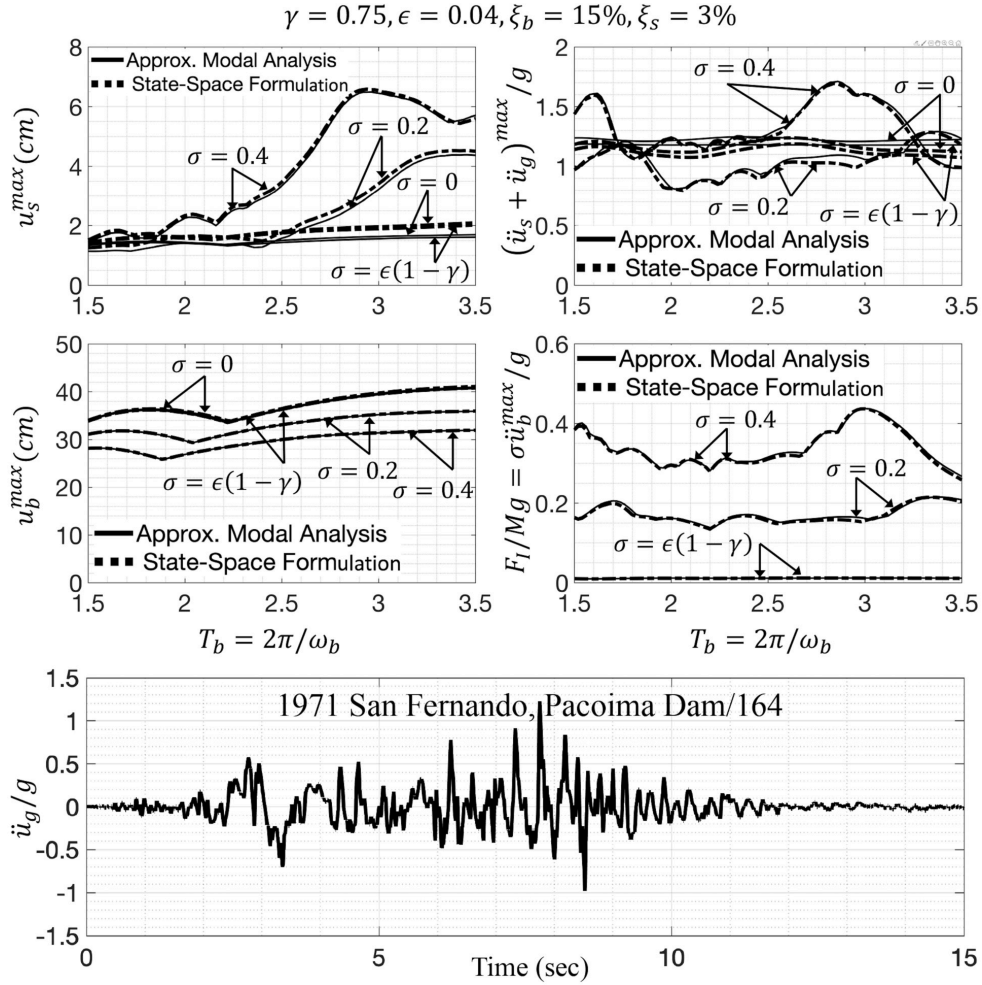


Figure 4.6: Left: Peak base u_b^{max} , and superstructure, u_s^{max} displacements of the 2DOF isolated structure shown in Figure 4.1 for a wide range of isolation periods ($1.5 \text{ sec} \leq T_b = 2\pi/\omega_b \leq 3.5 \text{ sec}$) and a constant value $\epsilon = \omega_b^2/\omega_s^2 = 0.04, \gamma = m_s/M = 0.75, \xi_b = 15\%, \xi_s = 3\%$ for various values of supplemental rotational inertia, $\sigma = 0, \epsilon(1 - \gamma) = 0.01, 0.2$ and 0.4 when subjected to the Pacoima Dam/164 ground motion recorded during the 1971 San Fernando, California earthquake shown at the bottom. The differences between the superstructure response when $\sigma = 0$ and when $\sigma = \epsilon(1 - \gamma)$ are marginal and within the error due to the approximations inherent to the approximate modal analysis procedure. Top-Right: Total superstructure accelerations. Bottom-Right: Force transferred to a non-compliant inerter-support.

4.3 SEISMIC RESPONSE OF A 2DOF STRUCTURE SUPPORTED ON A BILINEAR ISOLATION SYSTEM WITH SUPPLEMENTAL ROTATIONAL INERTIA

The linear theory of seismic isolation presented in the previous section offers insights on the advantages and challenges of supplemental rotational inertia when implemented in parallel with the isolation bearings. In an effort to better understand the role of supplemental rotational inertia in practical isolation systems, our study proceeds with the nonlinear time-history response analysis of the 2DOF structure shown in Figure 4.1, where now the isolation bearings exhibit bilinear behavior in association with some viscous damping ratio, c_b , that is relevant in the case where lead-rubber bearings (LRB) are used (Warburton and Soni 1977; Kelly 1997; Skinner et al. 1993; Makris and Kampas 2013; Wang et al. 2010).

With reference to Figure 4.7, the bilinear idealization which approximates satisfactorily the behavior of isolation bearings, including lead rubber bearings (LRB) and single concave sliding bearings (SCSB) (Mokha et al. 1990; Skinner et al. 1993; Al-Hussaini et al. 1994; Kelly 1997; Makris and Vassiliou 2011; Makris and Kampas 2013) is described with a preyielding stiffness k_1 , a postyielding stiffness $\alpha k_1 = k_b$ ($0 \leq \alpha < 1$), a yield displacement u_y , a yield force $F_y = k_1 u_y$ and a strength $Q = k_b u_y ((1/\alpha) - 1)$. With these parameters, the restoring force from a bilinear isolation system can be described with the Bouc-Wen model (Wen 1976; Baber and Noori 1985; Constantinou and Adnane 1987).

$$F = k_b u_b(t) + (1 - \alpha) k_1 u_y z(t) = k_b u(t) + (1 - \alpha) F_y z(t) \quad (4.33)$$

where $z(t)$ is a dimensionless internal variable given by

$$\frac{dz(t)}{dt} = \dot{z}(t) = \frac{1}{u_y} [\dot{u}_b(t) - \beta_z \dot{u}_b(t) |z(t)|^n - \gamma_z |\dot{u}_b(t)| z(t) |z(t)|^{n-1}] \quad (4.34)$$

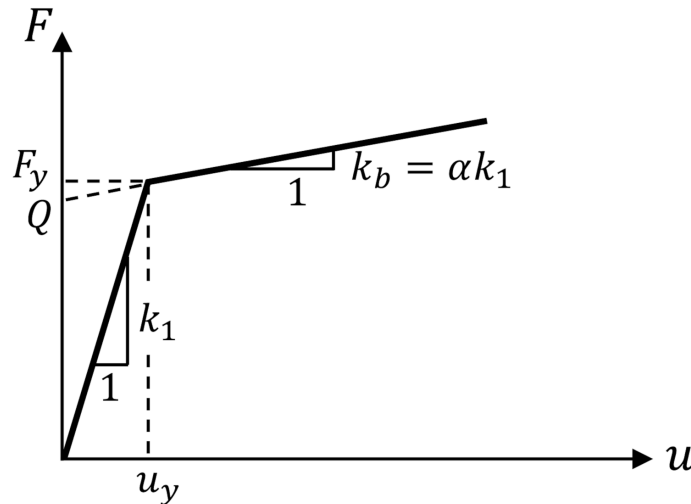


Figure 4.7: Bilinear idealization. From the five control parameters, k_1 , $k_b = \alpha k_1$, u_y , $F = k_1 u_y$ and $Q = (\frac{1}{\alpha} - 1) k_b u_y$ only these parameters are needed to define the bilinear behavior.

In equation (4.34), constants β_z , γ_z and n are model parameters. Parameter n controls the transition from the preyielding to the postyielding range; whereas parameters β_z and γ_z control the shape of the hysteretic loop. When $\beta_z + \gamma_z = 1$, then the dimensionless variable $z(t)$ is bounded by ± 1 ($-1 \leq z(t) \leq 1$) (Constantinou and Adnane 1987).

4.3.1 Response of Isolated Structure with Inerters Supported on a Non-Compliant Support

By virtue of equation (4.33), the dynamic equilibrium of the entire structure above the bilinear isolators in parallel with an inerter gives

$$(M + M_R) \ddot{u}_b + m_s \ddot{u}_s + c_b \dot{u}_b + k_b u_b + (1 - \alpha) F_y z = -M \ddot{u}_g \quad (4.35)$$

Equations (4.35) and (4.3) can be expressed in a matrix form in terms of the parameters defined in equations (4.4) and (4.5) after noting that $(1 - \alpha) F_y = Q$ and that $\frac{Q}{M} = \left(\frac{1}{\alpha} - 1\right) \omega_b^2 u_y$

$$\begin{bmatrix} 1 + \sigma & \gamma \\ 1 & 1 \end{bmatrix} \begin{Bmatrix} \ddot{u}_b \\ \ddot{u}_s \end{Bmatrix} + \begin{bmatrix} 2\xi_b \omega_b & 0 \\ 0 & 2\xi_s \omega_s \end{bmatrix} \begin{Bmatrix} \dot{u}_b \\ \dot{u}_s \end{Bmatrix} + \begin{bmatrix} \omega_b^2 & 0 \\ 0 & \omega_s^2 \end{bmatrix} \begin{Bmatrix} u_b \\ u_s \end{Bmatrix} + \frac{Q}{M} \begin{Bmatrix} z \\ 0 \end{Bmatrix} = - \begin{Bmatrix} 1 \\ 1 \end{Bmatrix} \ddot{u}_g \quad (4.36)$$

By multiplying equation (4.36) from the left with the inverse of the dimensionless mass matrix

$$\begin{bmatrix} 1 + \sigma & \gamma \\ 1 & 1 \end{bmatrix}^{-1} = \frac{1}{1 + \sigma - \gamma} \begin{bmatrix} 1 & -\gamma \\ -1 & 1 + \sigma \end{bmatrix} \quad (4.37)$$

The relative accelerations $\ddot{u}_b(t)$ and $\ddot{u}_s(t)$ of each degree-of-freedom become explicit expressions of the relative displacements and velocities of the degrees-of-freedom.

$$\ddot{u}_b(t) = \frac{1}{1 + \sigma - \gamma} [(-1 + \gamma) \ddot{u}_g(t) - 2\xi_b \omega_b \dot{u}_b(t) + 2\gamma \xi_s \omega_s \dot{u}_s(t) - \omega_b^2 u_b(t) + \gamma \omega_s^2 u_s(t) - \frac{Q}{M} z(t)] \quad (4.38)$$

$$\ddot{u}_s(t) = \frac{1}{1 + \sigma - \gamma} [-\sigma \ddot{u}_g(t) + 2\xi_b \omega_b \dot{u}_b(t) - 2(1 + \sigma) \xi_s \omega_s \dot{u}_s(t) + \omega_b^2 u_b(t) - (1 + \sigma) \omega_s^2 u_s(t) + \frac{Q}{M} z(t)] \quad (4.39)$$

The state vector of the system is $\{y(t)\} = \langle y_1(t), y_2(t), y_3(t), y_4(t), y_5(t) \rangle^T = \langle u_b(t), \dot{u}_b(t), u_s(t), \dot{u}_s(t), z(t) \rangle^T$. The solution of the system of nonlinear differential equations given by equations (4.38), (4.39) and (4.34) is computed by integrating the time-derivative of the state-vector

$$\{\dot{y}(t)\} = \begin{Bmatrix} \dot{u}_b(t) \\ \ddot{u}_b(t) \\ \dot{u}_s(t) \\ \ddot{u}_s(t) \\ \dot{z}(t) \end{Bmatrix} = \begin{Bmatrix} y_2(t) \\ \frac{1}{1 + \sigma - \gamma} [(-1 + \gamma) \ddot{u}_g - 2\xi_b \omega_b y_2(t) + 2\gamma \xi_s \omega_s y_4(t) - \omega_b^2 y_1(t) + \gamma \omega_s^2 y_3(t) - \frac{Q}{M} y_5(t)] \\ y_4(t) \\ \frac{1}{1 + \sigma - \gamma} [-\sigma \ddot{u}_g + 2\xi_b \omega_b y_2(t) - 2(1 + \sigma) \xi_s \omega_s y_4(t) + \omega_b^2 y_1(t) - (1 + \sigma) \omega_s^2 y_3(t) + \frac{Q}{M} y_5(t)] \\ \frac{1}{u_y} [y_2(t) - \beta_z y_2(t) |y_5(t)|^n - \gamma_z |y_2(t)| |y_5(t)|^{n-1}] \end{Bmatrix} \quad (4.40)$$

For the case of single concave sliding bearings (SCSB) with coefficient of friction, μ , the strength $Q = \mu M g$ so $Q/M = \mu g$. For the case of lead rubber bearings (LRB) with strength $Q = \beta_y M g$, so the ratio $Q/M = \beta_y g$ where $\beta_y g$ is the yield acceleration of the lead plugs. In order to compare the response of the 2DOF isolated structure supported on bilinear isolators with the response of the 2DOF linear isolated structure (elastic isolators with stiffness k_b) calculated with the approximate modal analysis procedure presented in the earlier sections, the hysteretic damping originating from

sliding or yielding of the lead plugs needs to be equivalent with the viscous damping of the linear isolation system, c_b . With reference to Figure 4.4 it is evident that during strong shaking the isolation system undergoes cyclic motion with period $T_b = 2\pi/\omega_b$ and amplitude u_b . Accordingly, the energy dissipated during each of the dominant cycles shown in Figure 4.4 is

$$W_D \approx \pi\omega_b u_b^2 c_b = \pi\omega_b^2 u_b^2 2\xi_b M \quad (4.41)$$

On the other hand, the energy dissipated per cycle from a bilinear isolation system (sliding or yielding) is

$$W_D \approx 4Q u_b \quad (4.42)$$

By equating the right-hand-sides of equations (4.41) and (4.42), the equivalent yield acceleration of the bilinear isolation system is

$$\frac{Q}{M} = \frac{\pi}{2}\omega_b^2 u_b \xi_b = \mu g \quad \text{or} \quad = \beta_y g \quad (4.43)$$

In the interest of simplicity, we focus on single-concave sliding spherical bearings with coefficient of friction μ and radius of curvature R_b . In this case $\omega_b^2 = g/R_b$ and equation (4.43) yields that the equivalent value of friction coefficient is

$$\mu = \frac{2\pi^3}{g} \frac{u_b}{T_b^2} \xi_b = \frac{\pi}{2} \frac{u_b}{R_b} \xi_b \quad \text{for (SCSB)} \quad (4.44)$$

Figure 4.8(left) plots the base, u_b^{max} , and the superstructure, u_s^{max} peak displacements of the 2DOF isolated structure, shown in Figure 4.1 when supported on bilinear isolation bearings for a wide range of isolation periods ($1.5 \text{ sec} \leq T_b = 2\pi/\omega_b \leq 3.5 \text{ sec}$) for a constant value $\epsilon = \omega_b^2/\omega_s^2 = 0.04$, $\gamma = m_s/M = 0.75$, $\xi_b = 0$, $\xi_s = 3\%$, coefficient of friction μ as offered by equation (4.44) for $\xi_b = 15\%$, $u_y = 0.25 \text{ mm}$ (Constantinou et al. 1990) and various values of supplemental rotational inertia, $\sigma = 0$, $\epsilon(1 - \gamma) = 0.01, 0.2$ and 0.4 , when subjected to the C02, N65E ground motion recorded during the 1966 Parkfield, California earthquake. The bottom-right plot offers the equivalent value of the friction coefficient μ as results from equation (4.44) for every isolation period value after reading the values of u_b^{max} that result from the linear modal analysis procedure (solid lines). Figure 4.8 reveals that when the response of the isolation bearings is bilinear, the approximate modal analysis captures satisfactorily the elastic response of the superstructure; however, noticeable differences are observed in the base displacements when computed with the rigorous state-space formulation of the nonlinear equation of motion and the approximate modal analysis. Figure 4.8 also reveals that supplemental rotational inertia aggravates both superstructure displacements and accelerations at larger isolation periods ($T_b > 2.5 \text{ sec}$). Figure 4.9 plots the same response quantities shown in Figure 4.8 when the 2DOF isolated structure shown in Figure 4.1 is subjected to the Pacoima Dam/164 ground motion recorded during the 1971 San Fernando, California earthquake. Trends similar to those discussed in Figure 4.8 are observed confirming that supplemental rotational inertia aggravates both superstructure displacements and accelerations at larger isolation periods ($T_b > 2.5 \text{ sec}$).

4.3.2 Response of Isolated Structure with Inerter Supported on a Compliant Support

Given the appreciable reaction forces that develop at the support of the inerter as the inertance $\sigma = M_R/M$ increases (see Figures 4.5 and 4.6), we now examine, the dynamic response of the

2DOF isolated structure shown in Figure 4.1, yet now the support of the inerter has finite stiffness k_f . Because of the compliance of the support, the force from the inerter is no-longer expressed with equation (4.1) which is for a non-compliant support, rather it is expressed from

$$F_I(t) + \frac{M_R}{k_f} \frac{d^2 F_I(t)}{dt^2} = M_R \frac{d^2 u_b(t)}{dt^2} \quad (4.45)$$

Equation (4.45) is the constitutive law of a spring-inerter in-series connection (Makris and Kampas 2016; Makris 2017, 2018) that was coined recently the inertoelastic fluid (Makris 2017). By defining the rotational frequency $\omega_R = \sqrt{k_f/M_R}$ (Makris 2017, 2018), the matrix equation (4.36) is replaced by

$$\begin{bmatrix} 1 & \gamma \\ 1 & 1 \end{bmatrix} \begin{Bmatrix} \ddot{u}_b \\ \ddot{u}_s \end{Bmatrix} + \begin{bmatrix} 2\xi_b\omega_b & 0 \\ 0 & 2\xi_s\omega_s \end{bmatrix} \begin{Bmatrix} \dot{u}_b \\ \dot{u}_s \end{Bmatrix} + \begin{bmatrix} \omega_b^2 & 0 \\ 0 & \omega_s^2 \end{bmatrix} \begin{Bmatrix} u_b \\ u_s \end{Bmatrix} + \frac{Q}{M} \begin{Bmatrix} z \\ 0 \end{Bmatrix} = - \begin{bmatrix} 1 & 1 \\ 0 & 1 \end{bmatrix} \begin{Bmatrix} \frac{F_I(t)}{M} \\ \ddot{u}_g(t) \end{Bmatrix} \quad (4.46)$$

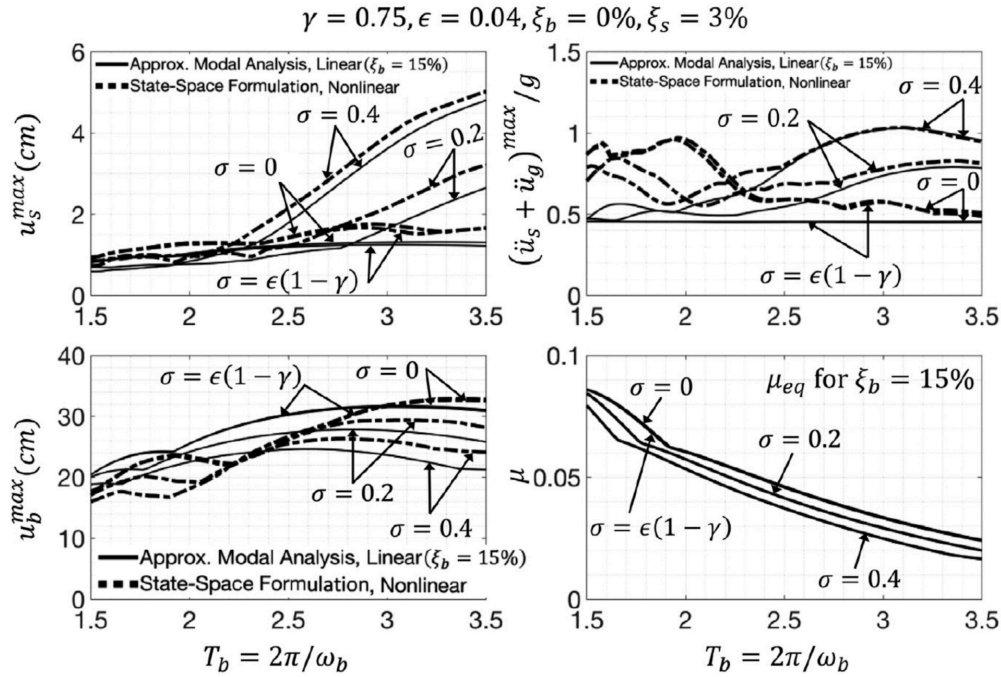


Figure 4.8: Left: Peak base u_b^{max} , and superstructure, u_s^{max} displacements of the 2DOF isolated structure shown in Figure 4.1 for a wide range of isolation periods ($1.5 \text{ sec} \leq T_b = 2\pi/\omega_b \leq 3.5 \text{ sec}$) for a constant value $\epsilon = \omega_b^2/\omega_s^2 = 0.04, \gamma = m_s/M = 0.75, \xi_b = 0, \xi_s = 3\%$, coefficient of friction μ as shown in bottom-right subplot, $u_y = 0.25 \text{ mm}$ and various values of supplemental rotational inertia, $\sigma = 0, \epsilon(1-\gamma) = 0.01, 0.2$ and 0.4 when subjected to the C02, N65E ground motion recorded during the 1966 Parkfield, California earthquake. The bottom-right plot offers the equivalent value of the friction coefficient μ as results from equation (4.44) for $\xi_b = 15\%$ (which is the isolation damping used in the approximate model analysis) for every isolation period value; whereas the top-right plot offers the total superstructure accelerations.

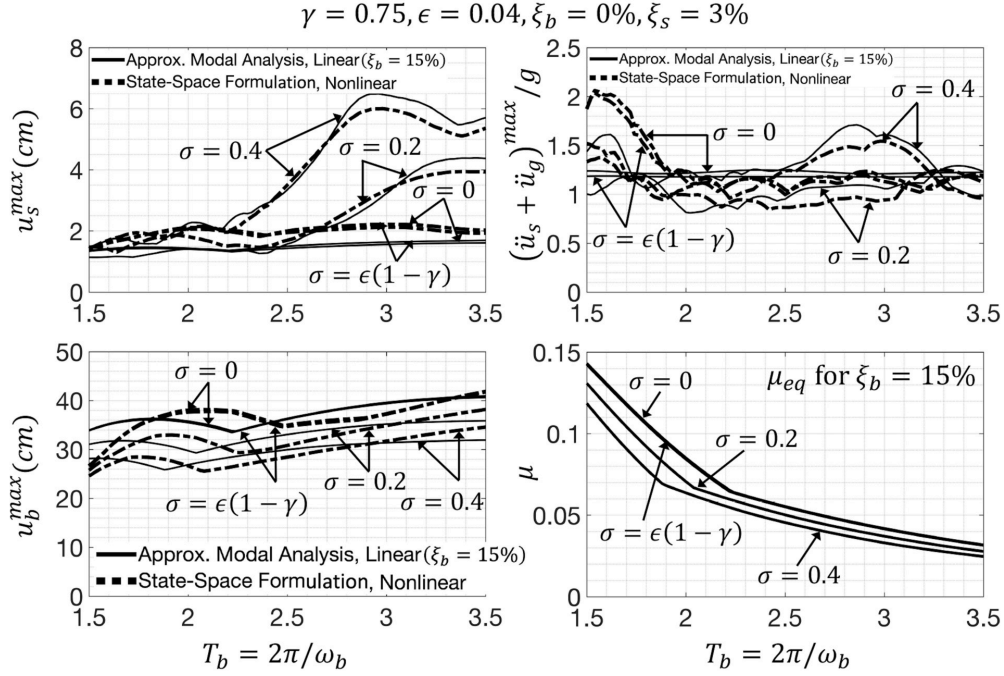


Figure 4.9: Left: Peak base u_b^{max} , and superstructure, u_s^{max} displacements of the 2DOF isolated structure shown in Figure 4.1 for a wide range of isolation periods ($1.5 \text{ sec} \leq T_b = 2\pi/\omega_b \leq 3.5 \text{ sec}$) for a constant value $\epsilon = \omega_b^2/\omega_s^2 = 0.04, \gamma = m_s/M = 0.75, \xi_b = 0, \xi_s = 3\%$, coefficient of friction μ as shown in bottom-right subplot, $u_y = 0.25 \text{ mm}$ and various values of supplemental rotational inertia, $\sigma = 0, \epsilon(1 - \gamma) = 0.01, 0.2$ and 0.4 when subjected to the Pacoima Dam/164 ground motion recorded during the 1971 San Fernando, California earthquake. The bottom-right plot offers the equivalent value of the friction coefficient μ as results from equation (4.44) for $\xi_b = 15\%$ (which is the isolation damping used in the approximate model analysis) for every isolation period value; whereas the top-right plot offers the total superstructure accelerations at a non-compliant support of the inerter.

By multiplying equation (4.46) from the left with the inverse of the dimensionless mass matrix

$$\begin{bmatrix} 1 & \gamma \\ 1 & 1 \end{bmatrix}^{-1} = \frac{1}{1-\gamma} \begin{bmatrix} 1 & -\gamma \\ -1 & 1 \end{bmatrix} \quad (4.47)$$

The relative accelerations $\ddot{u}_b(t)$ and $\ddot{u}_s(t)$ of each degree-of-freedom become explicit expressions of the relative displacements and velocities of the degrees-of-freedom.

$$\ddot{u}_b(t) = -\ddot{u}_g(t) + \frac{1}{1-\gamma} \left[-f_I(t) - 2\xi_b\omega_b\dot{u}_b(t) + 2\gamma\xi_s\omega_s\dot{u}_s(t) - \omega_b^2u_b(t) + \gamma\omega_s^2u_s(t) - \frac{Q}{M}z \right] \quad (4.48)$$

$$\ddot{u}_s(t) = \frac{1}{1-\gamma} \left[f_I(t) + 2\xi_b\omega_b\dot{u}_b(t) - 2\xi_s\omega_s\dot{u}_s(t) + \omega_b^2u_b(t) - \omega_s^2u_s + \frac{Q}{M}z \right] \quad (4.49)$$

where $f_I(t) = F_I(t)/M$ has units of acceleration. The state vector of the system is $\{y(t)\} = \langle y_1(t), y_2(t), y_3(t), y_4(t), y_5(t), y_6(t), y_7(t) \rangle^T = \langle u_b(t), \dot{u}_b(t), u_s(t), \dot{u}_s(t), f_I(t), \dot{f}_I(t),$

$z(t) >^T$. The solution of the system of nonlinear differential equations given by equations (4.48), (4.49) and (4.45) is computed by integrating the time-derivative of the state-vector

$$\{\dot{y}(t)\} = \begin{Bmatrix} \dot{u}_b(t) \\ \ddot{u}_b(t) \\ \dot{u}_s(t) \\ \ddot{u}_s(t) \\ \dot{f}_I(t) \\ \ddot{f}_I(t) \\ \dot{z}(t) \end{Bmatrix} = \begin{Bmatrix} y_2(t) \\ -\ddot{u}_g(t) + \frac{1}{1-\gamma} [-y_5(t) - 2\xi_b\omega_b y_2(t) + 2\gamma\xi_s\omega_s y_4(t) - \omega_b^2 y_1(t) + \gamma\omega_s^2 y_3(t) - \frac{Q}{M}y_7(t)] \\ y_4(t) \\ \frac{1}{1-\gamma} [y_5(t) + 2\xi_b\omega_b y_2(t) - 2\xi_s\omega_s y_4(t) + \omega_b^2 y_1(t) - \omega_s^2 y_3(t) + \frac{Q}{M}y_7(t)] \\ y_6(t) \\ \omega_R^2 (\sigma \ddot{u}_b(t) - y_5(t)) \\ \frac{1}{u_y} [y_2(t) - \beta_z y_2(t) |y_7(t)|^n - \gamma_z |y_2(t)| |y_7(t)|^{n-1}] \end{Bmatrix} \quad (4.50)$$

Figure 4.10(left) plots the base, u_b^{max} , and superstructure, u_s^{max} , peak displacements of the 2DOF isolated structure shown in Figure 4.1 when supported on bilinear isolation bearings for a wide range of isolation periods ($1.5 \text{ sec} \leq T_b \leq 3.5 \text{ sec}$) for a constant value of $\epsilon = \omega_b^2/\omega_s^2 = 0.04$, $\gamma = 0.75$, $\xi_b = 0\%$, $\xi_s = 3\%$, coefficient of friction μ as offered by equation (4.44) for $\xi_b = 15\%$, $u_y = 0.25 \text{ mm}$ and various values of supplemental rotational inertia, $\sigma = 0, \epsilon(1-\gamma) = 0.01, 0.2$

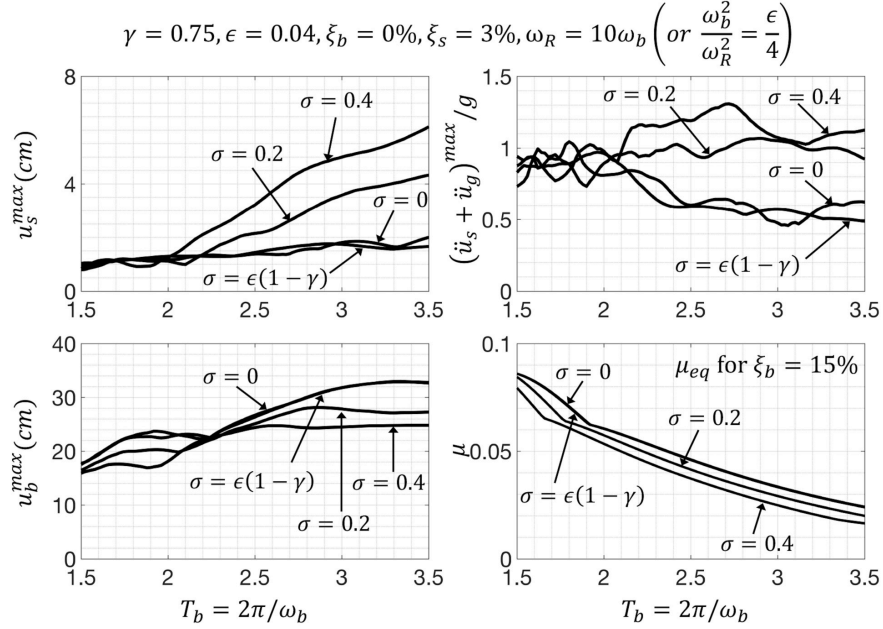


Figure 4.10: Left: Peak base u_b^{max} , and superstructure, u_s^{max} displacements of the 2DOF isolated structure shown in Figure 4.1 for a wide range of isolation periods ($1.5 \text{ sec} \leq T_b = 2\pi/\omega_b \leq 3.5 \text{ sec}$) for a constant value $\epsilon = \omega_b^2/\omega_s^2 = 0.04$, $\gamma = m_s/M = 0.75$, $\xi_b = 0$, $\xi_s = 3\%$, coefficient of friction μ as shown in bottom-right subplot, $u_y = 0.25 \text{ mm}$ and various values of supplemental rotational inertia, $\sigma = 0, \epsilon(1-\gamma) = 0.01, 0.2$ and 0.4 on a compliant support ($\omega_b/\omega_R = \epsilon/4$) when subjected to the C02, N65E ground motion recorded during the 1966 Parkfield, California earthquake. The bottom-left plot offers the equivalent value of the friction coefficient μ as results from equation (4.44) for $\xi_b = 15\%$ for every isolation period value; whereas the top-right plot offers the total superstructure accelerations.

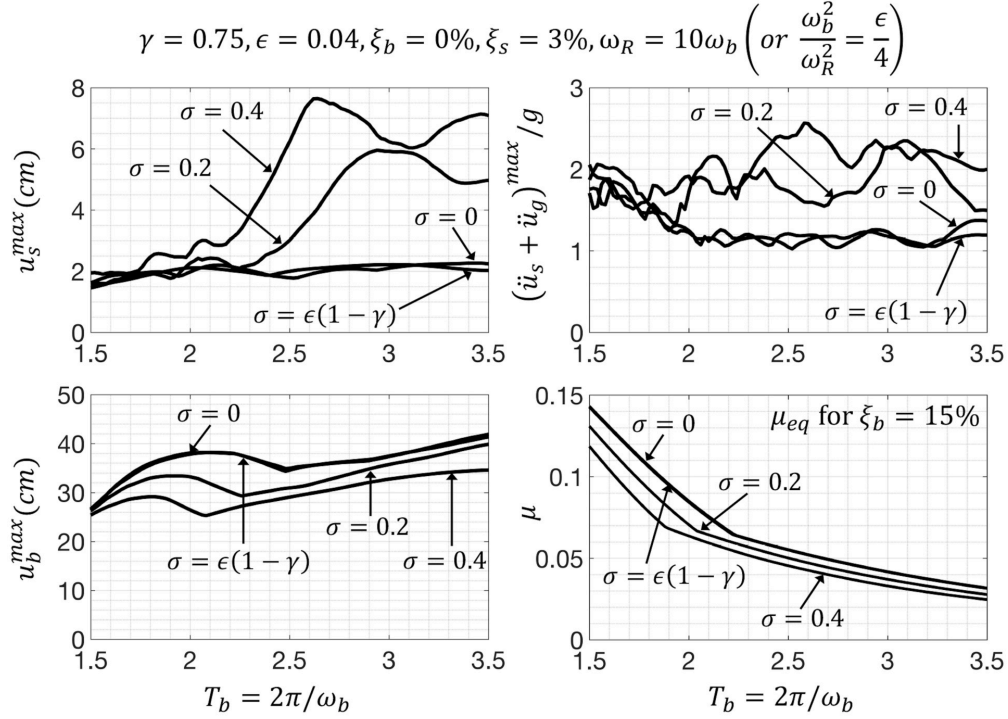


Figure 4.11: Left: Peak base u_b^{max} , and superstructure, u_s^{max} displacements of the 2DOF isolated structure shown in Figure 4.1 for a wide range of isolation periods ($1.5 \text{ sec} \leq T_b = 2\pi/\omega_b \leq 3.5 \text{ sec}$) for a constant value $\epsilon = \omega_b^2/\omega_s^2 = 0.04, \gamma = m_s/M = 0.75, \xi_b = 0, \xi_s = 3\%$, coefficient of friction μ as shown in bottom-right subplot, $u_y = 0.25 \text{ mm}$ and various values of supplemental rotational inertia, $\sigma = 0, \epsilon(1-\gamma) = 0.01, 0.2$ and 0.4 on a compliant support ($\omega_b/\omega_R = \epsilon/4$) when subjected to the Pacoima Dam/164 ground motion recorded during the 1971 San Fernando, California earthquake. The bottom-left plot offers the equivalent value of the friction coefficient μ as results from equation (4.44) for $\xi_b = 15\%$ for every isolation period value; whereas the top-right plot offers the total superstructure accelerations.

and 0.4 supported on a compliant support ($\omega_b^2/\omega_R^2 = \epsilon/4$), when subjected to the C02, N65E ground motion recorded during the 1966 Parkfield, California earthquake. Figure 4.10 reveals that when the support of the inerter is compliant, supplemental rotational inertia further aggravates superstructure displacements and accelerations at larger isolation periods ($T_b > 2.5 \text{ sec}$).

Similar trends are observed in Figure 4.11 which plots the nonlinear response of the 2DOF isolated structure when subjected to the Pacoima Dam/164 ground motion recorded during the 1971 San Fernando, California earthquake and the inerter in the isolation system is supported on a compliant support ($\omega_b^2/\omega_R^2 = \epsilon/4$).

4.4 CONCLUSIONS

The study presented in this chapter was partly motivated from the known and occasionally overstated property of inerters to eliminate the participation of the second mode of the classical 2DOF linear isolated structure and partly from the need to better understand the effect of supplemental rotational inertia when acting in parallel with bilinear isolators. Our study first shows that while a small amount of supplemental rotational inertia is needed to eliminate the participation of the second mode of the 2DOF isolated structure; the effect of this elimination is marginal on the structure response, since the participation of the second mode is invariably small even when isolation systems without inerters are used (Kelly 1990, 1997).

Within the context of linear analysis, our study brings forward inadvertent errors in a recent study (Ye et al. 2019) that violate the orthogonality of eigenmodes; and revisits how supplemental rotational inertia at the isolation level influences the modal frequencies, mode shapes and participation factors of the classical 2DOF linear seismically isolated, structure (Kelly 1990, 1997). Finally, our study proceeds with the nonlinear response analysis of the same 2DOF isolated structure by adopting a bilinear behavior for the isolation system in association with a formulation that accounts for the compliance of the support of the inverter and shows that supplemental rotational inertia aggravates superstructure displacements and accelerations at larger isolation periods ($T_b > 2.5 \text{ sec}$). In view of these findings in association with the small gains in reducing displacements above isolators, the use of inerters in isolation systems is not recommended.

5 Seismic Response of Yielding Structures Equipped with Inerters

All the aforementioned studies referenced in the previous chapters other than the studies by De Domenico and Ricciardi (2018b) and Moghimi and Makris (2021) examined invariably the response of elastic structures. In particular, chapter 3 and the study by Makris and Moghimi (2019) concluded that while the use of inerters may reduce effectively the first-story displacements of a 2DOF elastic structure, under certain strong ground motions, the first-story displacements are large enough, suggesting that an inelastic model for the structure is more appropriate. Furthermore, seismic design according to modern building codes allow damage in design basis level earthquakes and beyond, therefore it is needed to evaluate the efficacy of the inerters as a protective system in reducing or eliminating damage. In view of this finding and given the increasing number of strong acceleration records in urban areas, this chapter examines the inelastic response of a single degree of freedom (SDOF) and a two degree of freedom (2DOF) yielding structure equipped with inerters. Our interest in the inelastic response of a 2DOF yielding structure is primarily motivated from the need to understand to what extent the engagement of an inerter at the first story aggravates the inelastic deformation of the superstructure. In the 2DOF yielding structures, the inerter is placed only at the first story given that inerters, while suppressing displacements, they transfer appreciable shear forces which can be accommodated by the foundation.

5.1 INERTIA FORCES FROM AN INERTER SUPPORTED ON A STIFF CHEVRON FRAME

Figure 5.1(a) depicts a SDOF structure in which the mass, m_1 is engaged with a flywheel with radius R_1 and mass m_{w1} that can rotate about an axis O. Concentric to the flywheel; there is an attached pinion with radius ρ_1 engaged with a linear rack connected to the bottom of the vibrating mass m_1 of the SDOF structure. When the supporting chevron frame is stiff, the rotation, $\theta_1(t)$, of the flywheel is proportional to the relative displacement, $u_1(t)$, of the frame (Makris and Kampas 2016) as shown by equation (3.1).

For a positive displacement, $u_1(t)$, to the right, the internal force, $F_I(t)$ at the rack-pinion interface opposes the motion (to the left) [Figure 5.1(a)]. Moment equilibrium of the flywheel about point O is given by equation (3.2). Substituting equation (3.1) into equation (3.2) gives equation (3.3).

Equation (3.3) gives the inertial force, $F_I(t)$, at the rack-pinion interface-that is, the force trans-

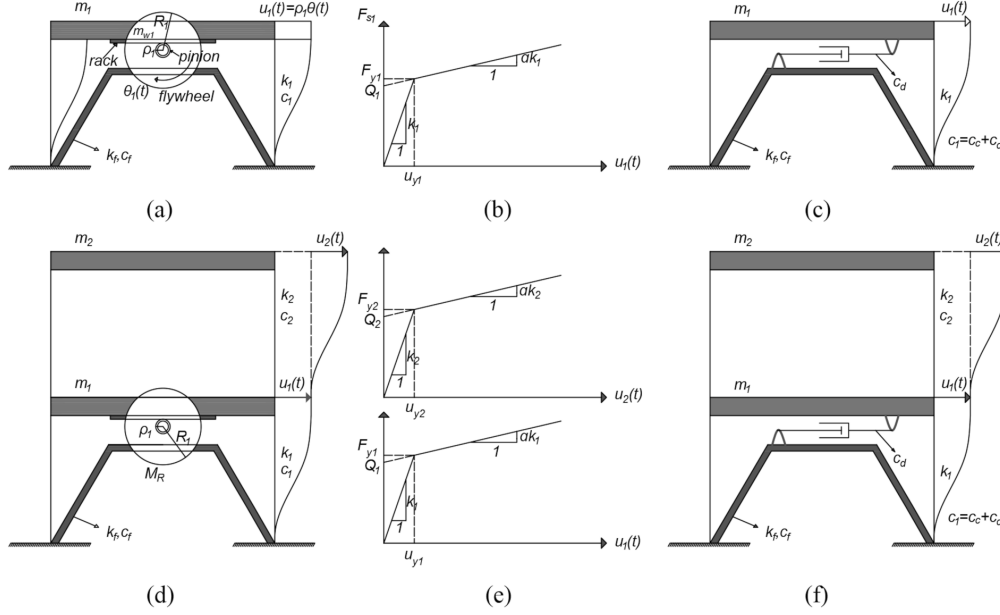


Figure 5.1: (a) SDOF yielding structure engaged with a rotational flywheel system; (b) Bilinear idealization of the inelastic behavior of the yielding SDOF structure; (c) SDOF yielding structure with supplemental damping; (d) 2DOF yielding structure engaged with a flywheel system; (e) Bilinear idealization of the inelastic behavior of each story of the 2DOF yielding structure; (f) 2DOF yielding structure with supplemental damping at its first story.

ferred to the stiff chevron frame. The constant of proportionality, $M_R = (1/2) m_{w1} (R_1^2 / \rho_1^2)$ is the inertance of the supplemental rotational inertia system and has units of mass [M]. The inertance, M_R , can be amplified by adding two (or more) flywheels in series, in which the first flywheel is a gearwheel Smith 2002; Makris and Kampas 2016.

5.2 EQUATION OF MOTION OF A YIELDING SDOF STRUCTURE WITH INERTERS SUPPORTED ON A STIFF CHEVRON FRAME

With reference to Figures 5.1(a) and (b), this chapter first examines the dynamic response of a yielding SDOF structure with mass, m_1 , preyielding stiffness, k_1 , postyielding stiffness, αk_1 ($0 \leq \alpha < 1$), and yielding displacement, u_{y1} , that is engaged with an inerter with inertance, M_R , supported on a stiff chevron frame. The dynamic equilibrium of the vibrating mass when subjected to a ground excitation, $\ddot{u}_g(t)$, gives:

$$m_1 [\ddot{u}_1(t) + \ddot{u}_g(t)] = -F_{s1}(t) - c_1 \dot{u}_1(t) - F_I(t) \quad (5.1)$$

where $F_I(t)$ = internal force from the inerter given by equation (3.3) and $F_{s1}(t)$ = inelastic restoring force of the structure that is described by the Bouc-Wen model (Wen 1976; Baber and Noori 1985).

$$F_{s1} = \alpha k_1 u_1(t) + (1 - \alpha) k_1 u_{y1} z_1(t) \quad (5.2)$$

where $\alpha =$ postyielding-to-preyielding stiffness ratio; and $-1 \leq z_1(t) \leq 1 =$ dimensionless internal variable described by

$$\dot{z}_1(t) = \frac{1}{u_{y1}} [\dot{u}_1(t) - \beta_z \dot{u}_1(t) |z_1(t)|^n - \gamma_z |\dot{u}_1(t)| z_1(t) |z_1(t)|^{n-1}] \quad (5.3)$$

In equation (5.3), constants β_z , γ_z and $n =$ model parameters. In the entire study $\beta_z = \gamma_z = 0.5$ and $n = 10$. Substitution of equations. (3.3) and (5.2) into equation (5.1) gives:

$$m_1 \ddot{u}_1(t) + M_R \ddot{u}_1(t) + c_1 \dot{u}_1(t) + \alpha k_1 u_1(t) + (1 - \alpha) k_1 u_{y1} z_1(t) = -m_1 \ddot{u}_g(t) \quad (5.4)$$

By introducing the nominal frequency ω_1 , viscous damping ratio ξ_1 and inertance ratio σ ,

$$\omega_1^2 = \frac{k_1}{m_1}, \quad 2\xi_1 \omega_1 = \frac{c_1}{m_1}, \quad \sigma = \frac{M_R}{m_1} \quad (5.5)$$

where $c_1 = c_c + c_d$ in witch $c_c =$ the damping from the framing action and $c_d =$ the damping constant of a possible supplemental damper; equation (5.4) assumes the form

$$(1 + \sigma) \ddot{u}_1(t) + 2\xi_1 \omega_1 \dot{u}_1(t) + \alpha \omega_1^2 u_1(t) + (1 - \alpha) \omega_1^2 u_{y1} z_1(t) = -\ddot{u}_g(t) \quad (5.6)$$

Upon dividing with the acceleration coefficient, $(1 + \sigma)$, equation (5.6) gives

$$\ddot{u}_1(t) + 2 \frac{\xi_1 \omega_1}{1 + \sigma} \dot{u}_1(t) + \alpha \frac{\omega_1^2}{1 + \sigma} u_1(t) + (1 - \alpha) \frac{\omega_1^2}{1 + \sigma} u_{y1} z_1(t) = -\frac{\ddot{u}_g(t)}{1 + \sigma} \quad (5.7)$$

Equation (5.7) indicates that the engagement of SDOF yielding structure with the inerter lengthens the preyielding period of the SDOF structure ($\omega_1^{apparent} = \omega_1 / \sqrt{1 + \sigma}$), reduces the apparent viscous damping, ($\xi_1^{apparent} = \xi_1 / \sqrt{1 + \sigma}$); yet, most importantly, it suppresses the level of ground shaking given that the denominator, $1 + \sigma$, in the right-hand-side of equation (5.7) is always larger than unity. The lengthening of the preyielding period of the structures implies that when a yielding structure is equipped with an inerter the equal-displacement rule (Veletsos et al. 1965) is established earlier in the response spectrum (at lower preyielding periods). It is recalled that the inelastic deformation of relative flexible structures (say preyielding period, $T_1 > 0.6sec$) is equal to the displacement of the elastic structure with the same period.

The solution of the system of equations given by equations (5.6) and (5.3) is computed numerically via a state-space formulation (Makris and Kampas 2016; Aghagholizadeh and Makris 2018; Makris and Moghimi 2019). The state-vector of the system is

$$\{y(t)\} = \langle y_1(t), y_2(t), y_3(t) \rangle^T = \langle u_1(t), \dot{u}_1(t), \dot{z}_1(t) \rangle^T \quad (5.8)$$

where the superscript, T , stands for the transpose of the line vector, $\langle \rangle$, and the time-derivative state-vector, $\{\dot{y}(t)\}$, is expressed solely in terms of the state variables appearing in the state-vector given by equation (5.8)

$$\{\dot{y}(t)\} = \left\{ \begin{array}{l} \dot{u}_1(t) \\ \ddot{u}_1(t) \\ \dot{z}_1(t) \end{array} \right\} = \left\{ \begin{array}{l} y_2(t) \\ \frac{1}{1+\sigma} [-\ddot{u}_g(t) - 2\xi_1 \omega_1 y_2(t) - \alpha \omega_1^2 y_1(t) - (1 - \alpha) \omega_1^2 u_{y1} y_3(t)] \\ \frac{1}{u_{y1}} [y_2(t) - \beta_z y_2(t) |y_3(t)|^n - \gamma_z |y_2(t)| y_3(t) |y_3(t)|^{n-1}] \end{array} \right\} \quad (5.9)$$

The numerical integration of the time-derivative of the state-vector, $\{\dot{y}(t)\}$, given by equation (5.9) is performed with standard ordinary differential equation (ODE) solvers available in MATLAB¹.

From the five parameters that appear in the bilinear idealization shown in Figure 5.1(b) ($k_1 =$ preyielding stiffness, $\alpha k_1 =$ postyielding stiffness, $u_{y1} =$ yield displacement, $Q_1 =$ strength and $F_{y1} =$ yield force), only three parameters are needed to fully describe the bilinear behavior (see for instance, Makris and Kampas 2013). In this work, we select the preyielding stiffness, $k_1 = m_1 \omega_1^2 = m_1 4\pi^2/T_1^2$, the postyielding stiffness, αk_1 , and the strength of the structure Q_1 . With reference to Figure 5.1(b), $F_{y1} = k_1 u_{y1} = Q_1 + \alpha k_1 u_{y1}$. Accordingly,

$$u_{y1} = \frac{Q_1}{k_1 - \alpha k_1} = \frac{Q_1}{m_1} \frac{T_1^2}{4\pi^2(1 - \alpha)} \quad (5.10)$$

5.2.1 The use of a pair of clutching inerters

One challenge with the implementation of inerters is that the rotating flywheels should only resist the motion of the structure, without inducing any deformations. This is feasible with the use of a clutch so that the pinion of the first gearwheel that is engaged with the rack is unable to drive the rack, and only the motion of the translating rack can drive the pinion-gearwheel (Makris and Kampas 2016). The sequential engagement of the two parallel-rotational-inertial systems that can only resist the motion is expressed mathematically as (Makris and Kampas 2016)

$$\frac{F_I(t)}{m_1} = \sigma \ddot{u}_1(t) \quad \text{when } \text{sgn} \left[\frac{\ddot{u}_1(t)}{\dot{u}_1(t)} \right] > 0 \quad (5.11a)$$

and

$$\frac{F_I(t)}{m_1} = 0 \quad \text{when } \text{sgn} \left[\frac{\ddot{u}_1(t)}{\dot{u}_1(t)} \right] \leq 0 \quad (5.11b)$$

Accordingly, when a pair of clutching inerters is employed, the equation of motion given in equation (5.6) is modified to

$$(1 + \delta\sigma) \ddot{u}_1(t) + 2\xi_1\omega_1\dot{u}_1(t) + \alpha\omega_1^2 u_1(t) + (1 - \alpha) \omega_1^2 u_{y1} z_1(t) = -\ddot{u}_g(t) \quad (5.12)$$

in which

$$\delta = \begin{cases} 1, & \text{when } \text{sgn} \left[\frac{\ddot{u}_1(t)}{\dot{u}_1(t)} \right] > 0 \\ 0, & \text{when } \text{sgn} \left[\frac{\ddot{u}_1(t)}{\dot{u}_1(t)} \right] \leq 0 \end{cases} \quad (5.13)$$

Response time histories for an elastic SDOF oscillator equipped with a single inerter and a pair of clutching inerters have been presented in (Makris and Kampas 2016; Makris 2017). Clearly, when a pair of clutching inerters is employed, the flywheels only resist the motion of the structure and do not give back any energy to the structure.

¹ MATLAB. (2021). High performance numerical computation and visualization software. The Math works, Natick,Mass.

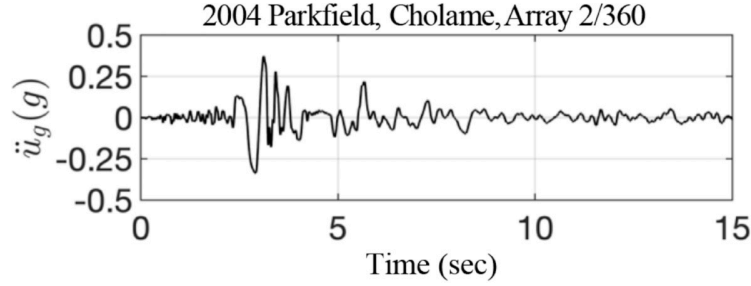


Figure 5.2: The Cholame, Array 2/360 acceleration time history recorded during the 2004 Parkfield, California earthquake.

5.3 RESPONSE SPECTRA OF A YIELDING SDOF STRUCTURE WITH INERTERS SUPPORTED ON A STIFF CHEVRON FRAME

The seismic response of a SDOF yielding structure equipped with an inerter as described by equation (5.6) or equation (5.12) and (5.13) is compared with the response of the same SDOF yielding structure where the inerter is replaced with a supplemental viscous damper with damping constant c_d [Figure 5.1(c)]. In this case, the value of the damping coefficient, $c_1 = c_c + c_d$, where c_c is the damping originating from the columns of the SDOF structure and c_d is the damping constant of the supplemental viscous damper. Together with the drift response, u_1 (relative displacement), of interest are the normalized base shear at the columns of the inelastic frame, $V_{columns}/(m_1g)$, the normalized base shear at the foundation of the inelastic structure, $V_b/(m_1g) = (\dot{u}_1 + \ddot{u}_g)/g$, which is the total acceleration of the first story normalized by g ; and the normalized force transferred to the mounting of the inerter, F_I/m_1g or to the mounting of the supplemental damper $c_d\dot{u}_1/m_1g = 2\xi_d\omega_1\dot{u}_1/g$. From equation (5.6) or equations (5.12) and (5.13), the normalized base shear at the columns is $[2\xi_c\omega_1\dot{u}_1(t) + \alpha\omega_1^2u_1(t) + (1 - \alpha)\omega_1^2u_{y1}(t)]/g$.

Figure 5.2 shows the recorded acceleration time history used for the response spectrum analysis presented in this chapter, the Cholame Number 2/360 ground motion recorded during the 2004 Parkfield California earthquake, together with the Gilroy Array 6/230 ground motion recorded during the 1979 Coyote Lake California earthquake shown in Figure 3.5(a). The response spectra shown in Figure 5.3 are the results of the solution of equation (5.6) for a single inerter (left plots) or equations (5.12) and (5.13) when a pair of clutching inerters is used (right plots) to modify the response of an elastoplastic ($\alpha = 0$) SDOF structure with normalized strength $Q_1/m_1 = 0.1g$ and $\xi_c = 0$ when subjected to the Gilroy Array 6/230 ground motion recorded during the 1979 Coyote Lake earthquake (Figure 3.5(a)). When $\sigma = 0$ (thin black line), the solution offers the response of the elastoplastic SDOF structure without any response modification device. The two heavier solid black lines are for values of normalized inertance, $\sigma = 0.5$ and $\sigma = 1.0$. The dashed lines are when the yielding SDOF structure is equipped with the supplemental damping $\xi_d = \xi_1 = 25\%$ given that the viscous damping of the yielding SDOF is taken to be equal to zero ($\xi_c = 0$). Together with the response of the elastoplastic oscillator (black lines), the spectra shown in Figure 5.3 plot for comparing the response of an elastic oscillator (red lines). When $\sigma = 0$, the thin red line meets the thin black line (no inerter, $\sigma = 0$) at a value of the preyielding period $T_1 \cong 1.4 \text{ sec}$, confirming the equal-displacement rule (Veletsos et al. 1965). The equal-displacement rule also holds when

$$\frac{Q_1}{m_1 g} = 0.1, \quad \alpha = 0.0, \quad \beta_z = 0.5, \quad \gamma_z = 0.5, \quad n = 10, \quad \xi_c = 0.0$$

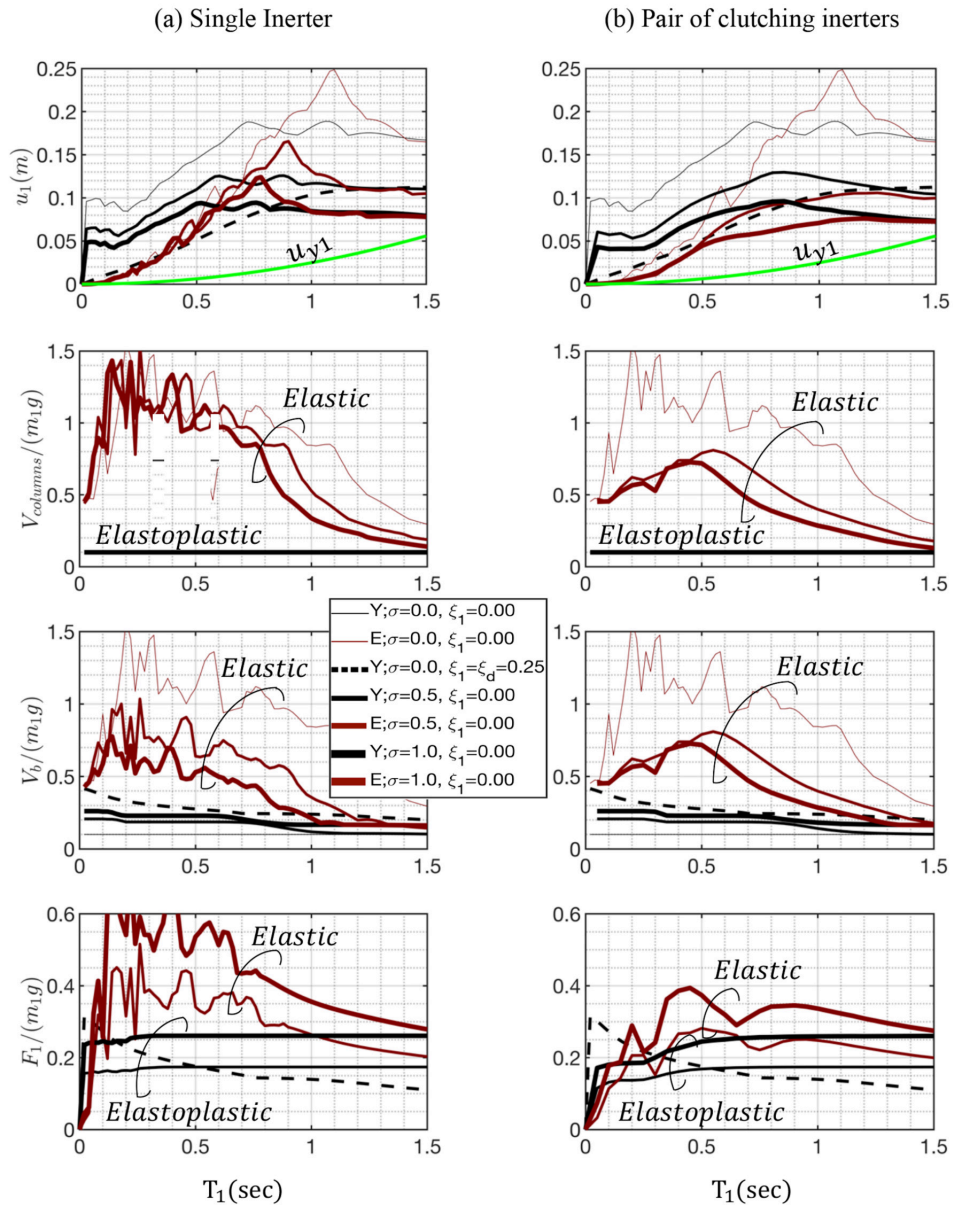


Figure 5.3: Response spectra of an elastoplastic ($\alpha = 0$) SDOF structure equipped with inerters (heavy solid black lines) or supplemental viscous damping (dashed lines) supported on a stiff frame when excited by the Gilroy Array 6/230 ground motion recorded during the 1979 Coyote Lake earthquake: (a) Single inerter; (b) Pair of clutching inerters. Red lines are for the corresponding elastic structures without (thin red lines) or with (heavier red lines) inerters.

$$\frac{Q_1}{m_1 g} = 0.1, \quad \alpha = 0.05, \quad \beta_z = 0.5, \quad \gamma_z = 0.5, \quad n = 10, \quad \xi_c = 0.0$$

(a) Single Inerter

(b) Pair of clutching inerters

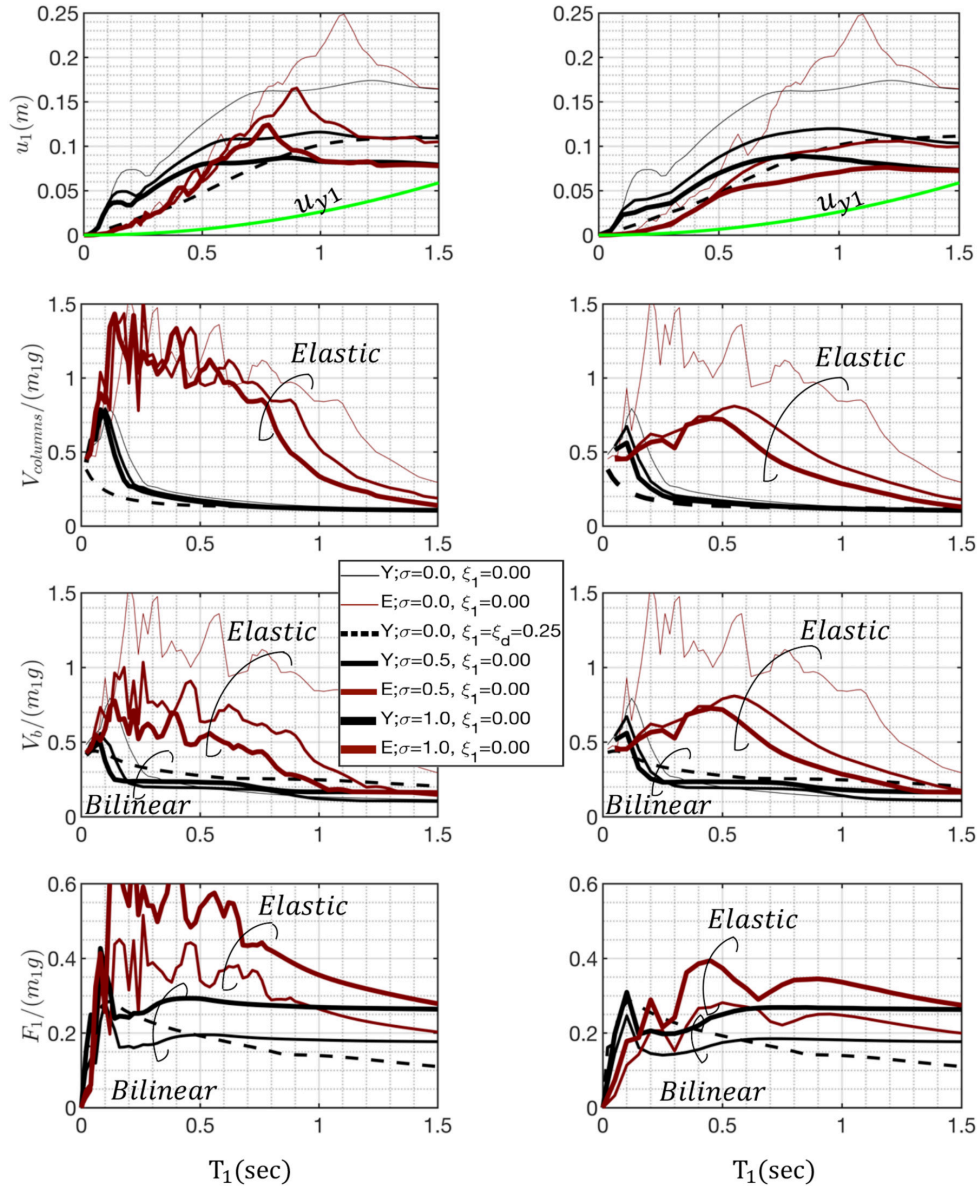


Figure 5.4: Response spectra of a bilinear ($\alpha = 0.05$) SDOF structure equipped with inerters (heavy solid black lines) or supplemental viscous damping (dashed lines) supported on a stiff frame when excited by the Gilroy Array 6/230 ground motion recorded during the 1979 Coyote Lake earthquake: (a) Single inerter; (b) Pair of clutching inerters. Red lines are for the corresponding elastic structures without (thin red lines) or with (heavier red lines) inerters.

$$\frac{Q_1}{m_1 g} = 0.1, \quad \alpha = 0.0, \quad \beta_z = 0.5, \quad \gamma_z = 0.5, \quad n = 10, \quad \xi_c = 0.0$$

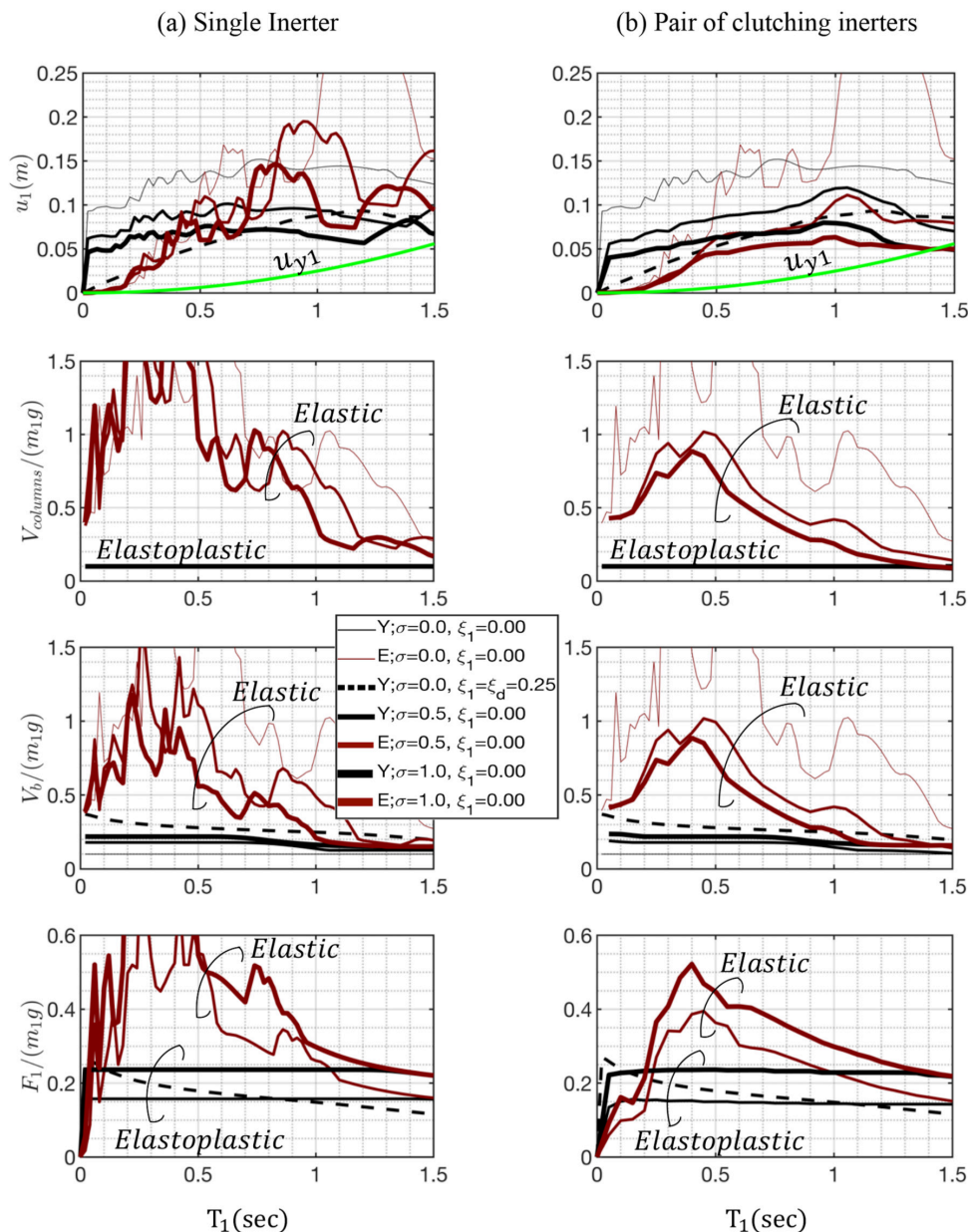


Figure 5.5: Response spectra of an elastoplastic ($\alpha = 0$) SDOF structure equipped with inerters (heavy solid black lines) or supplemental viscous damping (dashed lines) supported on a stiff frame when excited by the Cholame Number 2/360 ground motion recorded during the 2004 Parkfield California earthquake: (a) Single inerter; (b) Pair of clutching inerters. Red lines are for the corresponding elastic structures without (thin red lines) or with (heavier red lines) inerters.

$$\frac{Q_1}{m_1 g} = 0.1, \quad \alpha = 0.05, \quad \beta_z = 0.5, \quad \gamma_z = 0.5, \quad n = 10, \quad \xi_c = 0.0$$

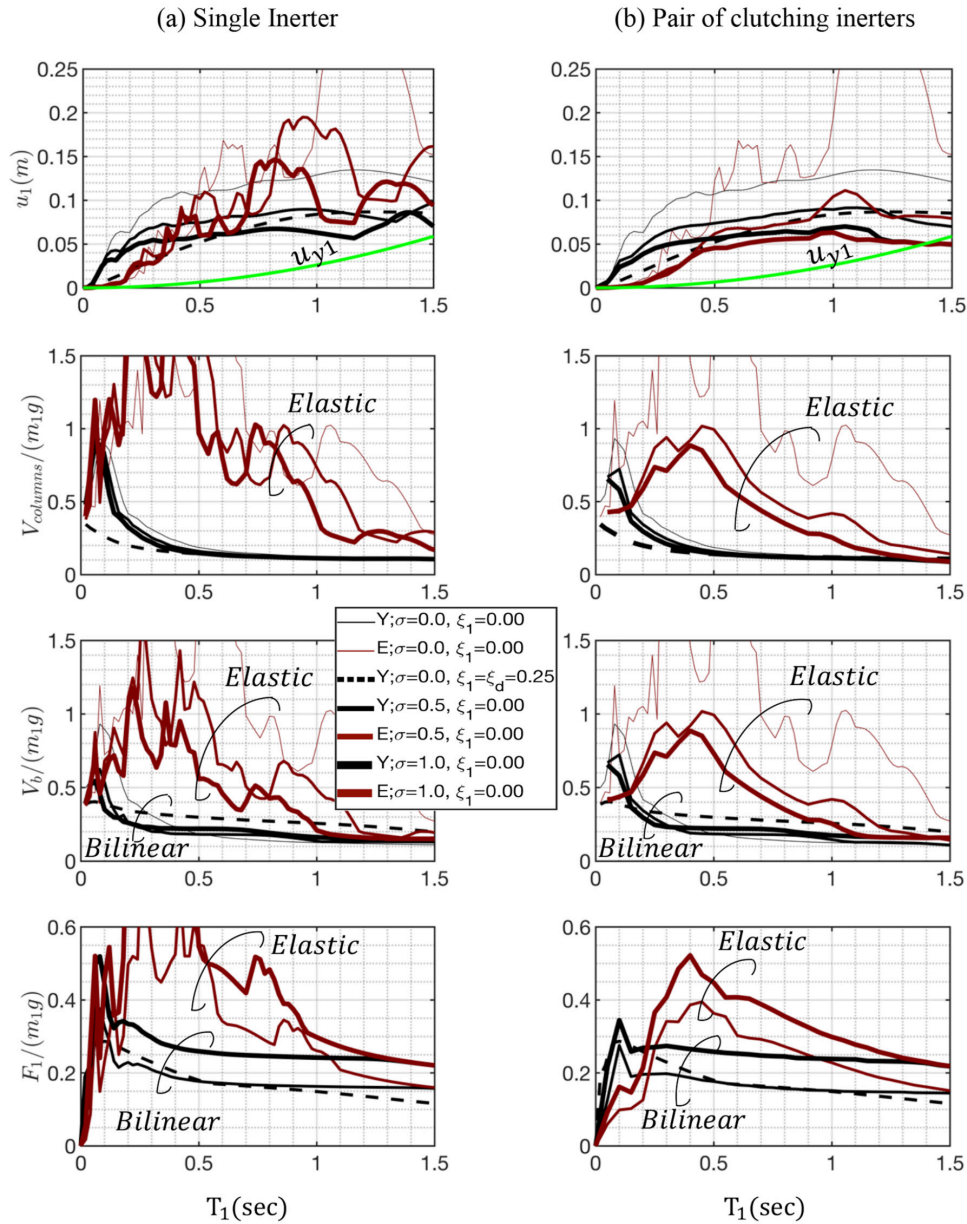


Figure 5.6: Response spectra of a bilinear ($\alpha = 0.05$) SDOF structure equipped with inerters (heavy solid black lines) or supplemental viscous damping (dashed lines) supported on a stiff frame when excited by the Cholame Number 2/360 ground motion recorded during the 2004 Parkfield California earthquake: (a) Single inerter; (b) Pair of clutching inerters. Red lines are for the corresponding elastic structures without (thin red lines) or with (heavier red lines) inerters.

the inelastic and the corresponding elastic structure are engaged with an inerter (heavier black and red lines). According to equation (5.7), when the yielding structure engages with an inerter, the apparent preyielding period of the structure lengthens and in this case, the equal-displacement rule is valid starting from lower preyielding periods ($T_1 \cong 1.15 \text{ sec}$ for $\sigma = 0.5$ and $T_1 \cong 0.95 \text{ sec}$ for $\sigma = 1.0$ for the case of a single inerter). Figure 5.3 reveals that the use of inerters supported on a stiff frame suppress effectively the displacements of SDOF yielding structures, while the resulting base shears are systematically lower than when large values of supplemental damping ($\xi_d = 0.25$) are used. Furthermore, the forces transferred to the mounting of the inerters are appreciably lower than the corresponding forces originating from an elastic structure.

All these observations indicate that supplemental rotational inertia (use of inerters) emerges as an attractive response modification strategy for elastoplastic structures with larger preyielding periods. In the case of an elastoplastic structure, the use of a pair of clutching inerters (right plots) does not offer any additional benefits when compared to the case where a single inerter is used. Pair of clutching inerters have advantages when suppressing the response of elastic structures.

Figure 5.4 plots the same response quantities as Figure 5.3 for a bilinear structure with $\alpha = 0.05$ and $\xi_c = 0$. Figure 5.4 reveals trends similar to those observed in Figure 5.3, supporting the finding that the use of inerters emerge as the most attractive response modification strategy for yielding structures with larger preyielding periods; while a pair of inerters does not offer any additional benefits than when a single inerter is employed. The right plots in Figure 5.4 indicate that a pair of inerters is attractive to reduce the columns shears and base shears of an elastic frame.

The response spectra shown in Figure 5.5 are for a single inerter (left plots) or when a pair of clutching inerters (right plots) is used to modify the response of an elastoplastic ($\alpha = 0$) SDOF structure with normalized strength $Q_1/m_1 = 0.1g$ and $\xi_c = 0$ when subjected to the Array 2/360 ground motion recorded during the 2004 Parkfield California earthquake. Figure 5.5 reveals trends similar to those observed in Figure 5.4, supporting the finding that the use of inerters emerges as the most attractive response modification strategy for yielding structure with larger preyielding periods; while a pair of clutching inerters (right plots) does not offer any additional benefits than when a single inerter is employed.

Figure 5.6 plots the same response quantities as Figure 5.5 for a bilinear structure with $\alpha = 0.05$ and $\xi_c = 0$, and reveals the same trends as those discussed earlier.

5.4 EQUATION OF MOTION OF A YIELDING 2DOF STRUCTURE WITH INERTERS SUPPORTED ON A COMPLIANT CHEVRON FRAME

With reference to Figure 5.1(d), this section examines the dynamic response of a yielding 2DOF structure with floor masses m_1 and m_2 , preyielding and postyielding stiffness at the first story k_1 and αk_1 ($0 \leq \alpha < 1$) respectively with a yield strength, Q_1 , and a yield displacement, u_{y1} . The preyielding and postyielding stiffness in the second story are k_2 and αk_2 respectively with a yield strength, Q_2 , and a yield displacement u_{y2} . Given that recent studies have shown that inerters in a multi-degree-of-freedom (MDOF) structure achieve the best performance when engaged to the first story of the MDOF structure (Lazar et al. 2014), this chapter examines the response of a yielding 2DOF structure when only the first floor is engaged to an inerter with inertance, M_R , supported

on a compliant chevron frame. Our interest in the inelastic response of a 2DOF yielding structure is motivated from the need to understand to what extent the engagement of the inerter at the first story aggravates the inelastic response of the second story. The dynamic equilibrium of the entire structure above the chevron frame gives

$$m_2 [\ddot{u}_1(t) + \ddot{u}_2(t) + \ddot{u}_g(t)] + m_1 [\ddot{u}_1(t) + \ddot{u}_g(t)] = -F_{s1}(t) - c_1 \dot{u}_1(t) - F_I(t) \quad (5.14)$$

where again $F_I(t)$ = the internal force from the inerter and $F_{s1}(t)$ = the inelastic restoring force of the structure at the first story described by the Bouc-Wen model (Wen 1976) expressed by equations (5.2) and (5.3). The dynamic equilibrium of the second story gives

$$m_2 [\ddot{u}_1(t) + \ddot{u}_2(t) + \ddot{u}_g(t)] = -F_{s2}(t) - c_2 \dot{u}_2(t) \quad (5.15)$$

where $F_{s2}(t)$ = inelastic restoring force of the structure at the second story described by the Bouc-Wen model.

$$F_{s2} = \alpha k_2 u_2(t) + (1 - \alpha) k_2 u_{y2} z_2(t) \quad (5.16)$$

where α = postyielding-to-preyielding stiffness ratio; and $-1 \leq z_2(t) \leq 1$ = dimensionless internal variable described by

$$\dot{z}_2(t) = \frac{1}{u_{y2}} [\dot{u}_2(t) - \beta_z \dot{u}_2(t) |z_2(t)|^n - \gamma_z |\dot{u}_2(t)| z_2(t) |z_2(t)|^{n-1}] \quad (5.17)$$

Following the notation introduced by Kelly (1997), the nominal frequencies and nominal damping ratios are given by equations (3.6) and (3.7); while, the mass ratio, γ , and the inertance ratio, σ , are defined by equation (3.8)

In this final section, we examine the dynamic response of the 2DOF structure shown in Figure 5.1(d), yet now the chevron frame that supports the inerter has finite stiffness, k_f , and damping constant, c_f . Because of its compliance, under the force transferred at the mounting of the inerter, the chevron frame deforms; therefore, the force from the inerter is no longer expressed with equation (3.3), which is for a rigid frame, but with equation (3.20) (Makris and Kampas 2016; Makris 2018).

Equation (3.20) is the constitutive law of a spring-dashpot parallel connection (k_f , c_f) that is connected in series with an inerter (M_R). This mechanical network is also known as the tuned inerter damper (TID) (Lazar et al. 2014), and was coined recently the inertoviscoelastic fluid A (Makris 2018). The term fluid expresses that the mechanical network undergoes infinite displacement under static loading.

The mechanical system described by equation (3.21) becomes critically damped when $\lambda \omega_R = 2$ (Makris 2018). In the case of a stiff frame $\lambda = c_f/k_f$ tends to zero, while $\omega_R = \sqrt{k_f/M_R}$ tends to infinity and equation (3.21) reduces to equation (3.3). Accordingly, the formulation presented in this section is for the most general case, and specific cases can be examined by taking limiting values of the parameters.

By using the frequencies, damping, mass, and inertance ratios defined by equations (3.6) to (3.8), the equations of motion of a yielding 2DOF structure with a compliant chevron frame is expressed

in a matrix form

$$\begin{aligned}
& \begin{bmatrix} 1 & \gamma \\ 1 & 1 \end{bmatrix} \begin{Bmatrix} \ddot{u}_1(t) \\ \ddot{u}_2(t) \end{Bmatrix} + \begin{bmatrix} 2\xi_1\omega_1 & 0 \\ 0 & 2\xi_2\omega_2 \end{bmatrix} \begin{Bmatrix} \dot{u}_1(t) \\ \dot{u}_2(t) \end{Bmatrix} + \begin{bmatrix} \alpha\omega_1^2 & 0 \\ 0 & \alpha\omega_2^2 \end{bmatrix} \begin{Bmatrix} u_1(t) \\ u_2(t) \end{Bmatrix} \\
& + \begin{bmatrix} (1-\alpha)\omega_1^2 u_{y1} & 0 \\ 0 & (1-\alpha)\omega_2^2 u_{y2} \end{bmatrix} \begin{Bmatrix} z_1(t) \\ z_2(t) \end{Bmatrix} = - \begin{bmatrix} 1 & 1 \\ 0 & 1 \end{bmatrix} \begin{Bmatrix} \frac{F_I(t)}{m_1+m_2} \\ \ddot{u}_g(t) \end{Bmatrix} \quad (5.18)
\end{aligned}$$

in which $F_I(t)$ is the solution of equation (3.21). By multiplying equation (5.18) from the left with the inverse of the normalized mass matrix given by equation (3.23), the relative accelerations $\ddot{u}_1(t)$ and $\ddot{u}_2(t)$ of each story become explicit expressions of the relative displacements and velocities of the stories.

$$\begin{aligned}
\ddot{u}_1(t) &= -\ddot{u}_g(t) - \frac{1}{1-\gamma} f_I(t) - \frac{2\xi_1\omega_1}{1-\gamma} \dot{u}_1(t) + \frac{2\gamma\xi_2\omega_2}{1-\gamma} \dot{u}_2(t) - \frac{\alpha\omega_1^2}{1-\gamma} u_1(t) \\
&+ \frac{\alpha\gamma\omega_2^2}{1-\gamma} u_2(t) - \frac{(1-\alpha)\omega_1^2 u_{y1}}{1-\gamma} z_1(t) + \frac{(1-\alpha)\gamma\omega_2^2 u_{y2}}{1-\gamma} z_2(t) \quad (5.19)
\end{aligned}$$

and

$$\begin{aligned}
\ddot{u}_2(t) &= \frac{1}{1-\gamma} f_I(t) + \frac{2\xi_1\omega_1}{1-\gamma} \dot{u}_1(t) - \frac{2\xi_2\omega_2}{1-\gamma} \dot{u}_2(t) + \frac{\alpha\omega_1^2}{1-\gamma} u_1(t) - \frac{\alpha\omega_2^2}{1-\gamma} u_2(t) \\
&+ \frac{(1-\alpha)\omega_1^2 u_{y1}}{1-\gamma} z_1(t) - \frac{(1-\alpha)\omega_2^2 u_{y2}}{1-\gamma} z_2(t) \quad (5.20)
\end{aligned}$$

where $f_I(t) = F_I(t) / (m_1 + m_2)$ has units of acceleration. The state-vector of the system is

$$\begin{aligned}
\{y(t)\} &= \langle y_1(t), y_2(t), y_3(t), y_4(t), y_5(t), y_6(t), y_7(t), y_8(t) \rangle^T \\
&= \langle u_1(t), \dot{u}_1(t), u_2(t), \dot{u}_2(t), f_I(t), \dot{f}_I(t), z_1(t), z_2(t) \rangle^T \quad (5.21)
\end{aligned}$$

From equation(3.21) it is evident that the time-derivative of $y_6(t)$, that is $\dot{y}_6(t) = \dot{f}_I(t)$, involves the third derivative of $u_1(t)$ which is given by

$$\begin{aligned}
\ddot{u}_1(t) &= -\ddot{u}_g(t) - \frac{1}{1-\gamma} \dot{f}_I(t) - \frac{2\xi_1\omega_1}{1-\gamma} \ddot{u}_1(t) + \frac{2\gamma\xi_2\omega_2}{1-\gamma} \ddot{u}_2(t) - \frac{\alpha\omega_1^2}{1-\gamma} \dot{u}_1(t) \\
&+ \frac{\alpha\gamma\omega_2^2}{1-\gamma} \dot{u}_2(t) - \frac{(1-\alpha)\omega_1^2 u_{y1}}{1-\gamma} \dot{z}_1(t) + \frac{(1-\alpha)\gamma\omega_2^2 u_{y2}}{1-\gamma} \dot{z}_2(t) \quad (5.22)
\end{aligned}$$

In terms of the state variables given by equation (5.21), equation (5.22) assumes the form

$$\begin{aligned}
\ddot{u}_1(t) = & - \left(\frac{1}{1-\gamma} y_6(t) + \ddot{u}_g(t) \right) \\
& - \frac{2\xi_1\omega_1}{1-\gamma} \left(-\frac{1}{1-\gamma} y_5(t) - \ddot{u}_g(t) - \frac{2\xi_1\omega_1}{1-\gamma} y_2(t) + \frac{2\gamma\xi_2\omega_2}{1-\gamma} y_4(t) - \frac{\alpha\omega_1^2}{1-\gamma} y_1(t) \right. \\
& \left. + \frac{\alpha\gamma\omega_2^2}{1-\gamma} y_3(t) - \frac{(1-\alpha)\omega_1^2 u_{y1}}{1-\gamma} y_7(t) + \frac{(1-\alpha)\gamma\omega_2^2 u_{y2}}{1-\gamma} y_8(t) \right) \\
& + \frac{2\gamma\xi_2\omega_2}{1-\gamma} \left(\frac{1}{1-\gamma} y_5(t) + \frac{2\xi_1\omega_1}{1-\gamma} y_2(t) - \frac{2\xi_2\omega_2}{1-\gamma} y_4(t) + \frac{\alpha\omega_1^2}{1-\gamma} y_1(t) - \frac{\alpha\omega_2^2}{1-\gamma} y_3(t) \right. \\
& \left. + \frac{(1-\alpha)\omega_1^2 u_{y1}}{1-\gamma} y_7(t) - \frac{(1-\alpha)\omega_2^2 u_{y2}}{1-\gamma} y_8(t) \right) \\
& - \frac{\alpha\omega_1^2}{1-\gamma} y_2(t) + \frac{\alpha\gamma\omega_2^2}{1-\gamma} y_4(t) - \frac{(1-\alpha)\omega_1^2}{1-\gamma} \left(y_2(t) - \beta_z y_2(t) |y_7(t)|^n - \gamma_z |y_2(t)| y_7(t) |y_7(t)|^{n-1} \right) \\
& + \frac{(1-\alpha)\gamma\omega_2^2}{1-\gamma} \left(y_4(t) - \beta_z y_4(t) |y_8(t)|^n - \gamma_z |y_4(t)| y_8(t) |y_8(t)|^{n-1} \right)
\end{aligned} \tag{5.23}$$

The solution of the system of differential equations given by equations (5.19), (5.20), and (3.21) is computed by integrating the time-derivative of the state-vector given by equation (5.21)

$$\left\{ \dot{y}(t) \right\} = \left\{ \begin{array}{l} \dot{u}_1(t) \\ \ddot{u}_1(t) \\ \dot{u}_2(t) \\ \ddot{u}_2(t) \\ \dot{f}_I(t) \\ \ddot{f}_I(t) \\ \dot{z}_1(t) \\ \dot{z}_2(t) \end{array} \right\} = \left\{ \begin{array}{l} y_2(t) \\ -\ddot{u}_g(t) - \frac{1}{1-\gamma} y_5(t) - \frac{2\xi_1\omega_1}{1-\gamma} y_2(t) + \frac{2\gamma\xi_2\omega_2}{1-\gamma} y_4(t) - \frac{\alpha\omega_1^2}{1-\gamma} y_1(t) \\ \quad + \frac{\alpha\gamma\omega_2^2}{1-\gamma} y_3(t) - \frac{(1-\alpha)\omega_1^2 u_{y1}}{1-\gamma} y_7(t) + \frac{(1-\alpha)\gamma\omega_2^2 u_{y2}}{1-\gamma} y_8(t) \\ y_4(t) \\ \frac{1}{1-\gamma} y_5(t) + \frac{2\xi_1\omega_1}{1-\gamma} y_2(t) - \frac{2\xi_2\omega_2}{1-\gamma} y_4(t) + \frac{\alpha\omega_1^2}{1-\gamma} y_1(t) \\ \quad - \frac{\alpha\omega_2^2}{1-\gamma} y_3(t) + \frac{(1-\alpha)\omega_1^2 u_{y1}}{1-\gamma} y_7(t) - \frac{(1-\alpha)\omega_2^2 u_{y2}}{1-\gamma} y_8(t) \\ y_6(t) \\ \omega_R^2 \sigma (\ddot{u}_1(t) + \lambda \ddot{u}_1(t)) - \omega_R^2 y_5(t) - \omega_R^2 \lambda y_6(t) \\ \frac{1}{u_{y1}} [y_2(t) - \beta_z y_2(t) |y_7(t)|^n - \gamma_z |y_2(t)| y_7(t) |y_7(t)|^{n-1}] \\ \frac{1}{u_{y2}} [y_4(t) - \beta_z y_4(t) |y_8(t)|^n - \gamma_z |y_4(t)| y_8(t) |y_8(t)|^{n-1}] \end{array} \right\} \tag{5.24}$$

When a pair of clutching inerters is employed that can only resist the motion of the structure without inducing any deformation (the pinion of the gearwheel that is engaged in the rack of the first story is unable to drive the rack and only the motion of the translating rack can drive the pinion), the normalized force, $f_I(t) = F_I(t)/(m_1 + m_2)$ appearing in equations (5.19) and (5.20) is given by equation (3.21) when $\text{sgn} [F_I(t)/\dot{u}_1(t)] \geq 0$ and by

$$f_I(t) = \frac{F_I(t)}{m_1 + m_2} = 0 \quad \text{when} \quad \text{sgn} \left[\frac{F_I(t)}{\dot{u}_1(t)} \right] < 0 \tag{5.25}$$

The time-derivative of the state-vector of the system is given by equation (5.24) when $\text{sgn} [F_I(t)/$

$\dot{u}_1(t)] > 0$ and by

$$\{\dot{y}(t)\} = \begin{Bmatrix} \dot{u}_1(t) \\ \ddot{u}_1(t) \\ \dot{u}_2(t) \\ \ddot{u}_2(t) \\ \dot{z}_1(t) \\ \dot{z}_2(t) \end{Bmatrix} = \begin{Bmatrix} y_2(t) \\ -\ddot{u}_g(t) - \frac{2\xi_1\omega_1}{1-\gamma} y_2(t) + \frac{2\gamma\xi_2\omega_2}{1-\gamma} y_4(t) - \frac{\alpha\omega_1^2}{1-\gamma} y_1(t) + \frac{\alpha\gamma\omega_2^2}{1-\gamma} y_3(t) \\ -\frac{(1-\alpha)\omega_1^2 u_{y1}}{1-\gamma} y_5(t) + \frac{(1-\alpha)\gamma\omega_2^2 u_{y2}}{1-\gamma} y_6(t) \\ y_4(t) \\ \frac{2\xi_1\omega_1}{1-\gamma} y_2(t) - \frac{2\xi_2\omega_2}{1-\gamma} y_4(t) + \frac{\alpha\omega_1^2}{1-\gamma} y_1(t) - \frac{\alpha\omega_2^2}{1-\gamma} y_3(t) \\ + \frac{(1-\alpha)\omega_1^2 u_{y1}}{1-\gamma} y_5(t) - \frac{(1-\alpha)\omega_2^2 u_{y2}}{1-\gamma} y_6(t) \\ \frac{1}{u_{y1}} [y_2(t) - \beta_z y_2(t) |y_5(t)|^n - \gamma_z |y_2(t)| y_5(t) |y_5(t)|^{n-1}] \\ \frac{1}{u_{y2}} [y_4(t) - \beta_z y_4(t) |y_6(t)|^n - \gamma_z |y_4(t)| y_6(t) |y_6(t)|^{n-1}] \end{Bmatrix} \quad (5.26)$$

when $\text{sgn} [F_I(t) / \dot{u}_1(t)] < 0$.

The response of the 2DOF structure with supplemental rotational inertia shown in Figure 5.1(d) with a compliant chevron frame with finite stiffness, k_f and damping c_f is compared with the response of a heavily damped 2DOF structure with supplemental viscous damping at the first story with damping constant $c_d = 2\xi_d\omega_1(m_1 + m_2)$ as shown in Figure 5.1(f). The constitutive equation of the mechanical network of a spring-dashpot parallel connection (k_f, c_f) that is connected in series with a dashpot (c_d) is given by (Makris and Kampas 2013; Makris and Moghimi 2019)

$$F_d(t) + \frac{c_d + c_f}{k_f} \frac{dF_d(t)}{dt} = c_d \left(\frac{du_1(t)}{dt} + \frac{c_f}{k_f} \frac{d^2u_1(t)}{dt^2} \right) \quad (5.27)$$

For the case of a 2DOF structure with supplemental damping supported by a compliant chevron frame with finite stiffness shown in Figure 5.1(f), the state-vector of the system is

$$\begin{aligned} \{y(t)\} &= \langle y_1(t), y_2(t), y_3(t), y_4(t), y_5(t), y_6(t), y_7(t) \rangle^T \\ &= \langle u_1(t), \dot{u}_1(t), u_2(t), \dot{u}_2(t), f_d(t), z_1(t), z_2(t) \rangle^T \end{aligned} \quad (5.28)$$

The solution of the system of differential equations given by equations (5.19), (5.20), and (5.27) is computed by integrating the time-derivative of the state-vector given by equation (5.28)

$$\{\dot{y}(t)\} = \begin{Bmatrix} \dot{u}_1(t) \\ \ddot{u}_1(t) \\ \dot{u}_2(t) \\ \ddot{u}_2(t) \\ \dot{f}_d(t) \\ \dot{z}_1(t) \\ \dot{z}_2(t) \end{Bmatrix} = \begin{Bmatrix} y_2(t) \\ -\frac{1}{1-\gamma} y_5(t) - \ddot{u}_g(t) - \frac{2\xi_1\omega_1}{1-\gamma} y_2(t) + \frac{2\gamma\xi_2\omega_2}{1-\gamma} y_4(t) - \frac{\alpha\omega_1^2}{1-\gamma} y_1(t) + \frac{\alpha\gamma\omega_2^2}{1-\gamma} y_3(t) \\ -\frac{(1-\alpha)\omega_1^2 u_{y1}}{1-\gamma} y_5(t) + \frac{(1-\alpha)\gamma\omega_2^2 u_{y2}}{1-\gamma} y_7(t) \\ y_4(t) \\ \frac{1}{1-\gamma} y_5(t) + \frac{2\xi_1\omega_1}{1-\gamma} y_2(t) - \frac{2\xi_2\omega_2}{1-\gamma} y_4(t) + \frac{\alpha\omega_1^2}{1-\gamma} y_1(t) - \frac{\alpha\omega_2^2}{1-\gamma} y_3(t) \\ + \frac{(1-\alpha)\omega_1^2 u_{y1}}{1-\gamma} y_6(t) - \frac{(1-\alpha)\omega_2^2 u_{y2}}{1-\gamma} y_7(t) \\ \frac{1}{\lambda_d} [-y_5(t) + 2\xi_d\omega_1(y_2(t) + \lambda(\dot{u}_1(t)))] \\ \frac{1}{u_{y1}} [y_2(t) - \beta_z y_2(t) |y_6(t)|^n - \gamma_z |y_2(t)| y_6(t) |y_6(t)|^{n-1}] \\ \frac{1}{u_{y2}} [y_4(t) - \beta_z y_4(t) |y_7(t)|^n - \gamma_z |y_4(t)| y_7(t) |y_7(t)|^{n-1}] \end{Bmatrix} \quad (5.29)$$

where $f_d(t) = F_d(t) / (m_1 + m_2)$ has units of acceleration.

5.5 RESPONSE SPECTRA OF A YIELDING 2DOF STRUCTURE WITH INERTERS SUPPORTED ON A COMPLIANT CHEVRON FRAME

The seismic response of the yielding 2DOF structure equipped with an inerter at the first story [Figure 5.1(d)] as described by equation (5.24) or equations (5.24) and (5.26) is compared with the seismic response of the same 2DOF structure where the inerter is replaced with a supplemental viscous damper with damping constant c_d given by equation (5.29). Together with the drift response u_1 and u_2 (relative displacements), of interest are the normalized shear above the first story, V_2/m_2g , the total normalized base shear at the ground level, $V_1/(m_1 + m_2)g$ which is essentially the left-hand side or the right-hand side of equation (5.14) and the normalized inerter force, $F_I/(m_1 + m_2)g$ transferred to the support of inerter.

The response spectra in Figures 5.7 and 5.8, which are for a 2DOF yielding structure with inerters supported on a stiff chevron frame, are obtained by setting in equation (3.21) $\lambda = 0$ and $1/\omega_R^2 = 0$. The thin solid lines in Figures 5.7 and 5.8 are for the yielding 2DOF structure without any response modification device, whereas the heavier solid lines are for the cases where inerters with $\sigma = 0.5$ and $\sigma = 1.0$ are used. The dashed lines are for when supplemental damping, ξ_d , is used so that $\xi_1 = \xi_c + \xi_d = 0.02 + 0.23 = 0.25$. Figure 5.7 present the response spectra for the two 2DOF yielding structural configurations shown in Figures 5.1(d) and (f) when subjected to the Gilroy Array 6/230 ground motion recorded during the 1979 Coyote Lake, California earthquake; while, Figure 5.8 presents the response spectra of the same 2DOF yielding structural configurations when subjected to the Array 2/360 ground motion recorded during the 2004 Parkfield, California earthquake.

The first observation is that supplemental rotational inertia supported on a stiff frame is most efficient in reducing displacements for structures with larger preyielding periods, T_1 ; nevertheless, the displacement reduction achieved is comparable to the reduction achieved with large values of supplemental damping ($\xi_d = 25\%$). However, the use of inerters does not amplify the inelastic response of the second story, as happens when large values of supplemental damping are used.

The use of a pair of clutching inerters, where only the structure can drive the inerters, has a marginal effect in further suppressing displacements and forces transferred at the support of the inerters.

The response spectra in Figures 5.9 and 5.10 are the results of the solution of the equation (5.24) (single inerter supported on a compliant frame) and of equations (5.24) and (5.26) when a pair of clutching inerters is used. Again, when $\sigma = 0$ (thin line), the solution offers the response of the 2DOF yielding structure without any seismic protection devices. The heavier solid lines are for the cases where inerters with $\sigma = 0.5$ and $\sigma = 1.0$ are used. The compliance of chevron frame is expressed with the relaxation time, $\lambda = c_f/k_f = 0.05$; whereas the stiffness of the chevron frame compared with the supplemental inertance, M_R , is expressed with the dimensionless product $\lambda\omega_R = 0.5$. For the structural system in Figure 5.1(f), values of $\xi_c = 2\%$ and $\xi_d = 23\%$ are used so that $\xi_1 = \xi_c + \xi_d = 0.02 + 0.23 = 0.25$. When supplemental damping, c_d is used, the compliance of the chevron frame is $\lambda_d = (c_d + c_f)/k_f = 0.5$. In all spectra $Q_1/(m_1 + m_2) = 0.1g$, $Q_2/m_2 = 0.2g$, $u_{y2} = u_{y1}/2$ and $m_1 = m_2$ so that $\gamma = 1/2$. Figure 5.9 present the response spectra for the two 2DOF yielding structural configurations shown in Figures 5.1(d) and (f) when subjected to the Gilroy Array 6/230 ground motion recorded during the 1979 Coyote Lake,

1979 Coyote Lake, Gilroy Array 6/230

$$\frac{Q_1}{(m_1 + m_2)g} = 0.1, \quad \frac{Q_2}{m_2g} = 0.2, \quad u_{y1} = 2u_{y2}, \quad T_1 = 2T_2, \quad \gamma = 0.5, \quad \xi_2 = 0.02, \quad \alpha = 0.05, \quad \beta_z = 0.5, \quad \gamma_z = 0.5, \quad n = 10$$

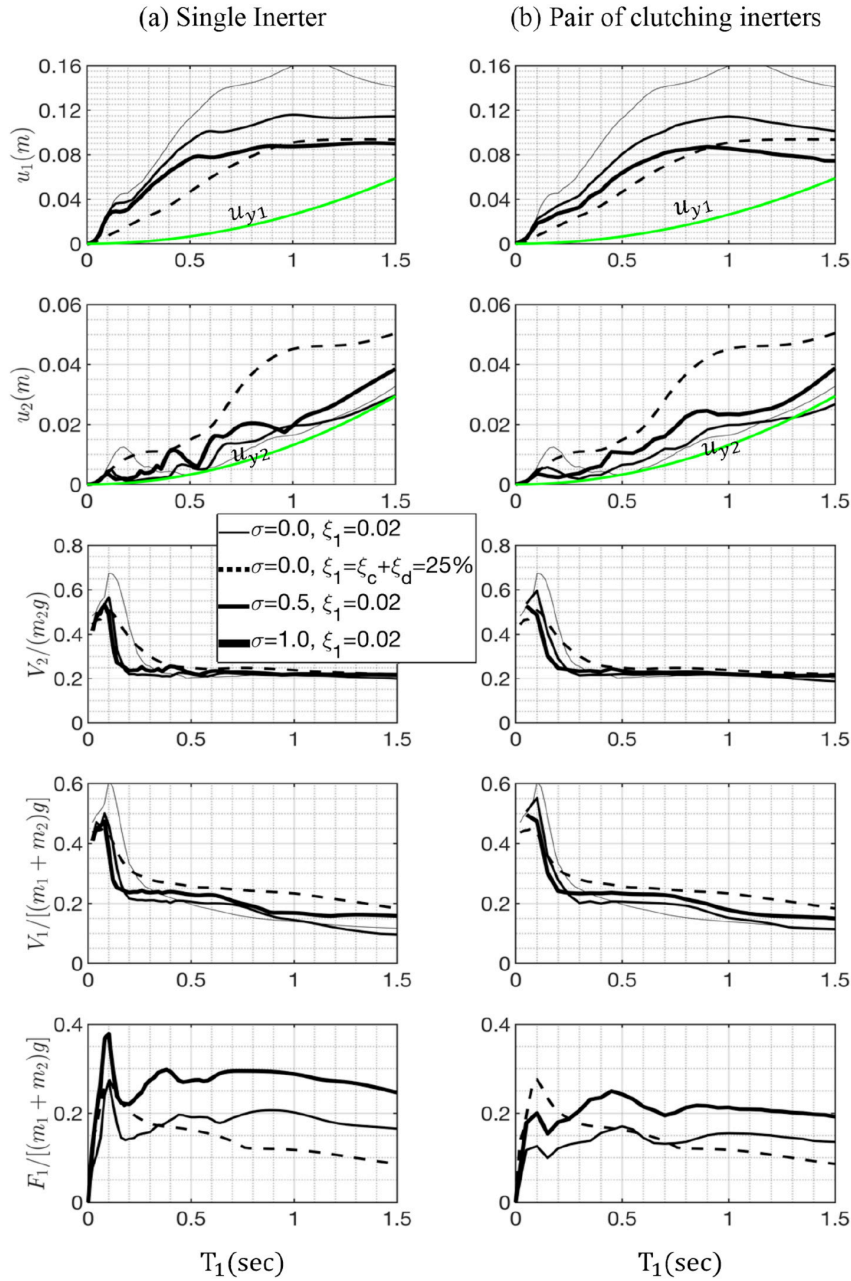


Figure 5.7: Response spectra of a yielding 2DOF structure equipped with inerters (heavy solid lines) or supplemental viscous damping (dashed lines) supported on a stiff frame when excited by the Gilroy Array 6/230 ground motion recorded during the 1979 Coyote Lake earthquake: (a) Single inerter; (b) Pair of clutching inerters.

2004 Parkfield, Cholame Number Array 2/360

$$\frac{Q_1}{(m_1 + m_2)g} = 0.1, \quad \frac{Q_2}{m_2g} = 0.2, \quad u_{y1} = 2u_{y2}, \quad T_1 = 2T_2, \quad \gamma = 0.5, \quad \xi_2 = 0.02, \quad \alpha = 0.05, \quad \beta_z = 0.5, \quad \gamma_z = 0.5, \quad n = 10$$

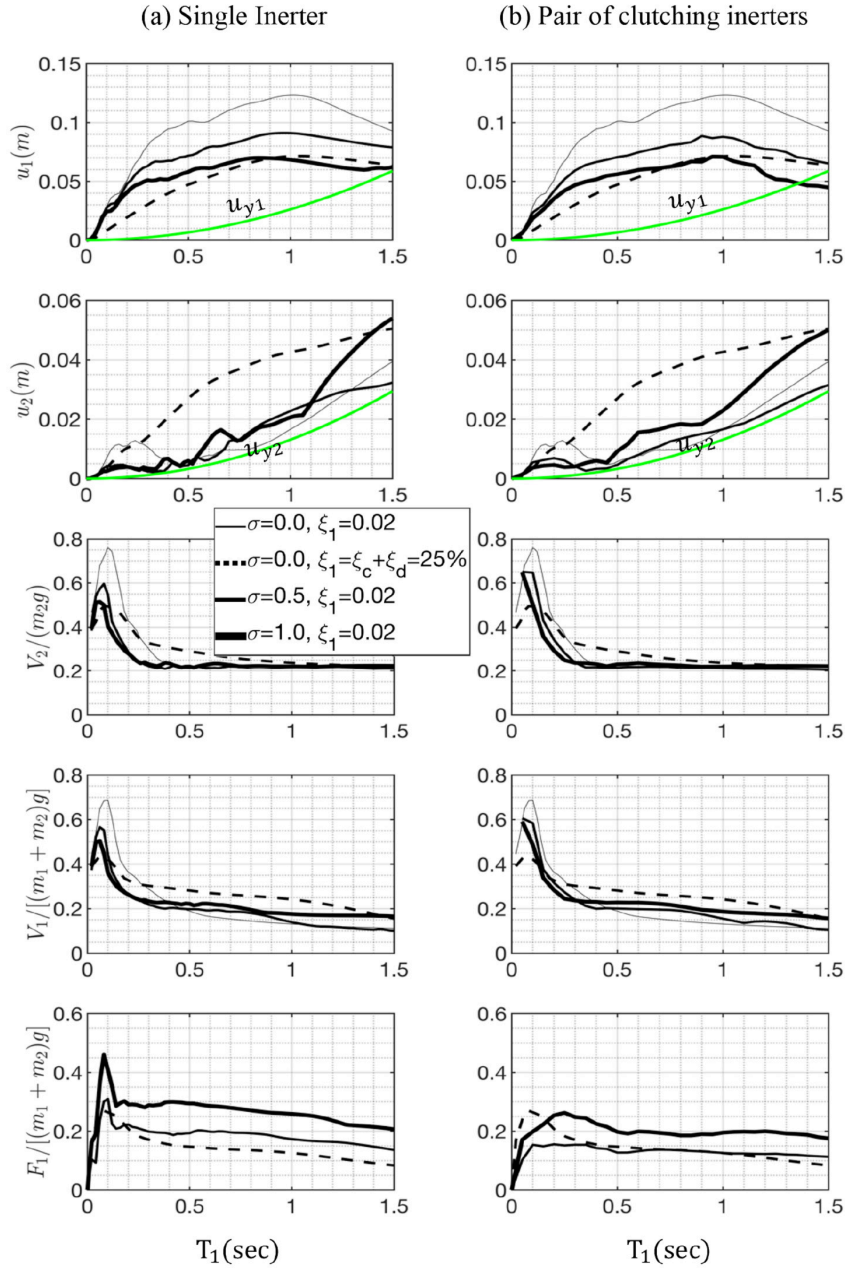


Figure 5.8: Response spectra of a yielding 2DOF structure equipped with inerters (heavy solid lines) or supplemental viscous damping (dashed lines) supported on a stiff frame when excited by the Cholame Number 2/360 ground motion recorded during the 2004 Parkfield California earthquake: (a) Single inerter; (b) Pair of clutching inerters.

1979 Coyote Lake, Gilroy Array 6/230

$$\frac{Q_1}{(m_1 + m_2)g} = 0.1, \quad \frac{Q_2}{m_2 g} = 0.2, \quad u_{y1} = 2u_{y2}, \quad T_1 = 2T_2, \quad \gamma = 0.5, \quad \xi_2 = 0.02$$

$$\alpha = 0.05, \quad \beta_z = 0.5, \quad \gamma_z = 0.5, \quad n = 10, \quad \lambda = \frac{c_f}{k_f} = 0.05 \text{ sec}, \quad \lambda_d = \frac{c_d + c_f}{k_f} = 0.5 \text{ sec}, \quad \lambda\omega_R = 0.5 \text{ rad/sec}$$

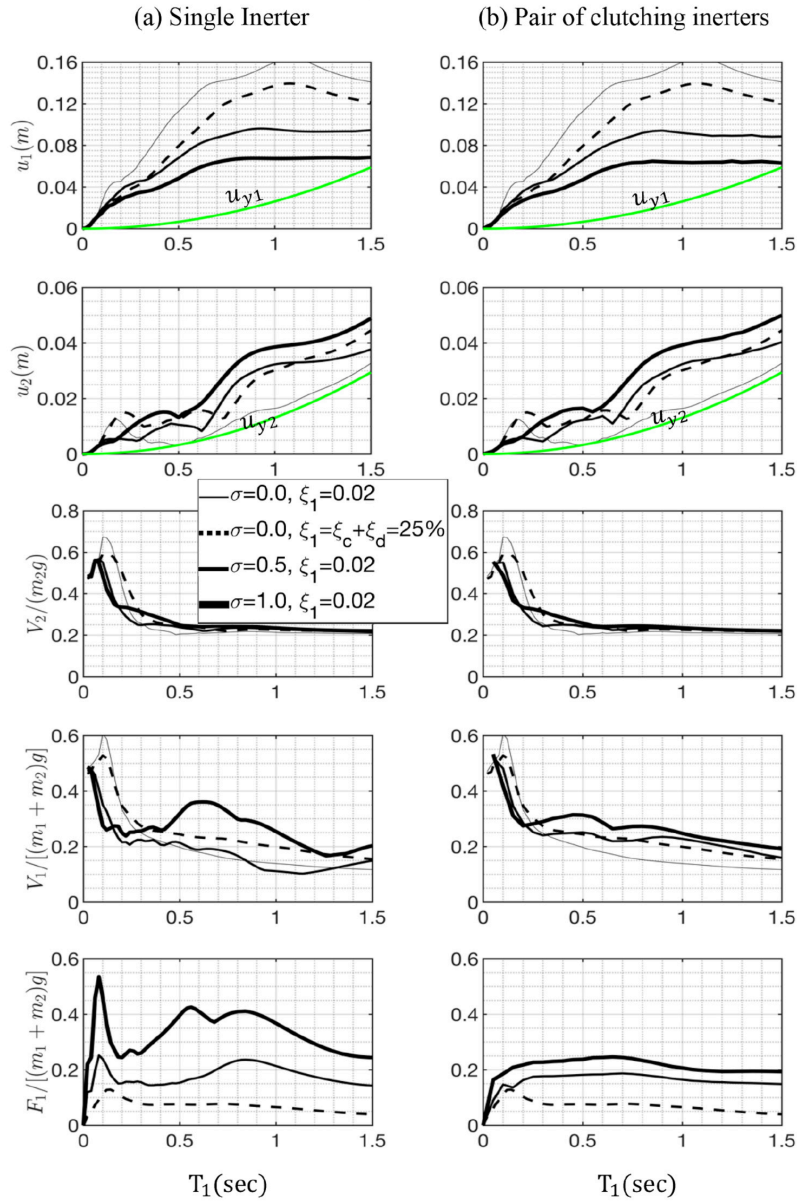


Figure 5.9: Response spectra of a yielding 2DOF structure equipped with inerters (heavy solid lines) or supplemental viscous damping (dashed lines) supported on a compliant chevron frame when excited by the Gilroy Array 6/230 ground motion recorded during the 1979 Coyote Lake earthquake: (a) Single inerter; (b) Pair of clutching inerters.

2004 Parkfield, Cholame Number Array 2/360

$$\frac{Q_1}{(m_1 + m_2)g} = 0.1, \quad \frac{Q_2}{m_2g} = 0.2, \quad u_{y1} = 2u_{y2}, \quad T_1 = 2T_2, \quad \gamma = 0.5, \quad \xi_2 = 0.02$$

$$\alpha = 0.05, \quad \beta_z = 0.5, \quad \gamma_z = 0.5, \quad n = 10, \quad \lambda = \frac{c_f}{k_f} = 0.05 \text{ sec}, \quad \lambda_d = \frac{c_d + c_f}{k_f} = 0.5 \text{ sec}, \quad \lambda\omega_R = 0.5 \text{ rad/sec}$$

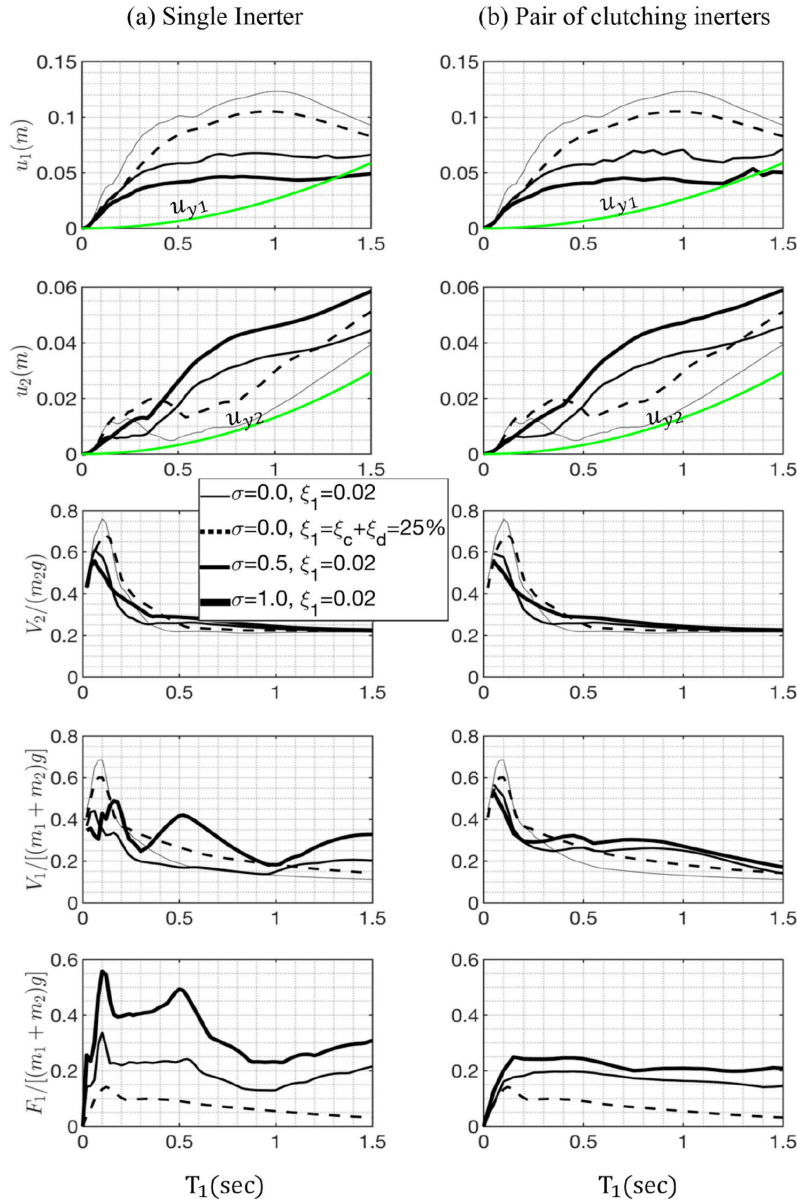


Figure 5.10: Response spectra of a yielding 2DOF structure equipped with inerters (heavy solid lines) or supplemental viscous damping (dashed lines) supported on a compliant chevron frame when excited by the Cholame Number 2/360 ground motion recorded during the 2004 Parkfield California earthquake: (a) Single inerter; (b) Pair of clutching inerters.

California earthquake; while, Figure 5.10 presents the response spectra of the same 2DOF yielding structural configurations when subjected to the Array 2/360 ground motion recorded during the 2004 Parkfield, California earthquake.

The main observation is that when the inerters are supported on a compliant frame they are much more efficient in suppressing inelastic displacement response than when large values of supplemental damping are used.

5.6 CONCLUSIONS

This chapter investigated the nonlinear seismic response of a one- and two-degree-of- freedom yielding structures equipped with inerters at the first story.

The response analysis of a SDOF elastoplastic and bilinear structure reveals that when the yielding structure is equipped with supplemental rotational inertia (inerters), the equal-displacement rule is valid starting from lower values of the preyielding period given that the presence of inerters lengthens the apparent preyielding period. Furthermore, inerters suppress effectively the inelastic displacements of SDOF yielding structures; while the resulting base shears are systematically lower than when large values of supplemental damping ($\xi_d = 0.25\%$) are used. The forces transferred at the mounting of the inerters are appreciably lower than the corresponding forces originating from an elastic structure analyzed in chapter 3. Consequently, the implementation of inerters emerges as an attractive response modification strategy for elastoplastic and bilinear SDOF structures with larger preyielding periods.

The use of a pair of clutching inerters does not offer any additional benefits compared to the case where a single inerter is used. Pair of clutching inerters are found to be attractive when suppressing the response of elastic structures.

Inerters are also most effective in suppressing the inelastic response of 2DOF yielding structures with pre-yielding periods up to $T_1 = 1.5sec$ without aggravating the inelastic response of the superstructure. The effectiveness of inerters to suppress the inelastic response of the 2DOF yielding structure outperforms appreciably the effectiveness of large values of supplemental damping ($\xi_d = 25\%$) when the support frame of the response modification device is compliant.

In view of these findings the use of inerters emerges as an attractive response modification strategy is recommended for yielding structures. For larger pre-yielding periods (say $T_1 > 2.0sec$), the effectiveness of inerters to suppress the inelastic response of 2DOF yielding structures reduces; and for very flexible first stories; as in the case of isolated structures examined in chapter 4, the use of inerters at the first level (isolation system) is not recommended given that they aggravate the response of the elastic superstructure.

6 The role of inerters when placed at floor-levels other than the first level

Following Furuhashi and Ishimaru's (2008) seminal contribution, Takewaki et al. (2012) explained that for inerters to suppress the induced ground acceleration they need to be installed without being interrupted, starting from the ground level; otherwise, the inerters which are installed above the "interrupted" level can no-longer suppress the ground induced acceleration. In spite of Takewaki et al. (2012) important finding-that solitary inerters when placed at higher levels do not suppress the ground induced acceleration, several subsequent publications investigated the response of structures equipped with a solitary inerter at a floor level other than the first level (Sugimura et al. 2012; Ogino and Sumiyama 2014; Lazar et al. 2014; Marian and Giaralis 2014; Taflanidis et al. 2019) within the context of proposing an enhanced tuned mass damper. Soon after Takewaki et al. (2012) publication, Lazar et al. (2014) examined in detail the role of a tuned inerter damper (TID)-which is essentially an inerter supported on a compliant support (a spring-dashpot parallel connection), as an alternative tuned mass damper (TMD) and they correctly concluded that the TID is more effective when placed at the ground level, reaffirming the findings of Takewaki et al. (2012). In view of the appreciable number of publications that examine the response of tall buildings when equipped at a higher level with a solitary mechanical network that involves inerters (Marian and Giaralis 2014; Giaralis and Taflanidis 2018; Taflanidis et al. 2019), in association that this concept has enjoyed full-scale implementations (Sugimura et al. 2012; Ogino and Sumiyama 2014), in this chapter we examine the role of inerters when placed at floor-levels other than the first level and we show that; whereas, they assume a reduced role since they can no-longer eliminate the participation of higher modes, nor they can suppress the ground induced acceleration, they maintain a distinct role as response modification devices, since it is not possible to replace a structure with a solitary inerter at a higher level with an equivalent traditional structure without inerters.

6.1 MULTI-STORY STRUCTURES

Our investigation on the role of inerters when placed at higher floor-levels commences with the analysis of the multi-story elastic structure ($NDOF$) shown in Figure 6.1. In this section the displacements of the floors $u_1(t), u_2(t), \dots, u_N(t)$ are measured relative to the ground by following the traditional formulation for the response analysis of multi-degree-of-freedom structures (Clough and Penzien 1975; Chopra 2000).

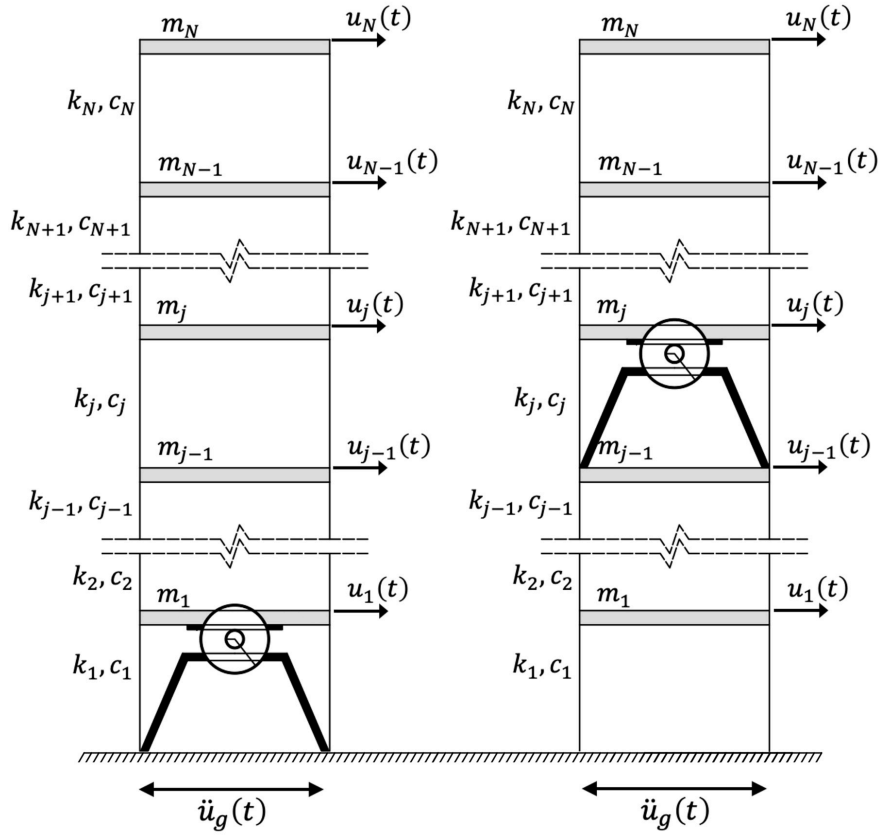


Figure 6.1: Multi-story structure with supplemental rotational inertia at its first level (left); or at some higher level j without any inerters at the levels below (right).

When the $NDOF$ structure is not equipped with inerters at any floor, the equation of motion that governs its response when subjected to a ground induced acceleration, $\ddot{u}_g(t)$, is (Clough and Penzien 1975; Chopra 2000)

$$\begin{bmatrix} m_1 & 0 & \dots & \dots & \dots & \dots & \dots & 0 \\ 0 & m_2 & & & & & & \dots \\ \vdots & & \ddots & & & & & \vdots \\ \vdots & & & m_{j-1} & & & & \vdots \\ \vdots & & & & m_j & & & \vdots \\ \vdots & & & & & \ddots & & \vdots \\ \vdots & & & & & & m_{N-1} & 0 \\ 0 & \dots & \dots & \dots & \dots & \dots & 0 & m_N \end{bmatrix} \begin{Bmatrix} \ddot{u}_1(t) \\ \ddot{u}_2(t) \\ \vdots \\ \ddot{u}_{j-1}(t) \\ \ddot{u}_j(t) \\ \vdots \\ \ddot{u}_{N-1}(t) \\ \ddot{u}_N(t) \end{Bmatrix} + [c] \begin{Bmatrix} \dot{u}_1(t) \\ \dot{u}_2(t) \\ \vdots \\ \dot{u}_{j-1}(t) \\ \dot{u}_j(t) \\ \vdots \\ \dot{u}_{N-1}(t) \\ \dot{u}_N(t) \end{Bmatrix} + [k] \begin{Bmatrix} u_1(t) \\ u_2(t) \\ \vdots \\ u_{j-1}(t) \\ u_j(t) \\ \vdots \\ u_{N-1}(t) \\ u_N(t) \end{Bmatrix} = - \begin{Bmatrix} m_1 \\ m_2 \\ \vdots \\ m_{j-1} \\ m_j \\ \vdots \\ m_{N-1} \\ m_N \end{Bmatrix} \ddot{u}_g(t) \quad (6.1)$$

where $[c]$ and $[k]$ are the damping and stiffness matrices

$$[c] = \begin{bmatrix} c_1 + c_2 & -c_2 & 0 & \cdot & \cdot & 0 & \cdot & 0 \\ -c_2 & c_2 + c_3 & -c_3 & & & & & \cdot \\ 0 & \ddots & \ddots & \ddots & & & & \cdot \\ \cdot & & -c_{j-1} & c_{j-1} + c_j & -c_j & & & \cdot \\ 0 & & 0 & -c_j & c_j + c_{j+1} & -c_{j+1} & & \cdot \\ \cdot & & & & \ddots & \ddots & \ddots & 0 \\ \cdot & & & & & -c_{N-1} & c_{N-1} + c_N & -c_N \\ 0 & \cdot & 0 & \cdot & \cdot & 0 & -c_N & c_N \end{bmatrix} \quad (6.2)$$

$$[c] = \begin{bmatrix} k_1 + k_2 & -k_2 & 0 & \cdot & \cdot & 0 & \cdot & 0 \\ -k_2 & k_2 + k_3 & -k_3 & & & & & \cdot \\ 0 & \ddots & \ddots & \ddots & & & & \cdot \\ \cdot & & -k_{j-1} & k_{j-1} + k_j & -k_j & & & \cdot \\ 0 & & 0 & -k_j & k_j + k_{j+1} & -k_{j+1} & & \cdot \\ \cdot & & & & \ddots & \ddots & \ddots & 0 \\ \cdot & & & & & -k_{N-1} & k_{N-1} + k_N & -k_N \\ 0 & \cdot & 0 & \cdot & \cdot & 0 & -k_N & k_N \end{bmatrix} \quad (6.3)$$

and $m_1, m_2, \dots, m_N, c_1, c_2, \dots, c_N, k_1, k_2, \dots, k_N$, are the masses, damping constants and stiffnesses of the N floors shown in Figure 6.1. Upon multiplying equation (6.1) from the left with the inverse of the diagonal mass matrix $[m]$, equation (6.1) assumes the form

$$\begin{Bmatrix} \ddot{u}_1(t) \\ \ddot{u}_2(t) \\ \vdots \\ \ddot{u}_{j-1}(t) \\ \ddot{u}_j(t) \\ \vdots \\ \ddot{u}_{N-1}(t) \\ \ddot{u}_N(t) \end{Bmatrix} + [m]^{-1}[c] \begin{Bmatrix} \dot{u}_1(t) \\ \dot{u}_2(t) \\ \vdots \\ \dot{u}_{j-1}(t) \\ \dot{u}_j(t) \\ \vdots \\ \dot{u}_{N-1}(t) \\ \dot{u}_N(t) \end{Bmatrix} + [m]^{-1}[k] \begin{Bmatrix} u_1(t) \\ u_2(t) \\ \vdots \\ u_{j-1}(t) \\ u_j(t) \\ \vdots \\ u_{N-1}(t) \\ u_N(t) \end{Bmatrix} = - \begin{Bmatrix} 1 \\ 1 \\ \vdots \\ 1 \\ 1 \\ \vdots \\ 1 \\ 1 \end{Bmatrix} \ddot{u}_g(t) \quad (6.4)$$

which shows that all degrees of freedom $u_j (j \in \{1, 2, \dots, N\})$ are loaded uniformly with the same acceleration excitation, $-\ddot{u}_g(t)$.

When the $NDOF$ structure is equipped with an inerter at the ground level that opposes the motion of the first floor, the equation of motion for the $NDOF$ structure shown in Figure 6.1(left), when the inerter is supported by a non-compliant support frame, is

$$\begin{bmatrix} m_1 + M_R & 0 & \cdot & \cdot & \cdot & \cdot & \cdot & 0 \\ 0 & m_2 & & & & & & \cdot \\ \cdot & & \ddots & & & & & \cdot \\ \cdot & & & m_{j-1} & & & & \cdot \\ \cdot & & & & m_j & & & \cdot \\ \cdot & & & & & \ddots & & \cdot \\ \cdot & & & & & & m_{N-1} & 0 \\ 0 & \cdot & \cdot & \cdot & \cdot & \cdot & 0 & m_N \end{bmatrix} \begin{Bmatrix} \ddot{u}_1(t) \\ \ddot{u}_2(t) \\ \vdots \\ \ddot{u}_{j-1}(t) \\ \ddot{u}_j(t) \\ \vdots \\ \ddot{u}_{N-1}(t) \\ \ddot{u}_N(t) \end{Bmatrix} + [c] \begin{Bmatrix} \dot{u}_1(t) \\ \dot{u}_2(t) \\ \vdots \\ \dot{u}_{j-1}(t) \\ \dot{u}_j(t) \\ \vdots \\ \dot{u}_{N-1}(t) \\ \dot{u}_N(t) \end{Bmatrix} + [k] \begin{Bmatrix} u_1(t) \\ u_2(t) \\ \vdots \\ u_{j-1}(t) \\ u_j(t) \\ \vdots \\ u_{N-1}(t) \\ u_N(t) \end{Bmatrix} = - \begin{Bmatrix} m_1 \\ m_2 \\ \vdots \\ m_{j-1} \\ m_j \\ \vdots \\ m_{N-1} \\ m_N \end{Bmatrix} \ddot{u}_g(t) \quad (6.5)$$

where the quantity $M_R = (1/2)M_W(R^2/\rho^2)$ appearing in the mass matrix is the inertance of the inerter with units of mass $[M]$ and $[c]$ and $[k]$ are the damping and stiffness matrices given by equations (6.2) and (6.6).

Upon multiplying equation (6.5) from the left with the inverse of the diagonal mass matrix, $[m]^{-1}$, appearing on the left of equation (6.5), equation (6.5) assumes the form

$$\begin{Bmatrix} \ddot{u}_1(t) \\ \ddot{u}_2(t) \\ \vdots \\ \ddot{u}_{j-1}(t) \\ \ddot{u}_j(t) \\ \vdots \\ \ddot{u}_{N-1}(t) \\ \ddot{u}_N(t) \end{Bmatrix} + [m]^{-1}[c] \begin{Bmatrix} \dot{u}_1(t) \\ \dot{u}_2(t) \\ \vdots \\ \dot{u}_{j-1}(t) \\ \dot{u}_j(t) \\ \vdots \\ \dot{u}_{N-1}(t) \\ \dot{u}_N(t) \end{Bmatrix} + [m]^{-1}[k] \begin{Bmatrix} u_1(t) \\ u_2(t) \\ \vdots \\ u_{j-1}(t) \\ u_j(t) \\ \vdots \\ u_{N-1}(t) \\ u_N(t) \end{Bmatrix} = - \begin{Bmatrix} \frac{1}{1 + \frac{M_R}{m_1}} \\ 1 \\ \vdots \\ 1 \\ 1 \\ \vdots \\ 1 \\ 1 \end{Bmatrix} \ddot{u}_g(t) \quad (6.6)$$

Equation (6.6) shows that when the inerter is installed at the first level of the $NDOF$ structure (see Figure 6.1(left)), the induced ground acceleration at DOF $u_1(t)$ (first level) is suppressed by the factor $1/(1 + M_R/m_1)$, in the same way that it is suppressed when a single degree of freedom structure is equipped with an inerter as shown by equation (1.3). Accordingly, when an inerter with inertance, M_R , is installed at the first level of a $NDOF$ structure it manifests its unique beneficial effect-that is it suppresses the ground induced acceleration at the first level by $1/(1 + M_R/m_1) = 1/(1 + \sigma_1)$.

We now examine the response of the $NDOF$ structure shown in Figure 6.1(right) where the inerter is installed at the j^{th} floor. Given that the force output of the inerter is proportional to the relative acceleration of the second floor to the first floor ($\ddot{u}_j(t) - \ddot{u}_{j-1}(t)$), the equation of motion of the $NDOF$ structure shown in Figure 6.1(right), when the inerter is supported by a non-compliant frame, is

$$\begin{bmatrix} m_1 & 0 & & & & & 0 & & 0 \\ 0 & m_2 & & & & & & & \\ & & \ddots & & & & & & \\ 0 & & 0 & m_{j-1} + M_R & -M_R & & 0 & & \\ 0 & & 0 & -M_R & m_j + M_R & & 0 & & \\ & & & & & \ddots & & & \\ & & & & & & m_{N-1} & 0 & \\ 0 & & 0 & & & & 0 & m_N \end{bmatrix} \begin{Bmatrix} \ddot{u}_1(t) \\ \ddot{u}_2(t) \\ \vdots \\ \ddot{u}_{j-1}(t) \\ \ddot{u}_j(t) \\ \vdots \\ \ddot{u}_{N-1}(t) \\ \ddot{u}_N(t) \end{Bmatrix} + [c] \begin{Bmatrix} \dot{u}_1(t) \\ \dot{u}_2(t) \\ \vdots \\ \dot{u}_{j-1}(t) \\ \dot{u}_j(t) \\ \vdots \\ \dot{u}_{N-1}(t) \\ \dot{u}_N(t) \end{Bmatrix} + [k] \begin{Bmatrix} u_1(t) \\ u_2(t) \\ \vdots \\ u_{j-1}(t) \\ u_j(t) \\ \vdots \\ u_{N-1}(t) \\ u_N(t) \end{Bmatrix} = - \begin{Bmatrix} m_1 \\ m_2 \\ \vdots \\ m_{j-1} \\ m_j \\ \vdots \\ m_{N-1} \\ m_N \end{Bmatrix} \ddot{u}_g(t) \quad (6.7)$$

where again $M_R = (1/2)m_W(R^2/\rho^2)$ is the inertance of inerter and $[c]$ and $[k]$ are the damping and stiffness matrices given by equations (6.5) and (6.6). Upon multiplying equation (6.7) from

the left with the inverse of the non-diagonal mass matrix

$$[m]^{-1} = \begin{bmatrix} m_1 & 0 & \cdot & \cdot & \cdot & \cdot & 0 & \cdot & 0 \\ 0 & m_2 & & & & & & & \\ \cdot & & \ddots & & & & & & \\ 0 & 0 & m_{j-1} + M_R & -M_R & 0 & 0 & 0 & 0 & \\ 0 & 0 & -M_R & m_j + M_R & 0 & 0 & 0 & 0 & \\ \cdot & & & & \ddots & & & & \\ \cdot & & & & & m_{N-1} & 0 & & \\ 0 & \cdot & 0 & \cdot & \cdot & \cdot & 0 & m_N \end{bmatrix}^{-1} = \begin{bmatrix} \frac{1}{m_1} & 0 & \cdot & \cdot & \cdot & \cdot & 0 & \cdot & 0 \\ 0 & \frac{1}{m_2} & & & & & & & \\ \cdot & & \ddots & & & & & & \\ 0 & 0 & \frac{m_j + M_R}{m_j M_R + m_{j-1}(m_j + M_R)} & \frac{M_R}{m_j M_R + m_{j-1}(m_j + M_R)} & 0 & 0 & 0 & 0 & \\ 0 & 0 & \frac{M_R}{m_j M_R + m_{j-1}(m_j + M_R)} & \frac{m_j + M_R}{m_j M_R + m_{j-1}(m_j + M_R)} & 0 & 0 & 0 & 0 & \\ \cdot & & & & \ddots & & & & \\ \cdot & & & & & \frac{1}{m_{N-1}} & 0 & & \\ 0 & \cdot & 0 & \cdot & \cdot & \cdot & 0 & \frac{1}{m_N} \end{bmatrix} \quad (6.8)$$

Equation(6.7) assumes the form

$$\begin{Bmatrix} \ddot{u}_1(t) \\ \ddot{u}_2(t) \\ \vdots \\ \ddot{u}_{j-1}(t) \\ \ddot{u}_j(t) \\ \vdots \\ \ddot{u}_{N-1}(t) \\ \ddot{u}_N(t) \end{Bmatrix} + [m]^{-1}[c] \begin{Bmatrix} \dot{u}_1(t) \\ \dot{u}_2(t) \\ \vdots \\ \dot{u}_{j-1}(t) \\ \dot{u}_j(t) \\ \vdots \\ \dot{u}_{N-1}(t) \\ \dot{u}_N(t) \end{Bmatrix} + [m]^{-1}[k] \begin{Bmatrix} u_1(t) \\ u_2(t) \\ \vdots \\ u_{j-1}(t) \\ u_j(t) \\ \vdots \\ u_{N-1}(t) \\ u_N(t) \end{Bmatrix} = - \begin{Bmatrix} 1 \\ 1 \\ \vdots \\ 1 \\ 1 \\ \vdots \\ 1 \\ 1 \end{Bmatrix} \ddot{u}_g(t) \quad (6.9)$$

where $[c]$ and $[k]$ are the damping and stiffness matrices of the $NDOF$ structure shown in Figure 6.1 and are given by equations (6.2) and (6.4).

The most interesting result of equation (6.9) is that its right-hand side is identical to the right-hand side of equation (6.4), showing that when the inerter is placed at any level other than the ground level all degrees of freedom $u_j(t)$ ($j \in \{1, 2, \dots, N\}$) are subjected uniformly to the same (non-suppressed) acceleration excitation, $-\ddot{u}_g(t)$. The same result-that when inerters are placed at floor levels other than the first level, all degrees of freedom are subjected uniformly to the same (non-suppressed) excitation, $-\ddot{u}_g(t)$, is true when more than one floors-levels, other than the ground level, are equipped with inerters. As an example, Figure 6.2 shows a 3-story structure where inerters are placed at the second and third floor.

Dynamic equilibrium of either 3-story structure shown in Figure 6.2 when subjected to a ground induced excitation, $\ddot{u}_g(t)$, gives

$$[m] \begin{Bmatrix} \ddot{u}_1(t) \\ \ddot{u}_2(t) \\ \ddot{u}_3(t) \end{Bmatrix} + [c] \begin{Bmatrix} \dot{u}_1(t) \\ \dot{u}_2(t) \\ \dot{u}_3(t) \end{Bmatrix} + [k] \begin{Bmatrix} u_1(t) \\ u_2(t) \\ u_3(t) \end{Bmatrix} = - \begin{Bmatrix} m_1 \\ m_2 \\ m_3 \end{Bmatrix} \ddot{u}_g(t) \quad (6.10)$$

where

$$[m] = \begin{bmatrix} m_1 + M_{R2} & -M_{R2} & 0 \\ -M_{R2} & M_{R2} + m_2 & -M_{R3} \\ 0 & -M_{R3} & m_3 + M_{R3} \end{bmatrix} [c] = \begin{bmatrix} c_1 + c_2 & -c_2 & 0 \\ -c_2 & c_2 + c_3 & -c_3 \\ 0 & -c_3 & c_3 \end{bmatrix} [k] = \begin{bmatrix} k_1 + k_2 & -k_2 & 0 \\ -k_2 & k_2 + k_3 & -k_3 \\ 0 & -k_3 & k_3 \end{bmatrix} \quad (6.11)$$

are the mass, damping and stiffness matrices of the 3-story structure. The inverse of the mass

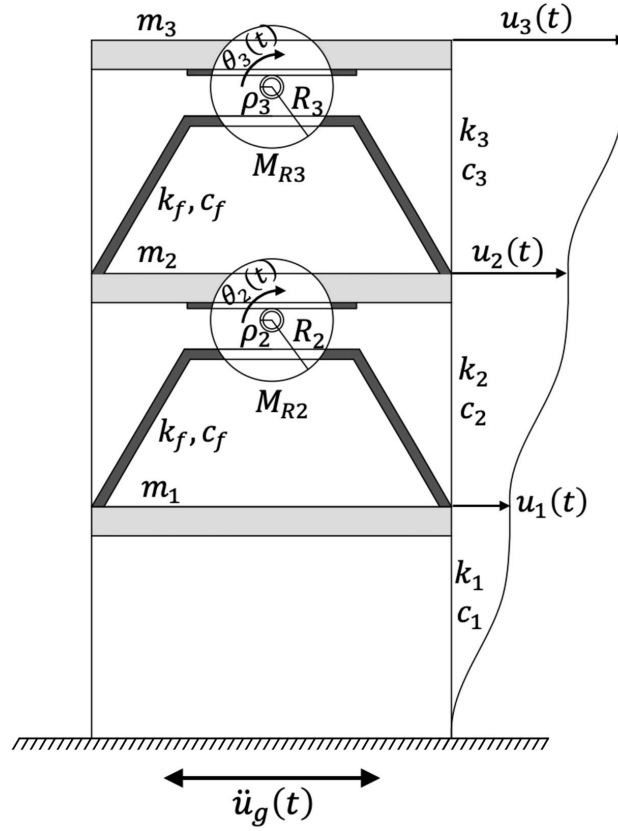


Figure 6.2: Three degree-of-freedom (3DOF) structure with supplemental rotational inertia at its 2nd and 3rd floors.

matrix of the 3-story structure shown in Figure 6.2, is

$$[m]^{-1} = \begin{bmatrix} \frac{m_3(m_2+M_{R2})+(m_2+m_3+M_{R2})M_{R3}}{\psi} & \frac{M_{R2}(m_3+M_{R3})}{\psi} & \frac{M_{R2}M_{R3}}{\psi} \\ \frac{M_{R2}(m_3+M_{R3})}{\psi} & \frac{(m_1+M_{R2})(m_3+M_{R3})}{\psi} & \frac{(m_1+M_{R2})M_{R3}}{\psi} \\ \frac{M_{R2}M_{R3}}{\psi} & \frac{(m_1+M_{R2})M_{R3}}{\psi} & \frac{MR2(m_2+M_{R3})+m_1(m_2+M_{R2}+M_{R3})}{\psi} \end{bmatrix} \quad (6.12)$$

where $\psi = m_1[m_3(m_2 + M_{R2}) + (m_2 + m_3 + M_{R2})M_{R3}] + M_{R2}[m_3M_{R3} + m_2(m_3 + M_{R3})]$. Upon multiplying equation (6.10) from the left with $[m]^{-1}$ given by equation (6.12) it assumes the form

$$\begin{Bmatrix} \ddot{u}_1(t) \\ \ddot{u}_2(t) \\ \ddot{u}_3(t) \end{Bmatrix} + [m]^{-1}[c] \begin{Bmatrix} \dot{u}_1(t) \\ \dot{u}_2(t) \\ \dot{u}_3(t) \end{Bmatrix} + [m]^{-1}[k] \begin{Bmatrix} u_1(t) \\ u_2(t) \\ u_3(t) \end{Bmatrix} = - \begin{Bmatrix} 1 \\ 1 \\ 1 \end{Bmatrix} \ddot{u}_g(t) \quad (6.13)$$

Equation (6.13) yields the same result initially presented by Takewaki et al. (2012)-that when the inerter is placed at the second and third floor of the 3-story structure shown in Figure 6.2, all three degrees of freedom u_1 , u_2 and u_3 are subjected uniformly to the same (non-suppressed) acceleration excitation, $-\ddot{u}_g(t)$.

6.2 INERTERS MANIFESTS A UNIQUE ROLE EVEN WHEN PLACED AT FLOOR-LEVELS OTHER THAN THE FIRST LEVEL

The equations of motion (6.9) and (6.13) which are for structures equipped with inerters at floor-levels other than the first level are of the same form as equation (6.7)-that is the equation of motion of the classical NDOF elastic structures without inerters. Accordingly, the natural question that arises is whether it is possible to adjust the mass and stiffness matrices of an equivalent classical NDOF structure without inerters so that its response to be identical to the response of a NDOF structure that is equipped with an inerter at its j^{th} level as is for instance, in the real-world applications reported by Sugimura et al. (2012) and Ogino and Sumiyama (2014).

With reference to equation (6.1) this equivalent NDOF structure has mass, damping and stiffness matrices of the same form as the matrices appearing in equations (6.1)-(6.6) where the $m_1, m_2, \dots, m_N, c_1, c_2, \dots, c_N, k_1, k_2, \dots, k_N$, are replaced with $m_1^e, m_2^e, \dots, m_N^e, c_1^e, c_2^e, \dots, c_N^e, k_1^e, k_2^e, \dots, k_N^e$.

Our analysis proceeds by assuming that such an equivalent structure exists and we examine the outcome of this assumption (Reductio ad absurdum). Accordingly, in the event that equation (6.9) is also the equation of motion of an equivalent NDOF classical structure without inerters, multiplication of equation (6.9) from the left with the diagonal mass $[m^e]$ gives

$$[m^e] \begin{Bmatrix} \ddot{u}_1(t) \\ \ddot{u}_2(t) \\ \vdots \\ \ddot{u}_{j-1}(t) \\ \ddot{u}_j(t) \\ \vdots \\ \ddot{u}_{N-1}(t) \\ \ddot{u}_N(t) \end{Bmatrix} + [m^e][m]^{-1}[c] \begin{Bmatrix} \dot{u}_1(t) \\ \dot{u}_2(t) \\ \vdots \\ \dot{u}_{j-1}(t) \\ \dot{u}_j(t) \\ \vdots \\ \dot{u}_{N-1}(t) \\ \dot{u}_N(t) \end{Bmatrix} + [m^e][m]^{-1}[k] \begin{Bmatrix} u_1(t) \\ u_2(t) \\ \vdots \\ u_{j-1}(t) \\ u_j(t) \\ \vdots \\ u_{N-1}(t) \\ u_N(t) \end{Bmatrix} = -[m^e] \begin{Bmatrix} 1 \\ 1 \\ \vdots \\ 1 \\ 1 \\ \vdots \\ 1 \\ 1 \end{Bmatrix} \ddot{u}_g(t) \quad (6.14)$$

where $[m]^{-1}$ is given by equation (6.8), and $[c]$ and $[k]$ are given by equations (6.2) and (6.3). For equation (6.14) to be the equation of motion of the equivalent NDOF structure without inerter, a necessary condition is that

$$[m^e][m]^{-1}[k] = [k^e] \quad (6.15)$$

where $[k^e]$ has the form of the stiffness matrix given by equation (6.3) where the entries k_1, k_2, \dots, k_N are replaced with $k_1^e, k_2^e, \dots, k_N^e$. Upon performing the matrix products on the left-hand side of equation (6.15), one obtains

$$\begin{bmatrix} \frac{(k_1+k_2)m_1^e}{m_1} & -\frac{k_2 m_1^e}{m_1} & 0 & \dots & \dots & \dots & 0 & \dots & \dots & 0 \\ -\frac{k_2 m_2^e}{m_2} & \frac{(k_2+k_3)m_2^e}{m_2} & -\frac{k_3 m_2^e}{m_2} & \dots & \dots & \dots & \dots & \dots & \dots & \dots \\ 0 & \dots & \dots & \dots & \dots & \dots & \dots & \dots & \dots & \dots \\ 0 & \dots & -\frac{k_{j-1} m_{j-1}^e (m_j + M_R)}{m_j M_R + m_{j-1} (m_j + M_R)} & \frac{m_{j-1}^e [k_j m_j + k_{j-1} (m_j + M_R)]}{m_j M_R + m_{j-1} (m_j + M_R)} & \frac{m_{j-1}^e (-k_j m_j + k_{j+1} M_R)}{m_j M_R + m_{j-1} (m_j + M_R)} & -\frac{k_{j+1} m_{j-1}^e M_R}{m_j M_R + m_{j-1} (m_j + M_R)} & \dots & \dots & \dots \\ 0 & \dots & -\frac{k_{j-1} m_j^e M_R}{m_j M_R + m_{j-1} (m_j + M_R)} & \frac{m_j^e [-k_j m_{j-1} + k_j M_R]}{m_j M_R + m_{j-1} (m_j + M_R)} & \frac{m_j^e [k_j m_{j-1} + k_{j+1} (m_{j-1} + M_R)]}{m_j M_R + m_{j-1} (m_j + M_R)} & -\frac{k_{j+1} m_j^e (m_{j-1} + M_R)}{m_j M_R + m_{j-1} (m_j + M_R)} & \dots & \dots & \dots \\ 0 & \dots & -\frac{k_{j-1} m_{j-1}^e (m_j + M_R)}{m_j M_R + m_{j-1} (m_j + M_R)} & \frac{m_{j-1}^e [-k_j m_{j-1} + k_j M_R]}{m_j M_R + m_{j-1} (m_j + M_R)} & \frac{m_{j-1}^e [k_j m_{j-1} + k_{j+1} (m_{j-1} + M_R)]}{m_j M_R + m_{j-1} (m_j + M_R)} & -\frac{k_{j+1} m_{j-1}^e M_R}{m_j M_R + m_{j-1} (m_j + M_R)} & \dots & \dots & \dots \\ \vdots & \dots & \dots & \dots & \dots & \dots & \dots & \dots & \dots & \dots \\ \vdots & \dots & \dots & \dots & \dots & \dots & \dots & \dots & \dots & \dots \\ 0 & \dots & 0 & \dots & \dots & \dots & \frac{k_{N-1} m_{N-1}^e}{m_{N-1}} & \frac{(k_{N-1} + k_N) m_{N-1}^e}{M_N} & -\frac{k_N m_{N-1}^e}{m_{N-1}} & \dots \end{bmatrix} = [k^e] \quad (6.16)$$

In the event that an equivalent NDOF structure without inerter exists, all corresponding entries k_{ij} ($i, j \in 1, \dots, N$) in the stiffness matrices appearing on the left and right-hand side of equation (6.16) shall be equal. Accordingly, by equating the entries $(j-1) * (j+1)$ of both matrices

$$-k_{j+1}m_{j-1}^e M_R = 0 \quad (6.17)$$

Since $m_{j-1}^e \neq 0$, and $k_{j+1} \neq 0$, equation (6.17) can be satisfied if and only if $M_R = 0$.

The above proof shows that the only way that equation (6.9) can be the equation of motion of an equivalent NDOF structure without inerter, is that $M_R = 0$ -that is the inertance of the inerter needs to be zero. Accordingly, while when placing inerters at floor levels other than the first level, the inerter is neither capable to suppress the ground induced acceleration (see right-hand side of equations (6.9) and (6.13)) nor to eliminate the contribution of higher modes (see Moghimi and Makris (2023) for the 2DOF structure), our analysis shows that inerters still have a unique distinct role since it is not possible to replace a structure with inerters with an equivalent structure without inerters. The above proof also contributes to support the merit of past investigations that examine the use of inerters installed at higher floor-levels as alternative tuned mass dampers Takewaki et al. (2012); Sugimura et al. (2012); Lazar et al. (2014); Marian and Giaralis (2014); Taflanidis et al. (2019); Giaralis and Taflanidis (2018).

The same result-that it is not possible to replace a structure with inerters at floor-levels other than the first level with an equivalent traditional structure without inerters, is true also for structures with inerters in more than one floors above the first floor. As an example, we investigate the case of the 3-story structure shown in Figure 6.2 which is equipped with inerters at the second and third floors. The equations of motion of this 3-story structure is offered by equation (6.13) where matrices $[c]$ and $[k]$ given by equations (6.11) and $[M]^{-1}$ is given by equation (6.12)). If an equivalent 3-story structure without inerters exists, this equivalent 3-story structure, will have mass, damping and stiffness matrices

$$[m^e] = \begin{bmatrix} m_1^e & 0 & 0 \\ 0 & m_2^e & 0 \\ 0 & 0 & m_3^e \end{bmatrix}, \quad [c^e] = \begin{bmatrix} c_1^e + c_2^e & -c_2^e & 0 \\ -c_2^e & c_2^e + c_3^e & -c_3^e \\ 0 & -c_3^e & c_3^e \end{bmatrix}, \quad [k^e] = \begin{bmatrix} k_1^e + k_2^e & -k_2^e & 0 \\ -k_2^e & k_2^e + k_3^e & -k_3^e \\ 0 & -k_3^e & k_3^e \end{bmatrix} \quad (6.18)$$

In the event that equation (6.13) is also the equation of motion of an equivalent 3DOF classical structure without inerters, multiplication of equation (6.13) from the left with its mass $[m^e]$ gives

$$\begin{bmatrix} m_1^e & 0 & 0 \\ 0 & m_2^e & 0 \\ 0 & 0 & m_3^e \end{bmatrix} \begin{Bmatrix} \ddot{u}_1(t) \\ \ddot{u}_2(t) \\ \ddot{u}_3(t) \end{Bmatrix} + \begin{bmatrix} m_1^e & 0 & 0 \\ 0 & m_2^e & 0 \\ 0 & 0 & m_3^e \end{bmatrix} [m]^{-1} [c] \begin{Bmatrix} \dot{u}_1(t) \\ \dot{u}_2(t) \\ \dot{u}_3(t) \end{Bmatrix} + \begin{bmatrix} m_1^e & 0 & 0 \\ 0 & m_2^e & 0 \\ 0 & 0 & m_3^e \end{bmatrix} [m]^{-1} [k] \begin{Bmatrix} u_1(t) \\ u_2(t) \\ u_3(t) \end{Bmatrix} = - \begin{bmatrix} m_1^e & 0 & 0 \\ 0 & m_2^e & 0 \\ 0 & 0 & m_3^e \end{bmatrix} \begin{Bmatrix} 1 \\ 1 \\ 1 \end{Bmatrix} \ddot{u}_g(t) \quad (6.19)$$

where $[m]^{-1}$ is given by equation (6.12) and $[c]$ and $[k]$ are given by equation (6.11)). For equation (6.19) to be the equation of motion of the equivalent 3DOF structure without inerters, a necessary condition is that

$$\begin{bmatrix} m_1^e & 0 & 0 \\ 0 & m_2^e & 0 \\ 0 & 0 & m_3^e \end{bmatrix} [m]^{-1} [k] = \begin{bmatrix} k_1^e + k_2^e & -k_2^e & 0 \\ -k_2^e & k_2^e + k_3^e & -k_3^e \\ 0 & -k_3^e & k_3^e \end{bmatrix} = [k^e] \quad (6.20)$$

Upon performing the matrix products on the left-hand side of equation (6.20), one obtains

$$\begin{bmatrix} \frac{m_1^e [m_3(k_2 m_2 + k_1(m_2 + M_{R2})) + (k_1 + k_2)(m_2 + m_3) + k_1 M_{R2}] M_{R3}}{\psi} & \frac{m_1^e [k_3 m_3 M_{R2} - k_2(m_3 M_{R3} + m_2(m_3 + M_{R3}))]}{\psi} & -\frac{m_1^e k_3 m_3 M_{R2}}{\psi} \\ -\frac{m_2^e (k_2 m_2 - k_1 M_{R2})(m_3 + M_{R3})}{\psi} & \frac{m_2^e [k_3 m_3 (m_1 + M_{R2}) + k_2 m_1 (m_3 + M_{R3})]}{\psi} & -\frac{m_2^e m_3 k_3 (m_1 + M_{R2})}{\psi} \\ \frac{m_3^e (-k_2 m_1 + k_1 M_{R2}) M_{R3}}{\psi} & \frac{m_3^e [-k_3 (m_2 M_{R2} + m_1 (m_2 + M_{R2})) + k_2 m_1 M_{R3}]}{\psi} & \frac{m_3^e [m_2 M_{R2} + m_1 (m_2 + M_{R2})] k_3}{\psi} \end{bmatrix} = [k^e] \quad (6.21)$$

where $\psi = m_1 [m_3(m_2 + M_{R2}) + (m_2 + m_3 + M_{R2})M_{R3}] + M_{R2} [m_3 M_{R3} + m_2(m_3 + M_{R3})]$.

In the event that an equivalent 3DOF structure without inerters exists, all corresponding entries k_{ij} ($i, j \in \{1, 2, 3\}$) in the stiffness matrices appearing on the left-and right-hand side of matrix equation (6.21) shall be equal.

By equating the entries 1 * 3 of both matrices

$$m_1^e k_3 m_3 M_{R2} = 0 \quad (6.22)$$

Since $m_1^e \neq 0$, $m_3 \neq 0$ and $k_3 \neq 0$, equation (6.22) can be satisfied if and only if $M_{R2} = 0$.

By equating the entries 3 * 1 of both matrices appearing in equation (6.21) in association with the result of equation (6.22)-that $M_{R2} = 0$, one obtains

$$-m_3^e k_2 m_1 M_{R3} = 0 \quad (6.23)$$

Since $m_3^e \neq 0$, $m_1 \neq 0$ and $k_2 \neq 0$, equation (6.23) can be satisfied if and only if $M_{R3} = 0$, showing that it is not possible to replace a structure with inerters with an equivalent structure without inerters.

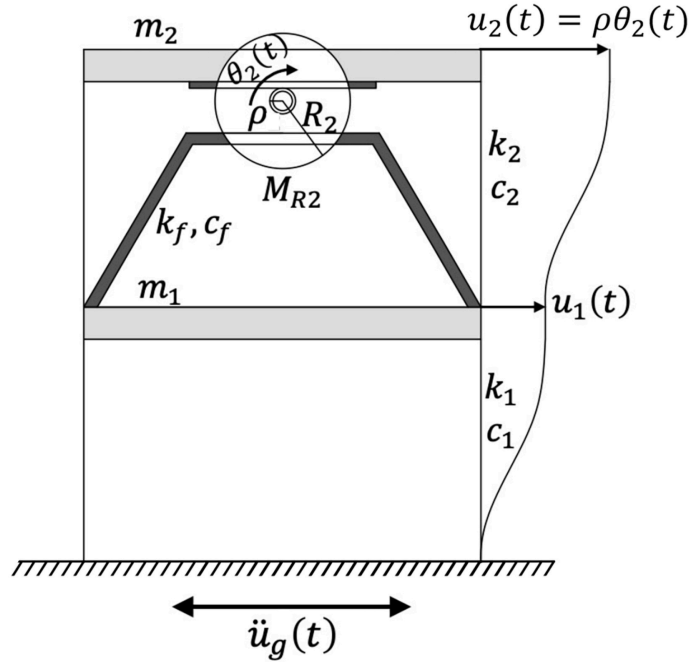


Figure 6.3: Two-degree-of-freedom (2DOF) structure with inverter installed only at its 2nd level

To further understand the unique role of inerters when placed at floor-levels other than the first level, our analysis examines the 2-story structure shown in Figure 6.3 that is equipped with the rotational inertia at the second level. In the interest of simplicity we assume that $\gamma = m_2/m_1 = 1$ ($m_1 = m_2 = m$) and $\alpha = k_2/k_1 = 1$ ($k_1 = k_2 = k$). For this special case, the equations for the modal frequencies (Moghimi and Makris 2023) reduce to

$$\omega_1^2 = p^2 \frac{3 + \sigma - \sqrt{5 + \sigma(\sigma - 2)}}{2(1 + 2\sigma)} \quad \omega_2^2 = p^2 \frac{3 + \sigma + \sqrt{5 + \sigma(\sigma - 2)}}{2(1 + 2\sigma)} \quad (6.24)$$

where $p = \sqrt{k/m}$ and $\sigma = M_R/m$ is the inertance ratio Makris and Kampas (2016); Moghimi and Makris (2021).

Figure 6.4 plots with solid lines the ratios ω_1^2/p^2 and ω_2^2/p^2 as a function of the added inertance ratio $\sigma = M_R/m$ and shows that the first modal frequency, ω_1 decreases mildly with increasing supplemental rotational inertia at the second level; whereas, the second modal frequency, ω_2 , drops drastically with increasing supplemental rotational inertia up to values of $\sigma \approx 2$ and subsequently decreases mildly following the rate of decrease of ω_1 .

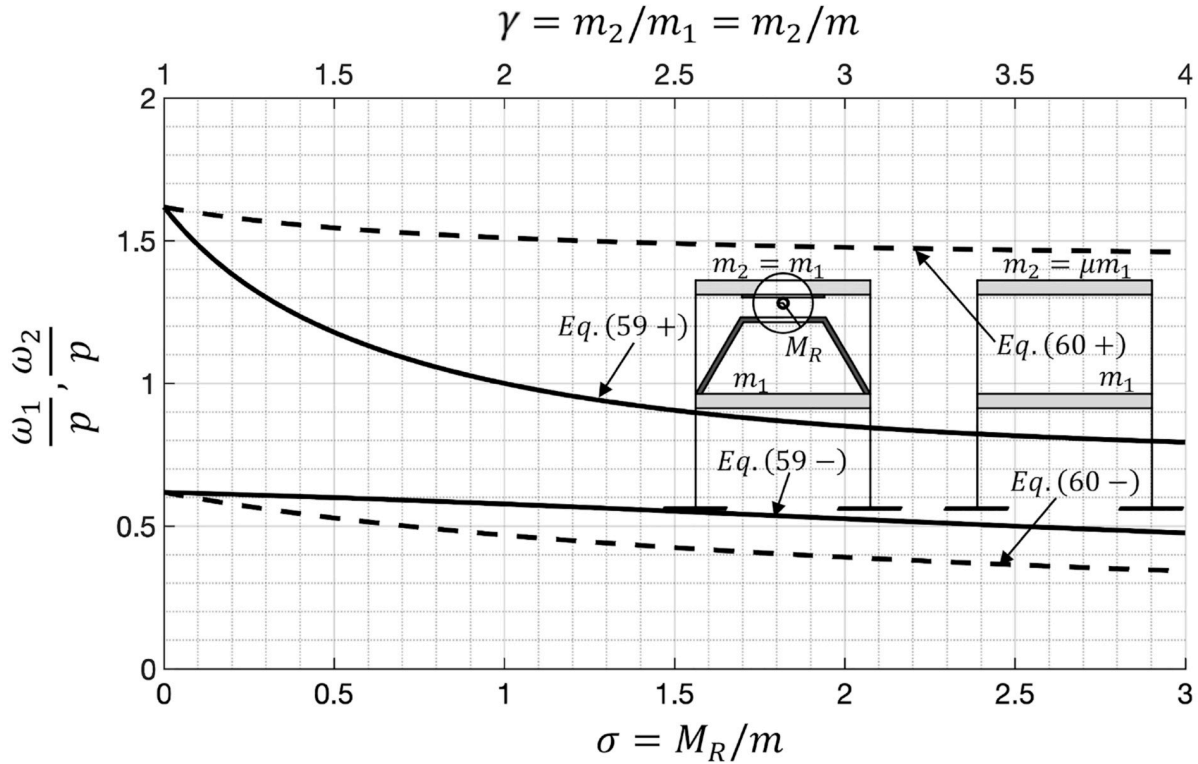


Figure 6.4: Comparison of modal frequencies ω_1 and ω_2 of the 2DOF structure as the rotational inertia at the second level increases (additional inertia forces are proportional to the relative acceleration of the second floor) with the modal frequencies of the traditional 2DOF structure (no inerters) by increasing the mass m_2 of the second level (additional inertia D'Alembert forces are proportional to the total acceleration of the second level).

Now consider the case that in order to lengthen the natural periods of the 2-story structure, instead of supplemental rotational inertia at the second level, we select to merely increase the mass m_2 of the second level. Accordingly, the mass of the second level is $m_2 = \gamma m_1$ with $\gamma \geq 1$.

By taking $k_1 = k_2 = k$ and $m_2 = \gamma m_1 = \gamma m$, and $\sigma = 0$, equations for frequencies (Moghimi and Makris 2023) reduce to

$$\omega_1^2 = p^2 \frac{2\gamma + 1 - \sqrt{4\gamma^2 + 1}}{2\gamma} \quad \omega_2^2 = p^2 \frac{2\gamma + 1 + \sqrt{4\gamma^2 + 1}}{2\gamma} \quad (6.25)$$

where again $p = \sqrt{k/m}$. Figure 6.4 also plots with dashed lines the ratios ω_1^2/p^2 and ω_2^2/p^2 as a function of $\gamma = m_2/m_1$. The four cases appearing in Figure 6.4 show the major differences by merely adding mass at the second level (increasing γ), which in this case the additional developing inertia forces (D'Alembert forces) are proportional to the total acceleration of the second floor; and by adding rotational inertia (increasing σ); which in this case the additional developing inertia forces are proportional to the relative acceleration of the second floor.

6.3 CONCLUSIONS

In view of the known distinct properties of inerters when installed without being interrupted, starting from the first level, namely: (a) their ability to eliminate the participation of higher modes and (b) their ability to suppress the ground induced excitation; in association with a growing number of publications that examine the response of tall buildings when equipped at a higher level with a solitary mechanical network that involves inerters, this chapter examines whether inerters have indeed a unique role when placed at floor-levels other than the first level.

Our study shows that in spite of the reduced role of inerters when placed at floor levels other than the first level, they still manifest a unique role since it is not possible to replace a structure with solitary inerters at higher levels with an equivalent traditional structure without inerters. Our proof contributes to support the merit of past investigations (Hoang and Warnitchai 2005; Miranda 2005; Papagiannopoulos and Beskos 2009; Sugimura et al. 2012; Garrido et al. 2013; Ogino and Sumiyama 2014; Lazar et al. 2014; Marian and Giaralis 2014; Giaralis and Taflanidis 2015; Giaralis and Petrini 2017; Luo et al. 2017; Pietrosanti et al. 2017; Wen et al. 2017; De Domenico and Ricciardi 2018a; Taflanidis et al. 2019) that examine the use of solitary inerters installed at higher floor-levels as alternative tuned mass dampers.

7 Conclusions

This report investigates the dynamics of single-story and multistory structures with supplemental rotational inertia and how inerters modify their elastic or inelastic response. In view that the inerter emerges as the third elementary mechanical element, Chapter 2 examines and constructs the basic frequency-response functions and subsequently derives the corresponding causal time-response functions of elementary mechanical networks which involve inerters. Because of the participation of the inerter, some basic time-response functions of the examined mechanical networks exhibit a causal oscillatory response and this behavior complements the decaying-exponential response due to the participation of the dashpot. Most importantly, the chapter shows that the inerter emerges as an attractive response-modification element given that in some cases it “absorbs” the impulsive response of the solitary spring or dashpot present in the mechanical network.

The basic response-functions derived in Chapter 2 and summarized in Table 2.1 in association with the mathematical operations outlined, extends the well-established theory of linear viscoelasticity to the inertoelastic and inertoviscoelastic behavior (combination of inerters, dashpots and springs) and introduces the subject of inertoviscoelasticity.

Chapter 3 shows that the supplemental rotational inertia controls effectively the displacements of the first story of a 2DOF elastic structure along a wide range of the response spectrum. The proposed seismic protection strategy can accommodate large relative displacements without suffering from the issue of viscous heating (Makris 1998; Makris et al. 1998; Black and Makris 2007) and potential leaking that challenges the implementation of fluid dampers under prolonged cyclic loading. When the chevron frame that supports the rotational inertia system is stiff, the use of two parallel rotational inertia systems offers improved results for the response of the 2DOF structure. However, as the compliance of the chevron frame that supports the inerters increases, the use of a single rotational inertia system offers more favorable response other than increasing the forces transferred to the chevron frame.

Chapter 4 shows that while a small amount of supplemental rotational inertia is needed to eliminate the participation of the second mode of the 2DOF linear isolated structure; the effect of this elimination is marginal on the structure response, since the participation of the second mode is invariably small even when isolation systems without inerters are used (Kelly 1990, 1997). The nonlinear response analysis of the same 2DOF isolated structure is examined by adopting a bilinear behavior for the isolation system in association with a formulation that accounts for the compliance of the support of the inerter. Our study shows that supplemental rotational inertia aggravates superstructure displacements and accelerations at larger isolation periods ($T_b > 2.5sec$). In view

of these findings in association with the small gains in reducing displacements above isolators, the use of inerters in isolation systems is not recommended.

The response analysis of a SDOF elastoplastic and bilinear structure in chapter 5 reveals that when the yielding structure is equipped with supplemental rotational inertia (inerters), the equal-displacement rule is valid starting from lower values of the preyielding period given that the presence of inerters lengthens the apparent preyielding period. Furthermore, inerters suppress effectively the inelastic displacements of SDOF yielding structures; while the resulting base shears are systematically lower than when large values of supplemental damping ($\xi_d = 25\%$) are used. The forces transferred at the mounting of the inerters are appreciably lower than the corresponding forces originating from an elastic structure analyzed in Chapter 3. Consequently, the implementation of inerters emerges as an attractive response modification strategy for elastoplastic and bilinear SDOF structures with larger preyielding periods.

The use of a pair of clutching inerters does not offer any additional benefits compared to the case where a single inerter is used. Pair of clutching inerters are found to be attractive when suppressing the response of elastic structures.

Inerters are also effective in suppressing the inelastic response of 2DOF yielding structures with pre-yielding periods up to $T_1 = 1.5\text{sec}$ without aggravating the inelastic response of the superstructure. The effectiveness of inerters to suppress the inelastic response of the 2DOF yielding structure outperforms appreciably the effectiveness of large values of supplemental damping ($\xi_d = 25\%$) when the support frame of the response modification device is compliant. In view of these findings the use of inerters emerges as an attractive response modification strategy and is recommended for yielding structures. For larger pre-yielding periods (say $T_1 > 2.0\text{sec}$), the effectiveness of inerters to suppress the inelastic response of 2DOF yielding structures reduces; and for very flexible first stories; as in the case of isolated structures examined in Chapter 4, the use of inerters at the first level (isolation system) is not recommended.

Motivated by the known distinct property of inerters when installed without being interrupted, starting from the first level, to suppress the ground induced excitation; in association with a growing number of publications that examine the response of tall buildings when equipped at a higher level with a solitary mechanical network that involves inerters in Chapter 6, we examine whether inerters have indeed a unique role when placed at floor-levels other than the first level. Our study shows that in spite of the reduced role of inerters when placed at floor levels other than the first level, they still manifest a unique role since it is not possible to replace a structure with solitary inerters at higher levels with an equivalent traditional structure without inerters. Our proof contributes to support the merit of past investigations (Sugimura et al. 2012; Ogino and Sumiyama 2014; Lazar et al. 2014; Marian and Giaralis 2014; Taflanidis et al. 2019) that examine the use of solitary inerters installed at higher floor-levels as alternative tuned mass dampers.

REFERENCES

- Aghagholizadeh, M. and Makris, N. (2018). “Seismic response of a yielding structure coupled with a rocking wall.” *Journal of Structural Engineering, ASCE*, 144(2), 04017196 (doi: [https://doi.org/10.1061/\(ASCE\)ST.1943-541X.0001894](https://doi.org/10.1061/(ASCE)ST.1943-541X.0001894)).
- Aiken, I. D. (1990). *Earthquake simulator testing and analytical studies of two energy-absorbing systems for multistory structures*. University of California Berkeley, U.S.A.
- Al-Hussaini, T. M., Constantinou, M. C., and Zayas, V. A. (1994). *Seismic isolation of multi-story frame structures using spherical sliding isolation systems. Report No. NCEER-94-0007*,. National Center for Earthquake Engineering Research, University at Buffalo.
- Antonopoulos, A. and Anagnostopoulos, S. (2017). “Partial strengthening of buildings with open ground stories.” *Proc., Int. Workshop on Performance Based Seismic Design of Structure*, Tongji University, Shanghai, China.
- Arakaki, T., Kuroda, H., Arima, F., Inoue, Y., and Baba, K. (1999a). “Development of seismic devices applied to ball screw: Part 1 basic performance test of rd-series.” *AIJ Journal of Technology and Design*, 5(8), 239–244 (doi: https://doi.org/10.3130/aijt.5.239_1).
- Arakaki, T., Kuroda, H., Arima, F., Inoue, Y., and Baba, K. (1999b). “Development of seismic devices applied to ball screw: Part 2 performance test and evaluation of rd-series.” *AIJ Journal of Technology and Design*, 5(9), 265–270 (doi: <https://doi.org/10.3130/aijt.5.265>).
- Arnold, C. (1984). “Soft first stories: truths and myths.” *Proc., 8th World Conference on Earthquake Engineering*, Vol. 5, San Francisco., 943–950.
- Baber, T. T. and Noori, M. N. (1985). “Random vibration of degrading, pinching systems.” *Journal of Engineering Mechanics, ASCE*, 111(8), 1010–1026 (doi: [https://doi.org/10.1061/\(ASCE\)0733-9399\(1985\)111:8\(1010\)](https://doi.org/10.1061/(ASCE)0733-9399(1985)111:8(1010))).
- Bendat, J. and Piersol, A. (1986). *Random data: Analysis and measurement procedures*. John Wiley and Sons, New York, NY, U.S.A.
- Bertero, V., Anderson, J., Krawinkler, H., Miranda, E., et al. (1991). *Design guidelines for ductility and drift limits*. Rept. No. EERC/UCB-91/15. Berkeley, CA: Univ. of California.
- Bertero, V. V., Mahin, S. A., and Herrera, R. A. (1978). “Aseismic design implications of near-fault san fernando earthquake records.” *Earthquake Engineering and Structural Dynamics*, 6(1), 31–42 (doi: <https://doi.org/10.1002/eqe.4290060105>).
- Bird, R. B., Armstrong, R. C., and Hassager, O. (1987). *Dynamics of polymeric liquids*. John Wiley and Sons, New York, NY, U.S.A.

- Black, C., Makris, N., and Aiken, I. (2002). *Component testing, stability analysis, and characterization of buckling-restrained unbonded braces (TM)*. Pacific Earthquake Engineering Research Center.
- Black, C., Makris, N., and Aiken, I. (2003). *Component testing and modeling of buckling restrained “unbonded” braces*. Proc., Conference on Behaviour of Steel Structures in Seismic Areas, Routledge, Netherlands.
- Black, C. J. and Makris, N. (2007). “Viscous heating of fluid dampers under small and large amplitude motions: experimental studies and parametric modeling.” *Journal of Engineering Mechanics, ASCE*, 133(5), 566–577 (doi: [https://doi.org/10.1061/\(ASCE\)0733-9399\(2007\)133:5\(566\)](https://doi.org/10.1061/(ASCE)0733-9399(2007)133:5(566))).
- Bode, H. W. et al. (1945). *Network analysis and feedback amplifier design*. Van Nostrand Reinhold, Princeton, NJ, U.S.A.
- Chang, S. and Makris, N. (2000). “Effect of various energy dissipation mechanisms in suppressing structural response.” *Proc., 12th World Conference on Earthquake Engineering*, Auckland, New Zealand.
- Chen, M. Z., Hu, Y., Huang, L., and Chen, G. (2014). “Influence of inerter on natural frequencies of vibration systems.” *Journal of Sound and Vibration*, 333(7), 1874–1887 (doi: <https://doi.org/10.1016/j.jsv.2013.11.025>).
- Chen, M. Z., Papageorgiou, C., Scheibe, F., Wang, F.-C., and Smith, M. C. (2009). “The missing mechanical circuit element.” *IEEE Circuits and Systems Magazine*, 9(1), 10–26 (doi: <https://doi.org/10.1109/MCAS.2008.931738>).
- Chopra, A., Clough, D., and Clough, R. (1972). “Earthquake resistance of buildings with a ‘soft’ first storey.” *Earthquake Engineering and Structural Dynamics*, 1(4), 347–355 (doi: <https://doi.org/10.1002/eqe.4290010405>).
- Chopra, A. K. (2000). *Dynamics of structures*. Prentice Hall, NJ, U.S.A.
- Clough, R. and Penzien, J. (1975). *Dynamics of structures*. Mc Graw-Hill, New York, U.S.A.
- Constantinou, M. and Adnane, M. (1987). *Dynamics of Soil-base-isolated-structure Systems Report 4: Evaluation of Two Models for Yielding Systems*. Drexel University, Philadelphia, U.S.A.
- Constantinou, M., Mokha, A., and Reinhorn, A. (1990). “Teflon bearings in base isolation ii: Modeling.” *Journal of Structural Engineering, ASCE*, 116(2), 455–474 (doi: [https://doi.org/10.1061/\(ASCE\)0733-9445\(1990\)116:2\(455\)](https://doi.org/10.1061/(ASCE)0733-9445(1990)116:2(455))).
- Constantinou, M., Soong, T., and Dargush, G. (1998). *Passive energy dissipation systems for structural design and retrofit*. Multidisciplinary Center for Earthquake Engineering Research Buffalo, NY, U.S.A.

- De Domenico, D., Deastra, P., Ricciardi, G., Sims, N. D., and Wagg, D. J. (2019). “Novel fluid inerter based tuned mass dampers for optimised structural control of base-isolated buildings.” *Journal of the Franklin Institute*, 356(14), 7626–7649 (doi: <https://doi.org/10.1016/j.jfranklin.2018.11.012>).
- De Domenico, D. and Ricciardi, G. (2018a). “An enhanced base isolation system equipped with optimal tuned mass damper inerter (tmdi).” *Earthquake Engineering and Structural Dynamics*, 47(5), 1169–1192 (doi: <https://doi.org/10.1002/eqe.3011>).
- De Domenico, D. and Ricciardi, G. (2018b). “Optimal design and seismic performance of tuned mass damper inerter (tmdi) for structures with nonlinear base isolation systems.” *Earthquake Engineering and Structural Dynamics*, 47(12), 2539–2560 (doi: <https://doi.org/10.1002/eqe.3098>).
- Efthymiou, E. and Makris, N. (2022). “Pulse-period–moment–magnitude relations derived with wavelet analysis and their relevance to estimate structural deformations.” *Earthquake Engineering and Structural Dynamics*, 51(7), 1636–1656 (doi: <https://doi.org/10.1002/eqe.3631>).
- Ferry, J. D. (1980). *Viscoelastic properties of polymers*. John Wiley and Sons, New York, NY, U.S.A.
- Fintel, M. and Khan, F. R. (1969). “Shock-absorbing soft story concept for multistory earthquake structures.” *ACI Structural Journal*, 66(5), 381–390 (doi: <https://doi.org/10.14359/7365>).
- Furuhashi, T. and Ishimaru, S. (2008). “Mode control seismic design with dynamic mass.” *Proc., 14th World Conference on Earthquake Engineering*, Beijing, China.
- Garrido, H., Curadelli, O., and Ambrosini, D. (2013). “Improvement of tuned mass damper by using rotational inertia through tuned viscous mass damper.” *Engineering Structures*, 56, 2149–2153 (doi: <https://doi.org/10.1016/j.engstruct.2013.08.044>).
- Giaralis, A. and Petrini, F. (2017). “Wind-induced vibration mitigation in tall buildings using the tuned mass-damper-inerter.” *Journal of Structural Engineering, ASCE*, 143(9), 04017127 (doi: [https://doi.org/10.1061/\(ASCE\)ST.1943-541X.0001863](https://doi.org/10.1061/(ASCE)ST.1943-541X.0001863)).
- Giaralis, A. and Taflanidis, A. (2018). “Optimal tuned mass-damper-inerter (tmdi) design for seismically excited mdof structures with model uncertainties based on reliability criteria.” *Structural Control and Health Monitoring*, 25(2), e2082 (doi: <https://doi.org/10.1002/stc.2082>).
- Giaralis, A. and Taflanidis, A. A. (2015). “Reliability-based design of tuned mass-damper-inerter (tmdi) equipped multi-storey frame buildings under seismic excitation.” *Proc., 12th International Conference on Applications of Statistics and Probability in Civil Engineering*, Vancouver, Canada.

- Giesekus, H. (1995). “An alternative approach to the linear theory of viscoelasticity and some characteristic effects being distinctive of the type of material.” *Rheologica Acta*, 34, 2–11 (doi: <https://doi.org/10.1007/BF00396050>).
- Green, N. B. (1935). “Flexible first-story construction for earthquake resistance.” *Transactions of the American Society of Civil Engineers*, 100(1), 645–652 (doi: <https://doi.org/10.1061/TACEAT.0004638>).
- Hoang, N. and Warnitchai, P. (2005). “Design of multiple tuned mass dampers by using a numerical optimizer.” *Earthquake Engineering and Structural Dynamics*, 34(2), 125–144 (doi: <https://doi.org/10.1002/eqe.413>).
- Hwang, J.-S., Kim, J., and Kim, Y.-M. (2007). “Rotational inertia dampers with toggle bracing for vibration control of a building structure.” *Engineering Structures*, 29(6), 1201–1208 (doi: <https://doi.org/10.1016/j.engstruct.2006.08.005>).
- Ikago, K., Saito, K., and Inoue, N. (2012a). “Seismic control of single-degree-of-freedom structure using tuned viscous mass damper.” *Earthquake Engineering and Structural Dynamics*, 41(3), 453–474.
- Ikago, K., Sugimura, Y., Saito, K., and Inoue, N. (2012b). “Modal response characteristics of a multiple-degree-of-freedom structure incorporated with tuned viscous mass dampers.” *Journal of Asian Architecture and Building Engineering*, 11(2), 375–382 (doi: <https://doi.org/10.3130/jaabe.11.375>).
- Inaudi, J. and Makris, N. (1996). “Time-domain analysis of linear hysteretic damping.” *Earthquake Engineering and Structural Dynamics*, 25(6), 529–545 (doi: [https://doi.org/10.1002/\(SICI\)1096-9845\(199606\)25:6<529::AID-EQE549>3.0.CO;2-P](https://doi.org/10.1002/(SICI)1096-9845(199606)25:6<529::AID-EQE549>3.0.CO;2-P)).
- Ishii, M., Kazama, H., Miyazaki, K., and Murakami, K. (2014). “Application of tuned viscous mass damper to super-high-rise buildings.” *Proc., 6th World Conference of the International Association for Structural Control and Monitoring (6WCSCM), Barcelona, Spain*.
- Ishimaru, S. (1994). “Outline of response control of structures against earthquakes, design mechanism and control dynamics of building structure.” *Architectural Institute of Japan*, 199–202.
- Jacobsen, L. S. (1938). “Effects of a flexible first story in a building located on vibrating ground.” *Proc., S. Timoshenko 60th Anniversary Volume*, The Macmillan New York, U.S.A.
- Jeffreys, H. (1929). *The earth*. Cambridge, Cambridge University Press, U.K.
- Kawamata, S. (1986). “Control of structural vibration by inertia pump damper: part i theoretical model and response to harmonic excitation.” *Proc., Summaries of Technical Papers of Annual Meeting Architectural Institute of Japan, 1986*, National Institute of Informatics (CiNii), Japan.
- Kelly, J. M. (1990). “Base isolation: linear theory and design.” *Earthquake Spectra*, 6(2), 223–244 (doi: <https://doi.org/10.1193/1.1585566>).
- Kelly, J. M. (1997). *Earthquake-resistant design with rubber*, Vol. 7. Springer, London, U.K.

- Kelly, J. M. and Konstantinidis, D. (2011). *Mechanics of rubber bearings for seismic and vibration isolation*. John Wiley and Sons, New York, NY, U.S.A.
- Kelly, J. M., Skinner, R., and Heine, A. (1972). “Mechanisms of energy absorption in special devices for use in earthquake resistant structures.” *Bulletin of the New Zealand Society for Earthquake Engineering*, 5(3), 63–88 (doi: <https://doi.org/10.5459/BNZSEE.5.3.63-88>).
- Konstantinidis, D. and Makris, N. (2005). “Seismic response analysis of multidrum classical columns.” *Earthquake Engineering and Structural Dynamics*, 34(10), 1243–1270 (doi: <https://doi.org/10.1002/eqe.478>).
- Kuznetsov, A., Mammadov, M., Sultan, I., and Hajilarov, E. (2011). “Optimization of improved suspension system with inerter device of the quarter-car model in vibration analysis.” *Archive of Applied Mechanics*, 81, 1427–1437 (doi: <https://doi.org/10.1007/s00419-010-0492-x>).
- Lazar, I., Neild, S., and Wagg, D. (2014). “Using an inerter-based device for structural vibration suppression.” *Earthquake Engineering and Structural Dynamics*, 43(8), 1129–1147 (doi: <https://doi.org/10.1002/eqe.2390>).
- Le Corbusier (1925). *Vers une architecture*. Les Editions G. Cres el C, Paris.
- Le Corbusier (1986). *Towards a new architecture*. Courier Corporation, New York, U.S.A.
- Lighthill, M. J. (1958). *An introduction to Fourier analysis and generalised functions*. Cambridge University Press, U.K.
- Liu, X., Jiang, J. Z., Titurus, B., and Harrison, A. (2018). “Model identification methodology for fluid-based inerters.” *Mechanical Systems and Signal Processing*, 106, 479–494 (doi: <https://doi.org/10.1016/j.ymssp.2018.01.018>).
- Luo, Y., Sun, H., Wang, X., Zuo, L., and Chen, N. (2017). “Wind induced vibration control and energy harvesting of electromagnetic resonant shunt tuned mass-damper-inerter for building structures.” *Shock and Vibration*, 2017 (doi: <https://doi.org/10.1155/2017/4180134>).
- Makris, N. (1997a). “Causal hysteretic element.” *Journal of Engineering Mechanics, ASCE*, 123(11), 1209–1214 (doi: [https://doi.org/10.1061/\(ASCE\)0733-9399\(1997\)123:11\(1209\)](https://doi.org/10.1061/(ASCE)0733-9399(1997)123:11(1209))).
- Makris, N. (1997b). “Stiffness, flexibility, impedance, mobility, and hidden delta function.” *Journal of Engineering Mechanics, ASCE*, 123(11), 1202–1208 (doi: [https://doi.org/10.1061/\(ASCE\)0733-9399\(1997\)123:11\(1202\)](https://doi.org/10.1061/(ASCE)0733-9399(1997)123:11(1202))).
- Makris, N. (1998). “Viscous heating of fluid dampers. i: Small-amplitude motions.” *Journal of Engineering Mechanics, ASCE*, 124(11), 1210–1216 (doi: [https://doi.org/10.1061/\(ASCE\)0733-9399\(1998\)124:11\(1210\)](https://doi.org/10.1061/(ASCE)0733-9399(1998)124:11(1210))).

- Makris, N. (2017). “Basic response functions of simple inertoelastic and inertoviscous models.” *Journal of Engineering Mechanics, ASCE*, 143(11), 04017123 (doi: [https://doi.org/10.1061/\(ASCE\)EM.1943-7889.0001348](https://doi.org/10.1061/(ASCE)EM.1943-7889.0001348)).
- Makris, N. (2018). “Time-response functions of mechanical networks with inerters and causality.” *Meccanica*, 53(9), 2237–2255 (doi: <https://doi.org/10.1007/s11012-018-0822-6>).
- Makris, N. (2020a). “On the physical meaning of time-domain constitutive models with complex parameters.” *Meccanica*, 55(3), 453–467 (doi: <https://doi.org/10.1007/s11012-020-01137-x>).
- Makris, N. (2020b). “Viscous-viscoelastic correspondence principle for brownian motion.” *Physical Review E*, 101(5), 052139 (doi: <https://link.aps.org/doi/10.1103/PhysRevE.101.052139>).
- Makris, N. (2021a). “Impulse response function for brownian motion.” *Soft Matter*, 17(21), 5410–5426 (doi: <https://doi.org/10.1039/D1SM00380A>).
- Makris, N. (2021b). “A rheological analog for brownian motion with hydrodynamic memory.” *Physics of Fluids*, 33(7), 072014 (doi: <https://doi.org/10.1063/5.0059452>).
- Makris, N. and Chang, S. (2000a). “Effect of viscous, viscoplastic and friction damping on the response of seismic isolated structures.” *Earthquake Engineering and Structural Dynamics*, 29(1), 85–107 (doi: [https://doi.org/10.1002/\(SICI\)1096-9845\(200001\)29:1<85::AID-EQE902>3.0.CO;2-N](https://doi.org/10.1002/(SICI)1096-9845(200001)29:1<85::AID-EQE902>3.0.CO;2-N)).
- Makris, N. and Chang, S. (2000b). “Response of damped oscillators to cycloidal pulses.” *Journal of Engineering Mechanics, ASCE*, 126(2), 123–131 (doi: [https://doi.org/10.1061/\(ASCE\)0733-9399\(2000\)126:2\(123\)](https://doi.org/10.1061/(ASCE)0733-9399(2000)126:2(123))).
- Makris, N., Constantinou, M., and Dargush, G. (1993a). “Analytical model of viscoelastic fluid dampers.” *Journal of Structural Engineering, ASCE*, 119(11), 3310–3325 (doi: [https://doi.org/10.1061/\(ASCE\)0733-9445\(1993\)119:11\(3310\)](https://doi.org/10.1061/(ASCE)0733-9445(1993)119:11(3310))).
- Makris, N., Dargush, G., and Constantinou, M. (1993b). “Dynamic analysis of generalized viscoelastic fluids.” *Journal of Engineering Mechanics, ASCE*, 119(8), 1663–1679 (doi: [https://doi.org/10.1061/\(ASCE\)0733-9399\(1993\)119:8\(1663\)](https://doi.org/10.1061/(ASCE)0733-9399(1993)119:8(1663))).
- Makris, N. and Efthymiou, E. (2020). “Time-response functions of fractional derivative rheological models.” *Rheologica Acta*, 59(12), 849–873 (doi: <https://doi.org/10.1007/s00397-020-01241-5>).
- Makris, N. and Kampas, G. (2009). “Analyticity and causality of the three-parameter rheological models.” *Rheologica Acta*, 48, 815–825 (doi: <https://doi.org/10.1007/s00397-009-0374-8>).
- Makris, N. and Kampas, G. (2013). “The engineering merit of the “effective period” of bilinear isolation systems.” *Earthquakes and Structures*, 4(4), 397–428 (doi: <https://doi.org/10.12989/eas.2013.4.4.397>).

- Makris, N. and Kampas, G. (2016). “Seismic protection of structures with supplemental rotational inertia.” *Journal of Engineering Mechanics, ASCE*, 142(11), 04016089 (doi: [https://doi.org/10.1061/\(ASCE\)EM.1943-7889.0001152](https://doi.org/10.1061/(ASCE)EM.1943-7889.0001152)).
- Makris, N. and Moghimi, G. (2019). “Displacements and forces in structures with inerters when subjected to earthquakes.” *Journal of Structural Engineering, ASCE*, 145(2), 04018260 (doi: [https://doi.org/10.1061/\(ASCE\)ST.1943-541X.0002267](https://doi.org/10.1061/(ASCE)ST.1943-541X.0002267)).
- Makris, N. and Moghimi, G. (2022). “Response of seismic isolated structures with supplemental rotational inertia.” *Earthquake Engineering and Structural Dynamics*, 51(12), 2956–2974 (doi: <https://doi.org/10.1002/eqe.3709>).
- Makris, N., Roussos, Y., Whittaker, A. S., and Kelly, J. M. (1998). “Viscous heating of fluid dampers. ii: Large-amplitude motions.” *Journal of Engineering Mechanics, ASCE*, 124(11), 1217–1223 (doi: [https://doi.org/10.1061/\(ASCE\)0733-9399\(1998\)124:11\(1217\)](https://doi.org/10.1061/(ASCE)0733-9399(1998)124:11(1217))).
- Makris, N. and Vassiliou, M. F. (2011). “The existence of ‘complete similarities’ in the response of seismic isolated structures subjected to pulse-like ground motions and their implications in analysis.” *Earthquake Engineering and Structural Dynamics*, 40(10), 1103–1121 (doi: <https://doi.org/10.1002/eqe.1072>).
- Marian, L. and Giaralis, A. (2014). “Optimal design of a novel tuned mass-damper-inerter (tmdi) passive vibration control configuration for stochastically support-excited structural systems.” *Probabilistic Engineering Mechanics*, 38, 156–164 (doi: <https://doi.org/10.1016/j.probengmech.2014.03.007>).
- Martel, R. (1929). “The effects of earthquakes on buildings with a flexible first story.” *Bulletin of the Seismological Society of America*, 19(3), 167–178 (doi: <https://doi.org/10.1785/BSSA0190030167>).
- Miranda, J. C. (2005). “On tuned mass dampers for reducing the seismic response of structures.” *Earthquake Engineering and Structural Dynamics*, 34(7), 847–865 (doi: <https://doi.org/10.1002/eqe.461>).
- Moghimi, G. (2022). *Response Modification and Seismic Protection of Yielding Structures Equipped with Inerters and Hysteretic Dampers*. Ph.D.dissertation. Southern Methodist University.
- Moghimi, G. and Makris, N. (2021). “Seismic response of yielding structures equipped with inerters.” *Soil Dynamics and Earthquake Engineering*, 141, 106474 (doi: <https://doi.org/10.1016/j.soildyn.2020.106474>).
- Moghimi, G. and Makris, N. (2023). “The role of inerters when placed at floor-levels other than the first level.” *Soil Dynamics and Earthquake Engineering*, 168, 107832 (doi: <https://doi.org/10.1016/j.soildyn.2023.107832>).

- Mokha, A., Constantinou, M. C., and Reinhorn, A. M. (1990). *Experimental study and analytical prediction of earthquake response of a sliding isolation system with a spherical surface. Report NCEER 90 0020*. National Center for Earthquake Engineering Research, University at Buffalo, NY, U.S.A.
- Morse, P. M. and Feshbach, H. (1953). *Methods of theoretical physics*. McGraw-Hill, New York, U.S.A.
- Ogino, M. and Sumiyama, T. (2014). “Structural design of a high-rise building using tuned viscous mass dampers installed across three consecutive storeys.” *Proc., 12th International Conference on Computational Structures Technology*, Vol. 225, Naples, Italy.
- Papageorgiou, C., Houghton, N. E., and Smith, M. C. (2009). “Experimental testing and analysis of inerter devices.” *Journal of Dynamic Systems, Measurement, and Control*, 131(1) (doi: <https://doi.org/10.1115/1.3023120>).
- Papageorgiou, C. and Smith, M. C. (2005). “Laboratory experimental testing of inerters.” *Proc., 44th IEEE Conference on Decision and Control*, IEEE, Seville, Spain, 3351–3356.
- Papagiannopoulos, G. A. and Beskos, D. E. (2009). “On a modal damping identification model for non-classically damped linear building structures subjected to earthquakes.” *Soil Dynamics and Earthquake Engineering*, 29(3), 583–589 (doi: <https://doi.org/10.1016/j.soildyn.2008.10.005>).
- Papoulis, A. (1987). *The Fourier integral and its applications*. Mc Graw-Hill, New York, U.S.A.
- Pietrosanti, D., De Angelis, M., and Basili, M. (2017). “Optimal design and performance evaluation of systems with tuned mass damper inerter (tmdi).” *Earthquake Engineering and Structural Dynamics*, 46(8), 1367–1388 (doi: <https://doi.org/10.1002/eqe.2861>).
- Pitilakis, D. and Makris, N. (2010). “Dimensional analysis of inelastic systems with soil-structures interaction.” *Bulletin of Earthquake Engineering*, 8(6), 1497–1514 (doi: <https://doi.org/10.1080/13632469.2012.691615>).
- Repapis, C., Zeris, C., and Vintzileou, E. (2006). “Evaluation of the seismic performance of existing rc buildings ii: A case study for regular and irregular buildings.” *Journal of Earthquake Engineering*, 10(03), 429–452 (doi: <https://doi.org/10.1080/13632460609350604>).
- Saitoh, M. (2007). “Simple model of frequency-dependent impedance functions in soil-structure interaction using frequency-independent elements.” *Journal of Engineering Mechanics, ASCE*, 133(10), 1101–1114 (doi: [https://doi.org/10.1061/\(ASCE\)0733-9399\(2007\)133:10\(1101\)](https://doi.org/10.1061/(ASCE)0733-9399(2007)133:10(1101))).
- Saitoh, M. (2012). “On the performance of gyro-mass devices for displacement mitigation in base isolation systems.” *Structural Control and Health Monitoring*, 19(2), 246–259 (doi: <https://doi.org/10.1002/stc.419>).

- Sarlis, A. A., Pasala, D. T. R., Constantinou, M., Reinhorn, A., Nagarajaiah, S., and Taylor, D. (2013). “Negative stiffness device for seismic protection of structures.” *Journal of Structural Engineering, ASCE*, 139(7), 1124–1133 (doi: [https://doi.org/10.1061/\(ASCE\)ST.1943-541X.0000616](https://doi.org/10.1061/(ASCE)ST.1943-541X.0000616)).
- Skinner, R., Kelly, J., and Heine, A. (1973). “Energy absorption devices for earthquake resistant structures.” *Proc. 5th World Conference on Earthquake Engineering*, Vol. 8, Rome, Italy.
- Skinner, R. I., Kelly, J. M., and Heine, A. (1974). “Hysteretic dampers for earthquake-resistant structures.” *Earthquake Engineering and Structural Dynamics*, 3(3), 287–296 (doi: <https://doi.org/10.1002/eqe.4290030307>).
- Skinner, R. I., Robinson, W., and GH, M. (1993). *An Introduction to Seismic Isolation*. John Wiley and Sons, New York, NY, U.S.A.
- Smith, M. C. (2002). “Synthesis of mechanical networks: the inerter.” *IEEE Transactions on Automatic Control*, 47(10), 1648–1662 (doi: <https://doi.org/10.1109/TAC.2002.803532>).
- Soong, T. and Dargush, G. (1997). *Passive Energy Dissipation Systems in Structural Engineering*. John Wiley and Sons, New York, NY, U.S.A.
- Sugimura, Y., Goto, W., Tanizawa, H., Nagasaku, T., Saito, K., Ninomiya, T., and Saito, K. (2012). “Response control effect of hi-rised steel building structure using tuned viscous mass dampers.” *AIJ Journal of Technology and Design*, 18(39) (doi: <https://doi.org/10.3130/aijt.18.441>).
- Swift, S., Smith, M. C., Glover, A., Papageorgiou, C., Gartner, B., and Houghton, N. E. (2013). “Design and modelling of a fluid inerter.” *International Journal of Control*, 86(11), 2035–2051 (doi: <https://doi.org/10.1080/00207179.2013.842263>).
- Symans, M., Charney, F., Whittaker, A., Constantinou, M., Kircher, C., Johnson, M., and McNamara, R. (2008). “Energy dissipation systems for seismic applications: current practice and recent developments.” *Journal of Structural Engineering, ASCE*, 134(1), 3–21 (doi: [https://doi.org/10.1061/\(ASCE\)0733-9445\(2008\)134:1\(3\)](https://doi.org/10.1061/(ASCE)0733-9445(2008)134:1(3))).
- Taflanidis, A., Giaralis, A., and Patsialis, D. (2019). “Multi-objective optimal design of inerter-based vibration absorbers for earthquake protection of multi-storey building structures.” *Journal of the Franklin Institute*, 356(14), 7754–7784 (doi: <https://doi.org/10.1016/j.jfranklin.2019.02.022>).
- Takewaki, I., Murakami, S., Yoshitomi, S., and Tsuji, M. (2012). “Fundamental mechanism of earthquake response reduction in building structures with inertial dampers.” *Structural Control and Health Monitoring*, 19(6), 590–608 (doi: <https://doi.org/10.1002/stc.457>).
- Tena-Colunga, A. (1997). “Mathematical modelling of the adas energy dissipation device.” *Engineering Structures*, 19(10), 811–821 (doi: [https://doi.org/10.1016/S0141-0296\(97\)00165-X](https://doi.org/10.1016/S0141-0296(97)00165-X)).

- Tschoegl, N. W. (2012). *The phenomenological theory of linear viscoelastic behavior: an introduction*. Springer Science and Business Media, Berlin, Germany.
- UnitedNations (2018). *United Nations, Department of Economic and Social Affairs*. (<https://www.un.org/development/desa/en/>).
- Vassiliou, M. F. and Makris, N. (2011). “Estimating time scales and length scales in pulslike earthquake acceleration records with wavelet analysis.” *Bulletin of the Seismological Society of America*, 101(2), 596–618 (doi: <https://doi.org/10.1785/0120090387>).
- Vassiliou, M. F. and Makris, N. (2012). “Analysis of the rocking response of rigid blocks standing free on a seismically isolated base.” *Earthquake Engineering and Structural Dynamics*, 41(2), 177–196 (doi: <https://doi.org/10.1002/eqe.1124>).
- Veletsos, A., Newmark, N., and Chelapati, C. (1965). “Deformation spectra for elastic and elasto-plastic systems subjected to ground shock and earthquake motions.” *Proc., 3rd world conference on earthquake engineering*, Vol. 2, New Zealand, 663–682.
- Veletsos, A. S. and Verbic, B. (1974). “Basic response functions for elastic foundations.” *Journal of the Engineering Mechanics Division, ASCE*, 100(2), 189–202 (doi: <https://doi.org/10.1061/JMCEA3.0001869>).
- Wang, F.-C., Hong, M.-F., and Chen, C.-W. (2010). “Building suspensions with inerters.” *Proc., Institution of Mechanical Engineers, Part C: Journal of Mechanical Engineering Science*, Vol. 224, SAGE Publications Sage, London, U.K., 1605–1616.
- Wang, F.-C., Hong, M.-F., and Lin, T.-C. (2011). “Designing and testing a hydraulic inerter.” *Proc., Institution of Mechanical Engineers, Part C: Journal of Mechanical Engineering Science*, Vol. 225, SAGE Publications Sage, London, U.K., 66–72.
- Warburton, G. and Soni, S. (1977). “Errors in response calculations for non-classically damped structures.” *Earthquake Engineering and Structural Dynamics*, 5(4), 365–376 (doi: <https://doi.org/10.1002/eqe.4290050404>).
- Watanabe, Y., Ikago, K., Inoue, N., Kida, H., Nakaminami, S., Tanaka, H., Sugimura, Y., and Saito, K. (2012). “Full-scale dynamic tests and analytical verification of a force-restricted tuned viscous mass damper.” *Proc., 15th World Conference on Earthquake Engineering*, Lisbon, Portugal.
- Wen, Y., Chen, Z., and Hua, X. (2017). “Design and evaluation of tuned inerter-based dampers for the seismic control of mdof structures.” *Journal of Structural Engineering, ASCE*, 143(4), 04016207 (doi: [https://doi.org/10.1061/\(ASCE\)ST.1943-541X.0001680](https://doi.org/10.1061/(ASCE)ST.1943-541X.0001680)).
- Wen, Y.-K. (1976). “Method for random vibration of hysteretic systems.” *Journal of the Engineering Mechanics Division, ASCE*, 102(2), 249–263 (doi: <https://doi.org/10.1061/JMCEA3.0002106>).

- Whittaker, A. S., Bertero, V. V., Thompson, C. L., and Alonso, L. J. (1991). “Seismic testing of steel plate energy dissipation devices.” *Earthquake Spectra*, 7(4), 563–604 (doi: <https://doi.org/10.1193/1.1585644>).
- Ye, K., Shu, S., Hu, L., and Zhu, H. (2019). “Analytical solution of seismic response of base-isolated structure with supplemental inerter.” *Earthquake Engineering and Structural Dynamics*, 48(9), 1083–1090 (doi: <https://doi.org/10.1002/eqe.3165>).
- Zhang, R.-H., Soong, T., and Mahmoodi, P. (1989). “Seismic response of steel frame structures with added viscoelastic dampers.” *Earthquake Engineering and Structural Dynamics*, 18(3), 389–396 (doi: <https://doi.org/10.1002/eqe.4290180307>).

Disclaimer

The opinions, findings, and conclusions or recommendations expressed in this publication are those of the author(s) and do not necessarily reflect the views of the study sponsor(s), the Pacific Earthquake Engineering Research Center, or the Regents of the University of California.

The Pacific Earthquake Engineering Research Center (PEER) is a multi-institutional research and education center with headquarters at the University of California, Berkeley. Investigators from over 20 universities, several consulting companies, and researchers at various state and federal government agencies contribute to research programs focused on performance-based earthquake engineering.

These research programs aim to identify and reduce the risks from major earthquakes to life safety and to the economy by including research in a wide variety of disciplines including structural and geotechnical engineering, geology/seismology, lifelines, transportation, architecture, economics, risk management, and public policy.

PEER is supported by federal, state, local, and regional agencies, together with industry partners.



PEER Core Institutions

University of California, Berkeley (Lead Institution)
California Institute of Technology
Oregon State University
Stanford University
University of California, Davis
University of California, Irvine
University of California, Los Angeles
University of California, San Diego
University of Nevada, Reno
University of Southern California
University of Washington

Pacific Earthquake Engineering Research Center
University of California, Berkeley
325 Davis Hall, Mail Code 1792
Berkeley, CA 94720-1792
Tel: 510-642-3437
Email: peer_center@berkeley.edu

ISSN 2770-8314
<https://doi.org/10.55461/TIHV1701>